

Smart Reporter Genes for Cellular Molecular Imaging in Tumor Immunology

Natasa Gaspar

Smart Reporter Genes for Cellular Molecular Imaging in Tumor Immunology

Slimme reportergenen voor cellulaire moleculaire beeldvorming in tumorimmunologie

Thesis

to obtain the degree of Doctor from the
Erasmus University Rotterdam
by command of the
rector magnificus

Prof. dr. F.A. Van der Duijn Schouten

and in accordance with the decision of the Doctorate Board.

The public defence shall be held on
Wednesday 15 September 2021 at 10:30 hrs

by

Natasa Gaspar

born in Benkovac, Croatia

Erasmus University Rotterdam



Promotor:

Prof. dr. C. Löwik

Other members:

Prof. dr. R. Fodde

Prof. dr. F. Verburg

Dr. M. Lamfers

Copromotors:

Dr. L. Mezzanotte

Dr. A. Chan

Smart Reporter Genes for Cellular Molecular Imaging in Tumor Immunology

Thesis, Erasmus MC, University Medical Centre, Rotterdam, The Netherlands

The research described in this thesis was performed at the Department of Molecular Genetics and the Department of Radiology and Nuclear Medicine, Erasmus Medical Center, Rotterdam, The Netherlands.

Financial support for this thesis was provided by Percuros B.V.

Financial support by the European Commission under the H2020-MSCA-RISE award grant number 777682 (CANCER) and under the H2020-MSCA-ITN award, grant number 675743 (ISPIC).

Table of Contents

Chapter 1	General Introduction and Thesis Outline	7
Chapter 2	NanoBiT System and Hydrofurimazine for Optimized Detection of Viral Infection in Mice - A Novel <i>in Vivo</i> Imaging Platform (International Journal of Molecular Sciences, 2020; 21 (16))	33
Chapter 3	Evaluation of NanoLuc Substrates for Bioluminescence Imaging of Transferred Cells in Mice (Journal of Photochemistry and Photobiology, 2021; 26 (216))	55
Chapter 4	Evaluating Brightness and Spectral Properties of Click Beetle and Firefly Luciferases Using Luciferin Analogues: Identification of Preferred Pairings of Luciferase and Substrate for <i>in Vivo</i> Bioluminescence Imaging (Molecular Imaging and Biology, 2020; 22 (6))	75
Chapter 5	Can We Transform a Bioluminescent Reporter Gene into a Reporter for Radionuclide-based Imaging? (Manuscript in preparation)	93
Chapter 6	Review: Active Nano-targeting of Macrophages (Current Pharmaceutical Design, 2019; 25 (17))	115
Chapter 7	Summary & Concluding remarks	143
	Nederlandse Samenvatting	155
	Scientific contributions	173
	PhD Portfolio	177
	Acknowledgements	181
	Curriculum Vitae	185

Chapter 1

General Introduction and Thesis Outline

INTRODUCTION

What if we could detect cancer at the earliest possible stage, already at a molecular level of tumor development?

Cancer is one of the major death causes worldwide- 1 in 5 people develop cancer during their lifetime. According to GLOBOCAN 2020 (International Agency for Research on Cancer) statistics, cancer burden has risen to 19.3 million cases and 10 million cancer deaths in 2020 (1). Perhaps, the best way to understand cancer is to think of it as a failure in the interplay of cell death versus cell growth. Cancer cells don't obey the rules, and do not follow the patterns of tissue homeostasis, they are proliferating without control, and producing increasing amounts of new cancer cells (2). The origin of the disease is set in the dynamic changes within the genome, where genes regulating proliferation and survival have become dysfunctional by mutations. It is suggested that the broad plethora of cancer genotypes is a result of alterations in cell homeostasis, known as cancer hallmarks: self-sufficiency in growth signals, insensitivity to growth-inhibitory (antigrowth) signals, evasion of programmed cell death (apoptosis), limitless replicative potential, sustained angiogenesis, tissue invasion and metastasis. Fact is that tumors are more than masses of proliferating cells, one way is to observe them as complex organs, consisting of distinct cell types that communicate with each other, forming the tumor microenvironment (TME) (2, 3).

TUMOR MICROENVIRONMENT- THE NICHE

We must imagine the tumor, not just simply as an accumulation of cancer cells, but rather as a heterogeneous population of infiltrating and resident cells, extracellular matrix and secreted factors, forming a complex, constantly growing 'organ' (3) (Figure 1). The make-up of most cancers involves the non-cellular (vascular and interstitial) and cellular compartment that remarkably differs from surrounding tissue. Within the non-cellular compartment there is a combination of densely vascularized areas that are growing and expanding faster, where in contrast there are regions of poor blood supply which are characterized with tumor necrosis (4). This is mostly caused by a disproportion in secretion of pro- and anti-angiogenic factors which further contributes to formation of poorly organized blood vessels, hypoxic and acidic regions and impaired blood flow (5, 6). There are 2 distinct populations of cancer cells within the tumor: cancer stem cells and fast proliferating cells. Cancer stem cells are the epicenter of TME, controlling all functions of both compartments, cellular and non-cellular, through complex signaling crosstalk in order to make benefit for further growth and expansion. The second population are fast proliferating cells that form most of the tumor mass and do not have the ability, neither to self-sustain nor metastasize (4). This tumor cell division probably explains best why

most therapies are not successful in fighting cancer: traditional chemotherapy is often not enough since it mainly targets non-cancer stem cells and leaves behind cancer cells which are able to regenerate the tumor all over again (7).

Chronic exposure to inflammatory cytokines within TME results in significant lack of antitumor response and immune cell anergy. TME reeducates immune cells, and they start over time to release pro-tumorigenic mediators keeping the tumor microenvironment alive. Understanding the language between cancer cells and its surrounding is key in order to develop reliable ways for successful anti-cancer therapy, all based on interruption of complex crosstalk within the TME (8). Due to diverse roles and key functions of immune cells within the TME, they have become an important target in design of novel cancer immunotherapy approaches.

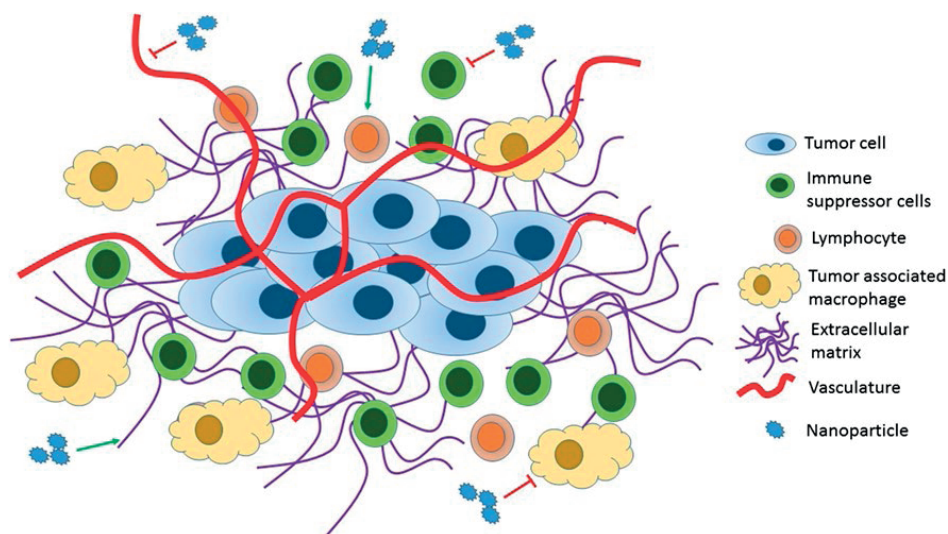


Figure 1 || Schematic representation of components of tumor microenvironment and nanoparticle therapies. The tumor microenvironment consists of tumor cells as well as many immunosuppressive cells and tumor-associated macrophages (TAMs), few immunostimulatory lymphocytes, abundant extracellular matrix (ECM) and vasculature. Nanoparticle therapies have been shown to inhibit immunosuppressive cells and TAMs and to hinder vascular development. From (9).

THE IMMUNE SYSTEM

The immune system is a network comprised of biological processes, chemicals and sets of cells that protect the organism from disease. It can be simplistically observed as having two major lines of defense: the innate and adaptive immunity. The innate immune system, provides already preconfigured responses, it represents the first line of defense to intruding

pathogens. It is not able to 'memorize' the same pathogen in case of future exposure to it. Numerous cells are involved in the innate immunity: phagocytes (macrophages and neutrophils), dendritic cells, mast cells, eosinophils, basophils and natural killer (NK) cells (10). NK cells can directly kill cancer cells even without MHC I marker, that is lost in some cancers (11).

On the other hand, the adaptive immune system, has a tailored response to each stimulus, and has the capacity for memory to protect against future challenges with the same pathogen (12). The cells of adoptive immune system include antigen-specific T- cells, activated through antigen presenting cells (usually dendritic cells or macrophages) and B- cells. These two systems collaborate with each other to ensure robust immune defense while avoiding auto-immune disease.

TUMOR INFILTRATING MYELOID CELLS (TIMCS)

TIMCs are of great interest in cancer immunology, since these phagocytic cells are most abundant within tumor stroma. Some of them modulate key cancer-associated activities, including immune invasion, where they can either favor or hinder therapy response (13). TIMCs are essential in tissue homeostasis and play a key role in sustaining, initiating or inhibiting T- cell immunity. The broad spectra of these cells is usually classified into mononuclear cells (macrophages, monocytes and dendritic cells) and polymorphonuclear cells (neutrophils, mast cells, basophils and eosinophils) (14). Macrophages (MQs) which are abundant in all tissues, perform tissue-specific functions like regulation of inflammation (15, 16). Dendritic cells (DCs) comprise most part of the mononuclear cell group. This cell subtype consists of distinct clusters, e.g. classic DCs (cDCs) are the most dominant subset, they sample antigens in tissues in order to move them towards the local draining lymph nodes to induce antigen-specific T- cell immunity or tolerance (17, 18). cDCs also control T- cell behavior within non-lymphoid tissues including solid tumors (18, 19). Another DC subset includes plasmacytoid DCs (pDCs), which uniquely produces interferon- α (IFN α) and therefore can regulate cancer state (20). MQs and DCs are derived from several origins (21), but the most abundant in tumors, are mainly derived from circulating precursors- the monocytes (22) and pre-DCs (23), which are produced by bone marrow-derived hematopoietic stem cells (HSCs) (24). Polymorphonuclear myeloid cells, are well known as granulocytes, they also are derived from HSCs. They accumulate in diseased sites releasing toxic and inflammation prone agents thereby protecting the host from parasitic and bacterial invaders (25-27).

These cell types still remain less studied, in comparison to T- lymphocytes, but started gaining attention in recent years, since their presence in tumors is linked to altered patient

survival (24). The specific cross talk between tumor-associated myeloid cells and adaptive immunity is an important regulator of cancer progression (24).

MACROPHAGES

Macrophages (MQs) are most spread immune cells in tumor stroma and they significantly affect cancer cell behavior (14, 28). MQs participate in maintenance of tissue integrity and homeostasis, by discriminating self from non-self, functioning as antigen presenting cells, sensing tissue damage, recognizing invading pathogens and eliminating them via phagocytosis (29). Their heterogeneity makes it challenging to define specific MQ markers, and in order to accurately identify this cell type, novel methods are needed. When MQs are being recruited to tumor site, they are known as tumor associated macrophages (TAMs). Currently CD68 and CD163- the scavenger receptor (M130 in humans) markers are widely used in clinical studies as TAM markers. The issue with these markers is that they detect other cell types as well, not specifically TAMs (24, 30, 31). Several studies revealed poor prognosis of cancer patients with high density of TAM-like cells in tumor areas (32). Numerous animal studies show that TAMs produce several growth factors and cytokines supporting tumor cell survival and growth (e.g. epidermal growth factor (EGF), tumor necrosis factor (TNF), interleukin IL-6, etc.) (32). They display broad activities and phenotypes but are usually categorized as either; classically activated (M1) cytotoxic phenotype, which contributes to an inflammatory environment by release of pro-inflammatory cytokines and reactive oxygen species (ROS) (9) and has an impairing role on tumor growth. In contra, the immunosuppressive, alternatively activated (M2) phenotype of TAMs (33), promotes tumor growth. Mostly these two subtypes are distinguished by activation stimuli: interferons (IFNs) for M1 activation and IL-13, IL-4 for M2 activation (34). This M1/M2 dogma of TAMs is an oversimplified division, since TAMs *in vivo* go beyond simple M1 and M2 denominations. Most tumors show to be enriched with the M2 subtype of TAMs which promote tumor cell growth and evasion, blunt the antitumor T- cell functions and enhance tumor angiogenesis (34). What is currently needed is a more sensitive characterization of TAMs in order to more specifically depict their true role in various cancer types.

T- CELLS

T- cells are type of white blood cells that play key roles within the immune system. They are distinguished from other lymphocytes by the presence of the surface TCR receptor. T- cells originate from hematopoietic stem cells and further mature within the thymus

gland that trains them to distinguish ‘foreign’ from ‘own’ tissue, in order to avoid autoimmunity. Two major subtypes of T- cells are known: ‘killer’ (CD8+) and ‘helper’ (CD4+) T- cells. ‘Killer’ T- cells (CD8+), also known as cytotoxic CD8+ T- cells, when activated are able to directly kill cancer cells or virus infected cells. ‘Helper’ T- cells (CD4+), on the contrary, indirectly kill foreign cells and help other parts of the immune system to respond to ‘foreign’ threat.

Regulatory T- cells (T_{reg}) are another distinguished subtype crucial for providing self-tolerance and are characterized by expression of the forkhead box protein P3 (FOXP3). Mutations in FOXP3 protein cause severe immune dysregulation characterized by development of several autoimmune disorders (35). T_{reg} cells for example, possess antitumor effect, but over time, they are reprogrammed within the TME; when $Foxp3^+CD25^+CD4^+$ (T_{reg} cells) infiltrate into the tumor, they start releasing inhibitory cytokines, such as IL-10 and transforming growth factor- β (TGF- β), thereby hindering immunosurveillance against tumor (36).

T- cells attack tumor cells expressing antigens that are bound to the major histocompatibility complexes (MHC) on the cell (37). They patrol within the TME and get activated by antigen recognition, where they start to differentiate, proliferate and in the end, eliminate cancer cells expressing specific antigen patterns. It is generally established that T- cell immunity is the primary immune effector system against tumors: cancers with high mutation percentage, show to contain more tumor epitopes and are best infiltrated and recognized by T- cells (‘hot tumors’). In contrast ‘cold tumors’ lack infiltrating T- cells demonstrating a dysfunctional immune system, for one or another reason. The lack of T-cells, within the tumor stroma, represents a problem for immunotherapy use, and the success rate of most modern cancer immunotherapies is particularly based on the induction/enhancement of T- cell responses (38).

THE IMMUNOTHERAPY TOOLBOX

Growing understanding of different cell types, especially the immune cells, within the TME and recent clinical success of cancer immunotherapy, led to development of new tools for imaging of the immune system (39, 40). Molecular imaging offers the advantage to depict alternations in cellular and biochemical processes that may reflect tumor response to therapy, far in advance of anatomic changes. To date, most imaging modalities are rather focused on assessment of shrinkage of tumor mass through anatomical imaging, whereas molecular imaging has the ability to image function, rather than the structure, with the ability to track changes in expression of molecular patterns including the state and location of cells of interest (41).

Paul Ehrlich introduced this concept of harnessing one's own immune system for cancer treatment. This concept started advancing with the development of hybridoma technologies and monoclonal antibodies (mAbs) (42). There are several mAbs that made a major impact in clinical practice and patient outcome, these mAbs are known to target tumor-specific antigens such as; CD20 (in lymphoma), epidermal growth factor receptor (EGFR) (43) in colon and head and neck cancer, and the human epidermal growth factor (HER2 or ERBB2) (44) in breast cancer. Despite their initial success in clinical trials, these mAbs were not the answer to the overall big problem: such therapies with mAbs provide 'passive immunity (immunity not derived from the host, transferred from another source), rather than 'active immunity' (derived from host's own immune system). When mAbs are once cleared from the system, the immunotherapy activity is completely lost (41). Harnessing 'active immunity' has been a recent focus in immunotherapy. This type of immunity depends on host's own immune system to generate an immune response, typically through B- and T- cell mediated processes. Such immune response depends on recognition of tumor specific antigens through humoral responses produced via B- cells (e.g. antibodies) or true cellular responses produced by T- cells (T cell receptor).

There is a number of methods currently available that focus on harnessing 'active immunity', such as cancer vaccines, checkpoint inhibition, cell-based therapies (CAR T-cells, dendritic cells) and oncolytic virotherapy.

Tumor vaccines are meant to provoke a therapeutic response (rather than prevent). Therapeutic vaccination against cancer involves administration of tumor epitopes in the form of protein or peptide antigens, or of DCs pre-loaded with such antigens (45). In this approach patients are immunized with their own inactivated tumor cells, provoking B- and T- cell responses (46). The biggest plus of such an approach, in comparison to mAbs, is that administration of whole cancer cells presents a range of tumor antigens, not just one. The bottleneck to this type of immunotherapy approach is the limited access to sufficient tumor tissue, which prevents large clinical trials.

In order to overcome this hurdle, of having to inject whole tumor cells, is to use recombinant proteins for vaccination. In 1991, MAGE-1 on melanoma cells, a tumor antigen was reported to evoke T- cell responses (47). Administration of a recombinant tumor antigen, provokes humoral, and as well cellular immunity. There are several tumor specific antigens that have been attempted; HER2 (48), CEA (49) and GFRv3 (50). Nevertheless, such approaches target again only one antigen, leaving a lot of space for resistance development.

A more comprehensive understanding how cancer cells manage to escape immune surveillance and immunotherapy has been developed. The presence of certain cell types within the tumor microenvironment has two sides of the story: presence of intratumoral CD8+ cytotoxic T- cells and CD4+ helper T- cells has a positive prognostic feature, where then again, a number of cell subtypes are linked to inhibition of immune function (51).

These cell types especially include: regulatory T- cells (T_{reg}) (52) which suppress other T- cell functions via expression of immune checkpoint molecules like CTLA4 and PD1, described below, but also immune suppressive molecules like TGF- β and IL-10; myeloid-derived suppressor cells (MDSCs) (53) which inhibit the immune system via metabolism of L-arginine and production of nitric oxide (NO); tumor associated macrophages (TAMs) (54) suppress immune function by production of proangiogenic invasion signals.

In addition to the cellular compartment, that inhibits the success of immunotherapy, there are as well some regulatory molecules that prevent the immune system in winning against cancer. These inhibitory molecules are called ‘immune checkpoints’ and their main function is to turn off immune response through interactions with effector T- cells. Blocking this signaling axis of immune checkpoints can lead to tumor regression.

All currently FDA-approved agents are blocking antibodies targeting immune checkpoint molecules; the cytotoxic T-lymphocyte-associated antigen 4 (CTLA-4) which represents an inhibitory surface receptor on T- cells and the programmed receptor-ligand pair PD-1 and PD-L1. CTLA-4 may regulate both, T- cell priming and effector function, and aid the suppressive function of a CD4 T- cell subset, the regulatory T- cells (55-57). Ipilimumab, an antibody which blocks CTLA-4 interaction with its ligands, CD80 and CD86, showed significant efficacy in malignant melanoma patients leading to FDA approval of the therapy in 2011 (57).

Programmed cell death protein 1 (PD-1) is an inhibitory receptor expressed on activated T- cells which upon ligation by PD-L1 induces T- cell apoptosis (58, 59). Blockade of PD-1/PD-L1 axis by antibodies was clinically effective in a range of cancer types including melanoma and non-small cell lung cancer (NSCLC) (60-62).

Combinations of PD-1 and CTLA-4 blocking antibodies were shown to further improve clinical responses (63-65).

Other approaches focus on *ex vivo* engineering of immune cells: by co-opting antigen presenting cells (APCs) to reveal tumor-specific antigens. Cellular immune responses are possible mostly coming from cytotoxic T and B lymphocytes and natural killer (NK) cells. Dendritic cell (DCs) vaccines are part of this concept where monocytes are isolated from patients’ peripheral blood and are engineered *ex vivo* into mature DC cells. Such cells are further incubated with tumor lysates, tumor-specific antigens and later on are reintroduced into patients. Vaccines like these, have been widely used in the clinics (66), nevertheless they did not make a significant change one has hoped for. Recent efforts in immunotherapy approaches are focusing on direct genetic engineering of T- cells, where harvested T- cells are transfected to express genes encoding for a receptor, specific for a tumor-specific antigen- the chimeric antigen receptor T (CAR-T). These CAR-T cells are reintroduced into patients leading to immune response. Success in the clinics has been observed with CAR-T cells targeted towards hematological cancers like CD19 chronic lymphocytic leukemia and acute lymphoblastic leukemia (67-69) where access of the

antibodies in the circulation is direct, this in contrast to solid tumors where access is more difficult and most therapies currently are not very effective.

Oncolytic viruses are as well gaining attention as an emerging therapy for cancer treatment, where engineered viruses are used to selectively infect and kill tumor cells.

Improving *in vivo* imaging of such viruses would improve safety, efficacy assessments and localization of viral biotherapeutics, with the potential to translate those findings towards the clinic (70). Novel imaging tools are expected to improve *in vivo* analysis over current methods, which are often not suitable for imaging the therapeutic efficacy of particular types of viruses (71).

With immunotherapies entering more in the clinic, and investigators noticing shortfalls of anatomic imaging modalities, since these modalities do not offer any information about the biology of therapy, there is a growing need for more precise imaging modalities that could better track patient's response (41).

MOLECULAR IMAGING

Recent clinical success of cancer immunotherapy requires development of tools to image the immune system. Molecular imaging of immune cells and molecular targets related to cancer, provide a unique viewpoint on a far deeper level: imaging a patient's underlying immune state before actual disease development. What if we could detect and measure molecular targets and biological processes non-invasively, in a living subject? What if we could image gene expression *in vivo*? What if we could detect cancer at the earliest stages, long before a patient or physician notices signs or symptoms (72)? Early detection and the following treatment of cancer is key in order to reduce cancer mortality.

Molecular imaging revolutionized the way we perceive and approach the human body, plan and approach drug design and diagnose disease (73). Visualization of complex biochemical processes in diseased states and healthy physiology, in real time, ranging from cells, tissues, organs to whole body images, was made possible with the definition of molecular imaging.

Molecular imaging is strongly tied to nuclear medicine which aims to facilitate patient management via imaging instrumentation and radionuclides, either alone, or bound to targets that specifically interact with molecular targets of interest (73, 74). Development of SPECT (single photon emission computed tomography) and PET (positron emission tomography) all in combination with the design of novel radiolabeled molecules that specifically bind to diverse biochemical targets opened a completely new era of molecular imaging (73, 75).

The importance of molecular imaging lies in the ability to translate common *in vitro* studies to an *in vivo* setting, therefore bridging preclinical and clinical research (Figure 2).

The fusion of *in vitro* molecular biology and *in vivo* imaging bridged many gaps across several areas of science.

There are several advantages of molecular imaging techniques compared to traditional *in vitro* methods, that is, non-invasive observation of cells in their natural environment; the combination of different imaging techniques made it easier to trace and visualize dynamic biological processes; rapid screening of drugs and therapies, thereby reducing the time needed to evaluate their safety and efficacy; performing studies in the same animal over time, thereby reducing the amount of needed animals; imaging techniques with appropriate and temporal spatial resolution, etc. (73).

Classical imaging modalities usually include SPECT (single photon emission computed tomography), PET (positron emission tomography), CT (Computed tomography), MRI (magnetic resonance imaging), US (Ultrasound), and Optical imaging (Figure 2).

Within the focus of this thesis, pre-clinical optical imaging modalities will be broadly explained, along with a short description on PET and SPECT, as main nuclear imaging modalities translated to the clinics.

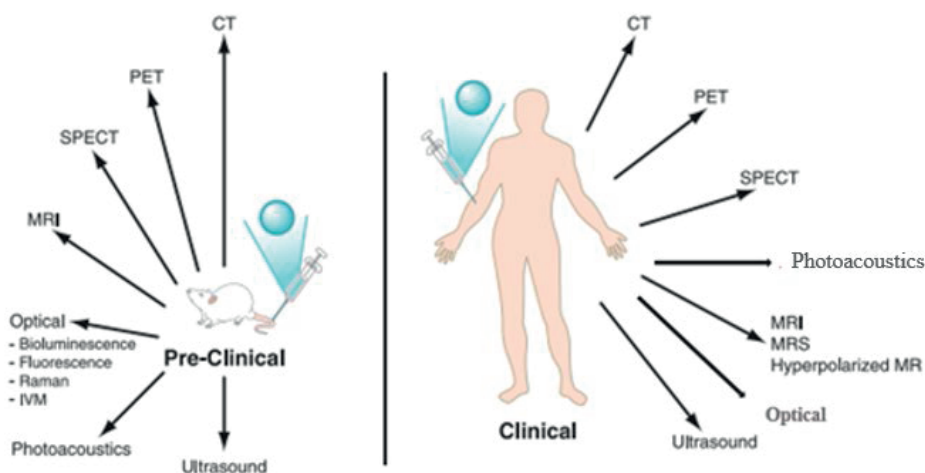


Figure 2 || Key molecular imaging modalities used for preclinical and/or clinical applications. CT, computed tomography; PET, positron emission tomography; SPECT, single photon emission computed tomography, MRI, magnetic resonance imaging; MRS, magnetic resonance spectroscopy; IVM, intravital microscopy. Blue circle, appropriate contrast agent or molecular imaging agent. From (73).

OPTICAL MOLECULAR IMAGING

Optical imaging uses light to examine molecular and cellular functions within the living body, as well as in animal and plant tissue. The images are created by use of light photons in the range from ultraviolet to near infrared wavelength. This use of light, ever since the

discovery of the first microscope in 1674 by Anton van Leeuwenhoek, has been a very informative and facile approach in research and medical imaging. The source of these optical signals can be fluorescent molecules, which emit light after being excited by an external light source (fluorescence imaging, FLI), or luciferase enzymes which produce light as a product of a chemical reaction converting an administered substrate (bioluminescence imaging, BLI). The necessary infrastructure for optical BLI and FLI are charge-coupled device (CCD) cameras and a source of filtered light, relatively inexpensive and easy to setup. The achieved imaging sensitivity with these techniques is usually very good (as low as picomolar to femtomolar concentrations). The use of low-energy photons represents a big hurdle for these 2 techniques: meaning that light penetration depth is limited to few centimeters making it impossible to study deep tissues in larger animals or humans, unless one uses an endoscope (76). Light absorptions, such as the one caused by hemoglobin or water, reduce fluorescent signals by a factor of ~10 per centimeter of tissue (77). One can overcome these hurdles, by a large extent by choosing fluorescent agents or proteins (e.g. iRFP) which emit in the near-infrared (NIR) part of the visible spectrum, with emission between 650 nm to 900 nm, where the absorption of cytochromes and hemoglobin, in living organisms is the lowest (77). These fluorescent agents and proteins, emitting in NIR part of visible spectrum, can be imaged at greater tissue depths, with a significant decrease in autofluorescence (fluorescent signal from tissues where no imaging agent is present) (76, 78).

FLUORESCENCE IMAGING

Fluorescence imaging is best described with administration of fluorescent dyes or expression of fluorescent proteins into either cells, tissues or animals, either as such or fused to molecules of interest, after which the administered molecules can be tracked in real time. Fluorescent molecules do not emit photons intrinsically, and therefore need to be excited with an external light source, such as a laser, where upon excitation, these molecules absorb energy resulting in photon emission on their own, which forms the actual fluorescent signal with a higher emission wavelength. One of the most exciting discoveries in the imaging field was the discovery of green fluorescent protein (GFP) in 1960, isolated from the jellyfish *Aequorea Victoria*. It rapidly became one of the most used proteins to study molecular mechanisms, due to the ability to generate GFP reporter systems or fusion proteins (79). It became very popular for studying gene expression and for protein targeting, especially in cells *in vitro* using fluorescence microscopy. Since light penetration of GFP is only 1- 2 mm, its use in living organisms is limited to superficial imaging or *ex vivo* analysis of GFP in tissue sections. Another problem of using GFP reporter systems is cellular/tissue autofluorescence that is very high at the excitation wavelength for GFP. To

overcome the problem of tissue penetration GFP and RFP (red fluorescent protein) have been used in intra-vital microscopy, where a glass window has been made to observe the cells tagged with GFP or RFP reporters (80).

Overall, FLI is mainly used for preclinical imaging, especially for *in vitro* cell imaging, since it allows high resolution multiplex imaging, but also *in vivo* in small animals, using either intravital microscopy to study cell behavior, or NIRF labeled tumor targeting probes for clinical translation in situations where tissue depth is not an issue e.g. in endoscopy settings and intraoperative techniques (73).

BIOLUMINESCENCE IMAGING

Bioluminescence is one of the oldest scientific studies which dates from the very first written words of ancient Greeks (Figure 3). It is a sort of chemiluminescence, the production and emission of light, occurring in a number of living organisms (81). This phenomenon, of so called 'living light' or 'cold light' is widely distributed among the biosphere and in the ocean. Already in ancient Greece, Aristotle (384-322 BCE) was the first one to mention the luminescence of bioluminescent organisms, where he noted that this sort of light emission was not accompanied with heat, like the light from a candle. He was describing the 'cold light' phenomena on death fish, now known to derive from infection of bioluminescent bacteria, the light on the sea-water, now known to originate from dinoflagellates. The first specific written word on bioluminescence was written by Pliny the Elder (23-79 CE) in his '*Naturalis Historia*', where he broadly described many bioluminescent animals, like the purple jellyfish, glow worm, fireflies etc. Later on, in the 17th century, Robert Boyle (1627-1691) discovered the importance of molecular oxygen for production of luminescent light (82).

The modern era of bioluminescence began, alongside with the advancement of chemical sciences, when Dubois demonstrated in 1885, the first example of a luciferase/luciferin reaction where he concluded that an enzyme and a specific, relatively heat stable substance, which he named 'luciferin' were key players for the light-emitting reaction. Edmund Newton Harvey (1887-1959) further advanced the knowledge behind the luminescence phenomena and published the book 'Bioluminescence' in 1952 which is considered to be one of the first and most important works in this field.

Nowadays, *in vivo* bioluminescence imaging (BLI) has enabled visualization of biological processes in intact living organisms, providing insight in all sort of molecular information that is far beyond classical *in vitro* assays. As already mentioned earlier, BLI is based on the catalytic activity of a luciferase enzyme which oxidases its substrate 'luciferin' (meaning 'light bearers'), generating an excited-state molecule that emits light (83). In comparison to fluorescence imaging, BLI does not require external light excitation, that in some cases

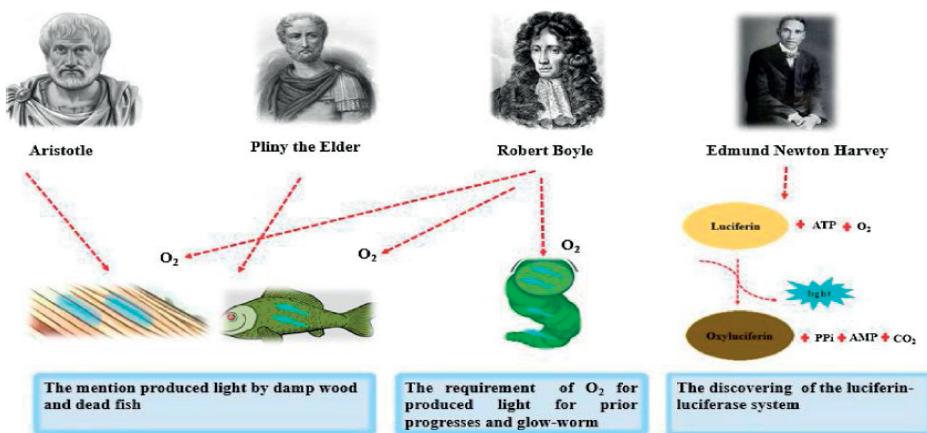


Figure 3 || The history of bioluminescence from the observations of Aristotle to the discovering of the luciferin-luciferase system by Harvey. The glowing of damp wood and dead fish was mentioned by both, Aristotle and Pliny the Elder. Later, Boyle showed the involving of oxygen in the process including wood and in glow-worms. Finally, the acting of light-emitting substances known as luciferins on by enzymes called luciferases was discovered by Harvey. From (82).

can cause background signal (autofluorescence), phototoxicity and photobleaching (84). The advancement in BLI field has led to sensitive *in vivo* imaging, in heterogeneous mammalian tissues, enabling monitoring of various biological processes, such as tumor growth, viral and bacterial infections, gene expression, etc.

The family of luciferase enzymes, that are nowadays used, emerge from a different species including beetles, sea pansy, copepods, and deep-sea shrimp. Every system is coupled with a distinct luciferin analogue; firefly luciferase (FLuc) requires D-luciferin, while marine Renilla and Oplophorus derived luciferases, RLuc and NLuc, use coelenterazine based analogues (85). Despite being similar, the color pallet (emission wavelength), intensity of emitted light, and the dependency on additional accessory molecules (e.g. ATP, Mg²⁺) differ among the luciferase/luciferin pairings. Selection of the proper luciferase/luciferin pairing, depending on the experimental setup, is key when performing imaging.

These bioluminescent systems have been used for non-invasive, *in vivo* imaging of biological processes due to possibility of genetic engineering of cells to express luciferases as reporter genes, and the ability to detect light by instrumentation equipped with CCD cameras (Figure 3).

The firefly luciferase (FLuc)/D-luciferin pairing is the most exploited BL reporter system, due to its relatively high quantum yield (0.44) and red-shifted light emission that penetrates better through tissue (530–640 nm). Compared to firefly luciferases, marine and bacterial luciferases are less commonly used for *in vivo* studies, because the light emitted from these systems falls in the blue/green region (430–490 nm) that is known for its poor tissue penetration. To date, many different BL systems have been developed by

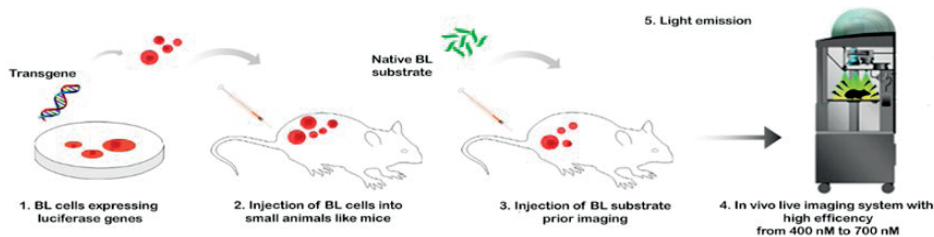


Figure 3 || Workflow of a BLI experiment. After establishment of genetically engineered cells for the expression of luciferase enzyme (1), a BL substrate is administered to animals that received an injection of bioluminescent cells (2). The animal is placed under anesthesia in the imaging system and the images are acquired (4).

discovery and cloning of novel luciferase genes, creation of mutants or synthetic enzymes. Moreover, intense research led to synthesis of luciferin analogues able to enhance brightness of BL systems and alter spectral emission. Some of them are reported in Table 1.

Light generated by different luciferase/luciferin pairings is able to travel diffusely through tissue. Photons are scattered in biological tissues approximately every 100 μm and are absorbed mainly by hemoglobin and melanin. The lowest absorption occurs in the region of 650–900 nm which is the optimal optical window for *in vivo* imaging. Firefly, click beetle red and AkaLuc luciferases emit ample amount of photons in this region.

BL imaging offers spatial resolution of millimeters in superficial tissue (0–1 mm) which decreases for light sources located in greater depths. 2D images can be acquired at a temporal resolution ranging from 1s to 5min, depending on the level of needed sensitivity. Scattering and absorption of light through biological tissue, in the visible or near-infrared wavelength, limits the applicability of BL imaging in the range of 1–10 millimeters. Both, sensitivity and spatial resolution, are affected by tissue depth. Sensitivity can be improved by increasing acquisition time, or by employing a brighter BL system, which generates

Table 1. || List of common luciferase reporter genes that are currently used for *in vivo* imaging applications.

Luciferase name	Origin and modifications	Emission peak <i>in vivo</i>
Firefly luciferase (FLuc)	<i>Photinus pyralis</i>	610 nm with D-luciferin
Firefly luciferase red (PPyRE8; PpyRE9)	<i>Photinus pyralis</i> mutants	618 nm with D-luciferin
Firefly luciferase green (PPyGR9)	<i>Photinus pyralis</i> mutant	547 nm with D-luciferin
Click beetle luciferase red (CBred)	<i>Pyrophorus plagiophthalmus</i> mutant	620 nm with D-luciferin
Click beetle luciferase red 2 (CBred2)	<i>Pyrophorus plagiophthalmus</i> mutant	720 nm with Naphthyl luciferin
Click beetle luciferase green (CBG99)	<i>Pyrophorus plagiophthalmus</i> mutant	542 nm with D-luciferin
Gaussia luciferase (Gluc)	<i>Gaussia princeps</i>	480 nm with Coelenterazine
Renilla luciferase	<i>Ophlophorus gracillocistris</i> mutant	480 nm with Coelenterazine
NanoLuc luciferase	<i>Ophlophorus gracillocistris</i> mutant	460 nm with Furimazine
Bacterial luciferase	<i>Vibrio fischeri</i>	480 nm with FMNH ₂
AkaLuc luciferase	Synthetic luciferase derived from <i>Photinus pyralis</i>	650 nm with Akalumine-HCl

a substantial number of near infrared photons. Tomographic reconstruction techniques may improve resolution. Therefore, BL emission is sufficient for imaging in small animals, particularly mice, but lacks translational potential to clinical applications, due to use of GMOs and the potential toxicity of some BL substrates in human cells (e.g. coelenterazine). Progress in development of novel bioluminescent systems, with different colors and brighter emission, engineering of new luciferase mutants and modification of luciferins to generate analogues, will further expand the range of BLI applications.

RADIONUCLIDE-BASED REPORTER GENE SYSTEMS

Radionuclide based imaging or scintigraphy can be simply described as detection of high-energy photons from decaying radioisotopes, most of the time coupled to specific molecules, which are administered in the subject of interest. The administered radiochemical probes are referred to as tracers or radiopharmaceuticals. When we talk about nuclear imaging modalities, we mostly refer to single photon emission tomography (SPECT) or positron emission tomography (PET). SPECT imaging makes use of gamma-emitting isotopes and is relatively less sensitive, requires longer scan time intervals and higher radioactivity administration, but provides the possibility to perform simultaneous multitracer studies (86). PET imaging, on the other hand, makes use of positron-emitting radioisotopes, and is a quantitative imaging modality, with an extremely high sensitivity which can be used to quantify gene expression (87). SPECT and PET offer outstanding imaging sensitivity, with detection limit as low as in the picomolar range, with deep tissue penetration, making them applicable for development and optimization of gene therapy approaches in pre-clinical models, which can be easily translated to clinics (88). A disadvantage of these two modalities is a relatively poor anatomical resolution with a low spatial resolution, which led to design of combined imaging modalities, mostly accompanied with computed tomography (CT) or X-ray (41).

Gene expression imaging is usually performed by using radionuclide probes with direct or indirect approaches (89). Direct labelling uses *ex vivo* labelling of cells prior administration: cells are being incubated with radioisotopes and are reintroduced in patients. This method is quite simple and convenient, but does not offer a longitudinal study of *in vivo* cell fate due to dilution effects, and it does not provide any information on cell survival, since cells that have died will still have the incorporated active agent (41). These limitations make direct labelling unsuitable for long term studies of fast proliferating cells (e.g. cancer cells).

Ex vivo labelling is as well related to low levels of radioactivity per cell, where cells are exposed to high levels of radioactivity during labelling, which affects their function (90).

Then again, indirect labelling with reporter genes, requires genetic engineering of cells to express the reporter gene and to ensure its long-term expression. Once the reporter gene is introduced to cells of interest, the cells are expanded *in vitro* and tested for radioactivity uptake, and finally these cells are being injected in the desired living organism. What follows is the systemic administration of a suitable labeling agent and the reporter gene can be targeted *in vivo* via molecular imaging (88).

Indirect labelling addresses issues of *ex vivo* labelling (direct labelling): it avoids *in vitro* exposure of cells to high quantities of activity and potential cell damage, and it supports long term studies of cell survival, proliferation and activation of immune cells.

Already a variety of radiolabeled probes for both, PET and SPECT, were developed for imaging of specific tumors and are clinically approved (e.g. [¹³¹I]MIBG for NET (91, 92) or [¹¹¹In]DTPA-octreotide for SSTR2 (93)).

An asset of radionuclide-based reporter imaging is the easy translation to clinical studies, when accompanied with well-equipped nuclear medicine infrastructure. The technology is sensitive and independent of tissue depth, unlike fluorescence- and bioluminescence-reporter based imaging systems (90).

However, clinical use of radionuclide-based reporter gene imaging raises some concerns about immunogenicity. An absolute necessity for these reporter gene systems is that they are biologically and immunologically inert (90). This concern is raised especially with respect to clinical use of viral-based reporter genes.

Nowadays, the focus of some research groups, is to develop humanized reporter systems, however the development process and integration in the clinic is rather slow. There are 7 well established humanized reporter genes (hNIS, hNET, hD2R, hSSTR2, PSMA, human thymidine kinase 2 (HSV-tk2), and human deoxycytidine kinase double mutant) with complementary radiolabeled substrates (gene + probe) available for clinical studies and only a single one (hNIS) is moving to clinical trials. These human genes are less probable to be immunogenic, than the currently used reporter genes, such as luciferases and fluorescent proteins, but also generate unspecific signals in non-target tissues. To perform human reporter gene studies, a good-manufacturing-practice (GMP) is absolute necessary in order to harvest, transduce, and expand human-derived cells for reinjection into patients, which are expensive and not available everywhere (90).

An interesting approach, in order to expand the pre-clinical use of reporter-based imaging, is development of multi-modality reporter imaging where 2 or 3 reporter genes are incorporated in one single expression cassette. Typically, these cassettes consist of fluorescent (e.g. GFP or RFP) or bioluminescence (e.g. FLuc or NanoLuc) genes in combination with a radionuclide-based reporter gene (90, 94-97). Such combined reporter gene cassettes compensate well for specific limitations of each imaging modality when used alone. Using multiple imaging modalities, can further increase knowledge related to a specific research question, and provides opportunities to monitor treatment success at the molecular level.

THESIS OUTLINE

This thesis focuses on development of improved imaging platforms for *in vivo* visualization of immune and cancer cells in preclinical models, that could potentially provide improved design of clinical protocols. Further improvement of novel imaging protocols for existing imaging modalities, will enable better disease visualization and understanding at the molecular level. The overall aim was to label cells with ‘smart’ reporter genes and track their fate *in vivo*, in real time.

Chapter 2 demonstrates bioluminescence imaging of viral infection using the NanoBiT system in combination with intraperitoneal injection of a novel furimazine analogue, hydrofurimazine. This new bioluminescent system served as an early-stage quantitative viral transduction reporter, for *in vitro* and *in vivo* studies in mice, and allows longitudinal monitoring of oncolytic viral persistence in infected tumor cells. The platform will not only provide novel opportunities for virus biology studies in animal models, but will also enable drug screening research.

In Chapter 3 we compared the performances of recently reported NanoLuc luciferase substrates for *in vivo* imaging in mice. Two substrates with improved aqueous solubility, hydrofurimazine and fluorofurimazine, were evaluated along with three stabilized O-acetylated furimazine analogues, the hikarazines. All five analogues were tested *in vitro* and the best performing ones were further selected for *in vivo* testing. We show that fluorofurimazine enables higher substrate loading and improved optical imaging sensitivity in small animals, upgrading the use of NanoLuc-based bioluminescent systems for deep tissue imaging.

Chapter 4 provides a detailed *in vivo* assessment of brightness and spectral characteristics of firefly (Luc2), click beetle green (CBG99), click beetle red 2 (CBR2) and AkaLuc luciferases when paired with different D-luciferin (D-LH2) analogues (e.g., Akalumine-HCl, CycLuc1 and amino naphthyl luciferin (NH₂-NpLH2)). The experimental results described within the study will be of importance for choosing the correct luciferase/luciferin pairing, for a variety of BLI applications, when performing imaging with terrestrial luciferases.

In Chapter 5 we developed a chimeric reporter gene, for stable transmembrane (TM) expression of a bioluminescent reporter gene, the TM-LgBiT, when combined with its radiolabeled HiBiT peptide probe, it supports bioluminescence imaging (BLI) in addition to nuclear (SPECT/PET) imaging, depending on the used radioisotope. As far as we can tell, this is the first report of a reporter gene that supports *in vivo* bioluminescence imaging (BLI) in addition to nuclear (SPECT/PET) modalities, and is derived from the BL Nano-BiT split-system. Within this study, we cover the whole issue ranging from radiolabeling, *in vitro* characterization, *in vivo* biodistribution studies to BLI and SPECT/CT imaging. We show specific tracer uptake in target positive cells, expressing TM-LgBiT, which was

confirmed by *ex vivo* biodistribution studies. This novel radionuclide-based reporter gene system, may accordingly find application in personalized health care for tracking, homing and persistence of cell-based therapies, including T- cells and stem cells. In **Chapter 6** we reflect on active targeting of macrophages using nanoparticles for therapeutic purposes. We highlight all the recent progress in active nanotechnology-based systems targeting various macrophage subsets in diseased tissues.

REFERENCES

1. Bray F, Ferlay J, Soerjomataram I, Siegel RL, Torre LA, Jemal A. Global cancer statistics 2018: GLOBOCAN estimates of incidence and mortality worldwide for 36 cancers in 185 countries. *CA Cancer J Clin.* 2018;68(6):394-424.
2. Hanahan D, Weinberg RA. Hallmarks of cancer: the next generation. *Cell.* 2011;144(5):646-74.
3. Anderson NM, Simon MC. The tumor microenvironment. *Curr Biol.* 2020;30(16):R921-R5.
4. Thakor AS, Gambhir SS. Nanooncology: the future of cancer diagnosis and therapy. *CA Cancer J Clin.* 2013;63(6):395-418.
5. Upreti M, Jyoti A, Sethi P. Tumor microenvironment and nanotherapeutics. *Transl Cancer Res.* 2013;2(4):309-19.
6. Omid Y, Barar J. Targeting tumor microenvironment: crossing tumor interstitial fluid by multifunctional nanomedicines. *Bioimpacts.* 2014;4(2):55-67.
7. Lobo NA, Shimono Y, Qian D, Clarke MF. The Biology of Cancer Stem Cells. *Annual Review of Cell and Developmental Biology.* 2007;23(1):675-99.
8. Baghban R, Roshangar L, Jahanban-Esfahlan R, Seidi K, Ebrahimi-Kalan A, Jaymand M, et al. Tumor microenvironment complexity and therapeutic implications at a glance. *Cell Communication and Signaling.* 2020;18(1):59.
9. Siegler EL, Kim YJ, Wang P. Nanomedicine targeting the tumor microenvironment: Therapeutic strategies to inhibit angiogenesis, remodel matrix, and modulate immune responses. *Journal of Cellular Immunotherapy.* 2016;2(2):69-78.
10. Marshall JS, Warrington R, Watson W, Kim HL. An introduction to immunology and immunopathology. *Allergy, Asthma & Clinical Immunology.* 2018;14(2):49.
11. Levy EM, Roberti MP, Mordoh J. Natural killer cells in human cancer: from biological functions to clinical applications. *J Biomed Biotechnol.* 2011;2011:676198-.
12. Flajnik MF, Kasahara M. Origin and evolution of the adaptive immune system: genetic events and selective pressures. *Nat Rev Genet.* 2010;11(1):47-59.
13. Murdoch C, Muthana M, Coffelt SB, Lewis CE. The role of myeloid cells in the promotion of tumour angiogenesis. *Nat Rev Cancer.* 2008;8(8):618-31.
14. Weissleder R, Pittet MJ. The expanding landscape of inflammatory cells affecting cancer therapy. *Nature Biomedical Engineering.* 2020;4(5):489-98.
15. Davies LC, Jenkins SJ, Allen JE, Taylor PR. Tissue-resident macrophages. *Nat Immunol.* 2013;14(10):986-95.
16. Murray PJ, Wynn TA. Protective and pathogenic functions of macrophage subsets. *Nature reviews Immunology.* 2011;11(11):723-37.
17. Steinman RM. Decisions about dendritic cells: past, present, and future. *Annu Rev Immunol.* 2012;30:1-22.
18. Merad M, Sathe P, Helft J, Miller J, Mortha A. The dendritic cell lineage: ontogeny and function of dendritic cells and their subsets in the steady state and the inflamed setting. *Annu Rev Immunol.* 2013;31:563-604.
19. Palucka K, Banchereau J. Cancer immunotherapy via dendritic cells. *Nat Rev Cancer.* 2012;12(4):265-77.
20. Swiecki M, Colonna M. The multifaceted biology of plasmacytoid dendritic cells. *Nat Rev Immunol.* 2015;15(8):471-85.
21. Guilliams M, Ginhoux F, Jakubzick C, Naik SH, Onai N, Schraml BU, et al. Dendritic cells, monocytes and macrophages: a unified nomenclature based on ontogeny. *Nat Rev Immunol.* 2014;14(8):571-8.

22. Pittet MJ, Nahrendorf M, Swirski FK. The journey from stem cell to macrophage. *Ann N Y Acad Sci.* 2014;1319(1):1-18.
23. Diao J, Zhao J, Winter E, Cattral MS. Recruitment and differentiation of conventional dendritic cell precursors in tumors. *J Immunol.* 2010;184(3):1261-7.
24. Engblom C, Pfirschke C, Pittet MJ. The role of myeloid cells in cancer therapies. *Nat Rev Cancer.* 2016;16(7):447-62.
25. Galli SJ, Borregaard N, Wynn TA. Phenotypic and functional plasticity of cells of innate immunity: macrophages, mast cells and neutrophils. *Nat Immunol.* 2011;12(11):1035-44.
26. Nathan C. Neutrophils and immunity: challenges and opportunities. *Nat Rev Immunol.* 2006;6(3):173-82.
27. Rosenberg HF, Dyer KD, Foster PS. Eosinophils: changing perspectives in health and disease. *Nat Rev Immunol.* 2013;13(1):9-22.
28. Barrett RL, Puré E. Cancer-associated fibroblasts and their influence on tumor immunity and immunotherapy. *eLife.* 2020;9:e57243.
29. Gaspar N, Zambito G, Löwik C, Mezzanotte L. Active Nano-targeting of Macrophages. *Curr Pharm Des.* 2019;25(17):1951-61.
30. Pulford KA, Sipos A, Cordell JL, Stross WP, Mason DY. Distribution of the CD68 macrophage/myeloid associated antigen. *Int Immunol.* 1990;2(10):973-80.
31. Kaiserling E, Xiao JC, Ruck P, Horny HP. Aberrant expression of macrophage-associated antigens (CD68 and Ki-M1P) by Schwann cells in reactive and neoplastic neural tissue. Light- and electron-microscopic findings. *Mod Pathol.* 1993;6(4):463-8.
32. Zhang QW, Liu L, Gong CY, Shi HS, Zeng YH, Wang XZ, et al. Prognostic significance of tumor-associated macrophages in solid tumor: a meta-analysis of the literature. *PLoS One.* 2012;7(12):e50946.
33. Eyileten C, Majchrzak K, Pilch Z, Tonecka K, Mucha J, Taciak B, et al. Immune Cells in Cancer Therapy and Drug Delivery. *Mediators Inflamm.* 2016;2016:5230219-.
34. Sica A, Mantovani A. Macrophage plasticity and polarization: in vivo veritas. *J Clin Invest.* 2012;122(3):787-95.
35. Bennett CL, Christie J, Ramsdell F, Brunkow ME, Ferguson PJ, Whitesell L, et al. The immune dysregulation, polyendocrinopathy, enteropathy, X-linked syndrome (IPEX) is caused by mutations of FOXP3. *Nat Genet.* 2001;27(1):20-1.
36. Nishikawa H, Sakaguchi S. Regulatory T cells in tumor immunity. *Int J Cancer.* 2010;127(4):759-67.
37. Sharma P, Allison JP. The future of immune checkpoint therapy. *Science.* 2015;348(6230):56-61.
38. Couzin-Frankel J. Breakthrough of the year 2013. Cancer immunotherapy. *Science.* 2013;342(6165):1432-3.
39. Brahmer JR, Tykodi SS, Chow LQM, Hwu W-J, Topalian SL, Hwu P, et al. Safety and Activity of Anti-PD-L1 Antibody in Patients with Advanced Cancer. *New England Journal of Medicine.* 2012;366(26):2455-65.
40. Hamid O, Robert C, Daud A, Hodi FS, Hwu W-J, Kefford R, et al. Safety and Tumor Responses with Lembrozumab (Anti-PD-1) in Melanoma. *New England Journal of Medicine.* 2013;369(2):134-44.
41. Kurtz DM, Gambhir SS. Tracking cellular and immune therapies in cancer. *Adv Cancer Res.* 2014;124:257-96.
42. Leavy O. The birth of monoclonal antibodies. *Nat Immunol.* 2016;17(1):S13-S.
43. Douillard J-Y, Oliner KS, Siena S, Tabernero J, Burkes R, Barugel M, et al. Panitumumab-FOLF- OX4 Treatment and RAS Mutations in Colorectal Cancer. *New England Journal of Medicine.* 2013;369(11):1023-34.

44. Slamon DJ, Leyland-Jones B, Shak S, Fuchs H, Paton V, Bajamonde A, et al. Use of Chemotherapy plus a Monoclonal Antibody against HER2 for Metastatic Breast Cancer That Overexpresses HER2. *New England Journal of Medicine*. 2001;344(11):783-92.
45. Guo C, Manjili MH, Subjeck JR, Sarkar D, Fisher PB, Wang XY. Therapeutic cancer vaccines: past, present, and future. *Adv Cancer Res*. 2013;119:421-75.
46. Hanna MG, Peters LC. Immunotherapy of Established Micrometastases with *Bacillus Calmette-Guérin*; Tumor Cell Vaccine. *Cancer Research*. 1978;38(1):204.
47. van der Bruggen P, Traversari C, Chomez P, Lurquin C, De Plaen E, Van den Eynde B, et al. A gene encoding an antigen recognized by cytolytic T lymphocytes on a human melanoma. *Science*. 1991;254(5038):1643.
48. Disis ML, Wallace DR, Gooley TA, Dang Y, Slota M, Lu H, et al. Concurrent trastuzumab and HER2/neu-specific vaccination in patients with metastatic breast cancer. *J Clin Oncol*. 2009;27(28):4685-92.
49. Tsang KY, Zaremba S, Nieroda CA, Zhu MZ, Hamilton JM, Schlom J. Generation of Human Cytotoxic T Cells Specific for Human Carcinoembryonic Antigen Epitopes From Patients Immunized With Recombinant Vaccinia-CEA Vaccine. *JNCI: Journal of the National Cancer Institute*. 1995;87(13):982-90.
50. Miao H, Choi BD, Suryadevara CM, Sanchez-Perez L, Yang S, De Leon G, et al. EGFRvIII-specific chimeric antigen receptor T cells migrate to and kill tumor deposits infiltrating the brain parenchyma in an invasive xenograft model of glioblastoma. *PloS one*. 2014;9(4):e94281-e.
51. Galon J, Costes A, Sanchez-Cabo F, Kirilovsky A, Mlecnik B, Lagorce-Pagès C, et al. Type, Density, and Location of Immune Cells Within Human Colorectal Tumors Predict Clinical Outcome. *Science*. 2006;313(5795):1960.
52. Zou W. Regulatory T cells, tumour immunity and immunotherapy. *Nat Rev Immunol*. 2006;6(4):295-307.
53. Gabrilovich DI, Nagaraj S. Myeloid-derived suppressor cells as regulators of the immune system. *Nat Rev Immunol*. 2009;9(3):162-74.
54. Noy R, Pollard Jeffrey W. Tumor-Associated Macrophages: From Mechanisms to Therapy. *Immunity*. 2014;41(1):49-61.
55. Grosso JF, Jure-Kunkel MN. CTLA-4 blockade in tumor models: an overview of preclinical and translational research. *Cancer Immun*. 2013;13:5.
56. Selby MJ, Engelhardt JJ, Quigley M, Henning KA, Chen T, Srinivasan M, et al. Anti-CTLA-4 antibodies of IgG2a isotype enhance antitumor activity through reduction of intratumoral regulatory T cells. *Cancer Immunol Res*. 2013;1(1):32-42.
57. Simpson TR, Li F, Montalvo-Ortiz W, Sepulveda MA, Bergerhoff K, Arce F, et al. Fc-dependent depletion of tumor-infiltrating regulatory T cells co-defines the efficacy of anti-CTLA-4 therapy against melanoma. *J Exp Med*. 2013;210(9):1695-710.
58. Iwai Y, Ishida M, Tanaka Y, Okazaki T, Honjo T, Minato N. Involvement of PD-L1 on tumor cells in the escape from host immune system and tumor immunotherapy by PD-L1 blockade. *Proc Natl Acad Sci U S A*. 2002;99(19):12293-7.
59. Dong H, Strome SE, Salomao DR, Tamura H, Hirano F, Flies DB, et al. Tumor-associated B7-H1 promotes T-cell apoptosis: a potential mechanism of immune evasion. *Nat Med*. 2002;8(8):793-800.
60. Topalian SL, Hodi FS, Brahmer JR, Gettinger SN, Smith DC, McDermott DF, et al. Safety, Activity, and Immune Correlates of Anti-PD-1 Antibody in Cancer. *New England Journal of Medicine*. 2012;366(26):2443-54.
61. Rosenberg JE, Hoffman-Censits J, Powles T, van der Heijden MS, Balar AV, Necchi A, et al. Atezolizumab in patients with locally advanced and metastatic urothelial carcinoma who have progressed fol-

- lowing treatment with platinum-based chemotherapy: a single-arm, multicentre, phase 2 trial. *Lancet*. 2016;387(10031):1909-20.
62. Fehrenbacher L, Spira A, Ballinger M, Kowanetz M, Vansteenkiste J, Mazieres J, et al. Atezolizumab versus docetaxel for patients with previously treated non-small-cell lung cancer (POPLAR): a multicentre, open-label, phase 2 randomised controlled trial. *Lancet*. 2016;387(10030):1837-46.
 63. Wolchok JD, Kluger H, Callahan MK, Postow MA, Rizvi NA, Lesokhin AM, et al. Nivolumab plus Ipilimumab in Advanced Melanoma. *New England Journal of Medicine*. 2013;369(2):122-33.
 64. Larkin J, Chiarion-Sileni V, Gonzalez R, Grob JJ, Cowey CL, Lao CD, et al. Combined Nivolumab and Ipilimumab or Monotherapy in Untreated Melanoma. *New England Journal of Medicine*. 2015;373(1):23-34.
 65. Callahan MK, Postow MA, Wolchok JD. CTLA-4 and PD-1 Pathway Blockade: Combinations in the Clinic. *Front Oncol*. 2015;4:385-.
 66. Qi CJ, Ning YL, Han YS, Min HY, Ye H, Zhu YL, et al. Autologous dendritic cell vaccine for estrogen receptor (ER)/progesterin receptor (PR) double-negative breast cancer. *Cancer Immunol Immunother*. 2012;61(9):1415-24.
 67. Grupp SA, Kalos M, Barrett D, Aplenc R, Porter DL, Rheingold SR, et al. Chimeric Antigen Receptor–Modified T Cells for Acute Lymphoid Leukemia. *New England Journal of Medicine*. 2013;368(16):1509-18.
 68. Porter DL, Levine BL, Kalos M, Bagg A, June CH. Chimeric Antigen Receptor–Modified T Cells in Chronic Lymphoid Leukemia. *New England Journal of Medicine*. 2011;365(8):725-33.
 69. Porter DL, Levine BL, Kalos M, Bagg A, June CH. Chimeric antigen receptor-modified T cells in chronic lymphoid leukemia. *N Engl J Med*. 2011;365(8):725-33.
 70. Pelin A, Wang J, Bell J, Le Boeuf F. The importance of imaging strategies for pre-clinical and clinical in vivo distribution of oncolytic viruses. *Oncolytic virotherapy*. 2018;7:25-35.
 71. Gaspar N, Zambito G, Dautzenberg IJC, Cramer SJ, Hoeben RC, Lowik C, et al. NanoBiT System and Hydrofurimazine for Optimized Detection of Viral Infection in Mice—A Novel in Vivo Imaging Platform. *International Journal of Molecular Sciences*. 2020;21(16).
 72. Mayer AT, Gambhir SS. The Immunoimaging Toolbox. *J Nucl Med*. 2018;59(8):1174-82.
 73. James ML, Gambhir SS. A molecular imaging primer: modalities, imaging agents, and applications. *Physiol Rev*. 2012;92(2):897-965.
 74. Williams L. Anniversary Paper: Nuclear medicine: Fifty years and still counting. *Medical physics*. 2008;35:3020-9.
 75. Keyes JW, Orlandea N, Heetderks WJ, Leonard PF, Rogers WL. The Humongotron--a scintillation-camera transaxial tomograph. *Journal of nuclear medicine : official publication, Society of Nuclear Medicine*. 1977;18(4):381-7.
 76. Debbage P, Jaschke W. Molecular imaging with nanoparticles: giant roles for dwarf actors. *Histochem Cell Biol*. 2008;130(5):845-75.
 77. Contag CH, Contag PR, Mullins JI, Spilman SD, Stevenson DK, Benaron DA. Photonic detection of bacterial pathogens in living hosts. *Mol Microbiol*. 1995;18(4):593-603.
 78. Luker GD, Luker KE. Optical imaging: current applications and future directions. *J Nucl Med*. 2008;49(1):1-4.
 79. Santos EB, Yeh R, Lee J, Nikhamin Y, Punzalan B, Punzalan B, et al. Sensitive in vivo imaging of T cells using a membrane-bound *Gaussia princeps* luciferase. *Nat Med*. 2009;15(3):338-44.
 80. Margarido AS, Bornes L, Vennin C, van Rheenen J. Cellular Plasticity during Metastasis: New Insights Provided by Intravital Microscopy. *Cold Spring Harb Perspect Med*. 2020;10(11).
 81. Lee J. Bioluminescence: the First 3000 Years (Review). *Biology*. 2008;3.

82. Sharifian S, Homaei A, Hemmati R, R BL, Khajeh K. The emerging use of bioluminescence in medical research. *Biomed Pharmacother.* 2018;101:74-86.
83. Hastings JW. Chemistries and colors of bioluminescent reactions: a review. *Gene.* 1996;173(1 Spec No):5-11.
84. Yan Y, Shi P, Song W, Bi S. Chemiluminescence and Bioluminescence Imaging for Biosensing and Therapy: In Vitro and In Vivo Perspectives. *Theranostics.* 2019;9(14):4047-65.
85. Endo M, Ozawa T. Advanced Bioluminescence System for In Vivo Imaging with Brighter and Red-Shifted Light Emission. *International journal of molecular sciences.* 2020;21(18):6538.
86. Khalil MM, Tremoleda JL, Bayomy TB, Gsell W. Molecular SPECT Imaging: An Overview. *Int J Mol Imaging.* 2011;2011:796025.
87. Basu S, Kwee TC, Surti S, Akin EA, Yoo D, Alavi A. Fundamentals of PET and PET/CT imaging. *Ann N Y Acad Sci.* 2011;1228:1-18.
88. Volpe A, Pillarsetty NVK, Lewis JS, Ponomarev V. Applications of nuclear-based imaging in gene and cell therapy: probe considerations. *Molecular Therapy - Oncolytics.* 2021;20:447-58.
89. Blasberg RG, Gelovani J. Molecular-genetic imaging: a nuclear medicine-based perspective. *Mol Imaging.* 2002;1(3):280-300.
90. Serganova I, Blasberg RG. Molecular Imaging with Reporter Genes: Has Its Promise Been Delivered? *J Nucl Med.* 2019;60(12):1665-81.
91. Shulkin BL, Shapiro B, Tobes MC, Shen SW, Wieland DM, Meyers LJ, et al. Iodine-123-4-amino-3-iodobenzylguanidine, a new sympathoadrenal imaging agent: comparison with iodine-123 metaiodobenzylguanidine. *J Nucl Med.* 1986;27(7):1138-42.
92. Glowniak JV, Kilty JE, Amara SG, Hoffman BJ, Turner FE. Evaluation of Metaiodobenzylguanidine Uptake by the Norepinephrine, Dopamine and Serotonin Transporters. *Journal of Nuclear Medicine.* 1993;34(7):1140.
93. Rogers BE, McLean SF, Kirkman RL, Della Manna D, Bright SJ, Olsen CC, et al. In vivo localization of [(111)In]-DTPA-D-Phe1-octreotide to human ovarian tumor xenografts induced to express the somatostatin receptor subtype 2 using an adenoviral vector. *Clin Cancer Res.* 1999;5(2):383-93.
94. Ponomarev V, Doubrovin M, Serganova I, Vider J, Shavrin A, Beresten T, et al. A novel triple-modality reporter gene for whole-body fluorescent, bioluminescent, and nuclear noninvasive imaging. *Eur J Nucl Med Mol Imaging.* 2004;31(5):740-51.
95. Doubrovin M, Ponomarev V, Serganova I, Soghomonian S, Myagawa T, Beresten T, et al. Development of a new reporter gene system--dsRed/xanthine phosphoribosyltransferase-xanthine for molecular imaging of processes behind the intact blood-brain barrier. *Mol Imaging.* 2003;2(2):93-112.
96. Ray P, De A, Min JJ, Tsien RY, Gambhir SS. Imaging tri-fusion multimodality reporter gene expression in living subjects. *Cancer Res.* 2004;64(4):1323-30.
97. Lee HW, Jeon YH, Hwang MH, Kim JE, Park TI, Ha JH, et al. Dual reporter gene imaging for tracking macrophage migration using the human sodium iodide symporter and an enhanced firefly luciferase in a murine inflammation model. *Mol Imaging Biol.* 2013;15(6):703-12.

Chapter 2

“NanoBiT System and Hydrofurimazine for Optimized Detection of Viral Infection in Mice - A Novel *in Vivo* Imaging Platform”

Authors: **Natasa Gaspar**^{1,2,3}, Giorgia Zambito^{1,2,4}, Iris J. C. Dautzenberg⁵, Steve J. Cramer⁵, Rob C. Hoeben⁵, Clemens Lowik^{1,2,6}, Joel R. Walker⁷, Thomas A. Kirkland⁷, Thomas P. Smith⁷, Wytse M. van Weerden⁸, Jeroen de Vrij⁹, Laura Mezzanotte^{1,2*}

Author affiliations:

¹ Erasmus Medical Center, Optical Molecular Imaging, Department of Radiology and Nuclear Medicine, Rotterdam, Netherlands

² Erasmus Medical Center, Department of Molecular Genetics, Rotterdam, Netherlands

³ Percuros B.V., Leiden, Netherlands

⁴ Medres Medical Research GMBH, Cologne, Germany

⁵ Leiden University Medical Center, Department of Cell and Chemical Biology, Leiden, Netherlands

⁶ Department of Oncology CHUV, UNIL and Ludwig Cancer Center, Lausanne, Switzerland

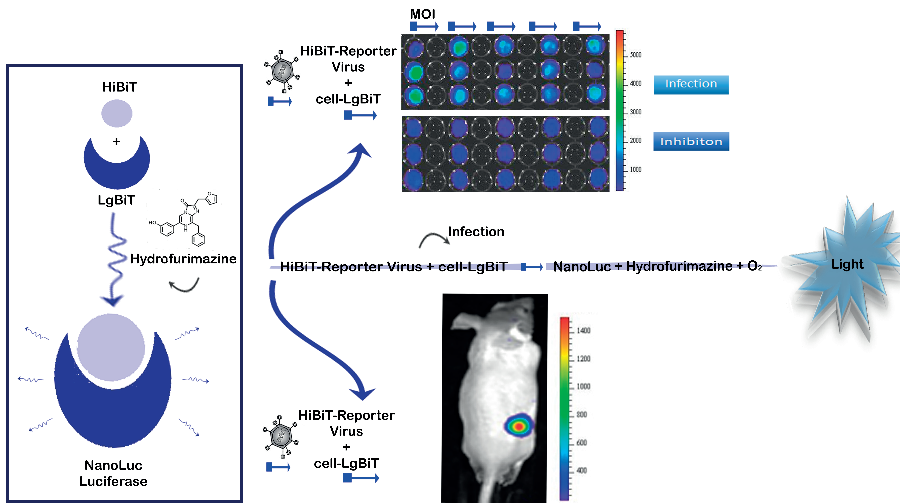
⁷ Promega Biosciences L.L.C., San Luis Obispo, California, United States of America

⁸ Erasmus Medical Center, Department of Urology, Rotterdam, Netherlands

⁹ Erasmus Medical Center, Department of Neurosurgery, Rotterdam, Netherlands

ABSTRACT

Reporter genes are used to visualize intracellular biological phenomena, including viral infection. Here we demonstrate bioluminescent imaging of viral infection using the NanoBiT system in combination with intraperitoneal injection of a furimazine analogue, hydrofurimazine. This recently developed substrate has enhanced aqueous solubility allowing delivery of higher doses for *in vivo* imaging. The small high-affinity peptide tag (HiBiT), which is only 11 amino-acids in length, was engineered into a clinically used oncolytic adenovirus, and the complementary large protein (LgBiT) was constitutively expressed in tumor cells. Infection of the LgBiT expressing cells with the HiBiT oncolytic virus will reconstitute NanoLuc in the cytosol of the cell, providing strong bioluminescence upon treatment with substrate. This new bioluminescent system served as both, an early stage quantitative viral transduction reporter *in vitro* and also *in vivo* in mice, for longitudinal monitoring of oncolytic viral persistence in infected tumor cells. This platform provides novel opportunities for studying the biology of viruses in animal models



INTRODUCTION

The development of novel strategies for pre-clinical and clinical imaging of viral replication and dissemination is of crucial importance [1]. An important tool used to deconvolute the pathways of viral infection are reporter viruses, which are constructed to study the course of infection. Bioluminescent imaging (BLI) is a highly effective imaging modality used in small animal models enabling longitudinal *in vivo* analysis of viral pathogenesis and determination of the efficacy of therapeutic interventions due to its high sensitivity and high signal to background ratio. BLI relies on luciferase-based gene reporters to detect sites of viral infection and to quantify viral transduction by correlation with *in vivo* photon emission within a single animal model [2]. A recombinant virus genetically engineered to express a luciferase produces light from infected cells after substrate (luciferin) administration, which can be detected using a sensitive, charged-coupled device (CCD) camera. This approach has been used in animal models for several viruses, e.g., Dengue virus, Herpes simplex virus 1 (HSV-1), Sindbis virus, Vaccinia virus, Influenza virus and oncolytic viruses (OVs) [3–9].

Generating recombinant reporter viruses remains a challenge. The smaller the inserted reporter gene, the more stable the viral genome remains, making small reporter tags applicable to different viral strains that do not tolerate large genome alterations such as RNA viruses, or being near the limit of their packaging capacity (e.g., armed oncolytic DNA viruses) [10]. Our proposed solution to this problem is the use of a small, multifunctional reporter tag that can be inserted anywhere in the viral genome without substantially altering its properties. HiBiT is a split-reporter tag derived from NanoLuc binary technology (NanoBiT) [9] with high affinity for the split-LgBiT reporter. The NanoBiT system is highly suitable for this purpose. NanoLuc (Nluc) luciferase is a relatively small (19 kDA), ATP independent bioluminescent enzyme and is significantly brighter than Firefly (Fluc) and Renilla (Rluc) luciferases [11].

In our system the very small HiBiT tag (33 base pairs/11 amino-acids) is inserted into the viral genome and interacts with the complementary large part (LgBiT) expressed in the infected cells upon infection of those cells with the tagged virus, reconstituting the full Nluc luciferase. Recently, a Flavivirus reporter has been generated using the NanoBiT complementation approach [7]. Tomokazu et al. demonstrated its utility for *in vitro* screening of active compounds and *ex vivo* measurement of viral persistence. However, with that system, *in vivo* imaging was not possible [7,11]. In fact, while the small size of NanoLuc is an asset as a reporter in viral imaging in small animals, a major limitation has been the poor solubility and pharmacokinetics of its substrate, furimazine, in biological environments. This limits the amount of the substrate that can be injected in one dose and makes intravenous injection the preferred route of administration in order to reach adequate *in vivo* imaging sensitivity [8]. To overcome the *in vivo* limitations of furimazine,

we used hydrofurimazine (HFz), along with a formulation enabling fast reconstitution. This allowed us to dissolve higher amounts of substrate for intraperitoneal (i.p.) injection in small animals, achieving optimal sensitivity [9,12,13].

OVs are gaining momentum as an emerging therapy for cancer treatment using engineered viruses to selectively kill tumor cells. Improving *in vivo* imaging of oncolytic viruses would improve safety and efficacy assessments and localization of viral biotherapeutics, with the potential to translate those findings towards the clinic [1]. A new generation of imaging tools is expected to improve *in vivo* analysis over current methods, which are often not suitable for imaging the therapeutic efficacy of particular types of OVs.

Here we demonstrate the power of our system for viral tracking over the course of 6 weeks post infection using an oncolytic adenovirus as model virus. This resulted in the HAdV-5-DELTA-24-RGD-GFP-T2A-HiBiT oncolytic adenovirus carrying the small HiBiT tag. The adenoviral infection and further replication were monitored via expression of HiBiT tag from the E3 promoter which is activated by the E1A proteins and expressed early after infection [14] and later reconstitution with the LgBiT protein expressed in the cytosol of PC-3 cells.

The approaches established within this study will have a direct application to various studies where sensitive detection is needed for a better understanding of infection dynamics *in vivo*, making it a preferable detection method especially for viruses not tolerating accommodation of large inserts or are at the limit of their packaging ability.

MATERIALS & METHODS

Cell Lines and Cell Culture Conditions

Human prostate cancer cell lines were used as a model system in this study. The PC-3 cell line was cultured in Roswell Park Memorial Institute (RPMI) 1640 Medium (Sigma, St. Louis, Mo, USA) supplemented with 10% of FBS and 1% Penicillin-Streptomycin. The cells were kept at 37°C in a humidified atmosphere containing 5% CO₂. Human embryonic kidney (HEK293T) cells were grown in Dulbecco's modified Eagle's medium DMEM (Sigma, St. Louis, Mo, USA), supplemented with 10% fetal bovine serum and 1% penicillin/streptomycin.

PC339C and PC346C cell lines are established from patient-derived xenografts and were chosen as bench mark models because of their known transduction potential [20]. PC339C and PC346C cell lines were cultured in prostate growth medium (PGM) as described previously [20]. In short, culture medium DMEM-F12 (Cambrex, BioWhittaker, Verviers, Belgium) was supplemented with 2% FCS (PAN Biotech, Aidenbach, Germany), 1% insulin-transferrin-selenium (GIBCO BRL, Gaithersburg, MD), 0.01% BSA (Boehringer-Mannheim, Germany), 10 ng/mL epidermal growth factor (Sigma-Al-

drich, Milan, Italy) and penicillin/streptomycin antibiotics (100 U/mL penicillin, 100 µg/mL streptomycin; (Cambrex, BioWhittaker, Verviers, Belgium). Cell lines were passaged when they reached 80% confluence (80% medium of T-175 flask covered by cell aggregates).

Lentiviral Vector Construction and Cell Transduction

Vector production and cell transduction were performed under appropriate biosafety level conditions (ML-II) in accordance with the National Biosafety Guidelines and Regulations for Research on Genetically Modified Organisms (GMO permit 99-163 from the Bureau of genetically modified organisms, The Netherlands). Procedures and protocols were reviewed and approved by the EMC Biosafety Committee. To create the pCDH-EF1-ATG-LgBiT-T2A-copGFP lentiviral vector, we first excised the 1929 luciferase gene from the vector pCDH-EF1-ATG-1929-T2A-copGFP (Promega, Madison, WI, USA) with restriction enzymes BamHI and NotI in NEB buffer 3.1. from New England BioLabs.

The LgBiT gene was amplified from the vector pBIT1.3.-C[LgBiT] (Promega) using the following primers; forward primer with a NotI restriction site 5'- TTT GCGGCCC-GCATGGTTACTCGGAAC-3' and 3'-GGATCCATGCTGGCTCGAGCGGTGG-5' with a BamHI restriction site. The amplified PCR product (LgBiT gene) was cloned in the above-prepared pCDH-EF1-ATG-T2A-copGFP recipient vector to create the pCDH-EF1-ATG-LgBiT-T2A-copGFP vector using the NotI and BamHI restriction sites. A self-inactivating lentivirus pCDH-EF1-LgBiT was produced by transfection of HEK293T packaging cells by transient transfection of HEK293T cells with three packaging plasmids pCMV-VSVG, pMDLg-RRE, pRSV-REV (Addgene, Cambridge, MA, USA) and PEI transfection reagent 1 mg/mL per µg DNA. Procedures were previously described in detail [21]. Lentiviral supernatant was collected after 48 and 72 hours and filtered (0.45 µm). Subsequent quantification of virus was performed using a standard antigen capture HIV p24 ELISA (ZeptoMetrix, Buffalo, NY, USA). PC-3, PC346C and PC339C cells were grown in culture dishes to 50% confluence in culture medium and were infected with the lenti-viral stock, resulting in LgBiT expression. Cells were transduced with MOI 1 particle per cell of pCDH-EF1-LgBiT-T2A-copGFP, lentivirus in the presence of polybrene (hexametride bromide, Sigma-Aldrich) at a final concentration of 8 µg/mL. Stable clones were selected via the limited dilution method.

HEK293T cells were seeded in a T-25 flask at a density of 5×10^5 cells and transduced with either EF1-NanoLuc-T2A-copGFP lentivirus plus polybrene (hexametridine bromide) (Sigma, St. Louis, Mo, USA) at a final concentration of 8 µg/mL. Cells were sorted for GFP expression using FACS (BD-FACS AriaIII, BD Biosciences). Transgene expression was confirmed by the presence of the green fluorescent protein copGFP from (excitation/emission maximum = 475/509 nm).

Reporter Virus Construction

The oncolytic HAdV-5-DELTA-24-RGD-GFP-T2A-HiBiT virus was constructed and produced according to previously described protocols [22]. The adenovirus has a 24-base pair deletion in the viral E1A gene, which disrupts the retinoblastoma protein (Rb)-binding capacity of this protein and facilitates selective replication in tumor cells with a dysfunctional Rb-pathway. The RGD peptide in the fiber protein allows the virus to bind and enter cells through cell surface integrins $\alpha v\beta 3/5$, which are often overexpressed on the surface of cancer cells. The virus contains the eGFP-T2A-HiBiT-expression cassette under control of the viral E3 promoter. Expression only occurs when viral replication is initiated. The 2A-HiBiT sequence was synthesized with BsrGI restriction site overhangs (TG TACAAGGCTGAGGGCAGAGGAAGTCTTCTAACATGCCGGTGACGTGGAGGAGAATCCCGGCCCTGTGAGCGGCTGGCGGCTGTTCAAGAAGATTAGCTAATGTACA) and was subsequently cloned in the plasmid pShuttle- Δ E3-Fib-RGD-ADP-EGFP-Kana. The GFP-2A-HiBiT containing fragment (after PacI+AatII+ScaI digestion) was recombined with SpeI-linearized pAdEasy-1 resulting in the plasmid pAE-RGD-GFP-2A-HiBiT. Using a standard recombination procedure [22] this plasmid was recombined with pSh+pIX resulting in HAdV-5-DELTA-24-RGD-GFP-T2A-HiBiT. The virus was rescued in HER911 cells [23]. To prevent heterologous recombination with the viral E1 sequence present in the HER911 genome, upscaling of the virus was performed in A549 cells. The virus was isolated by double cesium-chloride density gradient purification and a plaque assay on HER911 cells was performed to determine the titer of the virus in plaque forming units (PFU) per mL. The titer was 8.4×10^9 PFU/mL.

In vitro BLI and FLI

Transduced PC-3 cells transfected with pBIT1.2-N [CMV LgBiT] were plated with an equal seeding density (50,000 cells/well) in a black 96-well plate (Greiner-Bio-One, Frickenhausen, Germany) in 100 μ L of RPMI medium (Sigma, St. Louis, Mo, USA). Transduced Xenograft Human Prostate Cancer cells, the PC339C, expressing LgBiT were plated with an equal seeding density (500,000 cells/well) in 1 mL of growth medium in a black six-well plate with a clear bottom (Sigma-Corning 3506) and the PC346C cells expressing LgBiT were plated with an equal seeding in 100 μ L of growth media in a black 96-well plate (Greiner-Bio-One).

Oncolytic adenoviral infection was performed with several dilutions of the initial HAdV-5-DELTA-24-RGD-GFP-T2A-HiBiT viral stock (ranging from 4 to 0.03 MOI). Twenty-four hours after infection the cells were washed with PBS and the bioluminescence signal from wells was measured with IVIS spectrum system (PerkinElmer, Waltham, MA, USA) 1 min after substrate addition from the Nano-Glo Luciferase Assay System (Promega) with a final concentration of 0.01 mM. The photon flux (ph/s) was collected using open filter binning = medium, field of view = 12.9×12.9 cm, $f/\text{stop} = 1$ and either a 30 s or 60

s exposure time. The experiments were performed in triplicates and were repeated three times. Data were analyzed using Living Image 4.3 software (Perkin Elmer) by drawing the appropriate ROI and then plotted using GraphPad Prism 8. Cells were visualized at the microscopy for checking transfection rate using the GFP signal and viability.

Neutralization Assay

The intravenous immunoglobulin G (IvIg) (Sanquin, Leiden, The Netherlands) with a final concentration of 50 mg/mL has been incubated with the oncolytic reporter virus for 1 h and then inoculated to the cells. NanoLuc activity was measured 24 h post infection at the IVIS imager.

***In vivo* Bioluminescence**

Animal experiments were approved by the Bioethics Committee of Erasmus MC, Rotterdam, The Netherlands under the approved work protocol 17-867-42, covered by the national project license CCD number 2017867. The experiments are performed in accordance with national guidelines and regulations established by the Dutch Experiments on Animal Act (WoD) and by the European Directive on the Protection of Animals used for scientific purpose (2010/63/EU). BALB/C nude (males) were obtained from Charles River Laboratory (The Netherlands). All mice were provided access to food and water ad libitum and were hosted in the animal facility at the Erasmus MC, Rotterdam, The Netherlands. For the subcutaneous skin model experiments, eight-week-old nude BALB/C nude (males) were anesthetized using isoflurane and were injected with 2×10^6 PC-3-LgBiT expressing cells prepared in PBS and matrigel (Sigma-Corning) solution (50:50 ratio). After tumor cell implantation (PC-3-LgBiT) and tumor formation, mice were intratumorally (i.t.) injected, from three different sites, with 10 μ L (in total 30 μ L) of HAdV-5-DELTA-24-RGD-GFP-T2A-HiBiT (viral titer 8.49×10^9 PFU/mL) or PBS. Animals were monitored daily and were euthanized in case of unusual behavior e.g., weight loss > 20% of baseline, rapid tumor growth > 0.5 cm etc.

Mice were monitored over 6 weeks (43 dpi) for virus-treated mice ($n = 8$) and 20 days for control mice ($n = 4$) by non-invasive imaging. At different time points post intratumoral injection of the virus, 4.2 μ mole of formulated HFz [13] in a volume of 480 μ L of PBS was injected i.p. in nude mice. Mice were randomly assigned and were kept under (ketamine (25 mg/mL) (Vetalar) and Xylazine (1,7 mg/mL) (Rompun) anesthesia. Anesthetized mice (in groups of three) were placed in a specifically designed imaging box [24] for biosafety level 2 containment purpose.

Series of images were taken from 15 to 20 min after substrate administration using an IVIS Spectrum (Perkin Elmer) with open filter binning = medium, field of view = 12.9×12.9 cm, $f/\text{stop} = 1$ and a 3-min exposure time for the imaging of viral infection. At the peak of the bioluminescence signal, regions of interests (ROIs) were used as a tool to analyze the signals.

Immunohistochemistry

To detect the adenovirus hexon proteins, paraffin-embedded sections of the mouse tumors (obtained 43 days post intratumoral viral injection (dpi) for the treated ones and 20 dpi for the control) were deparaffinized and rehydrated with xylene and ethanol according to standard procedures [25]. The sections were then treated with primary polyclonal anti-adenovirus (clone Ab6982; Abcam, Cambridge, MA, USA) and Alexa Fluor 488-labeled goat anti-rabbit (Thermo Fisher-Molecular Probes, Waltham, MA, USA) antibodies. The nuclei were stained with Hoechst in TBS (1:1000). Stained slides were analyzed by confocal microscopy (Leica Microsystems, Wetzlar, Germany).

STATISTICAL ANALYSIS

Analysis of the bioluminescence output, where more than two groups were compared, was performed using a one-way ANOVA, followed by Tukey's t-test. All statistics were calculated using GraphPad Prism version 8 for Windows. Data from each animal were presented as means \pm SD. The results were statistically significant when $p < 0.05$.

RESULTS

Expression of HiBiT and Preserved Virulence of the Reporter Virus *in Vitro*

We performed a lentiviral transduction of prostate cancer cell lines PC-3, PC346C and PC339C to induce expression of LgBiT. PC-3 and PC346C are adherent cell lines while PC339C grows in suspension. In order to determine the functionality and the expression stability of the HiBiT tag from the NanoBiT system, a series of cell lines were infected with the oncolytic reporter virus (HAdV-5-DELTA-24-RGD-GFP-T2A-HiBiT). After the NanoBiT complex was reconstituted successfully, it formed a functional NanoLuc enzyme after infection with the virus (Figure 1A) over several dilutions of the initial viral stock (Figure 1B and Supplementary Figure 1A, C). The signal was clearly visible at 24 h post infection with all prostate cancer cell lines used, including the PDX-derived cell lines (Figure 1B and Supplementary Figure 1A, C). Moreover, the bioluminescent signal was specific and it quantitatively correlated with viral infectivity (Figure 1D and Supplementary Figure 1B, D). Furthermore, when we performed the assay with addition of intravenous immunoglobulins (IvIg) in order to neutralize the HiBiT-reporter virus (by adding IvIg) we observed 2- to 3-fold drop in luminescence output (Figure 1D and Supplementary Figure 1D). We have calculated an inter-assay variability of 16% and an intra-assay variability of 80%, parameters that are highly influenced by stochastic variability in virus-cell interactions. The reporter virus contains a GFP-T2A-HiBiT-expression

cassette under the control of a viral E3 promoter where expression of the cassette is only initiated after efficacious viral replication. Cells from this assay (Figure 1B, C) were imaged to visualize the presence of virus based on the amount of GFP positive cells. The GFP signal could be detected at multiple viral dilutions ranging from a multiplicity of infection (MOI) of 4 to 0.16 (Figure 1E).

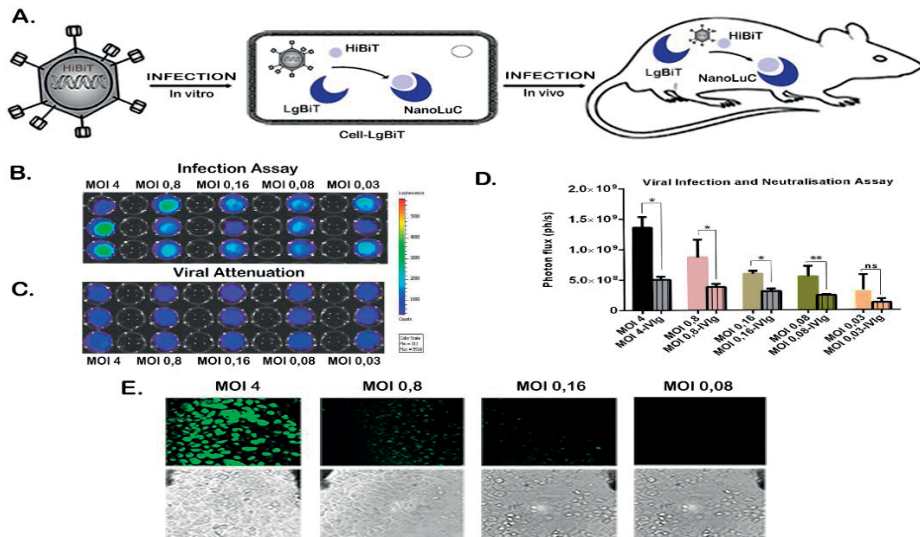


Figure 1. Detection of HiBiT-reporter *in vitro*. (A) Schematic representation of NanoBiT system applied for imaging of viral infection *in vivo* and *in vitro*. Bioluminescence *in vitro* imaging of HiBiT-reporter virus infection by applying the NanoBiT system (B and C). PC-3-LgBiT cells were infected with: (B) HiBiT-reporter virus or (C) with neutralized HiBiT-reporter virus by pre-incubation with intravenous immunoglobulin G (IVIg). The HiBiT-reporter virus infection was performed with several dilutions of viral stock (ranging from 4 to 0.03 MOI). The virus-exposed cells were imaged 24 h post infection by addition of substrate from the Nano-Glo Luciferase Assay System with a final concentration of 0.01 mM. (D) Signals were quantified with IVIS software. Quantification of detected signal as correlation between detected light and viral infectivity after background subtraction. Results are presented as means +SD. Data are significantly different (one-way ANOVA F-value of 30.16) and the signal of infected cells is significantly different from the neutralization assay (* p -value < 0.01, ** p -value < 0.001) (E) Fluorescence microscopy of PC-3-LgBiT cells infected with different HiBiT-GFP-reporter virus dilutions (varying from 4 to 0.03 MOI). For checking the transfection rate using the GFP signal, fluorescence was detected 24 h post infection. Size of the scale bar is 2 μ m.

Sensitive Longitudinal *in Vivo* monitoring of HiBiT-Reporter Oncolytic Virus

We next evaluated the *in vivo* efficacy of the HiBiT-reporter virus to monitor viral infection dynamics over time by stable expression of the HiBiT tag from the reporter-virus and successful infection of PC-3-LgBiT expressing cells. Three weeks after implantation of tumor cells, mice were infected intratumorally with the HiBiT-reporter virus ($n = 8$) or with Phosphate Buffered Saline (PBS) ($n = 4$) (control). The HFz substrate in its novel formulation proved particularly well-suited for these experiments, where a broad imaging

time window was required. In fact, the substrate showed a stable signal 15 min after intraperitoneal administration when formulated in P-407 in mice carrying NanoLuc expressing cells [13]. As early as 24 h post viral injection, all mice showed specific photon emission, suggesting successful infection of PC-3-LgBiT tumor cells *in vivo* and good distribution of HFz to the tumor site after i.p. injection, leading to sustained bioluminescent emission by the reconstituted NanoLuc luciferase (Figure 2B, C).

On the contrary, when furimazine was injected intraperitoneally (4 mg/kg) we could not detect any signal (data not shown). When imaging was repeated at day 10 post infec-

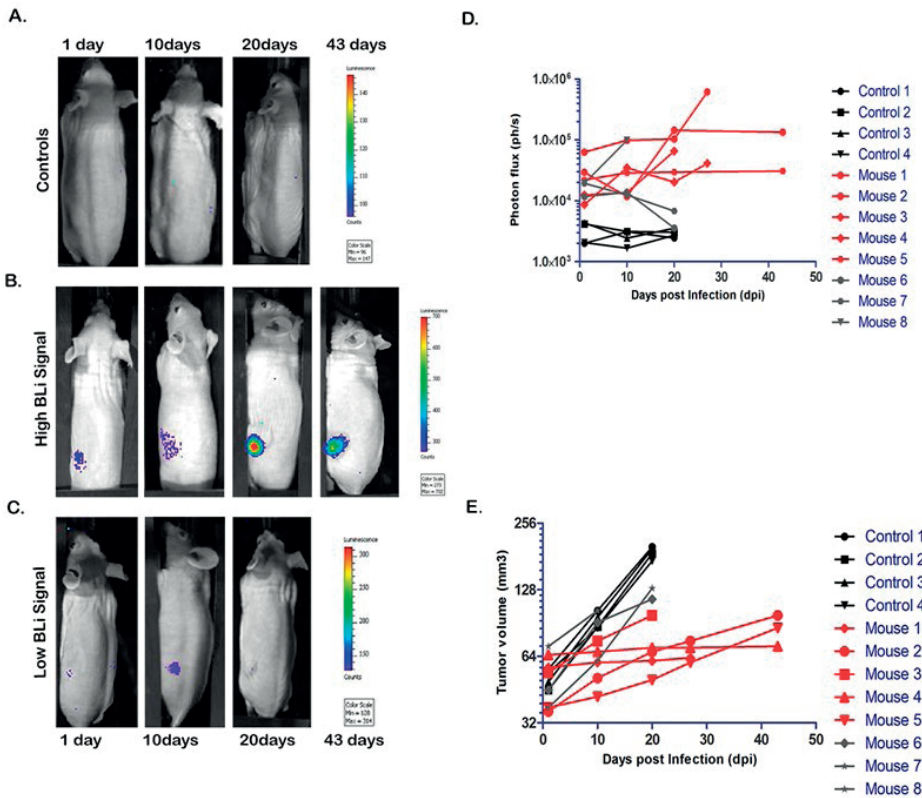


Figure 2. Longitudinal bioluminescence (BLI) imaging of HiBiT-reporter virus infection dynamics *in vivo* in PC-3-LgBiT xenografts. (A, B, C) Infection dynamics in nude BALB/C mice infected with 3.0×10^7 PFU of HiBiT-reporter virus. Representative infected mice were imaged at indicated time points by injecting $4.2 \mu\text{mol}$ of HFz intraperitoneally (i.p.) and monitoring the BLI signal over 43 days for the high BLI signal response group ($n = 5$), 20 days for the low BLI signal response group ($n = 3$) and 20 days for the control group ($n = 4$). (D) Signals were quantified at the IVIS software. Results are presented as median +SD ($n = 4$ for the control, $n = 5$ for 'high BLI signal group' and $n = 3$ for 'low BLI signal group'). Light signals were significantly different at 20 days post infection (dpi) (F-value of 4.84) where the 'high BLI signal group' was statistically different from the 'low BLI signal group' and the control group (p -value < 0.05 ; p -value < 0.01). (E) Tumor volume changes over time. The volume of tumors treated with oncolytic virus was significantly lower in the group of 'high BLI signal' ($n = 5$) when compared to the groups of the control mice ($n = 4$) and the group with 'low BLI signal' ($n = 3$) (p -value < 0.01) at day 20.

tion (dpi), most tumors still displayed photon emission, after substrate administration, suggesting the presence of the virus in these tumors (Figure 2C). In six out of nine mice the photon emission increased by 1.5-fold, and this group was designated the ‘high signal BLI group’ (Figure 2B, C). In the other three mice the light emission from the infected tumors decreased, and we referred to this group as the ‘low signal BLI group’ (Figure 2C, D). When mice were imaged on day 20 post viral administration, photon emission of the ‘low BLI signal group’ tumors was indistinguishable from the background levels (Figure 2C, D) measured in the control group with an average signal of 3.5×10^3 photons per second (ph/s) (Figure 2A, D). The ‘high BLI signal group’ showed a continuous increase in photon emission; on day 43 post viral administration, one mouse displayed a signal of 1.3×10^5 ph/s, 30 times higher than the average signal of the control group (Figure 2B, D) suggesting the persistence of HiBiT-reporter virus for 6 weeks post administration.

As for the tumor growth kinetics shown in Figure 2E, we observed that PC-3-LgBiT tumors treated with the HiBiT-reporter virus had a reduced tumor growth rate compared to the PBS control group (Figure 2E). The oncolytic virus intervention did not eradicate the tumor completely.

To confirm the presence of the reporter virus in tumor tissue and the specificity of the BLI signal, tumor sections (obtained 43 dpi for the treated mice and 20 dpi for the control mice) were analyzed for adenoviral capsid proteins. While staining was absent in control tumor sections injected with PBS (Figure 3A), the virus-treated tumors displayed a clearly visible signal (Figure 3B), indicating the presence of virus.

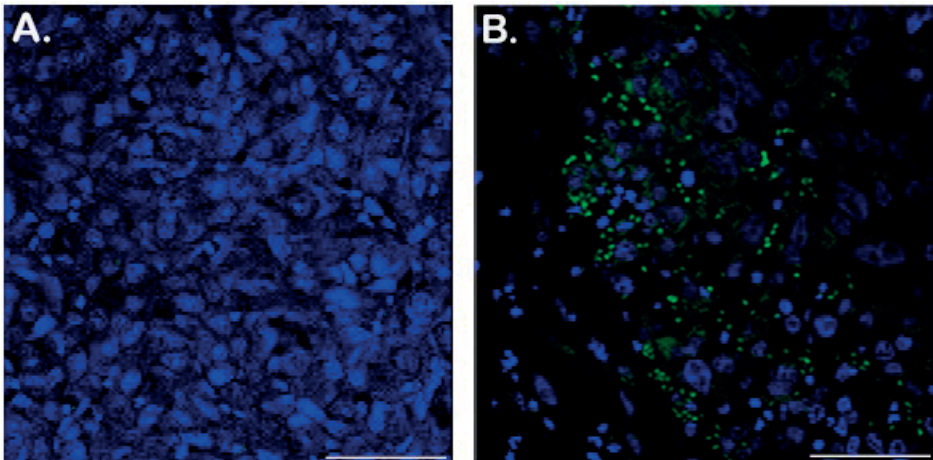


Figure 3. Immunohistochemistry of PC3-LgBiT tumor sections show HiBiT-reporter virus persistence within tumor xenografts 43 days post infection. Virus infected cells assessed via hexon detection in tumor xenografts. Frozen sections of tumors injected with PBS (A) or HiBiT-reporter virus (B) were stained by immunohistochemistry for adenovirus detection with an anti-hexon antibody and an Alexa Fluor 488-labeled secondary antibody; the sections were counterstained with Hoechst in TBS. (A) Representative control section from a tumor injected with PBS. (B) A representative section from virus-infected tumors at 43 days post infection. Size of the scale bar is 100 μ m.

DISCUSSION

Bioluminescent reporters have become routine tools for monitoring viral spread in living animals through sequential imaging [2,4]. Moreover, the ability to detect viral infection at the earliest possible time point and follow it up longitudinally over time in each animal provides valuable data about viral infection pathways as well as the progression of infection. Unfortunately, the large size of many luciferase reporter genes may alter the virulence and replication of viruses, which makes these genes unsuitable for introduction into most viral genomes, particularly those which do not tolerate incorporation of large transgenes. Other issues with recombinant viruses include reversion to unmodified virus (e.g., short single strand RNA viruses) and insufficient loading capacity (e.g., armed DNA or RNA oncolytic viruses), all of these viruses could benefit from an even smaller reporter in order to image them *in vivo*. For instance, the first *in vivo* BLI tracking of Influenza virus [15,16] was achieved using the very small and bright NanoLuc luciferase (19 kDa), allowing sensitive *in vivo* imaging of the recombinant virus in mice and ferrets.

Using the NanoBiT system, we engineered an oncolytic replication-competent HiBiT-reporter adenovirus harboring the smallest reporter tag reported for BLI imaging. In our initial *in vitro* experiments, we infected different LgBiT expressing cell lines with the HiBiT-reporter virus. Twenty-four hours post infection we could clearly detect a signal resulting from the successful viral transduction and NanoBiT system reconstitution. Furthermore, when we added a neutralizing antibody, we observed a 2- to 3-fold drop in the BLI signal as a result of antibody interference with viral uptake in cells. This demonstrates that our novel bioluminescent system can be used for screening of potential antivirals or for the screening of oncolytic in patients since oncolytic viruses also induce strong anti-tumor immune responses, which may act against all tumor cells. To further address this point, we plan to investigate the use of the NanoBiT system in the context of oncolytic virus performance in an immune-competent syngeneic mouse model.

We anticipate that pre-clinical research into (oncolytic) viral infections will strongly benefit from this non-invasive bioluminescent viral screening tool, enabling fast and simple longitudinal readout protocols applicable for rapid drug screening and viral-risk virus infectivity and transduction in a range of cell lines. To enable *in vivo* imaging of the infection course with our HiBiT-reporter virus, we employed hydrofurimazine, a substrate with improved solubility compared to furimazine [13]. The substrate was formulated this in a non-toxic, highly water-soluble excipient, which allows much higher substrate loading and extended light emission *in vivo* after a single substrate injection. This was necessary since these experiments required biosafety level 2 protocols and were carried out under containment in an imaging box. The animals were injected with the substrate and then transported to the animal imaging facility.

Having generated these tools, we were able to monitor infection dynamics of the HiBiT-reporter virus in living mice using established PC-3-LgBiT tumors over 6 weeks with hydrofurimazine. We detected infectious virus production as early as 24 h post viral administration and as late as 43 days post infection. These results suggest efficacious viral infection and successful *in vivo* complementation of the two NanoBiT subunits (LgBiT and HiBiT) within the transgenic xenografts.

The variation between the high and the low BLI signal we observed in this murine model is representative of the biological variation observed in clinical trials with oncolytic (adeno) viruses [16]. Using our imaging system, it was also evident that the oncolytic virus did not reach the entire tumor mass, in line with the performance of oncolytic adenoviruses evaluated in clinical trials. This could be the result of a number of different factors, e.g., presence of viral-limiting supportive tissue or extracellular matrix and/or lack of the viral CAR receptor (coxsackievirus and adenovirus receptor) on many tumor cells [17,18]. Still, the incomplete spread of oncolytic viruses to all tumor cells does not necessarily prevent complete tumor clearance in an actual human assessment [19]. This technology is applicable to study a wide range of viruses, and we predict that it will be particularly useful for viruses that do not tolerate larger transgene insertions.

AUTHOR CONTRIBUTIONS

N.G. and L.M. designed the experiments, N.G. performed the experiments, J.R.W., T.A.K. and T.P.S. synthesized and formulated hydrofurimazine. J.d.V., I.J.C.D. and S.J.C. designed and created the recombinant virus, N.G., T.A.K., J.R.W. and L.M. wrote the manuscript. J.d.V., I.J.C.D., W.M.v.W., T.A.K., C.L., R.C.H. and L.M. critically revised the manuscript for important intellectual content.

FUNDING

We acknowledge the funding for this work provided by the European Commission under the H2020-MSCA-RISE award grant number 777682 (CANCER) and under the H2020-MSCA-ITN award, grant number 675743 (ISPIC).

ACKNOWLEDGMENTS

We thank Mary Hall and Lance Encell for useful discussion on the use of the NanoBiT system, Sander Herfst for giving us the imaging box for animals and Sigrun Erkens for

technical help with the cell culture. This work was supported by the Applied Molecular Imaging Erasmus MC (AMIE) facility.

CONFLICTS OF INTEREST

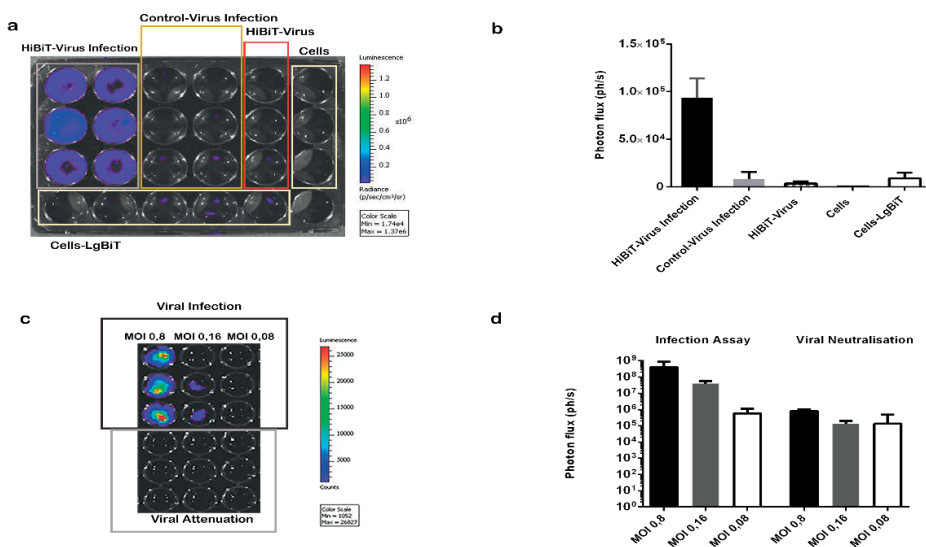
“The authors declare no conflict of interest.”

REFERENCES

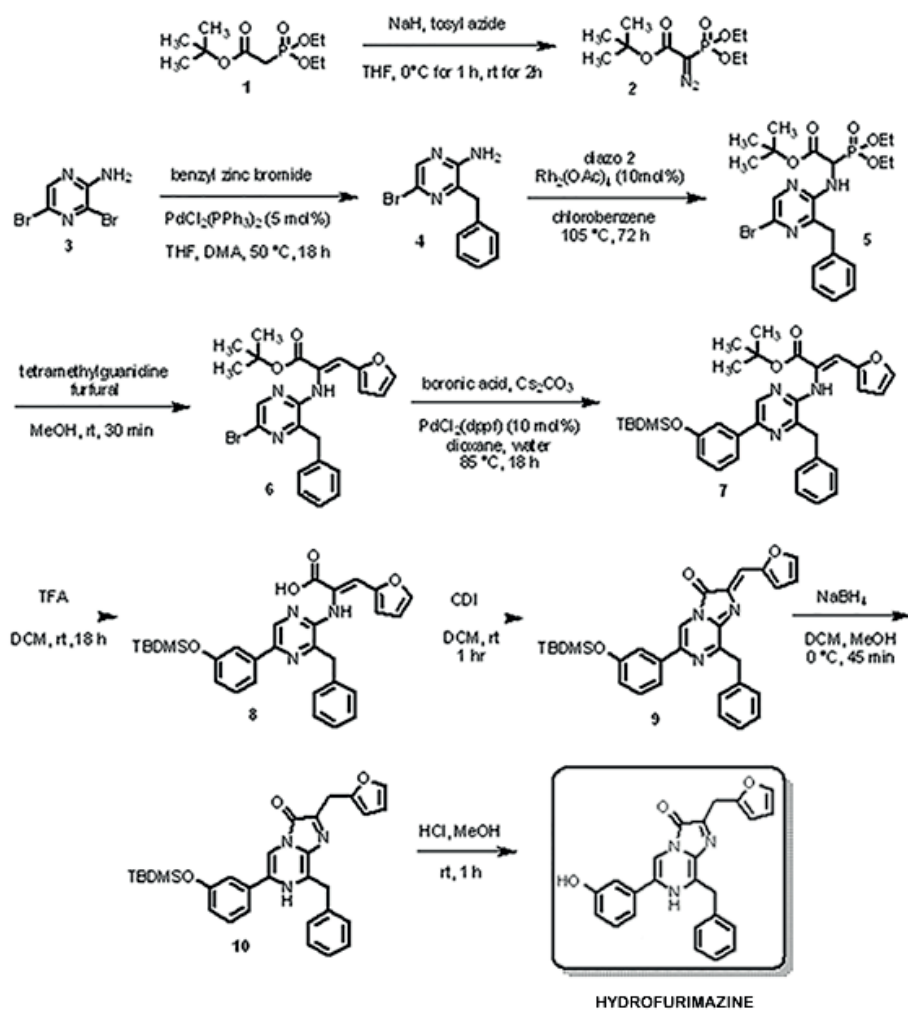
1. Pelin, A.; Wang, J.; Bell, J.; Boeuf, F. The importance of imaging strategies for pre-clinical and clinical in vivo distribution of oncolytic viruses. *Oncolytic Virotherapy* **2018**, *7*, 25–35, doi:10.2147/ov.S137159.
2. Coleman, S.M.; McGregor, A. A bright future for bioluminescent imaging in viral research. *Future Virol.* **2015**, *10*, 169–183, doi:10.2217/fvl.14.96.
3. Schoggins, J.W.; Dorner, M.; Feulner, M.; Imanaka, N.; Murphy, M.Y.; Ploss, A.; Rice, C.M. Dengue reporter viruses reveal viral dynamics in interferon receptor-deficient mice and sensitivity to interferon effectors in vitro. *Proc. Natl. Acad. Sci.* **2012**, *109*, 14610, doi:10.1073/pnas.1212379109.
4. Luker, G.D.; Leib, D.A. Luciferase real-time bioluminescence imaging for the study of viral pathogenesis. *Methods Mol. Biol.* **2005**, *292*, 285–296.
5. Cook, S.H.; Griffin, D.E. Luciferase Imaging of a neurotropic viral infection in intact animals. *J. Virol.* **2003**, *77*, 5333, doi:10.1128/jvi.77.9.5333-5338.2003.
6. Luker, K.E.; Hutchens, M.; Schultz, T.; Pekosz, A.; Luker, G.D. Bioluminescence imaging of vaccinia virus: Effects of interferon on viral replication and spread. *Virology* **2005**, *341*, 284–300, doi:10.1016/j.virol.2005.06.049.
7. Tamura, T.; Fukuhara, T.; Uchida, T.; Ono, C.; Mori, H.; Sato, A.; Fauzyah, Y.; Okamoto, T.; Kurosu, T.; Setoh, Y.X.; et al. Characterization of recombinant flaviviridae viruses possessing a small reporter tag. *J. Virol.* **2018**, *92*, e01582–01517, doi:10.1128/jvi.01582-17.
8. Taylor, A.; Sharkey, J.; Plagge, A.; Wilm, B.; Murray, P. Multicolour in vivo bioluminescence imaging using a nanoLuc-based BRET reporter in combination with firefly luciferase. *Contrast Media Mol. Imaging* **2018**, 2514796–2514796, doi:10.1155/2018/2514796.
9. Schwinn, M.K.; Machleidt, T.; Zimmerman, K.; Eggers, C.T.; Dixon, A.S.; Hurst, R.; Hall, M.P.; Encell, L.P.; Binkowski, B.F.; Wood, K.V. CRISPR-mediated tagging of endogenous proteins with a luminescent peptide. *ACS Chem. Biol.* **2018**, *13*, 467–474, doi:10.1021/acscmbio.7b00549.
10. Cai, H.; Liu, M.; Russell, C.J. Directed evolution of an influenza reporter virus to restore replication and virulence and enhance noninvasive bioluminescence imaging in mice. *J. Virol.* **2018**, *92*, e00593–00518, doi:10.1128/jvi.00593-18.
11. Sasaki, M.; Anindita, P.D.; Phongphaew, W.; Carr, M.; Kobayashi, S.; Orba, Y.; Sawa, H. Development of a rapid and quantitative method for the analysis of viral entry and release using a NanoLuc luciferase complementation assay. *Virus Res.* **2018**, *243*, 69–74, doi: 10.1016/j.virusres.2017.10.015.
12. Tran, V.; Moser, L.A.; Poole, D.S.; Mehle, A. Highly sensitive real-time in vivo imaging of an influenza reporter virus reveals dynamics of replication and spread. *J. Virol.* **2013**, *87*, 13321–13329, doi:10.1128/jvi.02381-13.
13. Su, Y.C.; Walker, J.R.; Park, Y.; Smith, T.P.; Liu, L.X.; Hall, M.P.; Labanieh, L.; Hurst, R.; Wang, D.C.; Encell, L.P.; et al. Novel NanoLuc substrates enable bright two-population bioluminescence imaging in animals. *Nat. Methods* **2020**, doi:10.1038/s41592-020-0889-6.
14. Farley, D.C.; Brown, J.L.; Leppard, K.N. Activation of the early-late switch in adenovirus type 5 major late transcription unit expression by L4 gene products. *J. Virol.* **2004**, *78*, 1782–1791, doi:10.1128/jvi.78.4.1782-1791.2004.
15. Karlsson, E.A.; Meliopoulos, V.A.; Savage, C.; Livingston, B.; Mehle, A.; Schultz-Cherry, S. Visualizing real-time influenza virus infection, transmission and protection in ferrets. *Nat. Commun.* **2015**, *6*, 6378.
16. Lang, F.F.; Conrad, C.; Gomez-Manzano, C.; Yung, W.K.A.; Sawaya, R.; Weinberg, J.S.; Prabhu, S.S.; Rao, G.; Fuller, G.N.; Aldape, K.D.; et al. Phase I study of DNX-2401 (Delta-24-RGD) oncolytic adenovirus: replication and immunotherapeutic effects in recurrent malignant glioma. *J. Clin. Oncol.* **2018**, *36*, 1419–1427, doi:10.1200/jco.2017.75.8219.

17. Sauthoff, H.; Hu, J.; Maca, C.; Goldman, M.; Heitner, S.; Yee, H.; Pipiya, T.; Rom, W.N.; Hay, J.G. Intratumoral spread of wild-type adenovirus is limited after local injection of human xenograft tumors: virus persists and spreads systemically at late time points. *Hum. gene Ther.* **2004**, *14*, 425–433, doi:10.1089/104303403321467199.
18. Douglas, J.T.; Kim, M.; Sumerel, L.A.; Carey, D.E.; Curiel, D.T. Efficient oncolysis by a replicating adenovirus (Ad) in vivo is critically dependent on tumor expression of primary Ad receptors. *Cancer Res.* **2001**, *61*, 813.
19. de Vrij, J.; Willemsen, R.A.; Lindholm, L.; Hoeben, R.C. Adenovirus-derived vectors for prostate cancer gene therapy. *Hum. Gene Ther.* **2009**, *21*, 795–805, doi:10.1089/hum.2009.203.
20. Marques, R.B.; Erkens-Schulze, S.; de-Ridder, C.M.; Hermans, K.G.; Waltering, K.; Visakorpi, T.; Trapman, J.; Romijn, J.C.; van Weerden, W.M.; Jenster, G. Androgen receptor modifications in prostate cancer cells upon long-term androgen ablation and antiandrogen treatment. *Int. J. Cancer* **2005**, *117*, 221–229, doi:10.1002/ijc.21201.
21. Mezzanotte, L.; An, N.; Mol, I.M.; Löwik, C.W.G.M.; Kaijzel, E.L. A new multicolor bioluminescence imaging platform to investigate nf- κ b activity and apoptosis in human breast cancer cells. *PLoS ONE* **2014**, *9*, e85550.
22. Balvers, R.K.; Belcaid, Z.; van den Hengel, S.K.; Kloezeman, J.; de Vrij, J.; Wakimoto, H.; Hoeben, R.C.; Debets, R.; Leenstra, S.; Dirven, C.; et al. Locally-delivered t-cell-derived cellular vehicles efficiently track and deliver adenovirus delta24-rgd to infiltrating glioma. *Viruses* **2014**, *6*, 3080–3096, doi:10.3390/v6083080.
23. He, T.-C. et al. A simplified system for generating recombinant adenoviruses. *Proc. Natl. Acad. Sci.* **1998**, *95*, 2509, doi:10.1073/pnas.95.5.2509.
24. Spronken, M.I.; Short, K.R.; Herfst, S.; Bestebroer, T.M.; Vaes, V.P.; van der Hoeven, B.; Koster, A.J.; Kremers, G.J.; Scott, D.P.; Gulyaev, A.P.; et al. Optimisations and challenges involved in the creation of various bioluminescent and fluorescent influenza A virus strains for in vitro and in vivo applications. *PLoS ONE* **2015**, *10*, e0133888.
25. Falkeholm, L.; Grant, C.A.; Magnusson, A.; Möller, E. Xylene-free method for histological preparation: A multicentre evaluation. *Lab. Investig.* **2001**, *81*, 1213–1221, doi:10.1038/labinvest.3780335.

SUPPLEMENTARY DATA



Supplementary Figure 1. NanoBiT system applied with different cell lines. (A) PC339C, expressing LgBiT were infected with the HiBiT-reporter virus or the control virus not containing the HiBiT tag. The infected cells were imaged 24 h post infection by addition of substrate from the Nano-Glo Luciferase Assay System with a final concentration of 0.1 mM. We show as well the minimum background signal coming from the infection of cells (PC339C-LgBiT) with the control virus; the PC339C cells on their own; the PC339C-LgBiT cells; HiBiT-reporter virus post substrate addition. **(B)** Signals were quantified with IVIS software. Quantification of detected signal as correlation between detected light and viral infectivity after background subtraction. Results are presented as means +SD. **(C)** PC346C cells expressing LgBiT were plated in 96 well plates and were infected with HiBiT-reporter virus dilutions of initial viral stock (ranging from 0.8 to 0.08 MOI) or with the neutralized HiBiT-reporter virus by pre-incubation with intravenous immunoglobulin G (IvIg) with a final concentration of 50 mg mL⁻¹. The infected cells were imaged 24 h post infection by addition of substrate from the Nano-Glo Luciferase Assay System with a final concentration of 0.1 mM. **(D)** Signals were quantified with IVIS software. Quantification of detected signal as correlation between detected light and viral infectivity after background subtraction. Results are presented as means +SD.



Supplementary Figure 2. Scheme of the synthesis of Hydrofurimazine.

Hydrofurimazine synthesis

tert-butyl 2-diazo-2-(diethoxyphosphoryl) acetate (2). To a solution of 4-methylbenzenesulfonyl azide (29.1 g, 147 mmol) in THF (300 mL) at 0°C was added sodium hydride (5.9 g, 147 mmol, 60% oil dispersion) in ~1 g batches. Tert-butyl 2-(diethoxyphosphoryl) acetate (31.0 g, 123 mmol) was added dropwise over 30 min. The mixture stirred for 1 h at 0°C and 2 h at room temperature. A mixture of ether and ice water was prepared in 2 L beaker and the reaction mixture was carefully added with stirring. The two layers were separated and the aqueous layer was extracted with ether. The organic layers were combined, dried with sodium sulfate, filtered, concentrated, and purified with silica gel chromatography in heptane and ethyl acetate to afford the desired product (32.9 g, 96%) as a yellow mobile oil. ¹H NMR (400 MHz, CDCl₃) δ 4.32 – 4.09 (m, 4H), 1.51 (s, 9H), 1.38 (td, J = 7.1, 0.8 Hz, 6H); ¹³C NMR (101 MHz, CDCl₃) δ 162.56 (d, J = 12.1 Hz), 128.06 (d, J = 323 Hz), 83.02, 63.44 (d, J = 5.7 Hz), 28.25, 16.17 (d, J = 6.9 Hz); HPLC 99.3% (AUC at 254 nm) 5.03 min (Synergi Max-RP, water/ACN 0.1%TFA).

tert-butyl 2-((3-benzyl-5-bromopyrazin-2-yl) amino)-2-(diethoxyphosphoryl) acetate (5). To a suspension of 4 (ref. Synthesis, 2014, 46, 646-652) (3.8 g, 14.4 mmol) in dichlorobenzene (30 mL) was added 2 (4.8 g, 17.3 mmol) and rhodium (II) acetate dimer (0.64 g, 1.44 mmol). The mixture was heated to 105 °C for 72 h. After cooling, the mixture was diluted with ethyl acetate, concentrated with celite, and purified with silica gel chromatography in heptane and ethyl acetate to afford the desired product (5.4 g, 73%) as a brown solid. ¹H NMR (400 MHz, CDCl₃) δ 8.05 (s, 1H), 7.38 – 7.21 (m, 5H), 5.27 – 5.19 (m, 1H), 5.01 (dd, J = 21.2, 8.0 Hz, 1H), 4.21 – 3.83 (m, 6H), 1.42 (s, 9H), 1.24 (dt, J = 21.2, 7.0 Hz, 6H); ¹³C NMR (101 MHz, CDCl₃) δ 166.16, 150.27 (d, J = 8.5 Hz), 142.90, 141.66, 135.53, 129.01, 128.74, 127.18, 126.33, 83.11, 63.66 – 63.24 (m), 52.54 (d, J = 146 Hz), 40.38, 27.84, 16.35 – 16.27(m); HRMS (ESI+) calcd for C₂₁H₂₉BrN₃O₅P [M + H]⁺ m/z 514.1107, found 514.1085; HPLC 98.1% (AUC at 254 nm) 6.59 min (Synergi Max-RP, water/ACN 0.1%TFA).

tert-butyl 2-((3-benzyl-5-bromopyrazin-2-yl) amino)-3-(furan-2-yl) acrylate (6). To a solution of 5 (5.4 g, 10.5 mmol) in methanol (100 mL) was added furfural (1.5 g, 15.7 mmol). Tetramethylguanidine (3.6 g, 31.5 mmol) was added dropwise and the reaction stirred at rt for 30 min. The reaction was diluted with dichloromethane and poured into a separatory funnel with HCl (0.1 M). The two layers were separated and the aqueous layer was extracted with dichloromethane. The organic layers were combined, dried with sodium sulfate, filtered, concentrated, and purified with silica gel chromatography in heptane and ethyl acetate to afford the desired product (4.0 g, 83%) as a brown solid. ¹H NMR (400 MHz, CDCl₃) δ 8.13 (s, 1H), 7.43 – 7.27 (m, 5H), 6.96 (d, J = 1.8 Hz, 1H), 6.90 (s, 1H), 6.70 (s, 1H), 6.29 (dd, J = 3.5, 1.8 Hz, 1H), 6.16 (d, J = 3.5 Hz, 1H), 4.27 (s, 2H), 1.45 (s, 9H); ¹³C NMR (101 MHz, CDCl₃) δ 164.01, 150.36, 149.59, 143.83, 143.25, 142.11, 136.21, 129.23, 128.81, 128.33, 127.53, 127.31, 112.71,

111.70, 110.84, 81.70, 40.50, 27.91; HRMS (ESI+) calcd for $C_{22}H_{22}BrN_3O_3$ $[M + H]^+$ m/z 456.0924, found 456.0913; HPLC 94.1% (AUC at 254 nm) 6.86 min (Synergi Max-RP, water/ACN 0.1%TFA).

tert-butyl 2-((3-benzyl-5-(3-((tert-butyldimethylsilyl) oxy) phenyl) pyrazin-2-yl) amino)-3-(furan-2-yl) acrylate (7). To a solution of 6 (0.32 g, 0.70 mmol) in dioxane (10 mL) was added (3-((tert-butyldimethylsilyl) oxy) phenyl) boronic acid (0.26 g, 1.05 mmol), [1,1'-bis(diphenylphosphino) ferrocene] dichloropalladium (II) (0.060 g, 0.070 mmol), and cesium carbonate (1.4 mL, 1.4 mmol, 1.0 M). The mixture was purged with nitrogen and heated to 85°C for 18 h. The reaction was diluted with ethyl acetate and water. The two layers were separated and the aqueous layer was extracted with ethyl acetate. The organic layers were combined, dried with sodium sulfate, filtered, concentrated, and purified with silica gel chromatography in heptane and ethyl acetate to afford the desired product (0.265 g, 64%) as a dark brown foam. 1H NMR (400 MHz, $CDCl_3$) δ 8.46 (s, 1H), 7.60 – 7.55 (m, 1H), 7.51 – 7.46 (m, 1H), 7.43 – 7.31 (m, 6H), 7.05 (s, 1H), 7.00 (d, $J = 1.8$ Hz, 1H), 6.89 (ddd, $J = 8.1, 2.6, 1.0$ Hz, 1H), 6.69 (s, 1H), 6.30 (dd, $J = 3.4, 1.8$ Hz, 1H), 6.17 (d, $J = 3.4$ Hz, 1H), 4.39 (s, 2H), 1.46 (s, 9H), 1.04 (s, 9H), 0.26 (s, 6H); ^{13}C NMR (101 MHz, $CDCl_3$) δ 164.48, 156.22, 150.70, 149.05, 143.46, 143.00, 142.50, 138.48, 137.11, 136.94, 129.90, 129.80, 129.06, 128.93, 128.17, 127.02, 120.07, 119.01, 117.76, 112.25, 111.64, 110.03, 81.57, 40.89, 27.91, 25.76, 18.29; HRMS (ESI+) calcd for $C_{34}H_{41}N_3O_4Si$ $[M + H]^+$ m/z 584.2945, found 584.2924; HPLC 88.5% (AUC at 254 nm) 10.43 min (Zorbax XDB-C8, water/ACN 0.1%TFA).

2-((3-benzyl-5-(3-((tert-butyldimethylsilyl) oxy) phenyl) pyrazin-2-yl) amino)-3-(furan-2-yl) acrylic acid (8). To a solution of 7 (0.26 g, 0.45 mmol) in dichloromethane (10 mL) was added trifluoroacetic acid (1 mL) and the reaction stirred at rt for 18 h. The mixture was diluted with toluene and concentrated. The process was repeated twice to afford crude product as an orange oil. ESI MS m/z 528 $[M + H]^+$.

8-benzyl-6-(3-((tert-butyldimethylsilyl) oxy) phenyl)-2-(furan-2-ylmethylene) imidazo[1,2-a] pyrazin-3(2H)-one (9). To a solution of 8 (0.45 mmol) in dichloromethane (10 mL) was added carbonyldiimidazole (147 mg, 0.91 mmol) and the reaction stirred at rt for 1 hr. The reaction was diluted with dichloromethane and poured into a separatory funnel with HCl (0.1 M). The two layers were separated and the aqueous layer was extracted with dichloromethane. The organic layers were combined, dried with sodium sulfate, filtered, and concentrated to afford crude product as a black solid. ESI MS m/z 510 $[M + H]^+$.

8-benzyl-6-(3-((tert-butyldimethylsilyl) oxy) phenyl)-2-(furan-2-ylmethyl) imidazo[1,2-a] pyrazin-3(7H)-one (10). To a solution of 9 (0.45 mmol) in dichloromethane/methanol (1:1, 20 mL) at 0°C was added sodium borohydride (85 mg, 2.3 mmol) and the reaction stirred for 45 min. The reaction was diluted with dichloromethane and poured into a separatory funnel with HCl (0.1 M). The two layers were separated and the aqueous

layer was extracted with dichloromethane. The organic layers were combined, dried with sodium sulfate, filtered, and concentrated to afford crude product as a red brown solid. ESI MS m/z 512 $[M + H]^+$.

8-benzyl-2-(furan-2-ylmethyl)-6-(3-hydroxyphenyl)imidazo[1,2-a]pyrazin-3(7H)-one (HFz). To a solution of 10 (0.45 mmol) in methanol (20 mL) was added HCl (1 mL, 6M) and the reaction stirred at rt for 1 h. The reaction was diluted with dichloromethane and poured into a separatory funnel with water. The two layers were separated and the aqueous layer was extracted with dichloromethane. The organic layers were combined, dried with sodium sulfate, filtered, concentrated, and purified with silica gel chromatography in dichloromethane and methanol to afford the desired product (0.091 g, 50% over 4 steps) as a brown solid. ^1H NMR (400 MHz, CD_3OD) δ 7.71 (s, 1H), 7.47 – 7.38 (m, 3H), 7.37 – 7.21 (m, 4H), 7.18 – 7.04 (m, 2H), 6.90 (ddd, $J = 8.1, 2.4, 0.9$ Hz, 1H), 6.34 (dd, $J = 3.2, 1.9$ Hz, 1H), 6.18 – 6.09 (m, 1H), 4.44 (s, 2H), 4.21 (s, 2H); HRMS (ESI+) calcd for $\text{C}_{24}\text{H}_{19}\text{N}_3\text{O}_3$ $[M + H]^+$ m/z 398.1505, found 398.1503; HPLC 97.1% (AUC at 254 nm) 4.55 min (Synergi Max-RP, water/ACN 0.1% TFA).

Chapter 3

“Evaluation of NanoLuc Substrates for Bioluminescence Imaging of Transferred Cells in Mice“

Authors: **Natasa Gaspar**^{1, 2, 3}, Joel R. Walker⁴, Giorgia Zambito^{1, 2, 5}, Kranthi Marella-Panth^{1, 2}, Clemens Lowik^{1, 2, 6}, Thomas A. Kirkland⁴, Laura Mezzanotte^{1, 2}

Author affiliations:

¹Erasmus Medical Center, Optical molecular Imaging, Department of Radiology and Nuclear Medicine, Rotterdam, Netherlands

²Erasmus Medical Center, Department of Molecular Genetics, Rotterdam, Netherlands

³Percuros B.V., Leiden, Netherlands

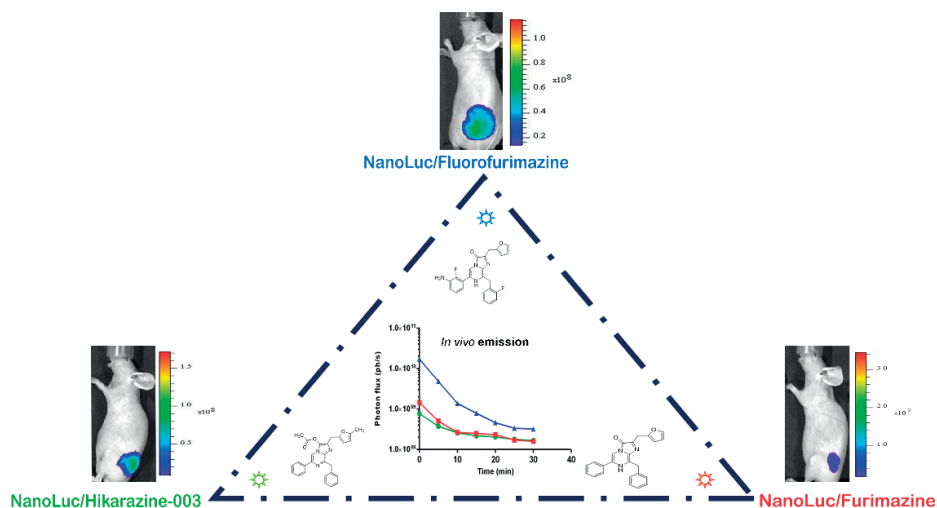
⁴Promega Biosciences L.L.C., San Luis Obispo, United States of America

⁵Medres Medical Research GMBH, Cologne, Germany

⁶University Hospital of Lausanne, CHUV-UNIL, Department of Oncology and Ludwig Cancer Center Lausanne, Switzerland

ABSTRACT

NanoLuc luciferase recently gained popularity due to its small size and superior bioluminescence performance. For *in vivo* imaging applications, NanoLuc has been limited by its substrate furimazine, which has low solubility and bioavailability. Herein, we compared the performances of recently reported NanoLuc luciferase substrates for *in vivo* imaging in mice. Two substrates with improved aqueous solubility, hydrofurimazine and fluorofurimazine, were evaluated along with three stabilized O-acetylated furimazine analogues, the hikarazines. All 5 analogues, when tested *in vitro*, displayed greater signal intensity and reaction duration, in comparison to the standard NanoLuc substrate, furimazine. The two best-performing analogues from the *in vitro* study were selected for further *in vivo* testing. The NanoLuc/fluorofurimazine pair demonstrated the highest bioluminescence intensity, post intravenous administration. It was found to be around 9-fold brighter compared to the NanoLuc/furimazine and 11-fold more intense than the NanoLuc/hikarazine-003 pair, with an average of 3-fold higher light emission when the substrate was injected intraperitoneally, in a subcutaneous model. Excitingly, despite the fact that NanoLuc/fluorofurimazine emits mostly blue light, we prove that cells trapped in mice lungs vasculature could be visualised via the NanoLuc/fluorofurimazine pair and compare the results to the AkaLuc/AkaLumine system. Therefore, among the tested analogues, fluorofurimazine enables higher substrate loading and improved optical imaging sensitivity in small animals, upgrading the use of NanoLuc derived bioluminescent systems for deep tissue imaging.



***Keywords:** AkaLuc; Bioluminescence imaging; Fluorofurimazine; Hikarazines; NanoLuc

INTRODUCTION

Bioluminescence imaging (BLI) is based on a biochemical reaction that is dependent on the oxidation of a luminophore containing substrate (luciferin) by luciferase enzymes with light emission as a result. Luciferase enzymes and their substrates are extensively used as effective, non-invasive screening tools in diverse research fields and have become a prominent method for live-cell visualization. Improving the performance of luciferase enzymes, substrates and their mutants for BLI is an important part in improving the tool box available for life science research [1].

Several thousand bioluminescent species are represented by ~700 genera among which 90% originate from marine organisms [2,3]. Luciferases from marine luminous organisms primarily utilise as substrates, coelenterazine [2], varguline [3] or analogues of these two. Coelenterazine (CTZ) is best-known as the substrate for luciferases derived from the sea pansy *Renilla reniformis* (RLuc), the luminous shrimp *Oplophorus gracilirostris* and the copepod *Gaussia princeps* (GLuc), yielding light with a fast enzymatic turnover and an emission maxima in the blue region (450–485 nm) of the visible spectrum.

NanoLuc (NLuc) is one of the smallest luciferases in size (19 kDa) and an important addition to the marine BLI-toolset [4]. Its small size, luminescence superiority and stability easily replaced other luciferases where increased sensitivity, fast response dynamics and low background auto-luminescence are vital [5]. The NLuc system is coupled with an optimized CTZ analogue, the 2-furanylmethyl-deoxycoelenterazine, known as furimazine, which when paired with NLuc gives ~2.5 million-fold brighter luminescence in mammalian cells and ~150-fold greater specific activity than firefly (*Photinus pyralis*) or *Renilla* luciferases [4].

Furimazine and its analogues are generally lipophilic and their solubility in aqueous solutions has limited the maximum injectable dose into small animals (*e.g.* 1.3 μmol in a polyethylene glycol (PEG) [6] based buffer and 0.016 μmol in Phosphate Buffered Saline (PBS) [7]. Therefore, furimazine analogues with improved solubility and bioavailability are needed to improve NanoLuc sensitivity for *in vivo* imaging [8]. Moreover, the NanoLuc/furimazine system mainly emits blue light, further limiting the sensitivity of detection in deep tissue.

Many synthetic analogues of CTZ have been reported in recent years, mostly focusing on the modification of the C-2, C-5, C-6 and C-8 substituents of the imidazopyrazinone core [4,9], with the most effort on modifying the C-2 and C-6 position [[5], [6], [7]]. The novel analogues were mostly optimized in order to improve *in vivo* imaging with NanoLuc, leading to better compound stability and more efficient light penetration through tissues [[5], [6], [7]]. A chemical library of 135 CTZ-analogues, the imidazo[1,2-*a*]pyrazin-3-one, have been recently synthesized as stabilized *O*-acetylated precursors (hikarazines) with an original synthesis route [10,11]. Some examples show robust bioluminescent

properties in terms of signal intensity and duration of the reaction. Particular examples turned out to be biochemically more efficient than furimazine with up to 2.5 increased light intensity and signal stability lasting up to 2 h [11]. Novel furimazine analogues, with increased aqueous solubility, were recently developed and named hydrofurimazine (HFz) and fluorofurimazine (FFz) [12]. These analogues enable *in vivo* applications by allowing the delivery of higher substrate doses *via* single intraperitoneal injection in mice leading to extended light emission *in vivo* for NanoLuc [13].

In the current work we investigated the BLI properties of novel furimazines (HFz and FFz) [11] and 3 different hikarazines (hikarazine-001, hikarazine-003 and hikarazine-097) [[14], [15], [16]] by evaluating their *in vivo* performance as substrates for imaging with NanoLuc, as the reference marine luciferase since recently they have demonstrated to be better suited for *in cellulo* and *in vivo* NLuc based imaging [[14], [15], [16]].

Although the above mentioned NanoLuc substrates have been reported to perform well *in vivo*, no direct comparison has been performed yet. In the present study, we first evaluated 5 recently reported analogues *in vitro*, through controlled conditions, using cells expressing a known amount of NanoLuc reporter, following with an *in vivo* comparison in a subcutaneous model. Secondly, since BLI in deep tissue is mostly dependent on the amount of generated photons and the emission wavelength, we tested the best performing NLuc/substrate pairing (NLuc/fluorofurimazine) in deep tissue, by imaging transferred bioluminescent cells that get entrapped in mice lungs, and compared it to the near-infrared AkaLuc/AkaLumine system [17], recently described by Iwano et al.

MATERIALS & METHODS

2.1. Cell Propagation for Life Cell Assays

Human embryonic kidney (HEK-293T) cells were grown in Dulbecco's Modified Eagle's Medium (DMEM) (Sigma-Aldrich), supplemented with 10% fetal bovine serum and 1% penicillin/streptomycin. Cells were cultured in T-175 flasks (Thermo Fisher Scientific) until reaching confluence; growth media was aspirated and cells were washed with PBS (Sigma-Aldrich). The PBS was aspirated and the cells were removed from the flask by the addition of 3 mL of TrypLE™ Express Trypsin (Life Technologies) and were incubated at 37 °C. Cells were centrifuged at 1500 RPM, washed, re-suspended in 5 mL of fresh growth media, and then counted using a BioRad TC20 cell counter. Cells were diluted to a desired final concentration and were plated in 96 well plates (Greiner Cell Star®) in total volume of 100 µL at 25000 cells/well. The culture was incubated at 37 °C with 5% CO₂.

2.2. Lentiviral Production

The plasmids pCDH-EF1-NanoLuc-T2A-copGFP and pCDH-EF1-AkaLuc-T2A-copGFP were engineered by NanoLuc or AkaLuc luciferase gene insertion into the vector backbone pCDH-EF1-T2A-copGFP. The inserted NanoLuc/AkaLuc luciferase genes were amplified with specific primers from pCDH-EF1-NanoLuc plasmid (Promega)/pcDNA3 Venus-AkaLuc plasmid (Riken BRC Repository) without a stop codon using BamHI and NotI sites into the cut vector: pCDH-EF1-MCS-T2A-copGFP. The pCDH-EF1-NanoLuc-copGFP/pCDH-EF1-AkaLuc-T2A-copGFP lentivirus were constructed using methods already described earlier in literature [18,19]. Virus production and cell transduction were performed under appropriate biosafety level conditions (ML-II) in accordance with the National Biosafety Guidelines and Regulations for Research on Genetically Modified Organisms. Procedures and protocols were reviewed and approved by the EMC Biosafety Committee (GMO permit 99-163).

Lentiviral particles were produced by transfection of HEK-293T packaging cells with three packaging plasmids (pCMV-VSVG, pMDLg-RRE (gag-pol), pRSV-REV) (Addgene) and the lentiviral vector plasmid using PEI transfection reagent (1 mg/mL)/ μ g DNA. The supernatant, containing lentiviral particles was collected after 48 h and 72 h. Viral quantification was performed using the standard antigen-capture HIV p24 ELISA (ZeptoMetrix).

2.3. Generation of Luciferase-Expressing HEK-293T Cell Lines

HEK-293T cells were grown in culture dishes to 50% confluency in culture medium and were infected with a lenti-viral stock, resulting in NanoLuc or AkaLuc expression, depending on the used lentivirus. Cells were transduced with MOI 1 of pCDH-EF1-NanoLuc-T2A-copGFP/pCDH-EF1-AkaLuc-T2A-copGFP lentivirus plus with polybrene (hexametride bromide) (Sigma-Aldrich) at the final concentration of 8 μ g/mL. Cells were sorted for GFP expression using FACS (BD-FACS AriaIII, BD Biosciences). Transgene expression was confirmed by the presence of the green fluorescent protein copGFP (excitation/emission maximum = 475/509 nm). Stably transduced cells (HEK-293T-EF1-NanoLuc-T2A-copGFP/HEK293T-EF1-AkaLuc-T2A-copGFP) were further cultured and expanded and have been used later for all experiments regarding measurement of photon production when using different furimazine analogues.

2.4. *In Vitro* Cell-Based Imaging

HEK-293T-NanoLuc cells were seeded in a 96-well black plate (Greiner Cell Star®) at a density of 25 000 cells per well. Post 24 h, cells were washed in PBS and imaged at the IVIS Imager (PerkinElmer) after addition of 6 different substrates profiled within this study; furimazine, hydrofurimazine (HFz), fluorofurimazine (FFz), all three provided by Promega and the hikarazine-001, hikarazine-003 and hikarazine-097 provided by Institute

Pasteur, Paris, France. The hikarazines (hikarazine-001, hikarazine-003, hikarazine-097) were dissolved (1 mg) in a mixture of 0,2 mL DMSO (Sigma-Aldrich) and then diluted in a solution of 0,3 mL of acidic ethanol made from addition of 37% hydrochloric acid (Sigma-Aldrich), 100 μ L on 12 mL of 100% ethanol (Sigma-Aldrich) to give a stock solution of 1 mg/mL which was then incubated at 50 °C for 2 h. Furimazine, hydrofurimazine (HFz) and flurofurimazine (FFz) were dissolved in 100% ethanol to give a 5 mM stock solution. All of the substrates were further diluted in DMEM medium to a final concentration of 10 μ M (100 μ L/well). Bioluminescence signal from wells was measured at the IVIS (Perkin Elmer) spectrum system every 5 min after substrate addition. All *in vitro* cell-based measurements were acquired after 1 min at 37 °C using a 30 s acquisition time with an open filter. Experiments were performed in triplicates and were repeated three times. Data was analyzed using Living Image 4.3 software (Perkin Elmer) by applying the appropriate region of interest (ROI).

As for the once-cell assay; HEK-293T-NanoLuc cells were plated in a black 96-well plate in seven dilutions starting at a density of approximately 100 cells per well as the starting cell-concentration. Further cell-dilutions were carried out with a 1/2 ratio; (50, 25, 12, 6, 3, 1, 0) cells per well. Luminescence images were acquired with the GloMax[®] Microplate Reader (Promega) immediately after substrates addition; furimazine, hydrofurimazine (HFz), fluorofurimazine (FFz), hikarazine-001, hikarazine-003 and hikarazine-097 with a final concentration of each substrate of 10 μ M. For measurement of total luminescence, we used 1 s of integration time. Measurements were performed at room temperature 18–20 °C. Experiments were performed in triplicates and were repeated three times. All data were plotted using GraphPad Prism.

2.5. Substrate Formulation for Use in Whole-Animal Imaging

The hikarazines (hikarazine-001, hikarazine-003, hikarazine-097) (Institute Pasteur, Paris, France) were dissolved (1 mg) in a mixture of 0.2 mL DMSO (Sigma-Aldrich) and then diluted in a solution of 0.3 mL of acidic ethanol made from addition of 37% hydrochloric acid (Sigma-Aldrich), 100 μ L on 12 mL of 100% ethanol (Sigma) to give a stock solution of 1 mg/mL which was then incubated at 50 °C for 2 h. The stock solution was then dissolved in PBS at a final concentration of 333 nmol in 100 μ L. Furimazine, hydrofurimazine (HFz) and fluorofurimazine (FFz) (Promega), powder formulations for intravenous administration, were dissolved in 100% ethanol to give a 5 mM stock solution. The stock solution was then dissolved in PBS to a final dose of 333 nmol in 100 μ L. Stock aliquots of the poloxamer-407 HFz and FFz, for the intraperitoneal administration, were prepared by the addition of 480 μ L of PBS to the vial and vortexed to create a plain solution resulting in a single injection dose of 12 mg poloxamer-407 and 4.3 μ mol HFz and FFz, and 1.3 μ mol (145 μ L).

AkaLumine (Sigma-Aldrich) was dissolved in PBS to a concentration of 33 mM (around 3 $\mu\text{mol}/100 \mu\text{L}$) for i.p. injection. These doses were chosen considering maximum solubility and tolerability in mice and maximum attainable signal based on previous findings.

2.6. *In Vivo* Bioluminescence Imaging of Subcutaneously Implanted NanoLuc Expressing Cells

Animal experiments were approved by the Bioethics Committee of Erasmus MC, Rotterdam, The Netherlands and performed in accordance with national guidelines and regulations established by the Dutch Experiments on Animal Act (WoD) and by the European Directive on the Protection of Animals used for scientific purpose (2010/63/EU). BALB/c nude (males) were obtained from Charles River Laboratory (The Netherlands). All mice aged 8 weeks were provided access to food and water *ad libitum* and were hosted in the animal facility at the Erasmus MC, Rotterdam, The Netherlands.

For the background assessment mice ($n = 3$ mice per tested analogue) were injected intraperitoneal (i.p.) with the following analogues; 4.3 μmol (in 480 μL PBS) and 1.3 μmol (in 145 μL PBS) of FFz; 333 nmol of furimazine and hikarazine-003, both in 100 μL of PBS and 3 μmol of AkaLumine (Sigma-Aldrich) in 100 μL of PBS. Mice were anesthetized with isoflurane (1.5%) and imaged 10 min post substrate administration at the IVIS Spectrum (PerkinElmer). Supine and prone BLI images were acquired at the IVIS, exposure time 1 min. For the subcutaneous skin model experiments, 8–10 week old BALB/c nude (males) mice received a subcutaneous injection of 1×10^6 HEK-293T-NanoLuc which were prepared in PBS (Sigma-Aldrich) and matrigel (Corning) solution (50:50 ratio) in a final injectable volume of 50 μL . Mice received an injection of 100 μL of the different substrate intravenously ($n = 6$ mice per group) or intraperitoneally (480 μL) ($n = 3$ mice per group) right after implantation of cells. The size of the group was determined using power analysis. Mice were kept under isoflurane anaesthesia (1.5%) and a series of images were taken using an IVIS Spectrum with open filter binning = medium, field of view = 12.9×12.9 cm, $f/\text{stop} = 1$ and 1 s exposure time every 5 min for half an hour. Data analysis was performed by drawing ROIs in the images taken at the peak of bioluminescence emission.

2.7. *In Vivo* BLI Comparison of HEK-293T Cells Trapped in the Mouse Lung (NLuc/Fluorofurimazine vs. AkaLuc/AkaLumine)

BALB/c nude (males) were used for the experimental purposes. Post cell selection at the flow-cytometry, either HEK-293T-AkaLuc or HEK-293T-NanoLuc cells were re-suspended and aliquoted (500000 cells/100 μL) each, and injected into the tail vein of mice.

10 to 15 min after the cell infusion, the mice were anesthetized with 1.5% isoflurane for induction and administered *via* intraperitoneal injection with the respective substrate

(100 μL of 3 μmol AkaLumine, 145 μL of 1.3 μmol fluorofurimazine (FFz). 10 min post substrate administration, dorsal BLI images were taken with 1,5% isoflurane and using the IVIS Spectrum (PerkinElmer) with following acquisition conditions: open for total bioluminescence, exposure time = 1 min, binning = medium: 4, field of view = 12.5 \times 12.5 cm, and f/stop = 1. Analysis of BLI images was performed with Living Image 4.3 software (PerkinElmer).

2.8. Statistical Analysis

For experiments where more than two groups were compared, one-way ANOVA, followed by Tukey's t -test was used to determine significant differences among treated groups.

RESULTS

3.1. *In Vitro* Performance Comparison of Novel Analogues Paired with NanoLuc Luciferase

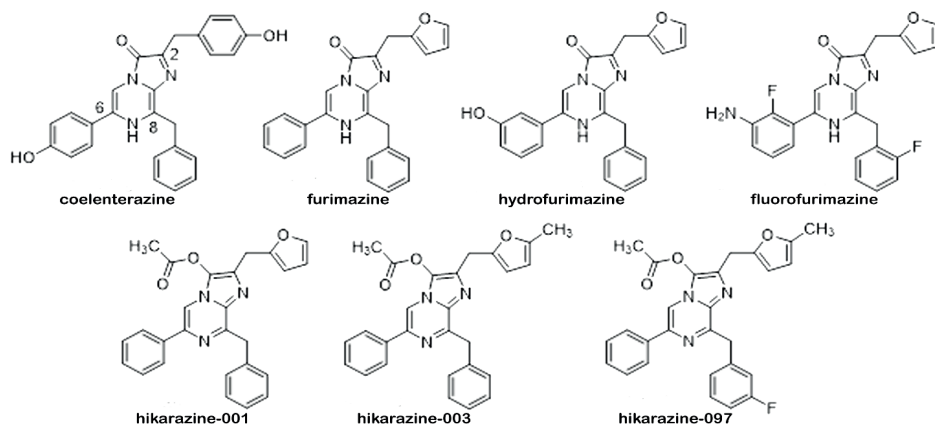


Figure 1. Chemical structures of furimazine analogues in this article; hikarazine-001, hikarazine-003, hikarazine-097, hydrofurimazine (HFz), fluorofurimazine (FFz) and furimazine.

Bioluminescence properties of the chosen furimazine analogues (Fig. 1), profiled with NLuc were assessed in live HEK-293T cells that were stably expressing NLuc luciferase in order to determine the best-performing NLuc/analogue pairs for *in vivo* testing. Cells were treated with substrates at a final concentration of 10 μM each and imaged in the IVIS imager at 5 minutes intervals after substrate administration for half an hour (Fig. 2a).

The imaging results in live cells showed brighter signals with the hikarazines (hikarazine-001, hikarazine-003 and hikarazine-097) than furimazine and its analogues hydrofurimazine (HFz) and fluorofurimazine (FFz) (Fig. 2b). We found that peak light

emission was highest with hikarazine-003, followed by hikarazine-001, hikarazine-097 and fluorofurimazine. The signal of all tested analogues proved to be extended and stable over the 30 minutes imaging duration.

We evaluated the correlation between reporter signal and number of cells, by plating a decreasing number of cells, ranging from 100 to 1 cell per well. Linear correlation was found and detection of single cells was achieved with all tested analogues. Again, the hikarazines showed to be brighter: hikarazine-003= 2.75×10^4 rlu/cell; hikarazine-001= 2.48×10^4 rlu/cell; hikarazine-097= 2.16×10^4 rlu/cell to the novel furimazine analogues and to furimazine itself: furimazine= 1.42×10^4 rlu/cell; hydrofurimazine= 1.07×10^4 rlu/cell and fluorofurimazine= 2.32×10^4 rlu/cell. (Fig. 2c).

Since the photon emission was comparable among the 3 tested hikarazines, we selected the brightest analogue (hikarazine-003) for further *in vivo* evaluation among with fluorofurimazine (FFz).

3.2. *In Vivo* Bioluminescence Imaging of Subcutaneously Implanted Cells

Prior to testing the compounds in mice, we assessed background emission of all substrates, including the AkaLuc substrate, AkaLumine, in nude mice not expressing a luciferase reporter. We administered the substrates intraperitoneally, allowing us to estimate autoluminescence in the absence of reporter enzymes (NanoLuc/AkaLuc). All substrates were administered with the doses recommended by the literature as appropriate for each substrate. Negligible signals were detected with AkaLumine, whereas all tested NLuc analogues gave background signal of around 10^2 ph/s in the abdomen in nude mice (Supplementary Fig. 1).

Given their intense *in vitro* brightness, we selected FFz and hikarazine-003 for further *in vivo* evaluation. Each substrate was administered via intravenous (i.v.) and intraperitoneal (i.p.) injection in mice. Around 1×10^6 HEK-293T cells were transferred in nude mice and injected subcutaneously in the lower flank, stably expressing NanoLuc luciferase.

For the i.v. administration route, the images were acquired after tail vein injection of equimolar substrate doses (injection volume 100 μ L); fluorofurimazine (333 nmol) (Fig. 3a), furimazine (333 nmol) (Fig. 3b) and hikarazine-003 (333 nmol) (Fig. 3c). The results demonstrated that the NanoLuc/fluorofurimazine pair was significantly brighter (around 8.6 fold) than the NanoLuc/furimazine pair and around 11.62 fold higher than the NanoLuc/hikarazine/003 pair (Fig. 3d) when administered i.v. at equimolar doses. The signal with the NanoLuc/fluorofurimazine pair showed a very high photon emission for the whole 30 minutes of acquisition, with an average of 3.58×10^9 ph/s and an initial luminescence (1 min post injection) of 1.70×10^{10} (Fig. 3d).

We further evaluated the BLI emission when administering the analogues i.p. We tested the newly formulated fluorofurimazine (FFz) in 3 different ways; with a dose of 4.3 μ moles (Fig. 4a) and 333 nmol derived from the solubilised poloxamer-P407 cake formulations¹¹

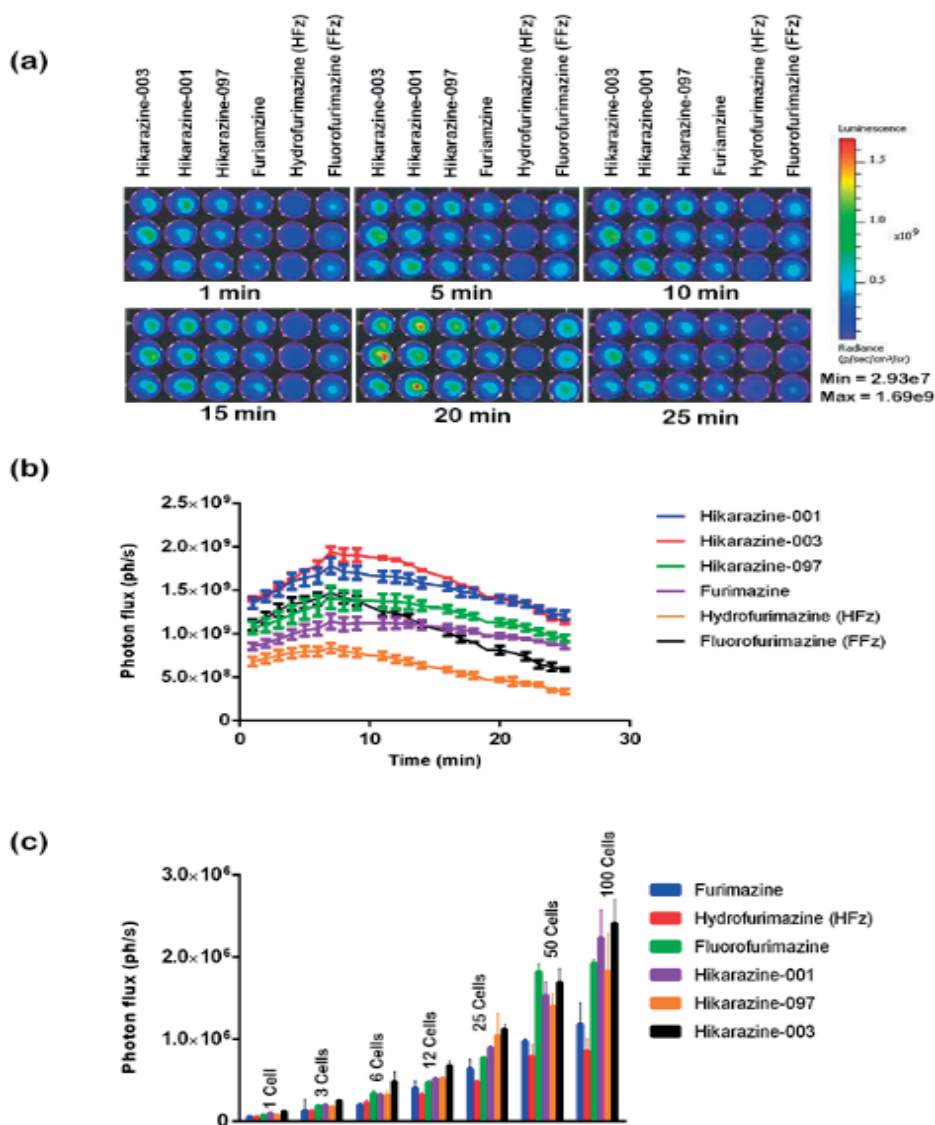


Figure 2. *In cellulo* performance of novel furimazine analogues in live HEK-293T cells transiently expressing NanoLuc luciferase. (a) Bioluminescence (BLI) imaging of substrates profiled with NanoLuc luciferase expressing cells. (b) Comparison of BLI-intensities of tested furimazine derivatives at a 10 μM concentration. BLI spectra were obtained at the IVIS Imager in triplicates, acquisition time of 1 s. Statistical analysis of triplicates was performed using ONE-Way Anova followed by Tukey's T test (p value < 0.001). (c) Comparison of bioluminescence intensities of the substrates in HEK-293T cells expressing NanoLuc luciferase (NLuc) at various cell-concentrations. Luminescence images were acquired the GloMax[®] Microplate Reader (Promega) immediately after substrates addition (10 μM), 1 s integration time.

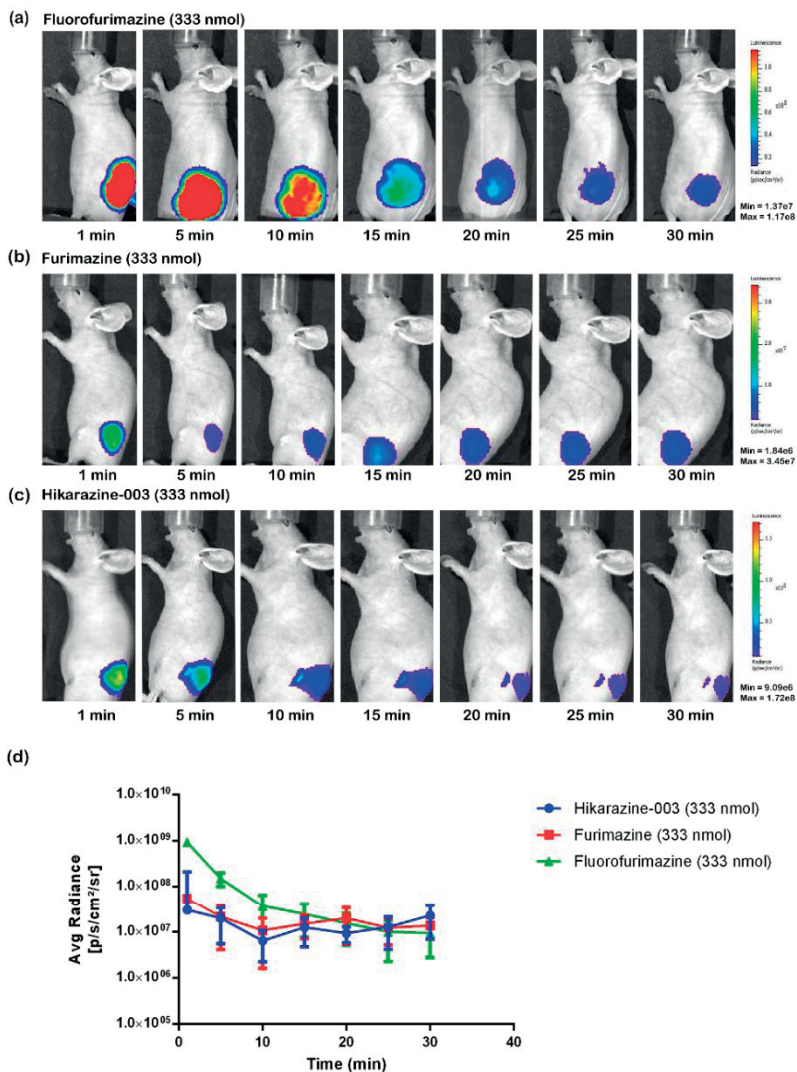


Figure 3. *In vivo* imaging of fluorofurimazine, hikarazine-003 and furimazine at 333 nmol after intravenous (i.v.) administration in a subcutaneous mice model. *In vivo* imaging after (i.v.) administration (n=6) of; (a) fluorofurimazine; (b) furimazine and (c) hikarazine-003. (d) Quantification of total maximum flux of fluorofurimazine, hikarazine-003 and furimazine at 333 nmol after intravenous administration. Spectral data was acquired for 30 min, every 5 minutes after substrate administration. Imaging data was collected at the IVIS Imager for 30 min using open filters and an exposure time of 1 s.

(Fig. 4c), and with fluorofurimazine derived stock powder formulation (333 nmol) (Fig. 4b). Hikarazine-003 and furimazine were administered with a final concentration of 333 nmol (Fig. 4d and 4e).

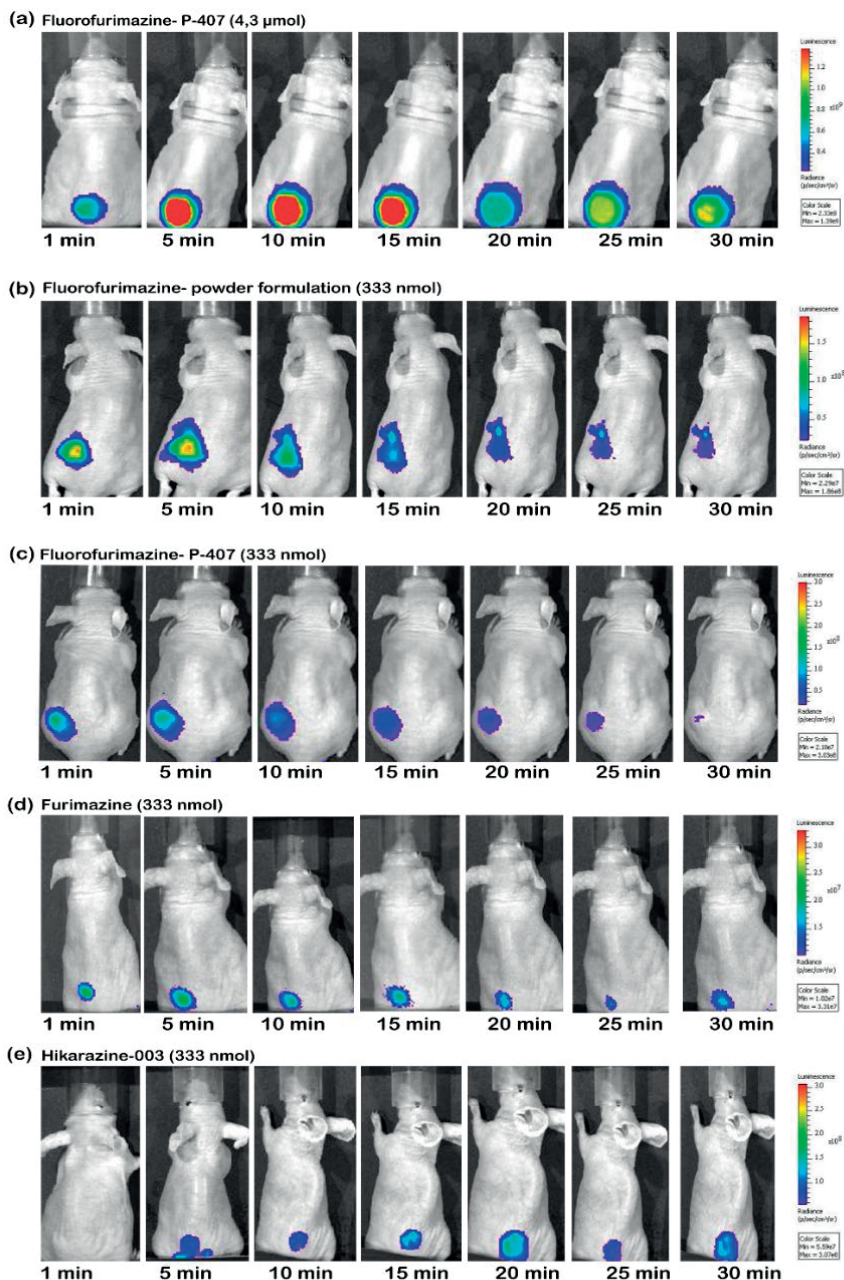


Figure 4. *In vivo* imaging of fluorofurimazine, hikarazine-003 and furimazine at different concentrations after intraperitoneal (i.p.) administration in a subcutaneous mice model. *In vivo* imaging after i.p. administration of (n=3); (a) fluorofurimazine-P407 formulation (4.3 μmol); (b) fluorofurimazine powder stock formulation (333 nmol); (c) fluorofurimazine-P407 formulation (333 nmol); (d) furimazine (333 nmol) and (e) hikarazine-003 (333 nmol). Spectral data was acquired for 30 min, every 5 minutes after substrate administration using open filters and an exposure time of 1 s.

As shown in figure 5 the 4.3 μmol NanoLuc/fluorofurimazine pair showed excellent BLI properties with a very high, sustained signal of an average of $1.22\text{E}+10$ ph/s, around 11 fold higher than the reference 333 nmol NanoLuc/furimazine pair and 3 fold higher than the 333 nmol NanoLuc/hikarazine-003 combination. The fluorinated FFz (333 nmol; $4.3\mu\text{mol}$) and its powder stock formulation (333 nmol) generated 3-fold brighter signal than hikarazine-003 (Fig. 5).

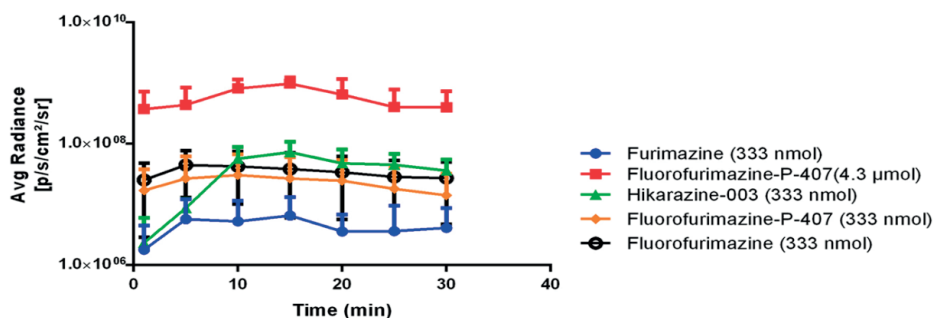


Figure 5. Signal quantification after intraperitoneal (i.p.) administration of fluorofurimazine, hikarazine-003 and furimazine at different concentrations. Fluorofurimazine (333 nmol and $4.3 \mu\text{mol}$)-P407 formulation and FFz (333 nmol) from the powder stock formulation showed significantly higher photon emission *in vivo* than furimazine and hikarazine-003 (p value < 0.0001).

3.3. *In Vivo* Deep Tissue BLI: NLuc/Fluorofurimazine vs. AkaLuc/AkaLumine

To assess how well NLuc in combination with FFz performs in deep tissue, we evaluated the brightness from HEK-293T cells stably expressing NanoLuc and copGFP, and compared it to photon emission of cells expressing AkaLuc and copGFP. We used GFP to ensure equimolar expression of both bioluminescent enzymes. The luciferase expressing cells were localised in mice lungs after tail vein injection of approximately 5×10^5 HEK-293T expressing either NLuc-copGFP or AkaLuc-copGFP [20,21] (Fig. 6a). A dose of $4.3 \mu\text{mol}$ FFz gives more light, but was found to cause weight loss and was associated with organ damage in mice: later on, a dose was established which showed no toxicity in mice consisting of $1.3 \mu\text{mol}$ FFz in P-407 [12], which we implemented in this experiment. Mice were imaged 10 min after cell administration and a kinetic analysis was performed after i.p. injection of substrate ($1.3 \mu\text{mol}/145 \mu\text{L}$ FFz; $3 \mu\text{mol}/100 \mu\text{L}$ AkaLumine) for 30 min. We were able to detect signals from both luciferase systems with a 1.5-fold higher photon emission arising from the AkaLuc/AkaLumine system (Fig. 6b). For the emission comparison, values at the time point of peak emission were used. The signals were corrected by a factor of 2.3 fold, given the higher-level of GFP expression of HEK-293T-AkaLuc expressing cells, determined prior the imaging session.

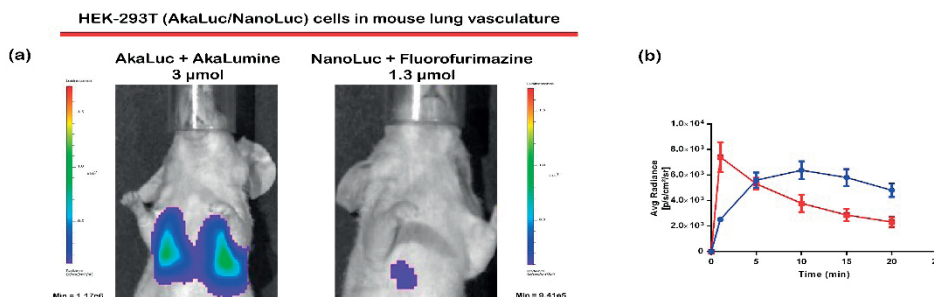


Figure 6. Bioluminescent signal detection from a minuscule number of AkaLuc- and NanoLuc-expressing cells trapped in mice lung vasculature. Performance comparison of AkaLuc/AkaLumine versus NanoLuc/fluorofurimazine. (a) Bioluminescent imaging of mice intravenously injected with 10^5 HEK-293T cells expressing NanoLuc (right) with fluorofurimazine and (a) HEK-293T cells expressing AkaLuc (left) with AkaLumine. Substrates were administered 10 min post cell administration via an intraperitoneal injection; the animals were injected with 3 μmol AkaLumine and 1.3 μmol of fluorofurimazine. (b) Data was collected at the IVIS (1 s exposure time) and are presented as \pm SD of $n=3$ mice per substrate analogue.

4. DISCUSSION

In the present study we tested novel furimazine analogues paired with NanoLuc luciferase to determine the most optimal NLuc/luciferin pair for *in vivo* imaging. We report on photon yields of two novel, furimazine analogues, recently published by Su, Y. et al., named hydrofurimazine (HFz) and fluorofurimazine (FFz) and three different *O*-acetylated furimazine analogue derivatives [9], known as ‘hikarazines’ (hikarazine-001, hikarazine-003 and hikarazine-097) and we confirm that many of these novel analogues improve the efficient brightness of NanoLuc *in vitro* and *in vivo*.

Our aim was to compare the best performing analogues in an *in vivo* setting based on different routes of administration. The comparison of BLI systems using cells expressing a known amount of luciferase injected subcutaneously in animals has been largely used in the past [[22], [23], [24], [25]]. As for coelenterazine based substrates, it is generally known that they produce higher light output when injected intravenously [26]. Yet for repeated measurements, intraperitoneal *in vivo* injections should be preferred, given the reproducibility of the technique being less prone to misinjections.

A recent study reported that furimazine possibly displays toxic side effects, when administered repeatedly in small animals with doses exceeding 40 μg of substrate per day [27]. Furimazine, *inter alia*, is poorly soluble in aqueous solution, whereas D-luciferin salt can be dissolved to high concentrations in simple buffered saline [12,28], and repeatedly administered *via* intraperitoneal administration (i.p.). The preferred furimazine administration route is *via* intravenous (i.v.) injection, since higher photon emission is achieved. However, signals appear faster after substrate injection and show a rapidly decay-

ing kinetic, limiting its use in certain areas of molecular imaging where a broader imaging window (longer substrate half-life) is required [13].

Based on our *in vivo* results we can clearly highlight on the importance of substrate solubility and bioavailability as the number one limitation for sensitive *in vivo* bioluminescent imaging [12]. The pairs, NanoLuc/fluorofurimazine (4.3 μmol and 333 nmol) and NanoLuc/hikarazine-003 (333 nmol), independent of the administration route, exhibited brighter (8 or 11-fold) *in vivo* BLI signals, than the standard NanoLuc/furimazine (333 nmol) pair. Moreover, it was clearly evident that the NanoLuc/fluorofurimazine (4.3 μmol and 333 nmol) pair was 11 or 3-fold brighter when administered intravenously or intraperitoneally, compared to the NLuc/hikarazine-003 pair (333 nmol). The photon generation from FFz is more prolonged and more intense, allowing *in vivo* tracking with the NLuc reporter over long time periods.

We also address *in vivo* coelenterazine analogues autoluminescence [17] by simply injecting the analogues in mice without the luciferase reporter being expressed. Such an approach provides accurate insight whether the compounds are prone to spontaneous light emission. Since dying cells expressing the NanoLuc reporter release the active luciferase in the bloodstream, which does not require any cofactors, and therefore can catalyze oxidation of its substrates and give background light. Our results demonstrate that NLuc substrate analogues (FFz, hikarazine-003) and furimazine itself also spontaneously oxidase, without the reporter being present in nude mice, and produce detectable light emission. This is important to take into account when performing imaging with furimazine and coelenterazine based analogues; performing a pre-scan and the proper positioning of animals is highly recommended in order to obtain accurate experimental results [12].

We next assessed the *in vivo* BLI performance of FFz with NLuc in deep tissue (lungs) and compared it to the near infra-red emission of AkaLuc/AkaLumine pair, as a near-infrared BLI system reference with an emission peak at 650 nm. The luciferase expression was localised in mice lung vasculature by tail vein injection of NLuc and AkaLuc expressing cells [20,21]. AkaLuc/AkaLumine, yielded a 1.5-fold higher signal than FFz with NLuc. Nevertheless, here we demonstrate clearly that NLuc can be used for deep tissue imaging in small animals, when combined with the novel FFz.

Multiple BL reporters are derived from NLuc luciferase that uses furimazine, or its analogues as substrates, like Antares [6] Antares 2 and LumiScarlet [24,29]. These protein fusions exhibit emission wavelengths above 600 nm due to intramolecular bioluminescence resonance energy transfer (BRET), and therefore transmit light more easily through mammalian tissues. Moreover, using a different strategy, furimazine analogues can generate red-shifted emission when paired with NanoLuc [30,31], and therefore could enable more sensitive visualization in deep tissue. However, all of these bioluminescent systems do not show peak of emission in the near infrared region as the AkaLuc/AkaLumine system.

In conclusion, the combination of superior brightness and signal duration, given by FFz, enables bioluminescence imaging with NanoLuc luciferase, in superficial and deep tissue, making it applicable for studying diverse physiological events over a substantial period of time.

AUTHOR CONTRIBUTIONS

L.M. and N.G. conceived and designed the whole study. N.G. performed all the experiments and analyzed the data. T.A.K and J.R.W. conceived designed and synthesized hydrofurimazine (HFz) and fluorofurimazine (FFz). K.M.P. performed the intravenous cell injections. G.Z. created the AkaLuc-HEK-293T stable cell line. N.G., T.A.K., J.R.W., C.L., and L.M. wrote the manuscript. L.M. supervised the project. All the authors read the manuscript and revised for important intellectual content.

FUNDING

We acknowledge the funding for this work provided by the European Commission under the H2020-MSCA-RISE award grant number [777682](#) (CANCER) and under the H2020-MSCA-ITN award, grant number [675743](#) (ISPIC).

DECLARATION OF COMPETING INTEREST

The authors declare that they have no known competing financial interests or personal relationships that could have appeared to influence the work reported in this paper.

ACKNOWLEDGMENTS

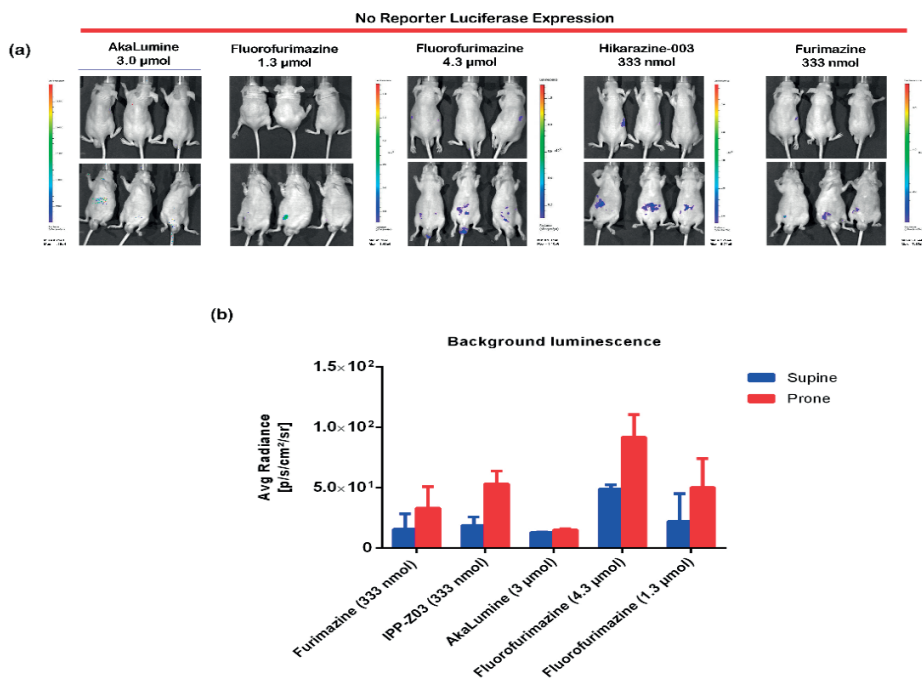
Yves L. Janin is acknowledged for kindly providing a sample of the luciferase prosubstrates; hikarazine-001, hikarazine-003 and hikarazine-097. This work was supported by the European H2020 MSCA award under proposal number [675743](#) (project acronym: ISPIC) and [777682](#) (project acronym: CANCER) and the Applied Molecular Imaging Erasmus MC (AMIE) facility.

REFERENCES

1. S.V. Markova, E.S. Vysotski Coelenterazine-dependent luciferases *Biochem. Mosc.*, 80 (2015), pp. 714-732, 10.1134/s0006297915060073
2. O. Shimomura *Bioluminescence: Chemical Principles and Methods* (revised edition) (2012)
3. S. Martini, S.H. Haddock Quantification of bioluminescence from the surface to the deep sea demonstrates its predominance as an ecological trait *Sci. Rep.*, 7 (2017), p. 45750
4. M.P. Hall, et al. Engineered luciferase reporter from a deep sea shrimp utilizing a novel imidazopyrazinone substrate *ACS Chem. Biol.*, 7 (2012), pp. 1848-1857, 10.1021/cb3002478
5. N.C. Dale, E.K.M. Johnstone, C.W. White, K.D.G. Pflieger NanoBRET: the bright future of proximity-based assays *Frontiers in Bioengineering and Biotechnology*, 7 (2019), 10.3389/fbioe.2019.00056
6. J. Chu, et al. A bright cyan-excitable orange fluorescent protein facilitates dual-emission microscopy and enhances bioluminescence imaging in vivo *Nat. Biotechnol.*, 34 (2016), pp. 760-767
7. A.C. Stacer, et al. NanoLuc reporter for dual luciferase imaging in living animals *Mol. Imaging*, 12 (2013), pp. 1-13
8. H.-W. Yeh, et al. ATP-independent bioluminescent reporter variants to improve in vivo imaging *ACS Chem. Biol.*, 14 (2019), pp. 959-965, 10.1021/acscchembio.9b00150
9. Y. Mizui, et al. Long-term single cell bioluminescence imaging with C-3 position protected coelenterazine analogues *Org. Biomol. Chem.* (2020), 10.1039/d0ob02020f
10. E.P. Coutant, et al. Gram-scale synthesis of luciferins derived from coelenterazine and original insights into their bioluminescence properties *Organic & Biomolecular Chemistry*, 17 (2019), pp. 3709-3713, 10.1039/c9ob00459a
11. E.P. Coutant, et al. Bioluminescence profiling of NanoKAZ/NanoLuc luciferase using a chemical library of coelenterazine analogues *Chem. Eur. J.*, 26 (2020), pp. 948-958, 10.1002/chem.201904844
12. Y. Su, et al. Novel NanoLuc substrates enable bright two-population bioluminescence imaging in animals *Nat. Methods*, 17 (2020), pp. 852-860
13. N. Gaspar, et al. Nanobit system and hydrofurimazine for optimized detection of viral infection in mice—a novel in vivo imaging platform *Int. J. Mol. Sci.*, 21 (2020), pp. 1-11, 10.3390/ijms21165863
14. D. Morse, B.A. Tannous A water-soluble coelenterazine for sensitive in vivo imaging of coelenterate luciferases *Mol. Ther.*, 20 (2012), pp. 692-693
15. M.K. Schwinn, et al. CRISPR-mediated tagging of endogenous proteins with a luminescent peptide *ACS Chem. Biol.*, 13 (2018), pp. 467-474
16. S. Inouye, et al. C6-Deoxy coelenterazine analogues as an efficient substrate for glow luminescence reaction of nanoKAZ: the mutated catalytic 19 kDa component of *Oplophorus* luciferase *Biochem. Biophys. Res. Commun.*, 437 (2013), pp. 23-28
17. S. Iwano, et al. Single-cell bioluminescence imaging of deep tissue in freely moving animals *Science*, 359 (2018), pp. 935-939, 10.1126/science. aaq1067
18. L. Mezzanotte, N. An, I.M. Mol, C.W. Löwik, E.L. Kaijzel A new multicolor bioluminescence imaging platform to investigate NF- κ B activity and apoptosis in human breast cancer cells *PLoS One*, 9 (2014), Article e85550
19. G. Zambito, et al. Evaluating brightness and spectral properties of click beetle and firefly luciferases using luciferin analogues: identification of preferred pairings of luciferase and substrate for in vivo bioluminescence imaging *Mol. Imaging Biol.*, 22 (6) (2020 Dec), pp. 1523-1531
20. S. Schrepfer, et al. Stem cell transplantation: the lung barrier *Transplant. Proc.*, 39 (2007), pp. 573-576
21. U.M. Fischer, et al. Pulmonary passage is a major obstacle for intravenous stem cell delivery: the pulmonary first-pass effect *Stem Cells Dev.*, 18 (2009), pp. 683-692

22. T. Miloud, C. Henrich, G. Hämmerling, T. Miloud, C. Henrich, G.J. Hammerling Quantitative comparison of click beetle and firefly luciferases for in vivo bioluminescence imaging *J Biomed Opt*, 12 (2007), p. 054018 *Journal of biomedical optics* 12, 054018 <https://doi.org/10.1117/1.2800386>
23. S. Bhaumik, S.S. Gambhir Optical imaging of *Renilla* luciferase reporter gene expression in living mice *Proc. Natl. Acad. Sci.*, 99 (2002), pp. 377-382, 10.1073/pnas.012611099
24. K. Saito, et al. Luminescent proteins for high-speed single-cell and whole-body imaging *Nat. Commun.*, 3 (2012), p. 1262, 10.1038/ncomms2248
25. H.W. Yeh, et al. Red-shifted luciferase-luciferin pairs for enhanced bioluminescence imaging *Nat. Methods*, 14 (2017), pp. 971-974
26. A. Taylor, J. Sharkey, A. Plagge, B. Wilm, P. Murray Multicolour in vivo bioluminescence imaging using a NanoLuc-based BRET reporter in combination with firefly luciferase *Contrast Media Mol Imaging*, 2018 (2018), p. 2514796
27. V.O. Shipunova, O.N. Shilova, E.I. Shramova, S.M. Deyev, G.M. Proshkina A highly specific substrate for NanoLUC luciferase furimazine is toxic in vitro and in vivo *Russian Journal of Bioorganic Chemistry*, 44 (2018), pp. 225-228, 10.1134/s1068162018020085
28. M. Edinger, et al. Noninvasive assessment of tumor cell proliferation in animal models *Neoplasia*, 1 (1999), pp. 303-310, 10.1038/sj.neo.7900048
29. Z. Hui, et al. Emission spectra of bioluminescent reporters and interaction with mammalian tissue determine the sensitivity of detection *in vivo* *J. Biomed. Opt.*, 10 (2005), pp. 1-9, 10.1117/1.2032388
30. A. Shakhmin, et al. Coelenterazine analogues emit red-shifted bioluminescence with NanoLuc *Organic & Biomolecular Chemistry*, 15 (2017), pp. 8559-8567, 10.1039/c7ob01985h
31. C. Yan, et al. Novel NanoLuc-type substrates with various C-6 substitutions *Bioorg. Med. Chem. Lett.*, 30 (2020), p. 127085

SUPPLEMENTARY DATA



Supplementary Figure 1. Assessment of background luminescence with no reporter expression. (a) Representative prone and supine images of autoluminescence in nude BALB/c mice post i.p. substrate administration; AkaLumine (3 μ mol), FFz (1.3 μ mol), FFz (4.3 μ mol), hikarazine-003 (333 nmol) and furimazine (333 nmol). (b) Mean signal intensity post 1 min acquisition at the IVIS, n=3 per substrate analogue.

Chapter 4

“Evaluating Brightness and Spectral Properties of Click Beetle and Firefly Luciferases Using Luciferin Analogues: Identification of Preferred Pairings of Luciferase and Substrate for *in Vivo* Bioluminescence Imaging”

Giorgia Zambito^{1,2,3}, **Natasa Gaspar**^{1,2,4}, Yanto Ridwan^{1,2}, Mary P. Hall⁵, Ce Shi⁶, Thomas A. Kirkland⁶, Lance P. Encell⁵, Clemens Löwik^{1,2,7}, Laura Mezzanotte^{1,2}

Author affiliation:

¹ Erasmus Medical Center, Optical Molecular Imaging, Radiology-Rotterdam, The Netherlands

² Erasmus Medical Center, Molecular Genetics-Rotterdam, The Netherlands

³ Medres medical research GmbH, Cologne, Germany

⁴ Percuros B.V.-Leiden, The Netherlands

⁵ Promega Corporation, Madison, Wisconsin, USA

⁶ Promega Biosciences Incorporated, San Luis Obispo, California, USA

⁷ CHUV Department of Oncology, University of Lausanne, Switzerland

ABSTRACT

Purpose: Currently a variety of red and green beetle luciferase variants are available for bioluminescence imaging (BLI). In addition, new luciferin analogues providing longer wavelength luminescence have been developed that show promise for improved deep tissue imaging. However, a detailed assessment of these analogues (e.g., Akalumine-HCl, CycLuc1 and amino naphthyl luciferin (NH₂-NpLH2)) combined with state of the art luciferases has not been performed. The aim of this study was to evaluate for the first time the *in vivo* brightness and spectral characteristics of firefly (Luc2), click beetle green (CBG99), click beetle red 2 (CBR2) and Akaluc luciferases when paired with different D-luciferin (D-LH2) analogues *in vivo*.

Procedures: Transduced human embryonic kidney (HEK 293T) cells expressing individual luciferases were analyzed both *in vitro* and in mice (via subcutaneous injection). Following introduction of the luciferins to cells or animals, the resulting bioluminescence signal and photon emission spectrum was acquired using a sensitive charge-coupled device (CCD) camera equipped with a series of band pass filters and spectral unmixing software.

Results: Our *in vivo* analysis resulted in four primary findings: 1. The best substrate for Luc2, CBG99 and CBR2 in terms of signal strength was D-luciferin; 2. The spectra for Luc2 and CBR2 were shifted to a longer wavelength when Akalumine-HCl was the substrate; 3. CBR2 gave the brightest signal with the near-infrared substrate, NH₂-NpLH2; and 4. Akaluc was brighter when paired with either CycLuc1 or Akalumine-HCl than when paired with D-LH2.

Conclusion: We believe that the experimental results described here should provide valuable guidance to end users for choosing the correct luciferin/luciferase pairs for a variety of BLI applications.

INTRODUCTION

Bioluminescence imaging (BLI) is a well-known, non-invasive technique employed during preclinical studies to track cells and monitor biological processes in living animals [1-3]. BLI is performed by capturing the light generated by a luciferase upon exogenous substrate (e.g., D-luciferin (D-LH2)) addition to report real-time, cellular and molecular events [4].

Over the last decade the bioluminescence toolbox has greatly expanded [1,5-6]. Novel luciferin analogues have been introduced that enhance light emission *in vivo* and increase detection sensitivity in deeper tissues [7]. Cycluc1 has been shown to enhance emission of codon optimized firefly luciferase (Luc2), especially in brain. Furthermore, this system provides slightly red-shifted emission resulting in deeper light penetration and less scattering of the bioluminescence signal [8-9]. Likewise, Akalumine-HCl has a spectral peak in the near infrared (NIR) (677 nm) as well as enhanced emission with Luc2 when administered at low concentration [10]. Akalumine-HCl paired with the recently engineered Akaluc luciferase is even brighter, although the spectral peak is blue-shifted to 650 nm [11]. Amino naphthyl luciferin (NH₂-NpLH2) represents another new substrate with potential for deeper tissue BLI [12]. This substrate was shown to emit in the NIR with a peak of 740 nm when reacting with an engineered version of click-beetle luciferase (CBR2). CBR2 can also utilize D-LH2 and this combination was shown to improve imaging in black mice compared to Luc2/D-LH2.

Research into the development of improved BLI reagents has generally focused on bioluminescence systems comprised of compatible luciferase/luciferin pairings [13-18]. Most comparative studies have been performed using D-LH2. For example, Miloud *et al.* compared firefly (Luc2) and click beetle luciferases *in vivo* with D-LH2 as substrate and concluded that click beetle green (CBG99) has sensitivity and total photon yield comparable to click beetle red [15]. In other studies, Luc2 was shown to have improved performance compared to a red-shifted firefly mutant (PpyRE9) and CBG99 for brain imaging [16-17], but D-LH2 was the only substrate examined. A direct comparison (either *in vitro* or *in vivo*) of emission spectra and relative brightness of bioluminescence systems comprised of different luciferase enzymes in combination with novel luciferins has, to date, not been reported.

Here, we provide a detailed *in vitro* and *in vivo* analysis of brightness and emission spectra for four luciferases when combined with four different substrates using a CCD camera equipped with a series of band pass filters and spectral unmixing software. We anticipate that the results of this comparative analysis will help enable researchers to choose the best enzyme/substrate pairs for different BLI applications. In addition, our findings revealed that depending on the luciferase/luciferin pair, a wide range of spectral emission peaks (i.e., multicolored luciferases) is available that could broaden the BLI toolbox for multiplex analysis both *in vitro* and *in vivo*.

MATERIALS & METHODS

Animals

Animal experiments were approved by the Bioethics Committee of Erasmus MC, Rotterdam, The Netherlands, and performed in accordance with national guidelines and regulations established by the Dutch Experiments on Animal Act (WoD) and by the European Directive on the Protection of Animals used for scientific purpose (2010/63/EU). BALB/C nude (females) were obtained from Charles River Laboratory (The Netherlands). All mice aged 6–8 weeks were provided access to food and water ad libitum and were hosted in the animal facility at the Erasmus MC, Rotterdam, The Netherlands.

Cell Line

Human embryonic kidney cells (HEK 293T) were cultured in Dulbecco's Modified Eagle's Medium (DMEM) (Sigma, St. Louis, MO, USA) supplemented with 10 % of FBS and 1 % Penicillin-Streptomycin. The culture was incubated at 37 °C with 5 % CO₂.

Lentivirus Production

Virus production and cell transduction were performed under appropriate biosafety level conditions (ML-II) in accordance with the National Biosafety Guidelines and Regulations for Research on Genetically Modified Organisms. Procedures and protocols were reviewed and approved by the EMC Biosafety Committee (GMO permit 99-163). The lentiviral plasmids pCDH-EF1-CBG99-T2A-copGFP, pCDH-EF1-Luc2-T2A-copGFP, and pCDH-EF1-CBR2-T2A-copGFP were previously described [12, 15]. The plasmid pCDH-EF1-Akaluc-T2A-copGFP was produced by inserting the sequence of Akaluc (amplified with specific primers from pcDNA3 Venus-Akaluc plasmid from RIKEN BRC repository) without stop codon using BamHI and NotI sites in pCDH-EF1-MCS-T2A-copGFP vector. Lentiviruses were produced by transfection of HEK 293T packaging cells with three packaging plasmids (pCMV-VSVG, pMDLgRRE, pRSV-REV; Addgene, Cambridge, MA, USA) and the lentiviral vector plasmids as previously described in details [16]. The supernatant containing lentiviral particles were collected after 48 and 72 h. Subsequent quantification of the virus was performed using a standard antigen-capture HIV p24 ELISA (ZeptoMetrix Corporation, NY, USA).

Cell Transduction and Transfection

Cell transduction was performed by culturing HEK 293T cells in DMEM supplemented with 10 % of FBS and 1 % of Penicillin-Streptomycin at the density of 200,000 cells in a T25-flask with 5 ml of medium. Expression in the lentiviral plasmid is driven by housekeeping elongation factor 1 α (EF1) promoter. Cells were transduced with MOI 1 of either pCDH-EF1-Luc2-T2A-copGFP, pCDH-EF1-CBG99-T2AcopGFP, pCDH-EF1-

CBR2-T2A-copGFP, or pCDH-EF1- Akaluc-T2A-copGFP lentivirus plus with polybrine (hexametrine bromide, Sigma-Aldrich) at the final concentration of 8 $\mu\text{g/ml}$. Transgene expression was confirmed by the presence of the super bright green fluorescent protein copGFP from the copepod *Potentilla plumata* (excitation/ emission maximum = 482/502 nm).

Flow Cytometry to Sort Stable Cell Lines

Positive stable clones were sorted for comparable levels of copGFP expression by cell sorting (BD-FACS ARIA III, BD Biosciences). Forward and side scatters were also drawn to eliminate cellular debris from the analysis and to select highly positive cells for GFP.

In Vitro BLI

Transduced cells were plated at a density of 2×10^4 cells per well in a black 96-well plate (Greiner Cell Star[®]) and imaged in 100 μl of D-PBS. Bioluminescence signal from wells was measured with IVIS[®] spectrum system (PerkinElmer, Boston, MA, USA) every 5 min after substrate addition (final concentration of each substrate was 0.1 mM). All in vitro measurements were acquired after 1 min at 37 °C using a 30-s acquisition time with an open filter or using a series of band pass filters ranging from 520 to 800 nm. Data were analyzed by the Living Image software version 4.3 (PerkinElmer). Data in every well were normalized for fluorescence emission detected using a GloMax[®]-Multi plate reader.

In Vivo BLI

Each stable expressing cell line was injected subcutaneously 1×10^5 cells/50 μl . The number of animals was chosen according to power analysis (p value at least G 0.05 and power 95 %) considering that we expected from the data generated in vitro that the brightest BL system would differ by 1–2 orders of magnitude in vivo. Mice (N = 3 per group) received two different cell lines, one in each flank. Animals were then imaged after intraperitoneal injection of D-LH2 substrate (150 mg/kg), NH2-NpLH2 substrate (220 mg/kg), CycLuc1 (7.6 mg/kg), and Akalumine-HCl substrate (50 mg/kg). These doses were chosen based on maximum solubility (for CycLuc1 and Akalumine-HCl), tolerability in mice, and maximum attainable signal based on previous findings. Mice were randomly assigned and anesthetized by isoflurane inhalation prior to performing BLI imaging. The person performing the subcutaneous injections was blind as to the cells being injected. Images were acquired with the IVIS[®] spectrum small animal imager system (PerkinElmer). Light was measured using open filter and a series of 20 nm wavelength band filters from 520 to 800 nm with acquisition time of 30 s during a time of about 30 min after substrate injection (kinetic analysis). Emission signals were measured with the Living Image software[®] version 4.3 (Perkin Elmer). Statistical Analysis All statistical

analyses were performed using the GraphPad Prism 6 software and one-way ANOVA followed by Tukey's post-test. p values ≤ 0.05 were considered statistically significant.

RESULTS

***In Vitro* Evaluation of Emission Properties for Different Combinations of Luciferase Variant and Luciferin Analogue**

The aim of this study was to evaluate *in vitro* and *in vivo* light emission and spectral differences between four luciferases (Luc2, CBG99, CBR2, and Akaluc) when combined with D-LH2 or three luciferin analogues (NH2-NpLH2, Akalumine-HCl, or CycLuc1) for bioluminescence imaging (BLI). To compare the different emissions, HEK 293T cells stably expressing each of the four luciferases were treated with substrates (0.1 mM) and imaged at 37 °C. Equimolar expression of each luciferase was achieved by selecting cells for GFP emission. We found that the luciferase/luciferin pairs yielding the highest photon emission (p value ≤ 0.001) were Luc2/D-LH2 and Akaluc/CycLuc1 when the substrate was added at a concentration of 0.1 mM. The combinations of Luc2/CycLuc1, Akaluc/Akalumine-HCl, CBG99/D-LH2, and CBR2/D-LH2 produced ~ 2-fold fewer photons (Fig. 1a), while cells expressing CBG99 were much less efficient (~ 100-fold dimmer with NH2-NpLH2/Akalumine-HCl; 10-fold dimmer with CycLuc1) (Fig. 1a). CBR2-expressing cells were more promiscuous compared with CBG99 cells. However, they generated 10-fold less luminescence (compared with Luc2/D-LH2) with Akalumine-HCl and NH2-NpLH2. The CBR2-expressing cells gave a signal comparable with Luc2/D-LH2 with CycLuc1. Finally, Akaluc produced similar luminescence intensity when either Akalumine-HCl or CycLuc1 was used as substrate (Fig. 1a). Akaluc also showed nearly 100-fold lower signal with DLH2 or NH2-NpLH2 compared with Akalumine-HCl and CycLuc1.

***In Vivo* Emission Spectrum of Luciferases Detected Using a Series of 20 nm Band Pass Filters**

The day of injection, HEK 293T cells (expressing the various luciferases) were prepared at a concentration of 2×10^6 cells/ml in PBS and fluorescence emission measured at IVIS, confirming the comparable average expression of GFP (Supplementary Fig. 1). Following subcutaneous injection of 1×10^5 HEK 293T cells (expressing the various luciferases) into both flanks of mice, images were acquired after injection of D-LH2 (150 mg/kg), NH2-NpLH2 (220 mg/kg), Akalumine-HCl (50 mg/kg), or CycLuc1 (7.6 mg/kg). We used the optimal concentration for each given substrate based on previous literature [8, 10, 12, 19]. For D-LH2, this was 150 mg/kg [19]. Because of poor aqueous solubility, CycLuc1 and Akalumine-HCl were injected at 7.6 mg/kg (5 mM in saline) and 50 mg/

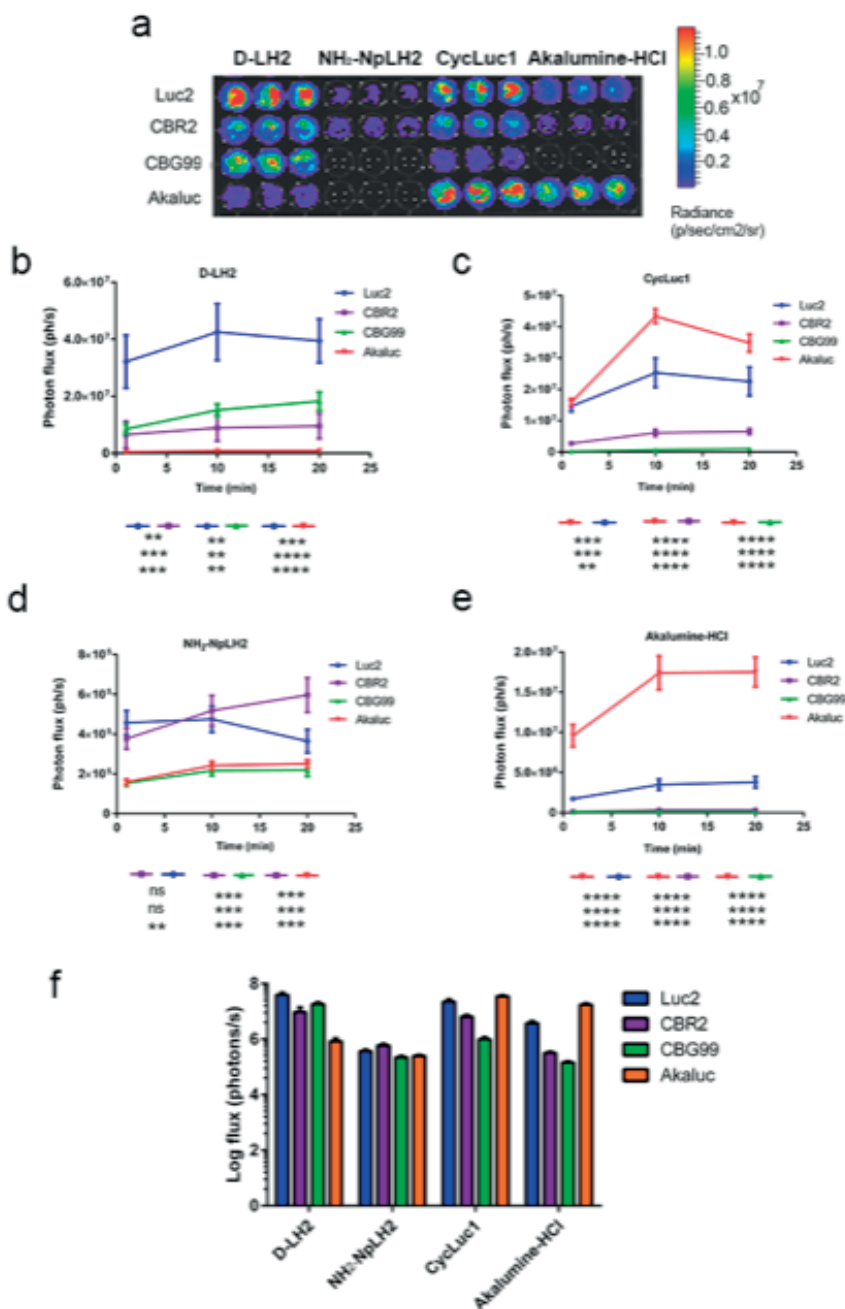


Figure 1. (a) Bioluminescence profiles for Luc2, CBR2, CBG99, and Akaluc luciferases combined with four different luciferin analogues in live cells. (b-f) Photon flux (ph/s) in HEK 293T cells expressing individual luciferases upon addition of substrates (0.1 mM) was quantified using an exposure time of 30 s. Statistical analysis (N = 3) was performed using one-way ANOVA followed by Tukey's T test (*p < 0.01 for Luc2/D-LH2 compared with all combinations with the exception of Akaluc/CycLuc1 which was not significantly different).

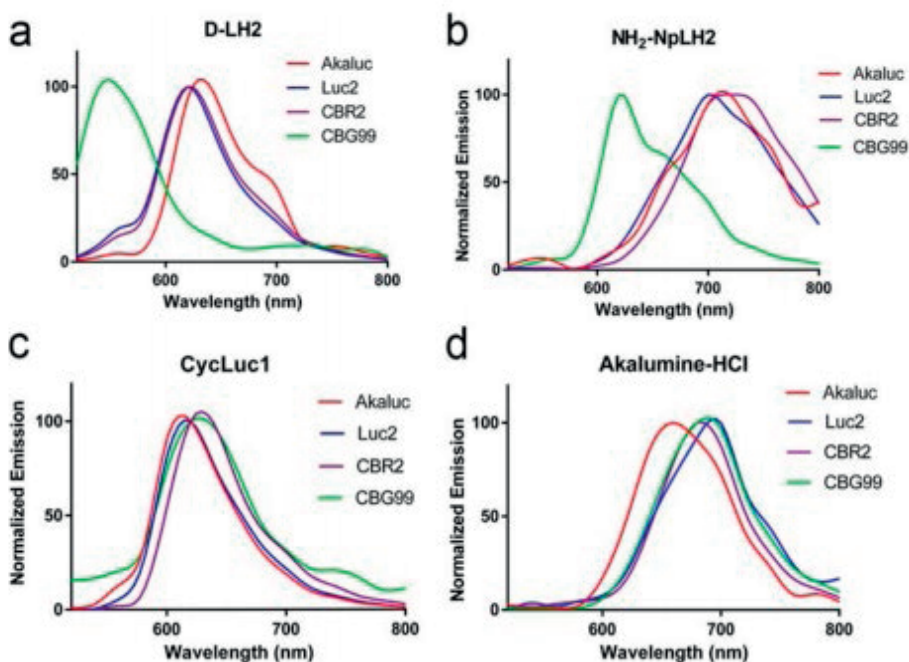


Figure 2. *In vivo* (BALB/C) emission spectra for different combinations of luciferase (Luc2, CBG99, CBR2, or Akaluc; expressed in HEK393T cells implanted subcutaneously in the flanks) and luciferin or luciferin analogue. (a) D-LH2 (150 mg/kg), (b) NH₂-NpLH2 (220 mg/kg), (c) CycLuc1 (7.6 mg/kg), and (d) Akalumine-HCl (50 mg/kg); substrates were injected intraperitoneally). Spectral data was acquired 15–20 min after injection.

kg (33 mM in saline), respectively [8, 10]. We previously demonstrated that the solubility of NH₂-NpLH2 allows injection of a maximal dose of 220 mg/kg (60 mM in saline) and that it produces significantly higher photon fluxes than a dose of 150 mg/kg [12]. Multiple acquisitions using a series of 20 nm band pass filters were performed with an exposure time of 30 s. The BLI measurements were performed at the time of peak of emission after injection of the luciferins into sedated animals. In terms of emission spectra, Luc2/D-LH2, CBG99/DLH2, CBR2/D-LH2, and Akaluc/D-LH2 produced peaks at 610 nm, 540 nm, 620 nm, and 640 nm, respectively (Fig. 2a). NH₂-NpLH2 caused a red shift of the peak of emission with all the luciferases (Luc2, 700 nm; Akaluc, 720 nm; CBR, 730 nm; and CBG99, 620 nm) (Fig. 2b). In contrast, when CycLuc1 was used as a substrate, the emission peak for each luciferase was in the range of 620 nm (Luc2 and Akaluc were green shifted towards 600 nm and CBG99 and CBR2 were red-shifted towards 640 nm) (Fig. 2c). Akaluc/ Akalumine-HCl, also referred to as the AkaBLI system [11], produced a peak of emission at 660 nm while the other luciferases peaked in the NIR (~ 680 nm) when paired with Akalumine-HCl (Fig. 2d).

***In Vivo* Comparison of Brightness of Luciferase/ Luciferin Pairing**

Next, we compared the total emission of each luciferase *in vivo* with D-LH2 or the luciferin analogues. Figure 3 shows the representative bioluminescent images of nude mice where CBG99, Luc2, CBR2, and Aka-Luc-expressing cells were implanted, and each of the different substrates was injected intraperitoneally. The data in Fig. 4 represents signals at peak of emission which differs slightly between BLI systems (Supplementary Fig. 2).

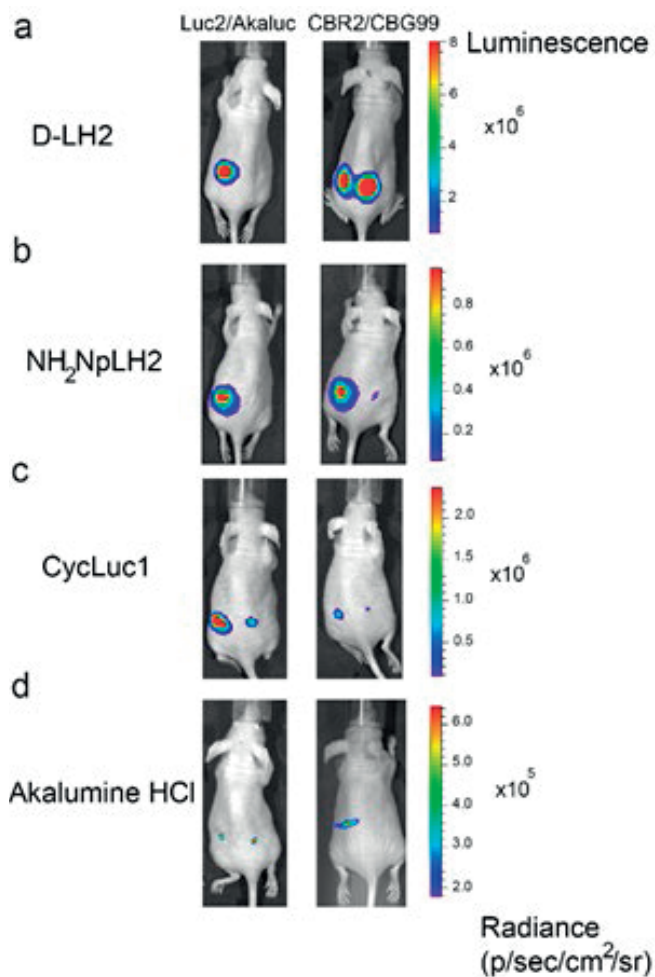


Figure 3. Superficial bioluminescence imaging of BALB/C mice in which 1×10^5 HEK293T cells transduced with Luc2 and Akaluc or CBR2 and CBG99 were implanted subcutaneously into the left and right flanks of mice, respectively, and treated (intraperitoneally) with (a) D-LH2 (150 mg/kg), (b) NH₂-NpLH2 (220 mg/kg), (c) CycLuc1 (7.6 mg/Kg), and (d) Akalumine-HCl (50 mg/kg). Imaging data was collected using open filters and with an exposure time of 30 s. Average luminescence is reported as photons/s/cm² /sr.

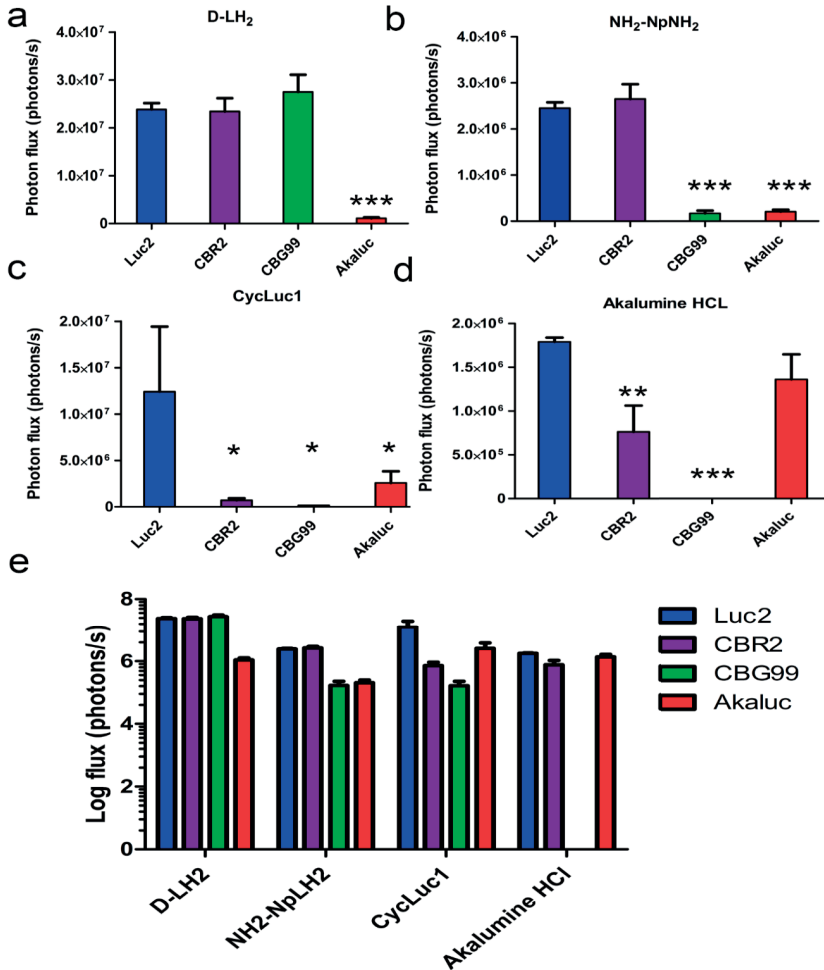


Figure 4. Quantification of photon flux (ph/s) measured in vivo for all combinations of luciferase and substrate (D-LH2 (a), Akalumine-HCl (b), CycLuc1 (c), and NH₂-NpLH₂ (d)). Combined data is also presented in logarithmic scale (e). Statistical analysis of data was performed using one-way ANOVA followed by Tukey's post-test (**p < 0.0019; ***p < 0.001; ****p < 0.0001).

Luc2, CBG99, and CBR2 paired with D-LH₂ produced the highest signals which were 20-fold higher compared with Akaluc/D-LH₂ (p value < 0.001) (Fig. 4a). When NH₂-NpLH₂ was used as a substrate, Luc2 and CBR2 produced approximately 10-fold higher signal output (p value, < 0.001) compared with both CBG99 and Akaluc (Fig. 4b). When CycLuc1 was used as a substrate, the strongest signal was detected for Luc2/CycLuc1. Akaluc, CBR2, and CBG99 paired with CycLuc1 produced ~ 5, 16, and 70-fold lower signal output, respectively (Fig. 4c). When Akalumine-HCl was used as a substrate, Luc2 and Akaluc produced ~ 2-fold higher signal compared with CBR2, and there was no

detectable signal for CBG99 (Fig. 4d). The luciferase/luciferin pairs that gave the highest photon yields *in vivo* were Luc2/D-LH2, Luc2/CycLuc1, CBG99/DLH2, and CBR2/D-LH2 ($1-2 \times 10^7$ ph/s). The following luciferin/luciferase pairs produced approximately 10-fold fewer photons: Akaluc/Cycluc1, Akaluc/Akalumine-HCl, Luc2/Akalumine-HCl, Luc2/NH2-NpLH2, and CBR2/NH2-NpLH2. Finally, the following pairs produced nearly 100-fold fewer photons: CBR2/CycLuc1, CBR2/AkalumineHCl, CBG99/Cycluc1, CBG99/NH2-NpLH2, and Akaluc/NH2-NpLH2 (Fig. 4e, Table 1).

Table 1 *In vivo* emission intensity relative to Luc2/D-LH2

Luciferase	D-LH2		NH ₂ NPLH2		CycLuc1		Akalumine-HCl	
	Spectral peak [nm]	Normalized intensity	Spectral peak [nm]	Normalized intensity	Spectral peak [nm]	Normalized intensity	Spectral peak [nm]	Normalized intensity
Luc2	620	1	700	0.1	620	0.5	700	0.8
CBR2	620	0.98	720	0.1	620	0.03	680	0.03
CBG99	540	1	620	0.01	620	0.01	680	0
AkaLuc	640	0.05	720	0.01	620	0.1	660	0.06

DISCUSSION

A variety of new luciferase enzymes and novel substrate analogues emerging in recent years have resulted in better tools for *in vivo* BLI. One example is CBR2/NH2-NpLH2, which was engineered specifically for enhanced NIR emission to improve imaging resolution in deeper tissues [12]. Another example is Akaluc/Akalumine-HCl [11], an engineered pair offering improved *in vivo* sensitivity. Another relatively new substrate, Cycluc1, has shown *in vivo* utility (including more efficient crossing of the blood brain barrier compared with D-LH2) when used in combination with the already well-established Luc2 [8]. With the emergence of these and other new bioluminescence systems, we felt it would be of interest and potential benefit for the *in vivo* BLI community, particularly for those interested in dual color readouts, to analyze different pairings of luciferase/substrate using a common set of test parameters. Here, we report on the photon yields and spectral characterization of Luc2, CBG99, CBR2, and Akaluc luciferases combined with four different substrates (D-LH2, NH2-NpLH2, Cycluc1, and Akalumine-HCl) both *in vitro* and *in vivo*. Our goal was to use these parameters to compare the various luciferase/substrate combinations in a standard subcutaneous *in vivo* BLI model, with the intention to provide guidance for the *in vivo* BLI community when choosing appropriate systems for specific applications involving dual color detection. Note the longer emission wavelengths for CBR2/NH2-NpLH2 and Akaluc/Akalumine-HCl provide a sensitivity advantage in deeper tissue [11, 12] that will not be fully realized in a subcutaneous model. However, we postulated that the peak emissions in the NIR for these systems would provide excellent spectral separa-

tion from shorter wavelength signals nonetheless. We have demonstrated *in vitro* that at a relatively low, but biologically relevant (*in vivo*) substrate concentration (0.1 mM), three of the four luciferases give maximum signal when combined with D-LH2. The exception was Akaluc, which produced more photons when using either Cycluc1 or Akalumine-HCl as substrate. We observed the same trend in a low-depth, superficial *in vivo* tissue model. Though we did not examine deeper tissues in this study, we predict based on our results that the red-shifted NIR systems (CBR2/NH2-NpLH2, Akaluc/Akalumine-HCl, and Luc2/Akalumine-HCl) would perform best.

To evaluate spectral properties *in vivo* as a way to determine the potential for multiplexing, we used the same superficial, subcutaneous model where different luciferase expressing cell lines were injected into the backs of mice. This minimally invasive model allowed us to determine the light emission characteristics for different BLI systems using a small cohort of animals. Based on the analysis, we are able to recommend new combinations of luciferases with distinct colors having potential for multiplexing with a single substrate in superficial tissue e.g., CBG99/D-LH2 (540 nm) and CBR2/D-LH2 (620 nm) (examples of spectral unmixing showed in Supplementary Fig. 3); CBG99/D-LH2 (540 nm) and Luc2/D-LH2 (610 nm); and Luc2/Akalumine (680 nm) and Akaluc/Akalumine (650 nm). Such an approach could be useful for analyzing multiple parameters or biological processes in animals using either engrafted cells or transgenes expressed in particular tissues or organs, and as part of a single imaging session requiring fewer animals.

Successful multiplexing of luminescence systems with different emission spectra relies on the acquisition of images using multiple filters followed by accurate, algorithm-based spectral unmixing to resolve the contributions from each luciferase to total light output. This can be a challenge with shorter wavelength systems (e.g., CBG99/D-LH2), as they tend to shift their apparent emission peak to significantly longer wavelengths when imaged in deeper tissues or even in superficial tissue when using mice with dark fur [20–22]. For these more challenging imaging targets, it is therefore desirable to use bioluminescence pairs that emit in the NIR (9 650 nm), as emission peaks are essentially constant in this range of the spectrum [22, 23]. In this regard, we found that click beetle luciferases have high photon emission with NH2-NpLH2 [12] and that there is a broad spectral separation between CBG99 (620 nm) and CBR2 (720 nm) (spectral unmixing is shown in Supplementary Fig. 2). However, before giving serious consideration to this pair with NH2-NpLH2 as a multiplexing opportunity for deep tissue imaging in mice, it will likely be necessary to improve the photon yield for CBG99/NH2-NpLH2.

FUNDING

This study is funded by the European Commission under the H2020-MSCA-RISE award grant number 777682 (CANCER) and under the H2020-MSCA-ITN award, grant number 675743 (ISPIC), and the Applied Molecular Imaging Erasmus MC (AMIE) facility.

COMPLIANCE WITH ETHICAL STANDARDS

CONFLICT OF INTEREST

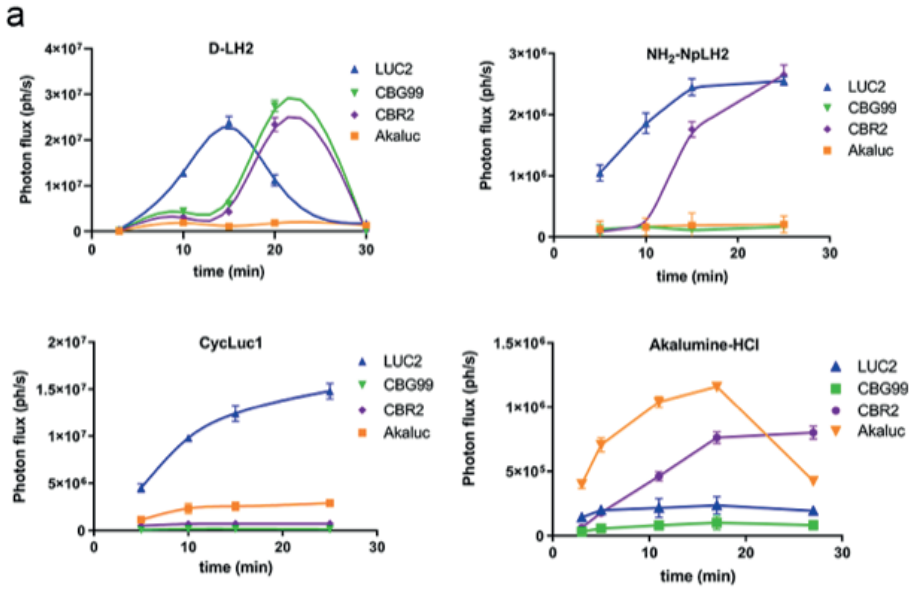
“The authors declare that they have no conflict of interest”

REFERENCES

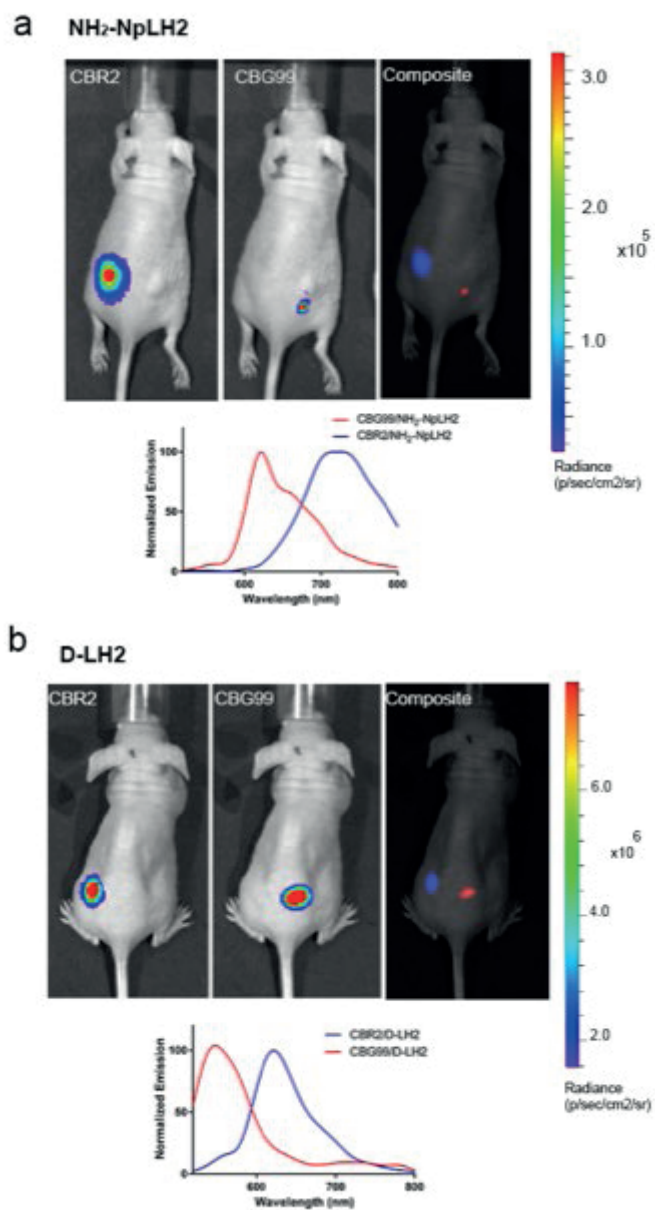
1. Contag CH, Bachmann M (2002) Advances in In Vivo bioluminescence imaging of gene expression. *Annu Rev Biomed Eng* 4:235-260.
2. Brader P, Serganova I and Blasberg RG, (2013) Noninvasive Molecular Imaging Using Reporter Genes. *J Nucl Med* 54:167-172.
3. Close DM, Xu T, Saylor GS, Ripp S (2010) In vivo bioluminescent imaging (BLI): noninvasive visualization and interrogation of biological processes in living animals. *Sensors (Basel, Switzerland)* 11:180-206.
4. Wilson TA, Hastings JW (1998) *Bioluminescence Annual Review of Cell and Developmental Biology* 14:197-230.
5. Mezzanotte L, vant Root M, Karatas H et al. (2017) In Vivo molecular bioluminescence imaging: new tools and applications *Trends in Biotechnology* 35:640-652.
6. Xu T CD, Handagama W, Marr E, et al. (2016) The expanding Toolbox of In Vivo Bioluminescent imaging. *Frontiers in Oncology* 6:150.
7. Adams ST, Miller SC (2014) Beyond D-luciferin: expanding the scope of bioluminescence imaging in vivo. *Current Opinion in Chemical Biology* 21:112-120.
8. Evans MS, Chaurette JB, Adams ST et al. (2014) A synthetic luciferin improves bioluminescence imaging in live mice. *Nat Methods* 11:393-395.
9. Simonyan H, Hurr C, Young CN (2016) A synthetic luciferin improves in vivo bioluminescence imaging of gene expression in cardiovascular brain regions. *Physiological Genomics* 48(10): 762-770.
10. Kuchimaru T, Iwano S, Kiyama M, et al. (2016) A luciferin analogue generating near-infrared bioluminescence achieves highly sensitive deep-tissue imaging. *Nat Commun* 7:11856.
11. Iwano S, Sugiyama M, Hama H et al. (2018) Single-cell bioluminescence imaging of deep tissue in freely moving animals. *Science* 359:935-939.
12. Hall MP, Woodrooffe CC, Wood MG, et al. (2018) Click beetle luciferase mutant and near infrared naphthyl-luciferins for improved bioluminescence imaging. *Nature Communications* 9:132.
13. Ohmiya Y (2015) Simultaneous multicolor luciferase reporter assays for monitoring of multiple genes expressions. *Combinatorial Chemistry & High Throughput Screening* 18: :937.
14. Branchini BR, Southworth TL, Fontaine DM, Kohrt D, Florentine CM, Grossel MJ (2018) A Firefly Luciferase Dual Color Bioluminescence Reporter Assay Using Two Substrates To Simultaneously Monitor Two Gene Expression Events. *Scientific Reports* 8:5990.
15. Miloud T, Gunter CH, Hammerling J, Quantitative comparison of click beetle and firefly luciferases for in vivo bioluminescence imaging. *J Biomed Opt* 12(5).
16. Mezzanotte L, Aswendt M, Tennstaedt A, et al. (2013) Evaluating reporter genes of different luciferases for optimized in vivo bioluminescence imaging of transplanted neural stem cells in the brain. *Contrast Media Mol Imaging* 8:505-513.
17. Branchini BR, Ablamsky DM, Davis AL, et al. (2010) Red-emitting luciferases for bioluminescence reporter and imaging applications. *Analytical Biochemistry* 396:290-297.
18. Kaskova ZM, Tsarkova AS, Yampolsky IV (2016) 1001 lights: luciferins, luciferases, their mechanisms of action and applications in chemical analysis, biology and medicine. *Chemical Society Reviews* 45:6048-6077.
19. Contag CH, Spilman SD, Contag PR et al. (1997) Visualizing gene expression in living mammals using a bioluminescent reporter. *Photochem Photobiol.* 66(4):523-31.
20. Mezzanotte L, Que I, Kaijzel E et al. (2011) Sensitive dual color in vivo bioluminescence imaging using a new red codon optimized firefly luciferase and a green click beetle luciferase. *PLoS One*: 10.1371/journal.pone.0019277.

21. Aswendt M, Vogel S, Schäfer C et al. (2019) Quantitative in vivo dual-color bioluminescence imaging in the mouse brain. *Neurophotonics*. 6(2):025006.
22. Stowe CL, Burley TA, Allan H, et al (2019) Near-infrared dual bioluminescence imaging in mouse models of cancer using infraluciferin. *Elife*: 10.7554/eLife.45801.

SUPPLEMENTARY DATA



Supplementary Figure 1. *In vivo* kinetics of D-LH2, NH₂-NpLH2, CycLuc1 and Akalumine-HCl at various time points ranged between 5 and 30 minutes after injection of substrates. Data are presented as means (n=3) and SD and curves are generated using loess smoothing function.



Supplementary Figure 2. Representative spectral unmixing images of CBR2 and CBG99 luciferases. Mice were imaged after administration of NH₂-NpLH2 (a) or of D-LH2 (b) substrates using a series of band pass filters at IVIS spectrum (Perkin Elmer). A spectral unmixing algorithm applied to the images extracted and measured each luciferase contribution and generated the two reported spectra of emission.

Chapter 5

“Can We Transform a Bioluminescent Reporter Gene into a Reporter for Radionuclide-based Imaging?”

Natasa Gaspar^{1,2,3}, Maryana Handula¹, Marcus C. M. Stroet^{1,2}, Kranthi Marella-Panth^{1,2}, Joost Haeck⁴, Thomas Kirkland⁵, Mary Hall⁵, Lance Encell⁵, Simone Dalm¹, Marion De Jong¹, Clemens Lowik^{1,2}, Yann Seimbille¹, Laura Mezzanotte^{1,2}

1 Erasmus Medical Center, Department of Radiology and Nuclear Medicine, Rotterdam, Netherlands

2 Erasmus Medical Center, Department of Molecular Genetics, Rotterdam, Netherlands

3 Percuros B.V., Leiden, Netherland

4 Erasmus Medical Center, AMIE core facility, Rotterdam, Netherlands

5 Promega corporation, Madison, Wisconsin, USA

***Manuscript in preparation.**

ABSTRACT

Purpose (Background): Reporter gene imaging enables longitudinal tracking of cell survival and biodistribution *in vivo*. Advantages of multimodality imaging include high sensitivity and high resolution, resulting in better cancer management and outcome. In this study we developed a reporter gene system, derived from the ‘NanoBiT’ split-system, that enables multiplex bioluminescence (BLI) with radionuclide imaging using PET or SPECT.

Experimental design: We constructed a chimeric transmembrane reporter gene (TM-LgBiT) by fusion of LgBiT to a C-terminal transmembrane anchoring domain of platelet-derived growth factor receptor (PDGFR), for membrane expression on HEK-293T and PC-3 cells. Furthermore we conjugated the HiBiT peptide to DOTA chelator via a 6-amino hexanoic acid (Ahx) linker and radiolabeled it for single-photon emission-computed tomography (SPECT), yielding [^{111}In]In-DOTA-6-Ahx-HiBiT. *In vitro* characterization of reporter probes was followed by *in vivo* evaluation. We determined the characteristics of our reporter system using bioluminescence and radioactivity as detection techniques.

Results: We established a reliable procedure for labelling HiBiT peptide with indium-111, using the [^{111}In]In-DOTA-6-Ahx-HiBiT tracer we synthesized. Specific uptake of DOTA-6-Ahx-HiBiT was detected using bioluminescence imaging *in vitro* in cells, and *in vivo* from tumors cells expressing the TM-LgBiT reporter. After a preliminary SPECT/CT scan, we found specific [^{111}In]In-DOTA-6-Ahx-HiBiT tracer uptake in mice implanted with target positive cells which we confirmed using *ex vivo* biodistribution studies. Additionally, and importantly, uptake by tumours expressing TM-LgBiT was shown to be specific by blocking uptake with excess of unlabeled peptide.

Conclusion: We have generated and preliminary validated a novel multi-modality gene reporter system for cell tracking *in vivo* that has the potential to be applied in personalized health care for cell tracking in diagnostic/prognostic settings, or in therapeutic methods.

INTRODUCTION

Reporter genes represent a straightforward means to detect emerging tumor masses or cell based therapeutics (e.g. stem cells or immune cells) in mice. Multimodality molecular imaging is greatly contributing to non-invasive detection of engineered cells, allowing *in vivo* visualization and tracking, with high sensitivity and resolution, by combining optical, nuclear and magnetic resonance imaging modalities. The ability to monitor treatment efficacy, safety concerns and further biodistribution of target tracers, in an easy, non-invasive way will significantly influence the success rate of any given therapy¹.

There are already several reporter genes for visualization of engineered cells, including genes used preclinically such as fluorescence (FLI) and bioluminescence (BLI) imaging²⁻⁴, as well primarily clinical modalities, like positron emission tomography (PET/ SPECT), magnetic resonance imaging (MRI) and photoacoustic imaging⁵⁻⁷. In order to maximize the information gathered, these reporters, are usually co-expressed as fusion proteins or in tandem which enables multimodality imaging.

An attractive approach, that compensates for the limitations of individual imaging techniques, is the coupling of nuclear (SPECT/PET) with optical (BLI/FLI) imaging modalities. Here, SPECT/PET scans provide us with 3D images and quantitative analyses of reporter expression while optical imaging modalities (BLI/FLI) provide 2D images with high sensitivity of detection^{8,9}. Such approaches make use of specific reporter genes which can be detected in animals by administration of bioluminescence substrates (luciferins) or radiotracers^{8,9}. The strength of these technologies lies in the possibility to repeatedly and non-invasively image the same animal over time. More specifically multiplexing these techniques allows imaging of the location(s), time variation and magnitude of reporter gene expression with a reporter system incorporating radioisotope and optical imaging potential, thus providing more comprehensive information than either single modality on its own⁸. Nuclear reporter genes have been recently translated into the clinic for tracking therapeutic cells: cytotoxic T- cells have been engineered to express a chimeric antigen receptor (CAR) to target glioma cells, as well as a herpes simplex virus type 1 thymidine kinase (HSV1-TK), a dual reporter-suicide gene which selectively accumulates the PET tracer [¹⁸F]FHBG for tracking of injected cell localization and viability in glioma patients^{10,11}. Development of new generation reporter genes that are more specific and sensitive and that can be expressed in therapeutic cells, is essential to improve translation to the clinic and for a more customized and individualized imaging^{9,12,13}.

Herein we developed a unique, chimeric reporter gene, which enables simultaneous optical (BLI) and nuclear (SPECT/PET) tumor cell visualization. Our reporter gene encodes a reporter protein (LgBiT) that represents the large fragment of a bioluminescent split-system derived from NanoLuc luciferase^{14,15}. NanoLuc luciferase is ca. 100-fold brighter than Renilla or firefly luciferase, and another favourable property is its small size (19 kDa),

notably less than GFP (28kDa)¹⁶. The LgBiT reporter protein is, one of the split pieces of NanoLuc luciferase showing very little bioluminescence in the absence of its complementation partner HiBiT. We expressed and anchored LgBiT in the membrane of engineered cells through a C-terminal transmembrane anchoring domain of platelet-derived growth factor receptor (PDGFR), which is fused to the LgBiT marker, together with an HA tag. Our reporter gene is small (0.8 kB) and therefore easy to clone in viral vectors together with other genes, allowing multimodal and specific imaging of the tagged cells. The small part of the ‘NanoBiT’ split-system, the HiBiT tag (11 AA), reconstitutes the full NanoLuc protein spontaneously upon colocalization with LgBiT. HiBiT has nanomolar affinity for LgBiT¹⁶.

We now show that HiBiT can be labelled with radionuclides for targeting of (over) expressed reporters (LgBiT) on a cell membrane, making it attractive for multiplex BLI and radionuclide-based imaging¹⁷. In general, tracer peptides are very small (less than 50 AA), easy to synthesize, display very fast pharmacokinetics with high target selectivity, have a rapid clearance from the blood and non-target tissues and are generally non-immunogenic, properties that combine to give a high target to-background ratio *in vivo*¹⁷. Some pitfalls of peptide-receptor radionuclide imaging are; fast clearance from the target tissue, short biological half-life and renal elimination causing kidney toxicity. The delicate balance between these attributes is key to achieving the desired performance^{17,18}.

The purpose of this study was to evaluate the potential of TM-LgBiT, a chimeric reporter gene, and its linked tracer, DOTA-6-Ahx-HiBiT, for dual modality SPECT/ BLI *in vivo* imaging. To date no study has performed labeling of HiBiT, in order to bridge together optical (BLI) and nuclear imaging modalities (SPECT/PET). In the work presented here, we generated the DOTA-6-Ahx-HiBiT peptide and labelled it with indium-111. Furthermore, we developed a chimeric reporter gene (TM-LgBiT) and modified it for membrane expression, resulting in a unique translational reporter system, combining for the first time, radionuclide (SPECT/PET) and optical (BLI). We discovered that LgBiT and HiBiT have a strong tendency to form their native and active structures *in vivo* in small animals, but also that the small size of TM-LgBiT subunit (18 kDa)¹⁵, which when combined with the radioactively labeled HiBiT tag, allows multimodal and non-invasive *in vivo* cell imaging with both modalities.

RESULTS

Synthesis and Radiolabeling

The preparation of the peptide sequence, VSGWRLFKKIS, was performed following a *N*^α-Fmoc solid-phase peptide synthesis strategy. Coupling of the linker to the N-terminal valine residue was achieved using a commercially available Fmoc-6-Ahx-OH. Conjugation

tion of the chelate was carried out using DOTA-tris(*t*Bu) ester under basic conditions in the presence of PyBOP. Cleavage of the peptide from the solid support and concomitant removal of the protecting groups was performed under acidic conditions. Purification of the crude compound resulted in 16.8% yield. Radiolabeling of DOTA-Ahx-VS-GWRLFKKIS was setup with $^{111}\text{InCl}_3$ to give 97% radiochemical yield and a molar activity corresponding to 150 MBq/nmol. Stability studies were performed by incubation of [^{111}In]In-DOTA-Ahx-VS-GWRLFKKIS in PBS and mouse serum up to 4 h. The results showed that approximately 90% of the peptide remains intact up to 4 h after incubation in PBS, proving that the compound is barely sensitive to radiolytic degradation over this time period. However, in mouse serum, the obtained results indicate that the compound undergoes enzymatic degradation after 4 h incubation resulting in 72% intact ligand. Lipophilicity of [^{111}In]In-DOTA-Ahx-VS-GWRLFKKIS was determined by measurement of the $\text{LogD}_{7.4}$ value according to the shake-flask method. The $\text{LogD}_{7.4}$ value was -2.03 ± 0.72 , showing that our compound is hydrophilic and more prone to be cleared by the kidneys.

***In Vitro* Reporter Gene Expression on Engineered Cells**

We first assessed the functionality of TM-LgBiT protein as part of the NanoBiT system when expressed on the membrane or within the cytosol of PC-3 cells using BLI imaging. Luminescence signals were detected with the IVIS validating the expression of LgBiT reporter gene in transduced PC-3 cells and preserved 'HiBiT-TM-LgBiT' high affinity interaction; even lowest HiBiT peptide concentrations of 1 pM resulted in signal detection (Fig. 1A). Next, the HiBiT peptide was linked to DOTA for nuclear imaging purposes using different types of linkers. We evaluated binding affinity of DOTA-HiBiT and DOTA-6-Ahx-HiBiT towards the TM-LgBiT reporter expressed on HEK-293T. Results showed that the affinity of the HiBiT peptide for TM-LgBiT improved with about a 10-fold decrease in K_D value, indicating of an impaired future for *in vivo* studies (Fig. 1B). A calculation of the K_D value (reaction between TM-LgBiT reporter and HiBiT peptide), using one site specific binding function is shown in Figure 1B. The calculated K_D values were 6.8 nM for intact HiBiT peptide, 1.3 nM for HiBiT-DOTA-HiBiT and 0.7 nM for DOTA-6-Ahx-HiBiT that showed the highest affinity.

All further studies were carried out with HiBiT linked to DOTA-6-Ahx due to increased affinity towards TM-LgBiT.

***In Vitro* BLI Wash/ Non-Wash Binding & Radioactivity Cell Uptake Demonstrate Specificity**

We further examined the binding specificity of DOTA-6-Ahx-HiBiT and HiBiT, on control PC-3 and PC-3-TM-LgBiT cells based on obtained luminescence signals after furimazine addition (Fig. 1C, D). After addition of HiBiT peptide (10 nmol) to PC-3-TM-LgBiT

cells, and not washing the cells (removing peptide), we found that the signal was higher than from washed PC-3-TM-LgBiT cells, where the signal was almost absent (Fig. 1C). Compared to signals obtained by addition of HiBiT peptide to the reaction, there was a consistently higher signal (around 1.04E+02-fold) when DOTA-6-Ahx-HiBiT (10 nmol) was administered to PC-3-TM-LgBiT cells (Fig. 1D). Observing the control cell line (PC-3), we did not notice any signal after addition of original HiBiT or DOTA-6-Ahx-HiBiT peptide. For both peptides, the change in luminescent signals in different concentrations

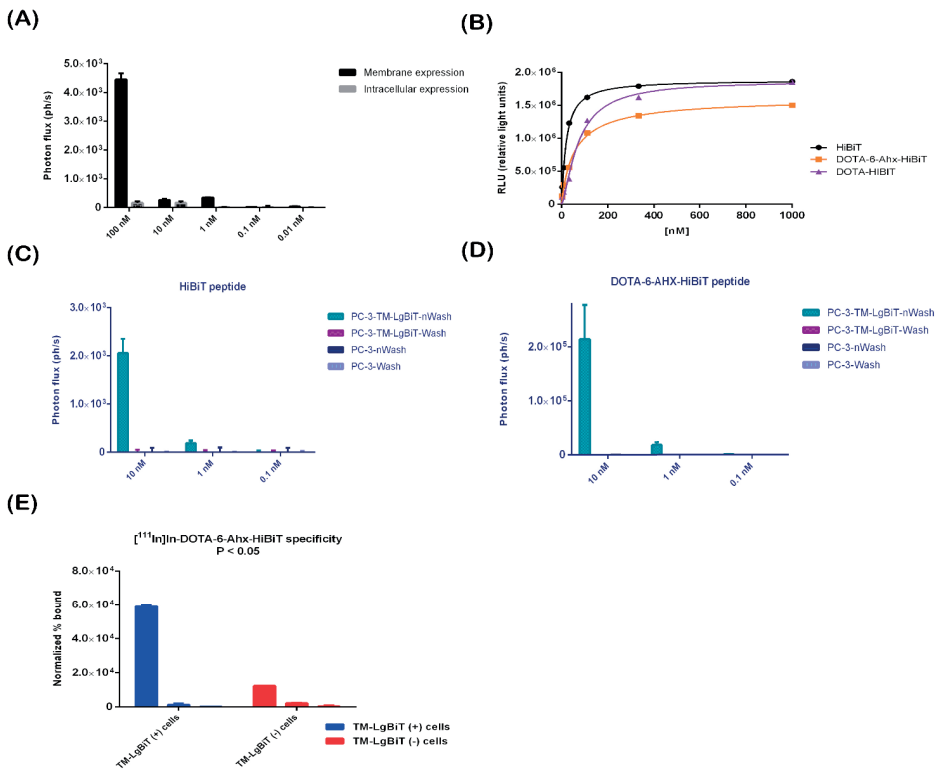


Figure 1. *In vitro* evaluation of TM-LgBiT expression and HiBiT probe affinity. Luminescence signals were detected at the IVIS, validating the expression of reporter (TM-LgBiT) when expressed on the membrane or within the cytosol of PC-3 cells, upon administration of different concentrations of HiBiT probe (A). To assess how the conjugation affects the HiBiT probe characteristics, functional and affinity data were obtained using one site specific binding function. The calculated K_D values; HiBiT= 6.8 nM; The DOTA-HiBiT= 1.3 nM and DOTA-6-Ahx-HiBiT= 0.7 nM. The equilibrium dissociation constant (K_D) was determined by a protocol, as suggested from the manufacturer (Promega) at the GloMax Multi Luminometer (B). DOTA-6-Ahx-HiBiT and HiBiT probes binding specificity was evaluated on TM-LgBiT-positive and-negative PC-3 cells based on obtained luminescence signals. DOTA-6-Ahx-HiBiT demonstrated high specificity for TM-LgBiT expressing PC-3 cells compared to controls (C, D). Specific binding after 1h of incubation with 10^{-9} M of [¹¹¹In]In-DOTA-6-Ahx-HiBiT in cells expressing TM-LgBiT in comparison to control cells. Shown results were performed in triplicates and values are indicated as means ± SD (E).

ranges can be clearly observed in figure 1 (C, D), evidently showing a signal decrease when the peptide is removed from cells in the ‘wash’ step. When we performed a similar assay, by using radioactive HiBiT peptide, we obtained a difference in radioactive signals between TM-LgBiT expressing and non-expressing cells, after incubation and washing, only when using a 1 nM concentration of peptide (Fig. 1E). The use of lower concentrations did not result in detectable difference probably because the washing step was affecting the results.

***In Vivo* BLI TM-LgBiT Sensitivity**

To assess reporter gene expression and the sensitivity of the BLI split-system *in vivo* with both, the native HiBiT peptide and its synthetic analogue DOTA-6-Ahx-HiBiT, we performed imaging studies with an IVIS in living mice (n=6) by subcutaneously injecting control PC-3 cells (n=3) and PC-3-TM-LgBiT cells (n=3) stably expressing the LgBiT reporter gene. The tumours were allowed to grow until they reached a palpable size of approx. ~ 4-6 mm in diameter. Prior to testing the *in vivo* system performance, we assessed background emission of LgBiT expressed from tumour cells (PC-3-TM-LgBiT) upon intraperitoneal administration of fluorofurimazine (NanoLuc *in vivo* substrate, 1.3 μ mol), allowing us to estimate autoluminescence of the LgBiT protein in this context. An average background signal of 2.63E+04 ph/s was detected, mostly coming from the abdomen. After separate i.v. injections of HiBiT peptides (native and DOTA-6-Ahx-HiBiT), the NanoBiT complex was successfully reconstituted into a functional enzyme, resulting in specific light emission coming from PC-3-TM-LgBiT tumours (Fig. 2A). Moreover, we detected a strong and specific bioluminescent signal emerging from NanoLuc luciferase, at the tumour site, 30 min post peptide administration (HiBiT and DOTA-6-Ahx-HiBiT) and 1 minute post substrate administration, with a significantly higher average maximum of 8.98E+05 ph/s for native HiBiT peptide and an average maximum of 5.84E+04 ph/s

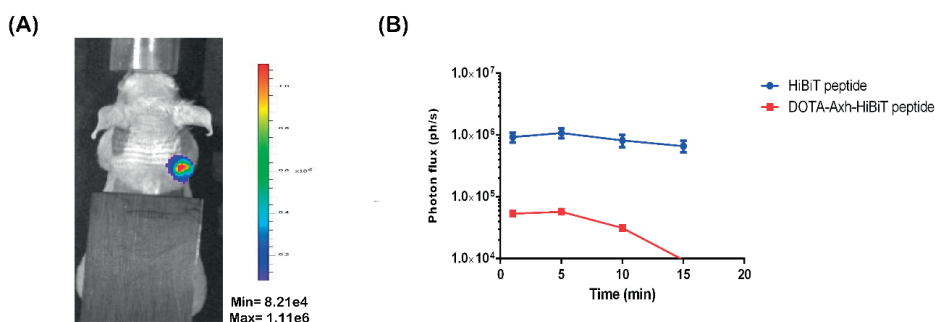


Figure 2. Longitudinal bioluminescence (BLI) imaging of HiBiT probe distribution in mice xenografts implanted with target (TM-LgBiT) positive tumors (A) A strong and specific bioluminescent signal was detected at the tumour site, 30 min post peptides (HiBiT and DOTA-6-Ahx-HiBiT), and 1 minute upon substrate administration, with an average maximum of 8.98E+05 ph/s for native HiBiT peptide and 5.84E+04 ph/s for DOTA-6-Ahx-HiBiT (B).

for DOTA-6-Ahx-HiBiT (Fig. 2B) These data were consistent across all mice bearing PC-3-TM-LgBiT tumors showing that we could detect reporter gene expression and enzyme complementation *in vivo* via BLI.

***In Vivo* SPECT/CT Scan & *Ex Vivo* Biodistribution**

We used HEK-293T-TM-LgBiT cells as a proof-of-principle cell line, and the PC3-TM-LgBiT cells as an oncology-relevant prostate cancer model cell line, in order to test our reporter system for nuclear SPECT/CT imaging. Initially nude mice were injected with HEK-293T cells expressing TM-LgBiT (right flank) and HEK-293T control cells (left flank) (n=3). The mice were subjected to a 1 h dynamic SPECT/CT after subcutaneous administration of 0.13 nmol/20 MBq of [¹¹¹In]In-DOTA-6-Ahx-HiBiT. HEK-293T-LgBiT cells showed specific uptake of peptide tracer with approx. 3.6-fold higher uptake than control HEK-293T at 1-hour post tracer administration (Fig. 3).

Moving into a tumor model, we implanted another set of nude mice with PC-3-TM-LgBiT cells (n=8). The tumors were allowed to grow until they reached a palpable size of approx. ~ 4-6 mm in diameter. Again the mice were subjected to a 1h dynamic SPECT/CT scan after i.v. administration of 0.13 nmol/20 MBq of

[¹¹¹In]In-DOTA-6-Ahx-HiBiT. As can be seen in figure 4A, the signal from target-positive tumor (PC-3-TM-LgBiT) is delineated, indicating the presence of [¹¹¹In]In-DOTA-6-Ahx-HiBiT on PC-3-TM-LgBiT site. This was confirmed by *ex vivo* biodistribution study (Fig. 4B), where the uptake of PC-3-TM-LgBiT tumors was shown to be 11.73% ID/g.

Non-specific background activity, predominantly in the kidneys (59.33% ID/g) and the tail (17.80% ID/g) was seen in all animals (Fig. 4B). In addition, tumor uptake was blocked by excess of unlabeled peptide further confirming [¹¹¹In]In-DOTA-6-Ahx-HiBiT specific inhibition. Co-injection of 13 nmol of DOTA-6-Ahx-HiBiT (100-fold excess) led to almost complete loss of tumor uptake (total of 2.30% ID/g). TM-LgBiT blocking with

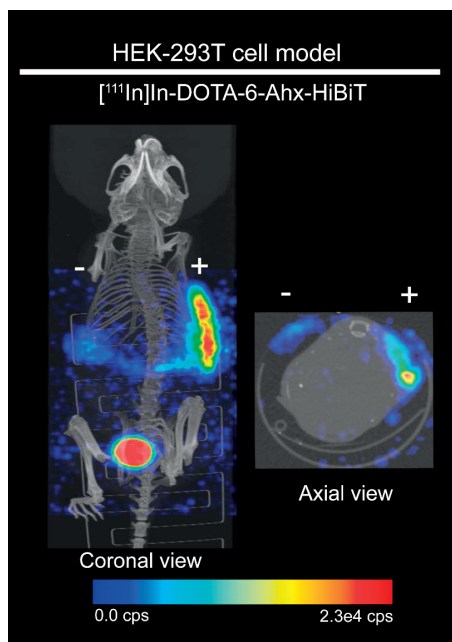


Figure 3. [¹¹¹In]In-DOTA-6-Ahx-HiBiT SPECT/CT imaging of mice implanted with target –positive and –negative HEK-293T cells. [¹¹¹In]In-DOTA-6-Ahx-HiBiT showed higher uptake (3.6-fold) in HEK-293T target positive cells (right flank,+) compared with the target negative HEK-293T cells (left flank, -) at 1h post subcutaneous administration of [¹¹¹In]In-DOTA-6-Ahx-HiBiT probe.

an excess of DOTA-6-Ahx-HiBiT led to an overall decrease in tissue and organ radioactivity with the exception of strong kidney uptake (45.81% ID/g) (Fig. 4B). Tumor-to-muscle uptake ratios for $[^{111}\text{In}]\text{In-DOTA-6-Ahx-HiBiT}$ in non-blocking mice were 11.24 ± 0.96 and for mice blocked with tracer excess 4.88 ± 0.04 (Fig. 4C).

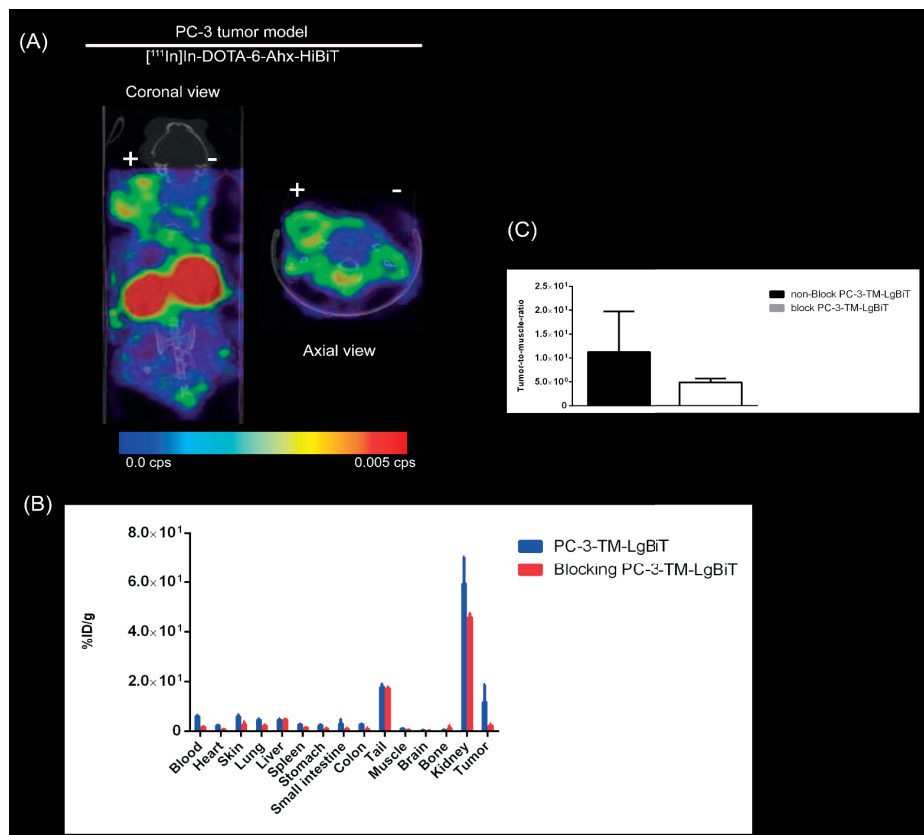


Figure 4. $[^{111}\text{In}]\text{In-DOTA-6-Ahx-HiBiT}$ SPECT/CT imaging and *ex vivo* biodistribution in PC-3 tumor xenografts. $[^{111}\text{In}]\text{In-DOTA-6-Ahx-HiBiT}$ showed higher uptake in the TM-LgBiT positive tumor (left flank, +) compared with the TM-LgBiT negative tumor (right flank, -) at 1h post i.v. administration of $[^{111}\text{In}]\text{In-DOTA-6-Ahx-HiBiT}$ tracer (A). *Ex vivo* biodistribution confirmed the $[^{111}\text{In}]\text{In-DOTA-6-Ahx-HiBiT}$ specificity (B). Tumor-to-muscle ratios of 11.24 ± 0.96 demonstrate specific uptake of $[^{111}\text{In}]\text{In-DOTA-6-Ahx-HiBiT}$ in TM-LgBiT positive tumor, with a reduced ratio in mice that were pre-administered with 100-fold excess of cold In-DOTA-6-Ahx-HiBiT (C).

Immunohistochemistry

To confirm the presence of TM-LgBiT in tumors, cryosections were analyzed with rabbit monoclonal antibody to HA tag present in the chimeric TM-LgBiT reporter construct. PC-3-TM-LgBiT tumors displayed a clearly visible signal (Fig. 5A), indicating of successful reporter expression, the staining was absent in control tumor sections (PC-3) (Fig. 5B).

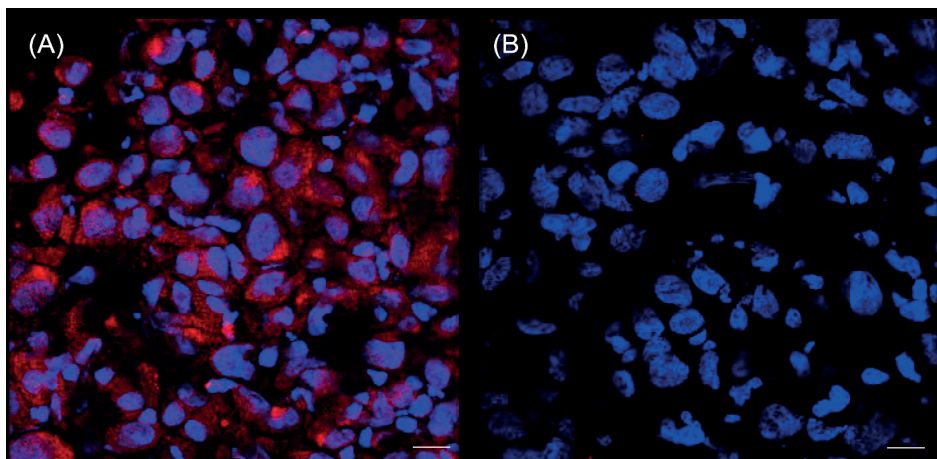


Figure 5. Characterization of xenograft tumor model. Prostate cancer (PC-3) was employed to establish a xenograft model with both target -positive (PC-3-TM-LgBiT) and -negative (PC-3) tumors. Immunostaining of tumor sections revealed TM-LgBiT staining in red (A), whereas the target negative tumors showed no signal (B). Size of the scale bar is 100 μm .

MATERIALS & METHODS

Synthesis of HiBiT Peptide

HiBiT (VSGWRLFKKIS), was synthesized using a $N\alpha$ -Fmoc solid-phase peptide synthesis strategy. The conjugation of Fmoc protected sequence (Val-Ser(tBu)-Gly-Trp(Boc)-Arg(Pbf)-Leu-Phe-Lys(Boc)-Lys(Boc)-Ile-Ser(tBu)) to the 2-chlorotrityl chloride resin was carried out in dimethylformamide (DMF) using hexafluorophosphate azabenzotriazole tetramethyl uronium (HATU) (3.8 equivalent) and *N,N*-diisopropylethylamine (DIPEA) (7.8 equivalent) for 45 minutes. Fmoc deprotection was accomplished by treatment of the resin with a 20% solution of piperidine in DMF. Amide formation and Fmoc deprotection were monitored by Kaiser test. Double couplings or Fmoc deprotection were performed when the reaction was not completed. The peptide synthesis was started by loading Fmoc-L-Ser(tBu)-OH (1.6 mmol, 4 equivalent) onto the solid support (0.25 g, loading capacity: 1.6 mmol/g). The resin was shaken for 90 min at room temperature. The resin was capped using dichloromethane/methanol/*N,N*-diisopropylethylamine (DCM/MeOH/DIPEA) (10 mL, 80:15:5, v/v/v) for 15 min at room temperature. Subsequent Fmoc deprotection and coupling with Fmoc-L-Ile-OH, Fmoc-L-Lys(Boc)-OH, Fmoc-L-Lys(Boc)-OH, Fmoc-L-Phe-OH, Fmoc-L-Leu-OH, Fmoc-L-Arg(Pbf)-OH, Fmoc-L-Trp(Boc)-OH, Fmoc-Gly-OH, Fmoc-L-Ser(tBu)-OH and Fmoc-L-Val-OH were achieved with 4 equivalents of the respective protected amino acids following the protocol described above.

Synthesis of DOTA-6-Ahx-HBiT Conjugate

Conjugation of the linker to the N-terminal valine residue was accomplished by using Fmoc-6-Ahx-OH (2 equivalent), HATU (3.8 equivalent) and DIPEA (7.8 equivalent) in DMF. The resin was stirred for 2 h at room temperature. Then, the resin was washed thrice with DMF and the Fmoc protecting group was removed by treatment of the resin with a 20% solution of piperidine in DMF. DOTA-tris(tBu) ester (3 equivalent) was coupled to the peptide in presence of benzotriazol-1-yl-oxytripyrrolidinophosphonium hexafluorophosphate (PyBoP) (3 equivalent), DIPEA (6 equivalent) and DMF. The reaction was carried out overnight at room temperature. Cleavage of the peptide from the solid support and its concomitant global deprotection were performed by treatment of the resin with a solution of trifluoroacetic acid/water/triisopropylsilane (TFA/H₂O/TIPS) (95:2.5:2.5, v/v/v) for 6 h at room temperature. Upon filtration, the filtrate was collected, and the solvent was evaporated under vacuum. Trituration of the residue with cold diethyl ether gave the final crude product, which was purified by HPLC to give pure DOTA-6-Ahx-VSGWRLFKKIS, as a white solid (12 mg, 16.8%). ESI-MS: m/z 910.80 [M + 2H]²⁺, 922.21 [M + Na + H]²⁺ and 930.19 [M + 2Na]²⁺.

Radiolabelling of DOTA-6-Ahx- HiBiT Peptide

¹¹¹InCl₃ (93.3 μL, 150 MBq) was added to a mixture of DOTA-6-Ahx-VSGWRLFKKIS (1 nmol), ascorbic acid/gentisic acid (10 μL, 50 mM), sodium acetate (1 μL, 2.5 M) and H₂O (29.7 μL). The mixture was incubated for 20 min at 90°C. The reaction was monitored by instant thin-layer chromatography (iTLC) on silica gel impregnated glass fiber sheets eluted with a solution of sodium citrate (0.1 M, pH 5.0). The reaction mixture was cooled down for 5 min and diethylenetriaminepentaacetic acid (DTPA) (5 μL) was added to complex the remaining free indium-111. The radiochemical yield and molar activity of [¹¹¹In] In-DOTA-6-Ahx-VSGWRLFKKIS were determined to be 93 % and 150 MBq/nmol, respectively.

Cell Lines and Cell Culture Conditions

Human embryonic kidney 293T cells (HEK-293T) and human prostate cancer cell line (PC-3) were used for purposes of this study. Human embryonic kidney (HEK-293T) cells were grown in Dulbecco's Modified Eagle's Medium (DMEM) (Sigma-Aldrich) and the PC-3 cell line was cultured in Roswell Park Memorial Institute (RPMI) 1640 Medium (Sigma, St. Louis, MO, USA). Both cell lines were supplemented with 10% fetal bovine serum and 1% penicillin/streptomycin. Cells were cultured in T-175 flasks (Thermo Fisher Scientific) until reaching confluence.

Construction of Chimeric Transmembrane LgBiT reporter (TM-LgBiT) and Cell Transduction

Vector production and cell transduction were performed under appropriate biosafety level conditions (ML-II) in accordance with the National Biosafety Guidelines and Regulations for Research on Genetically Modified Organisms (GMO permit 99-163 from the Bureau of genetically modified organisms, The Netherlands). Procedures and protocols were reviewed and approved by the EMC Biosafety Committee. The transmembrane LgBiT sequence (TM-LgBiT) was created by construction of pCDH1-LgBiT-EF1-copGFP lentiviral vector. Initially we cut the pDisplay vector (Thermo Fisher, Massachusetts, USA), a mammalian expression vector that allows display of proteins on the

cell surface, with restriction enzymes Bgl II and Sal I in NEB 3.1 from New England BioLabs. The LgBiT gene was amplified from the vector pBIT1.3.-C[LgBiT] (Promega) using the following primers; forward primer with a forward Sal I restriction site 5'-GTC-GACGCTGTTGATGGTTAC TCGGAAC-3' and 5'-AGATCTGTCTTCACACTC-GAAGATTTTC G-3' and a reverse primer with a Bgl II restriction site. The amplified PCR product (LgBiT gene) was cloned in the above-prepared pDisplay recipient vector to create the pDisplay-TM-LgBiT vector using Sal I and Bgl II restriction sites. Furthermore, in order to enable cell sorting and stable expression of TM-LgBiT in cells of interest, we cut the pCDH1-MCS2-EF1-copGFP vector (Addgene, Cambridge, MA, USA), a mammalian expression vector, with restriction enzymes BamHI and NotI in NEB 3.1 Buffer from New England BioLabs. The LgBiT sequence was cut from the above created vector construct (pDisplay-TM-LgBiT) with BamHI and NotI restriction enzymes (New England Biolabs) and inserted into the cloning site of the cut pCDH1-MCS2-EF1-copGFP Vector (Addgene, Cambridge, MA, USA). A self-inactivating lentivirus pCDH-EF1-LgBiT-copGFP was produced by transfection of HEK-293T packaging cells by transient transfection of HEK-293T cells with three packaging plasmids pCMV-VSVG, pMDLg-RRE, pRSV-REV (Addgene, Cambridge, MA, USA) and PEI transfection reagent 1 mg/mL per μg DNA as previously described in detail by Mezzanote et al.¹⁹ After 48 and 72 hours, the lentiviral supernatant was collected and filtered through a 0.45 μm membrane. Viral quantification was performed by use of a standard antigen capture HIV p24 ELISA (ZeptoMetrix, Bu_alo, NY, USA). PC-3 cells were grown in culture dishes until 70% confluence and were infected with the above described lenti-viral stock, with a final result of transmembrane LgBiT expression. Cells were transduced by addition of pseudoviral particles containing the chimeric transmembrane construct (40 ng virus per 1×10^5 cells) in the presence of polybrene (hexametride bromide, Sigma-Aldrich) at a final concentration of 8 $\mu\text{g}/\text{mL}$. Stable clones were sorted for GFP expression using FACS (BD-FACS AriaIII, BD Biosciences). Transgene expression was confirmed by the presence of the green fluorescent protein copGFP from (excitation/emission maximum = 475/509 nm).

Construction of LgBiT Reporter for Cytosolic Expression

Vector production and cell transduction were performed under appropriate biosafety level conditions (ML-II) in accordance with the National Biosafety Guidelines and Regulations for Research on Genetically Modified Organisms (GMO permit 99-163 from the Bureau of genetically modified organisms, The Netherlands). Procedures and protocols were reviewed and approved by the EMC Biosafety Committee. To create the pCDH-EF1-ATG-LgBiT-T2A-copGFP lentiviral vector we first excised the 1929 luciferase gene from the vector pCDH-EF1-ATG-1929-T2A-copGFP (Promega) with restriction enzymes BamHI and NotI in NEB buffer 3.1. from New England Biolabs. The LgBiT gene was amplified from the vector pBIT1.3-C[LgBiT] (Promega) using the following primers; forward primer with a NotI restriction site 5'-GGGTTTAAACTTAGCTGTTGATG-GTTACTC-3' and 3'-GGATCCATGCTGGCTCGAGCGGTGG-5' with a BamHI restriction site. The amplified PCR product (LgBiT gene) was cloned in the above prepared pCDH-EF1-ATG-T2A-copGFP recipient vector to create the pCDH-EF1-ATG-LgBiT-T2A-copGFP vector using the NotI and BamHI restriction sites. A self-inactivating lentivirus (pCDH-EF1-LgBiT) was produced by transfection of HEK-293T packaging cells by transient transfection of HEK-293T cells with three packaging plasmids (pCMV-VSVG, pMDLg-RRE, pRSV-REV; Addgene) which were previously described in detail¹⁹ using PEI transfection reagent (1mg/mL) per μ g DNA. Lentiviral supernatant was collected after 48 and 72 hours and filtered (0.45mm). Subsequent quantification of virus was performed using a standard antigen-capture HIV p24 ELISA (ZeptoMetrix). The PC-3 cell line, expressing LgBiT in the cytosol was produced as previously described by Gaspar et al.²⁰. PC-3 cells were grown in culture dishes to 50% confluence in culture medium and were infected with the lenti-viral stock, resulting in LgBiT expression. Cells were transduced with MOI 1 particle per cell of pCDH-EF1-LgBiT-T2A-copGFP, lentivirus in the presence of polybrene (hexamethide bromide, Sigma-Aldrich) at the final concentration of 8 μ g/mL. Stable clones were selected via the limited dilution method.

HEK-293T cells were seeded in a T-25 flask at a density of 500,000 cells and transduced with either EF1-NanoLuc-T2A-copGFP lentivirus²¹ plus polybrene (hexamethidine bromide) (Sigma) at a final concentration of 8 μ g/mL. Cells were sorted for GFP expression using FACS (BD-FACS AriaIII, BD Biosciences). Transgene expression was confirmed by the presence of the green fluorescent protein copGFP from (excitation/emission maximum= 475/509 nm).

Functionality Assessment of TM- LgBiT Expression

PC-3 cells stably expressing LgBiT reporter at the membrane (TM-LgBiT) and PC-3 cells stably expressing LgBiT within the cytosol, were seeded with an equal seeding density (50,000 cells/well) in a black 96-well plate (Greiner-Bio-One, Frickenhausen, Germany). HiBiT peptide was added to the wells in dilutions ranging from 100 nM-1pM containing

the NanoLuc substrate (furimazine), prepared as suggested from the manufacturer (1:50 dilution in PBS). Bioluminescence signals from wells were acquired at the GloMax® Microplate Reader (Promega) with 1s acquisition time, immediately after peptide+substrate solution addition. Measurements were performed at room temperature 18-20°C. Experiments were performed in triplicates and were repeated three times. All data were plotted using GraphPad Prism.

Binding Affinity of Native HiBiT, DOTA-6-Ahx-HiBiT and DOTA-HiBiT peptides to TM-LgBiT Reporter

The equilibrium dissociation constant (K_D) was determined by a protocol, as suggested from the manufacturer (Promega) at the GloMax Multi Luminometer (Promega). An OptiMEM solution with 10% Fetal Bovine Serum (FBS) was prepared where the LgBiT protein from the Nano-Glo® HiBiT Lytic Detection System (Promega N3030) was diluted to a final concentration of 2 nM (each 500 μ L) with a starting concentration of 200 nM in OptiMEM plus 10% FBS. A three-time dilution series of synthesized peptides (DOTA-6-Ahx-HiBiT, DOTA-HiBiT) and native HiBiT was prepared and diluted: 150 μ L of peptide solution with 350 μ L of OptiMEM plus 10% FBS. 90 μ L of the above prepared solutions were added in triplicates to a white assay plate (Costar 3600) and 10 μ L of 2 nM LgBiT solution (0.2 nM final concentration) was added to the wells with the peptide solutions and was incubated on an orbital shaker for 30 minutes at 600 RPM. A solution of furimazine (Promega) and

1 mM DTT (Thermo Fisher Scientific) was prepared in OptiMEM plus 10% FBS and 10 μ L was added to each well with the peptide solutions plus LgBiT. The plate was incubated on orbital shaker at 600 RPM for 5 minutes, after addition of the solution. Luminescence was measured at the GloMax Multi Luminometer (Promega) with 0.5 s integration time per well. K_D was calculated using GraphPad Prism- one site specific binding.

***In Vitro* Wash/ non-Wash Bioluminescence Assay**

Both, target expressing (PC-3-TM-LgBiT) and target non-expressing (PC-3) cells, were seeded in a black 96-well plate (Greiner-Bio-One, Frickenhausen, Germany), typically 10 000 cells per well. The next day, medium from the wells, was removed. 3 different concentrations (10 nmol, 1 nmol and 0.1 nmol) of either DOTA-6-Ahx-HiBiT or original HiBiT peptide were added to the wells in a final volume of 100 μ L. The cells were incubated for 4 h at 37°C. After the incubation step, for cells from the 'washing' assay, supernatant, either containing HiBiT or DOTA-6-Ahx-HiBiT peptide, was removed and the cells were washed three times with phosphate-buffered saline (PBS) (Lonza). The NanoLuc substrate, furimazine, from the Nano-Glo Luciferase Assay System (Promega), with a final concentration of 0.01 mmol, was added to all wells, both, washed and non-washed.

Luminescence images were acquired at the GloMax® Microplate Reader (Promega) immediately after substrate addition. For measurement of total luminescence, we used 1 s of integration time. Measurements were performed at room temperature 18-20°C. Experiments were performed in triplicates and were repeated three times. All data were plotted using GraphPad Prism.

***In Vitro* Radioactivity Cell Uptake Assay**

The membrane-bound fraction of [¹¹¹In]In-DOTA-6-Ahx-HiBiT radiotracer was determined after incubation with 3 different concentrations of [¹¹¹In]In-DOTA-6-Ahx-HiBiT with HEK-293T-TM-LgBiT cells, and control cells not expressing TM-LgBiT (HEK-293T). 24 h before the uptake experiment, cells were seeded in 24-well plates (100 000 cells/ well) (Greiner-Bio-One, Frickenhausen, Germany). Next day, cells were incubated with 1x10⁻⁸ M, 1x10⁻⁹ M and 1x10⁻¹⁰ M of [¹¹¹In]In-DOTA-6-Ahx-HiBiT in 1 mL of culture medium for 1 h at 37°C. After the incubation step, cells were placed on ice, the supernatant was removed and the cells were washed three times with ice-cold phosphate-buffered saline (PBS) (Lonza). In order to determine the membrane-bound fraction of peptide tracer ([¹¹¹In] In-DOTA-6-Ahx-HiBiT), cells were incubated for 10 min with an acid solution (50 mM glycine and 100 mM NaCl, pH 2.8). The membrane-bound fraction of radiotracer was counted in an γ -counter (1480 WIZARD automatic γ counter; PerkinElmer) using a radionuclide-specific energy window, a counting time of 60 s, and a counting error of 5% or less. Data are expressed as percentage added dose.

***In Vivo* BLI**

All animal experiments were approved by the Bioethics Committee of Erasmus MC, Rotterdam, The Netherlands, and performed in accordance with national guidelines and regulations established by the Dutch Experiments on Animal Act (WoD) and by the European Directive on the Protection of Animals used for scientific purpose (2010/63/EU). BALB/c nude (males) were obtained from Charles River Laboratory (The Netherlands). All mice aged 8 weeks were provided access to food and water ad libitum and were hosted in the animal facility at the Erasmus MC, Rotterdam, The Netherlands.

Prior i.v. peptide administration (HiBiT and DOTA-6-Ahx-HiBiT) background signal was estimated: tumour bearing mice (PC-3-TM-LgBiT) were intraperitoneally (i.p) injected with the recently formulated, water soluble substrate, the fluorofurimazine (FFz), with a final concentration of 1.3 μ mol in a total volume of 120 μ L. Mice were anesthetized with isoflurane (1.5%) and imaged post substrate administration at the IVIS Spectrum (PerkinElmer). Prone BLI images were acquired at the IVIS, exposure time 30s. As for the bioluminescence light assessment, nude BALB/c mice (n=6) with subcutaneously implanted PC-3-TM-LgBiT cells, stably expressing TM-LgBiT, were intravenously injected with 1 nmol of either native HiBiT peptide (n=3) or 1 nmol of DOTA-6-Ahx-HiBiT

(n=3), both in a total volume of 100 μ L. 30 min post peptide administration, all mice received an intraperitoneal (i.p.) injection of FFz (1.3 μ mol/120 μ L). Mice were kept under isoflurane anaesthesia (1.5%) and a series of images were taken using an IVIS Spectrum (PerkinElmer) with open filter; binning=medium, field of view=12.9 \times 12.9 cm, f/stop=1 and 1 min exposure time every 5 minutes for 20 minutes. Data analysis was performed by drawing ROIs in the images taken at the peak of bioluminescence emission.

***In vivo* SPECT/CT**

For the subcutaneous skin HEK-293T-LgBiT model, 8–10 week old BALB/ c nude (males) mice (n=3) received were implanted with 1×10^6 HEK-293T-TM-LgBiT cells in the right flank and 1×10^6 HEK-293T (control) in the left flank. As for the subcutaneous tumor model, eight-week-old nude BALB/C male mice (n=12) were injected with 5×10^6 PC-3-TM-LgBiT expressing cells (n=8) and with 5×10^6 PC-3 cells (control, n=4). Both cell lines were prepared for injections in PBS (Sigma-Aldrich) and matrigel (Corning) solution with a 50:50 ratio and a final injectable volume of 50 μ L. Tumors were left to grow approximately 3-4 weeks post tumor cell implantation. To determine the functionality of our imaging system, a dynamic whole body SPECT/CT scan (VECT/CT Milabs) was performed. Mice were anesthetized using 1-2% isoflurane/O₂ and the body temperature was maintained at 37°C during the time of imaging (1h) by using a heated bed aperture. The 1-hour dynamic SPECT/CT scan was performed immediately after tail vein injection of [¹¹¹In]In-DOTA-6-Ahx-HiBiT for the PC-3 tumor model, or subcutaneous injection of [¹¹¹In]In-DOTA-6-Ahx-HiBiT in case of the HEK-293T cell model, (20 MBq labeled to 0.13 nmol in 200 μ L PBS). In order to determine the effect of unlabeled peptide on PC-3 tumour uptake, 13 nmol of DOTA-6-Ahx-HiBiT (approximately 100-fold excess), was co-injected along with [¹¹¹In]In-DOTA-6-Ahx-HiBiT (n=4). Dynamic scans were obtained over a total duration of 1 h with 30 time frames, directly after injection of [¹¹¹In] In-DOTA-6-Ahx-HiBiT. Acquired images were reconstructed using SR-OSEM with 9 iterations and 128 subsets on a 36 \times 36 \times 35 mm matrix with 0.80 \times 0.80 mm isotropic voxels. The images were further analyzed in Pi-Mod and VivoQuant. Regions of interest were manually drawn around the tumors, heart, and muscle. Subsequently, the percentage of injected dose (%ID) and the tumor to background ratio (TBR) were determined.

***Ex Vivo* Analysis: Biodistribution**

Mice were sacrificed and dissected one hour after tail vein injection of approx. 20 MBq [¹¹¹In] In-DOTA-6-Ahx-HiBiT peptide (n=4 per treated group/control). The organs (blood, heart, skin, lungs, liver, spleen, stomach, small intestine, colon, tail, muscle, brain, tumor, kidney and bone) were weighted and the radioactivity uptake in tumor and other organs was determined and expressed as percentage injected dose per gram of tissue (%ID/g). Tumors and organs were counted in a γ -counter (PerkinElmer). Counting

time was 60 s per sample with an isotope-specific energy window and a counting error not exceeding 5%. After counting, the tumors were frozen in liquid nitrogen for further analysis.

Immunofluorescence Staining

For immunofluorescence staining of tumor tissue, frozen xenografts were embedded in Tissue-Tek O.C.T Compound (Sakura Finetek,) and trimmed by cryostat (10 μm) and transferred to glass slides (Thermo Fisher Scientific). Xenografts were fixed with 4% formalin for 15 minutes at room temperature. After washing with PBS (Sigma-Aldrich), the sections were blocked with 5% normal serum + 0.3 M glycine (Sigma-Aldrich) in TBS/Tween for 1 hour at room temperature. Again, slides were washed in PBS and further on incubated with primary rabbit monoclonal antibody to HA tag (ab236632; abcam); in a ratio of 1:300 in TBS/Tween + 1% normal serum, in a wet chamber over night at 4°C. Next day, after the washing step with PBS, the sections were incubated with the secondary antibody, goat anti-rabbit Alexa Fluor 594 nm (ab150080; abcam) in a ratio of 1:1000 in TBS/Tween + 1% normal serum for 1 hour at room temperature. The slides were washed with PBS; the nuclei were stained with Hoechst (Thermo Fisher Scientific) in a ratio of 1:1000 in TBS for 5 minutes at room temperature. Slides were rinsed in distilled water and mounted with prolong diamond antifade (Thermo Fisher Scientific) and analyzed by fluorescent microscopy (Leica Microsystems).

Statistical Analysis

Analysis of the data output, was performed using column statistics (T test). Where more than two groups were compared one-way ANOVA, followed by Tukey's t-test. All statistical analysis was performed using GraphPad Prism version 8 for Windows. Data from each conditions or animal group were presented as means and SD. The results were statistically significant when $p < 0.05$.

Data Availability

The authors confirm that all relevant data are included in the paper and/ or its supplementary information files. Other data that support the findings of this study are available from the corresponding author on request.

DISCUSSION

In this study we developed a chimeric reporter gene for stable transmembrane (TM) expression of the large NanoLuc subunit, the TM-LgBiT, for multimodality imaging purposes, when combined with a radiolabeled HiBiT peptide probe.

To the best of our knowledge, this is the first report of a reporter gene that supports *in vivo* bioluminescence imaging (BLI), in addition to nuclear (SPECT/PET) modalities, and is derived from the NanoBiT split-luciferase system. Within this study, we cover radiolabeling, *in vitro* characterization, *in vivo* biodistribution studies to BLI and SPECT/CT imaging of implanted HEK-293T-LgBiT cells and PC-3-LgBiT tumors in mice.

Initially, we engineered cells (HEK-293T and PC-3) with the TM-LgBiT reporter gene where we demonstrated the ability to image cells, both in culture and *in vivo* in nude mice, via both imaging modalities. Such an approach offers several advantages. The NanoLuc luciferase gene (NLuc), in combination with its substrate fluorofurimazine (FFz), allows us to directly visualize engineered cells *in vivo*. In preclinical small animal cancer models, BLI genes are valuable tools which are relatively inexpensive and allow one to track cell migration, access cell viability and follow cell/ tumor growth longitudinally²². In clinical settings, the leading imaging technologies are radionuclide technologies like SPECT and PET, where the level of measured radioactivity is a direct correlation with the amount of trapped tracer in the desired tissue^{23,24}. Since radioisotope emission is not attenuated by body mass and other factors, like optical modalities⁹, it allows 3D detection of signals in deep tissue.

We then set out to engineer HiBiT peptide conjugates (DOTA-HiBiT and DOTA-6-Ahx-HiBiT) enabling SPECT/CT imaging. Upon conjugation to the DOTA chelator and the DOTA-6-Ahx chelator-linker complex, the affinity of HiBiT conjugates was significantly increased, in comparison to native HiBiT peptide ($K_D = 6.8$ nM); the lowest K_D value of 0.7 nM (highest affinity towards TM-LgBiT reporter protein) was measured for DOTA-6-Ahx-HiBiT (Fig. 1B). These results were unforeseen, since other reported conjugates have caused an impairment of binding upon conjugation with chelators and linkers²⁵⁻²⁸, but we believe this unexpected result can be explained by the increased hydrophilicity of our DOTA labeled peptide.

Considering that successful *in vivo* interaction between TM-LgBiT and HiBiT is dependent on the bioavailability of the HiBiT peptide conjugate, and its affinity at physiological temperature, we initially investigated if PC-3-TM-LgBiT tumors could be visualized via BLI imaging using HiBiT or HiBiT-6-Ahx-DOTA. The BLI signal obtained was significantly higher than background, unequivocally detecting tumor cells in mice 4 weeks post tumor cell implantation (Fig. 2). This means that both HiBiT and HiBiT-6-Ahx-DOTA peptides may be employed as imaging tags to follow *in vivo* distribution of small molecules, drugs or antibodies to target tissues (expressing TM-LgBiT) with BLI.

Initial, proof-of-concept *in vivo* SPECT/CT studies administering HEK-293T cells expressing TM-LgBiT and [¹¹¹In]In-DOTA-6-Ahx-HiBiT tracer subcutaneously to nude mice, revealed a clear difference in uptake of approx. 3.6 fold difference in favor of target-positive cells, indicating the specificity of our probes (Fig. 3). Next, we evaluated a prostate cancer tumor model, stably expressing TM-LgBiT on the cell membrane, with

the [¹¹¹In]In-DOTA-6-Ahx-HiBiT tracer administered i.v. This model revealed a slight difference in tracer uptake (>2%) in favor of target-positive tumors (Fig. 4A) at 1 hour. Importantly, with the exception of the kidneys, no other tissue showed significant signal, indicating that HiBiT peptide is not actively uptaken in non-target tissues. Other reporter genes for radionuclide imaging derived from human receptors have the disadvantage of uptake in tissues where the receptors are expressed (e.g. hNIS reporter shows uptake in salivary glands, thyroid and stomach²⁹).

Blocking studies with a 100-fold excess of cold labelled peptide decreased the SPECT signals in tumors and other organs, demonstrating successful blocking of complementation of the HiBiT conjugate with LgBiT *in vivo*. Future work will focus on further optimization of the system by injecting higher concentrations of HiBiT tracer (e.g. 1 nmol) to animals, in order to enhance ‘HiBiT-TM-LgBiT’ interaction and obtain more tracer uptake at the target site. Evaluating the most suitable imaging time point after probe administration will also be essential for protocol optimization.

The stable expression of our chimeric reporter gene (TM-LgBiT), that we clearly demonstrate in our preliminary study, represents a valuable tool in diagnostics. It will allow indirect labeling of many cell types, including T- cell therapies or other therapeutic cells, allowing noninvasive disease monitoring and yielding whole body information via optical and SPECT/PET imaging modalities in living subjects. This will allow rapid evaluation of anatomical localization of engineered cells and also their viability via BLI.

Ultimately, we believe that these tools, not only are useful for clinical cell-based therapies, but also are extremely useful in preclinical studies for investigating cancer progression/ regression, metastatic burden, and treatment.

REFERENCES

- 1 Gambhir, S. S. Molecular imaging of cancer with positron emission tomography. *Nat Rev Cancer* **2**, 683-693 (2002).
- 2 Prescher, J. A. & Contag, C. H. Guided by the light: visualizing biomolecular processes in living animals with bioluminescence. *Curr Opin Chem Biol* **14**, 80-89 (2010).
- 3 Hong, H., Yang, Y. & Cai, W. Imaging gene expression in live cells and tissues. *Cold Spring Harb Protoc* **2011**, pdb top103 (2011).
- 4 Kim, J. E., Kalimuthu, S. & Ahn, B. C. In vivo cell tracking with bioluminescence imaging. *Nucl Med Mol Imaging* **49**, 3-10 (2015).
- 5 Li, M., Wang, Y., Liu, M. & Lan, X. Multimodality reporter gene imaging: Construction strategies and application. *Theranostics* **8**, 2954-2973, doi:10.7150/thno.24108 (2018).
- 6 Gilad, A. A. & Shapiro, M. G. Molecular Imaging in Synthetic Biology, and Synthetic Biology in Molecular Imaging. *Mol Imaging Biol* **19**, 373-378 (2017).
- 7 Kang, J. H. & Chung, J. K. Molecular-genetic imaging based on reporter gene expression. *J Nucl Med* **49 Suppl 2**, 164S-179S (2008).
- 8 Kang, J. & Chung, J.-K. Molecular-Genetic Imaging Based on Reporter Gene Expression. *Journal of nuclear medicine: official publication, Society of Nuclear Medicine* **49 Suppl 2**, 164S-179S, doi:10.2967/jnumed.107.045955 (2008).
- 9 Akins, E. J. & Dubey, P. Noninvasive Imaging of Cell-Mediated Therapy for Treatment of Cancer. *Journal of Nuclear Medicine* **49**, 180S, doi:10.2967/jnumed.107.045971 (2008).
- 10 Yaghoubi, S. S. *et al.* Noninvasive detection of therapeutic cytolytic T cells with 18F-FHBG PET in a patient with glioma. *Nat Clin Pract Oncol* **6**, 53-58 (2009).
- 11 Keu, K. V. *et al.* Reporter gene imaging of targeted T cell immunotherapy in recurrent glioma. *Sci Transl Med* **9**, eaag2196, doi:10.1126/scitranslmed. aag2196 (2017).
- 12 De, A., Lewis, X. Z. & Gambhir, S. S. Noninvasive imaging of lentiviral-mediated reporter gene expression in living mice. *Mol Ther* **7**, 681-691 (2003).
- 13 Haywood, T. *et al.* Positron emission tomography reporter gene strategy for use in the central nervous system. *Proceedings of the National Academy of Sciences* **116**, 11402, doi:10.1073/pnas.1901645116 (2019).
- 14 Dixon, A. S. *et al.* NanoLuc Complementation Reporter Optimized for Accurate Measurement of Protein Interactions in Cells. *ACS Chemical Biology* **11**, 400-408, doi:10.1021/acscchembio.5b00753 (2016).
- 15 Hall, M. P. *et al.* Engineered luciferase reporter from a deep sea shrimp utilizing a novel imidazopyrazinone substrate. *ACS Chem Biol* **7**, 1848-1857 (2012).
- 16 Schwinn, M. K. *et al.* CRISPR-Mediated Tagging of Endogenous Proteins with a Luminescent Peptide. *ACS Chemical Biology* **13**, 467-474, doi:10.1021/acscchembio.7b00549 (2018).
- 17 Laverman, P., Sosabowski, J. K., Boerman, O. C. & Oyen, W. J. G. Radiolabelled peptides for oncological diagnosis. *Eur J Nucl Med Mol Imaging* **39 Suppl 1**, S78-S92, doi:10.1007/s00259-011-2014-7 (2012).
- 18 Mather, S. J. *et al.* Selection of Radiolabeled Gastrin Analogs for Peptide Receptor-Targeted Radionuclide Therapy. *Journal of Nuclear Medicine* **48**, 615, doi:10.2967/jnumed.106.037085 (2007).
- 19 Mezzanotte, L., An, N., Mol, I. M., Löwik, C. W. G. M. & Kaijzel, E. L. A New Multicolor Bioluminescence Imaging Platform to Investigate NF- κ B Activity and Apoptosis in Human Breast Cancer Cells. *PLOS ONE* **9**, e85550 (2014).

- 20 Gaspar, N. *et al.* NanoBiT System and Hydrofurimazine for Optimized Detection of Viral Infection in Mice-A Novel in Vivo Imaging Platform. *Int J Mol Sci* **21** (2020).
- 21 Gaspar, N. *et al.* Evaluation of NanoLuc substrates for bioluminescence imaging of transferred cells in mice. *J Photochem Photobiol B* **216**, 112128 (2021).
- 22 Parkins, K. M. *et al.* A multimodality imaging model to track viable breast cancer cells from single arrest to metastasis in the mouse brain. *Sci Rep* **6**, 35889 (2016).
- 23 Cherry, S. R. & Gambhir, S. S. Use of Positron Emission Tomography in Animal Research. *ILAR Journal* **42**, 219-232, doi:10.1093/ilar.42.3.219 (2001).
- 24 Chatziioannou, A., Tai, Y. C., Doshi, N. & Cherry, S. R. Detector development for microPET II: a 1 microl resolution PET scanner for small animal imaging. *Phys Med Biol* **46**, 2899-2910 (2001).
- 25 Fani, M. *et al.* PET of somatostatin receptor-positive tumors using ⁶⁴Cu- and ⁶⁸Ga-somatostatin antagonists: the chelate makes the difference. *J Nucl Med* **52**, 1110-1118 (2011).
- 26 Zhang, X. *et al.* Improved Tumor Targeting and Longer Retention Time of NIR Fluorescent Probes Using Bioorthogonal Chemistry. *Theranostics* **7**, 3794-3802, doi:10.7150/thno.20912 (2017).
- 27 Chen, Y. *et al.* Synthesis and biological evaluation of low molecular weight fluorescent imaging agents for the prostate-specific membrane antigen. *Bioconjug Chem* **23**, 2377-2385, doi:10.1021/bc3003919 (2012).
- 28 Mankoff, D., Link, J., Linden, H., Sundararajan, L. & Krohn, K. Tumor Receptor Imaging. *Journal of nuclear medicine: official publication, Society of Nuclear Medicine* **49 Suppl 2**, 149S-163S, doi:10.2967/jnumed.107.045963 (2008).
- 29 Emami-Shahri, N. *et al.* Clinically compliant spatial and temporal imaging of chimeric antigen receptor T-cells. *Nature Communications* **9**, 1081, doi:10.1038/s41467-018-03524-1 (2018).

Chapter 6

“Active Nano-targeting of Macrophages”

Authors: **Natasa Gaspar**^{1,2,3}, Giorgia Zambito^{1,2,4}, Clemens M.W.G. Löwik^{1,2,5},
Laura Mezzanotte^{1,2}

Author affiliations:

¹ Erasmus Medical Center, Optical Molecular Imaging, Department of Radiology and Nuclear Medicine, Rotterdam, Netherlands

² Erasmus Medical Center, Department of Molecular Genetics, Rotterdam, Netherlands

³ Percuros B.V., Leiden, Netherlands

⁴ Medres Medical Research GMBH, Cologne, Germany

⁵ Department of Oncology CHUV, UNIL and Ludwig Cancer Center, Lausanne, Switzerland

ABSTRACT

Macrophages play a role in almost every disease such as cancer, infections, injuries, metabolic and inflammatory diseases and are becoming an attractive therapeutic target. However, understanding macrophage diversity, tissue distribution and plasticity will help in defining precise targeting strategies and effective therapies. Active targeting of macrophages using nanoparticles for therapeutic purposes is still at its infancy but holds promises since macrophages have shown high specific uptake of nanoparticles. Here, we highlight recent progress in active nanotechnology-based systems gaining pivotal roles to target diverse macrophage subsets in diseased tissues.

Keywords: Nanoparticles, Active and Passive Nano-targeting, Macrophage polarization, Macrophage reprogramming, Macrophage depletion, Cancer, Asthma, Metabolic diseases, Inflammatory diseases, Cardiovascular diseases

1. INTRODUCTION

Macrophages have several origins during ontogeny and they develop in the mouse embryo in three waves: First with phagocytes derived from the yolk sac independently of blood monocytes; second with blood monocytes produced in the fetal liver; third with blood monocytes derived from bone marrow, hematopoietic stem cells that can replace tissue adapted resident macrophages [1-3]. First and second wave generate tissue resident macrophages and each tissue has its own composition of embryonically derived and adult-derived macrophages. Tissue resident macrophages have adapted to the environment and show different phenotypes and function. To date a clear distinction can be seen among gut, liver (Kupffers cells), lung (alveolar macrophages), skin (Langerhans cells) and brain (microglia) macrophages but subsets have been described in almost every tissue (lymph nodes, skin, artery, pancreas, kidney and brown adipose tissue) [4, 5]. Additionally, they are also part of the tumor stroma and are named tumor associated macrophages (TAMs) [6, 7]. Macrophages, originally discovered by Metchnikoff [8], participate in the maintenance of tissue integrity and homeostasis by discriminating self from non-self, functioning as antigen presenting cells, sensing tissue damage, recognizing invading pathogens and eliminating them *via* phagocytosis. Macrophages play a role in many diseases like cancer, allergies, asthma, autoimmunity, atherosclerosis, and fibrosis acting as pro-inflammatory M1 macrophages (classical activation) or as tissue repair M2 macrophages (alternative activation). M1 macrophages are involved in upregulating the expression of genes involved in the clearance of pathogens while M2 type upregulates the expression of genes related to clearance of apoptotic cells. Therefore, M2 type modulates the anti-inflammatory response. However, the M1 and M2 classification paradigm is oversimplified since macrophages are very heterogeneous cells and their phenotype and functions are affected by the micro-environment. Hence to the micro-environment, macrophages can switch from one phenotype to another depending on the stimuli released in their surroundings. The activation and polarization of macrophages are reviewed in detail elsewhere [9, 10] and it is beyond the scope of this review. Given their important role in pathogenesis and progression of diseases they have recently become an interesting therapeutic target. Moreover, given their phagocytic nature, they represent an attractive target for nanoparticle-based drug intervention. In the following sections, we first describe the different molecules used to efficiently and specifically target macrophages and then we highlight recent literature about active nano-targeting approaches in asthma, cancer, inflammatory bowel diseases and cardiovascular and metabolic diseases (Fig. 1).

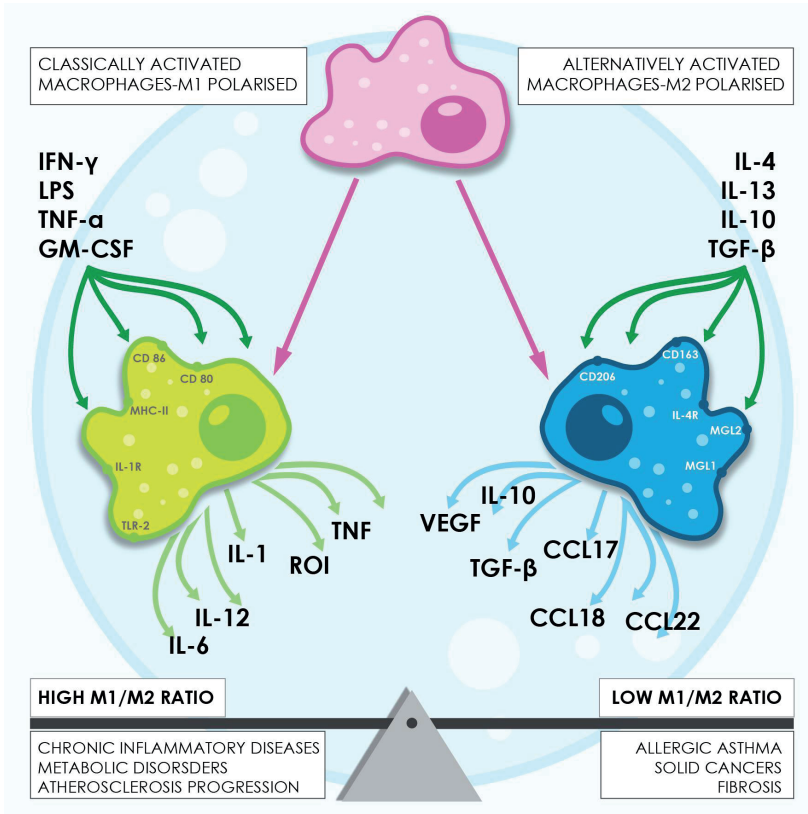


Fig. (1). Illustration of macrophage polarization concept and role of macrophages in diseases.

2. ACTIVE AND PASSIVE NANO-TARGETING OF MACROPHAGES

Currently, several strategies related to target pathological macrophages have been adopted. To manipulate the depletion and re-education of macrophages presents a challenge in the field of nanotechnology-based systems. In the section below, we highlight the difference between active and passive targeting of macrophages with a summary of specific surface ligands leading to the development of improved preclinical active-nanoparticle targeting systems. Macrophages are a target of a plethora of nanoparticle-based therapies due to their multifunctional intracellular capacity. Such targeting can be performed via a passive or an active process. The passive targeting exploits the leakiness of blood vessels in inflamed tissues. This unique phenomenon relies on passive enhanced permeability and retention (EPR effect) on which most of the passive nanoparticle-based therapies are designed [11]. For instance, due to the leaky vasculature and impaired drainage from the tumor site, nanoparticles (size 50-100 nm) can passively enter the vessels and accumulate

at the target area [12, 13]. However, the EPR phenomenon seems highly variable and heterogeneous amongst patients due to differences in tumor growth, vascular distribution and intra-tumoral blood flow [14]. This issue affects nanoparticle distribution in tumors especially when nanocarriers are employed [15,16]. Moreover, tumor associated M2-like macrophages were used as nanoparticle drug-reservoir themselves since they showed high uptake of nanoparticles and to be able to release the antitumor drug over time into the surrounding tissue [17].

The active nano-targeting is based on decorating nanoparticles with ligands specifically binding to overexpressed surface cell receptors. There is a large spectrum of targeting ligands, which can be monoclonal antibodies, peptides, oligomers, antibodies or either small molecules like mannose, legumain [13, 18]. With such ligand-receptor interaction, therapeutic agents will be released into the specific region of interest. As such active targeting exploits the strong interaction between ligand-receptor and reduces the non-specific recognition, avoiding the delivery of cargo in off-target tissues [19].

1.1. Strategies

1.1.1. Legumain

Legumain, a member of asparaginyl endopeptidase, has been identified as an overexpressed protease in cancers and inflammatory disease. Furthermore, the legumain mRNA is more strongly expressed in M2 polarized macrophages than in M1 polarized cells [20-22]. In a nanoparticle-based study, legumain was targeted by coating the surface of liposomes with RR-11a, a synthetic enzyme inhibitor of legumain. When these liposomes were loaded with doxorubicin, they were shown to efficiently target TAMs and release doxorubicin as an encapsulated drug in a breast cancer model [23].

In another study, Liu *et al.* described specific targeting and cellular internalization of macrophages by developing a drug carrier using alanine-alanine-asparagine (AAN), a substrate of legumain, that was attached to the cell-penetrating peptide (TAT) increasing the penetrating capacity of TAT. Moreover, AAN-TAT liposomes carrying doxorubicin were shown to have an antitumor effect in 4T1 breast tumor-bearing mice [24]. Re-education of TAMs by polarizing them to M1-like phenotypes could be performed by hydrazine-curcumin encapsulated nanoparticles targeted to legumain. The application of these nanoparticles aims to modulate the STAT3 pathway and to inhibit the cross talk between tumor cells and TAMs [25].

1.1.2. Lectins

Different families of endogenous lectins are used as a defense strategy against pathogens. Lectins, carbohydrate-binding proteins, can distinguish non-self glycans found on pathogens. In general, collectin and galectin families are widely used to enhance phagocytosis. Especially in lungs, collectin binds different microorganisms and elicits phagocytosis

by alveolar macrophages [26]. For example, pathogen-like amphiphilic polyanhydride nanoparticles offer the advantage of targeting C-type lectin receptors (CLRs) on alveolar macrophages, tailoring the immune response by presenting galactose and di-mannose to the CLRs and reducing inflammation [27].

1.1.1. Mannose Receptor

CD206, the mannose receptor (MR), is a scavenger receptor that is over-expressed on the surface of TAMs and M2 macrophages in general. Mannosylated nanoparticles that target the MR in macrophages result in an increase in endocytosis. In earlier studies, high-mannoside cationic liposomes were used to actively target macrophages [28-30].

Recently, Ortega *et al.* [31] have demonstrated that mannosylated nanoparticles can deliver siRNA against IkBa that could modulate the gene targets within the NF- κ B pathway in TAMs, resulting in a therapeutic effect. Indeed, restoration of the NF- κ B signaling pathway by inhibiting IkBa induced immune-stimulatory activities and cytotoxicity towards TAMs.

Another elegant example of multi-functionalized nanoparticles was shown by Song Y. *et al.* where nanoparticles were used to suppress breast tumor growth and M2 like macrophages. These mannosylated chitosan nanoparticles were loaded with vascular endothelial growth factor (VEGF) and placental growth factor (PIGF) siRNAs, which are over-expressed in breast cancer cells and TAMs macrophages. Therefore, the simultaneous gene depletion of VEGF and PIGF revealed a synergistic antitumor immunotherapeutic effect [32].

In a tuberculosis model, solid nanoparticles could be administered *via* inhalation achieving high drug concentration in the infected macrophages. Indeed, rifampicin-loaded nanoparticles with a mannosylated surface were developed in order to improve drug uptake. Further investigations revealed that the mannosylated solid nanoparticles improved the cellular uptake overtime [33].

1.1.2. Folate Receptor (FR)

The folate receptor gene family includes four members (FR α or FOLR1, FR β or FOLR2, FR γ or FOLR3 and FR δ or FOLR4), which bind the folic acid with high affinity. The FR α and FR β encode glycosyl phosphatidylinositol anchored endocytotic receptors expressed in certain epithelial tissues or in normal myeloid cells. Within this the myeloid lineage FR β is specifically expressed by M-CSF-polarized M2 macrophages involved in inflammatory and autoimmune disease [34, 35]. The high affinity of FR α and FR β for folate binding and the consequential endocytic activity make folate-drug conjugates a selective strategy for cancer treatments and M2-depletion therapy. Dyes or radioactive agents can be linked to folate in order to selectively visualize TAMs in inflammatory diseases. For instance, the conjugation of folate with the radioactive agent ^{99m}Tc allowed imaging

the migration of macrophages to an inflamed area both *in vitro* and *in vivo* in healthy rats with adjuvant-induced arthritis (AIA), and arthritic rats that had been depleted of macrophages [35]. Folate coupled to the peptide EC20 that can chelate radioactive technetium ($[^{99m}\text{Tc}] \text{Tc-EC20}$) can also be conjugated to PEG-coated liposomes, improving the total uptake in activated macrophages in a mouse model of ulcerative colitis [36]. In another recent study polyamidoamine dendrimer nanoparticles conjugated with methotrexate (G5-MTX Nps) and FR β reduced TAM recruitment and was more effective than cisplatin in ovarian cancer [37].

1.1.1. Peptides

Peptides have also shown great potential in terms of targeting and delivering various chemotherapeutic hydrophobic agents. The use of peptides is very cost-effective and easy to synthesize. Notably, Cieslewicz *et al.* identified the M2 macrophage specific peptide named M2pep, which can bind selectively to M2 macrophages. In this approach they fused M2pep to a pro-apoptotic peptide, causing a decrease of TAM cells in murine colon carcinoma [38]. Another similar investigation was performed by Kakoschky B. *et al.*, in which the target efficiency of M2pep varies in different tumor entities. However, they showed that M2pep binding to TAMs was higher than Kupffer cells in the liver [39]. Qian Y. and colleagues developed a dual-targeting nanoparticle using the α -peptide (a scavenger receptor B type 1 (SR-B1) targeting peptide) fused to the M2pep (α M2NPs). The α M2NPs were then loaded with anti-colony stimulating factor-1 receptor (anti-CSF-1R) siRNA. This dual targeting nanoparticle demonstrated itself to efficiently target and reduce TAMs and to decrease the size of the tumor in hepatocellular (HCC) and in 4T1 breast carcinoma [40]. Recently in a study by Scodeller P. *et al.* TAMs were selectively targeted *via* the MRC1 (mannose receptor C type 1) by using a peptide called UNO. This peptide conjugated with a fluorescent dye (FAM-UNO) binds specifically to the MRC1 receptor. FAM-UNO decorated liposomes were tested as drug-loaded nanoparticles against tumor-associated macrophages in melanoma tumors [41].

Chanju Lee *et al.* demonstrated the possibility of inducing apoptotic cell death after cell membrane penetration. A hybrid peptide MEL-dKLA can target preferentially M2-like TAMs, induces cell death by disrupting mitochondrial membranes *in vitro* and inhibits tumor growth *in vivo* [42]. In another study, the nanoparticle surface was modified with a peptide sequence containing tuftsin (TKPR). This peptide interacts with macrophages by binding the Fc receptor and neuropilin-1 receptors on the macrophage surface. The successful binding promotes efficient phagocytosis of IL10 containing alginate nanoparticle into active macrophages in rheumatoid arthritis [43].

1.1.3. Beta-Glucans

β -glucans serve as immune-stimulants that nonspecifically activate cellular and humoral components of the host immune system so that they increase the functional activity of macrophages. Dectin-

1 receptor recognizes β -glucans and modulates macrophages towards the M1 phenotype. In a recent study, endocytosis of macrophages has been stimulated using glucan particles (GPs) prepared from *Saccharomyces cerevisiae*. The GPs were shown to be dectin-1 dependent *in vitro*. In the same study, they tried to load the GPs with different molecules like proteins, DNA, siRNA, and small drug molecules, such as the antibiotic rifampicin and deliver them to macrophages. The ability to target phagocytic cells like macrophages makes GPs an attractive target for drug delivery [44, 45]. A recent study reported the development of a spray dried glucan particle-based formulation able to encapsulate a large payload of rifabutin, an anti-tuberculosis drug. The spray dried batch displayed greater characteristics in terms of size, uniformly comparing to the particles dried *via* lyophilization. Such particle-formulation showed to enhance target delivery of rifabutin to macrophages in less than 2 minutes after exposure. The system represents a slow-drug delivery system in which rifabutin is released continuously. This strategy can reduce the dosage and frequency of administration of the drug needed for treatment of tuberculosis and potentially could be applied in other disease models [46].

2.2. Active Nano-targeting of Macrophages for Asthma

Allergic asthma is associated with airway inflammation and hyperactivity. As the inflammation becomes established after repeated antigen exposures, alveolar macrophages can polarize across a continuum of activation phenotypes losing their suppressive functions and gaining pathogenic functions. M1 and M2 macrophages secrete high levels of interleukins and chemokines that activate T cells and promote further infiltration of B cells and eosinophil into the lungs [47, 48]. Recent studies have indicated that M2 macrophages (polarized by exposure to IL-4 and IL-13) may be elevated in asthma based on marker molecule expression [49-51]. Currently, many studies have been performed to test nanoparticle-based drug delivery systems targeting the lungs that offer many advantages. This is mostly due to their longer retention time, their ability to release drugs and their biodegradability. Al Faraj A. *et al.* synthesized a superparamagnetic iron-oxide nanoparticle conjugated with anti-IL4R α that simultaneously blocks IL-4 and IL-13 signaling. IL4R α has been recognized as an asthma biomarker that is expressed in inflammatory M2 macrophages. The simultaneous inhibition of this signaling in the inflammatory sites in the lungs has been assessed by MRI. SPIONs conjugated with IL4R α antibodies and functionalized with PEG have been validated to efficiently target IL4R α positive inflammatory cells. In this study, it was possible to target IL4R α in allergic diseases to block the signaling pathway and give additional relief to asthma. These anti-IL4R α -conjugated

nanocarriers can be directly administrated to the in- flamed lungs, thus improving treatment efficacy and decrease side effects [52, 53].

Intranasal treatment with biocompatible nanoparticles conjugated with anti-IL4Ra has shown to control lung inflammation in asthma. OVA-sensitized mice were treated with dextran coated- SPION anti-IL4Ra nanoparticles that efficiently decreased the expression of pro-inflammatory cytokines [54].

In another approach, the FOXO1 gene was found to be significantly upregulated in M2 lung macrophages that localize in the airways of patients with mild asthma after an allergen challenge. Inhibition of FOXO1 gene downregulated pro-asthmatic and pro-fibrotic gene expression by macrophages further supporting the theory that FOXO1 may be a good target for the development of drugs to treat asthma [55].

2.3. Active Nano-targeting of Macrophages in Inflammatory Diseases

Nanomedicine aims to efficiently target dysfunctional macro- phages through active targeting. Based on their physiological role in disease emerging nanotechnology has opened up new opportunities to treat inflammatory diseases.

2.3.1. Rheumatoid Arthritis (RA)

RA is an autoimmune disorder that affects articular tissues and evolves as chronic systemic inflammation. Macrophages amplify the local and systemic inflammation and contribute to matrix deg- radation [56]. The reinforcement of macrophages in the synovium is a relevant sign of inflammatory lesions. Furthermore, the degree of macrophage infiltration is correlated to the degree of joint erosion.

Currently, therapies mainly focus on decrease of pro- inflammatory cytokines expressed by active macrophages, upregulate anti-inflammatory cytokines and inhibit dysfunctional macro- phages located in the inflammatory foci.

Macrophages in RA can also be targeted *via* tuftsin peptide- functionalized nanoparticles to deliver IL-10, an anti-inflammatory cytokine. This method aims to repolarize macrophages from M1 to M2 phenotype and reduce significantly systemic and joint-tissue pro-inflammatory cytokines [43].

In a study conducted by Nogueira E. *et al.* they used folate conjugated NPs that can actively target folate receptor β (FR β) on activated macrophages. They demonstrated that the receptor mediates the cellular internalization of the cargo *via* endocytosis for effective drug delivery [57]. In a similar study, a recombinant antibody that has high specificity for FR β and the data produced suggested that this antibody can selectively bind activated monocytes in the synovial fluid of patients [58].

Interestingly methotrexate (MTX), the first line therapy indicated for the treatment of RA, has been encapsulated in a new liposomal formulation using folate coating to enhance drug delivery efficacy [59]. In another approach, the glucocorticoid prednisolone (PD)

was encapsulated within solid lipid nanoparticles coated with hyaluronic acid. Hyaluronic acid has been demonstrated to target CD44 expressed on the surface of synovial macrophages in a mouse model of collagen-induced arthritis [60]. Current RA drugs target the production of cytokines derived from macrophages and still additional research needs to be done to target the macrophages as cells.

2.3.2. Inflammatory Bowel Disease (IBD)

In the inflammatory bowel disease (IBD) the immune system attacks the intestines. Ulcerative colitis and Crohn's disease are the two major disorders of IBD. In a healthy state, macrophages are located in the lamina propria and Peyer's patch and they function as effector cells. Upon inflammation, macrophages are activated and are able to elicit a pro-inflammatory response as well as produce pro-inflammatory cytokines as TNF- α . Therapeutic strategies, such as nanomedicine delivered anti TNF- α treatments, have demonstrated strong therapeutic potential; they conferred advantages because they could efficiently penetrate epithelial and inflammatory cells [61].

For example, targeting activated macrophages by mannose- conjugated bio-reducible cationic polymers (PPM) and sodium triphosphate (TTP) improved their endocytosis. It was shown that nanoparticles encapsulating a small interference RNA (siTNF- α) could efficiently release the siRNA, resulting in reduced TNF- α expression both *in vitro* and *in vivo* in IBD therapy [62].

Getts *et al.* demonstrated the use of "immune-modifying microparticles" (IMPs) that target macrophages in inflammatory diseases. These microparticles have a negative surface charge and are taken up through the scavenger receptor MARCO. The electrostatic interaction seems to mediate the binding of the IMPs to MARCO receptors, inducing cellular uptake and subsequent death by caspase-3 mediated apoptosis [63].

Another approach is to exploit the mannan polysaccharide, a ligand for mannose receptors (MR), which has been used in several studies and used to decorate nanoparticles [33, 39]. For instance, Gan J. *et al.* induced the clustering of mannose receptors (MR) on the cell surface by using glucomannan-decorated silicon oxide (KSiNP30). Unexpectedly this approach could polarize M1 macrophages into the anti-inflammatory M2 phenotype and alleviate the inflammatory bowel disease [64].

2.4. Active Nano-targeting of Tumor-associated Macrophages

Macrophages take part in both tumor initiation and progression. Despite their high plasticity macrophages are still the main interest for researchers as the most promising therapeutic target within the tumor microenvironment. The design of therapeutic tools has been very challenging due to the fact that macrophages display a high grade of plasticity in response to the diverse chemokine secretion coming from the tumor microenvironment. Many strategies emerged and have been put to use with the aim of manipulating, repro-

graming and depleting macrophages from the tumor microenvironment. In this scenario nanotechnology-based systems have been greatly implicated and have led to important results in preclinical studies [65, 66] (Table 1).

2.4.1. Macrophage Reprogramming

Macrophage re-education is one of the most promising strategies in the field of anti-cancer therapy. The aim is to re-program M2-like pro-tumor macrophages into M1-like macrophages endowed with anti-tumor functions. In one study, tri-block copolymers nanoparticles were developed specifically targeting macrophages for the delivery of siRNA *in vitro* and *in vivo*. The particle core is a hydrophobic, pH responsive block that triggers endosomal escape and cytoplasmic delivery of siRNA. The second block is a poly (DMAEMA) polymer with a polycationic charge that condenses polyanionic oligonucleotides within the particle, which serves to carry and protect siRNA for delivery to the target cell. The third block of the nanoparticles is an azide-presenting block that triggers the particles towards the targeting molecules, in this case the mannose receptor (CD206). The surface of the nanoparticles was functionalized with a mannose ligand (MnNP) to specifically target macrophages *via* the mannose receptor (CD206). Macrophages were efficiently transfected both *in vitro* and *in vivo* with the particles and labelled nucleotides were effectively delivered to macrophages in mice with primary mammary tumors. Enhanced uptake was notable in lung metastasis associated macrophages [67]. Once the macrophage population was successfully targeted *via* MnNPs, researchers incorporated siRNA to manipulate the NF-Kb pathway where *in vitro* this resulted in cytotoxicity and immune-stimulation [68]. Zhang and *et al.* coupled the small molecular legumain inhibitor RR-11a to liposomes and loaded the nanoparticles with doxorubicin, which led to total tumor growth inhibition [69].

In another approach, glucan-based nanoparticles were used to systemically deliver therapeutic siRNA to TAMs and reduce the expression of the migration inhibitory factor (MIF), which is upregulated in disease macrophages and plays an important role in regulating the immune system [70, 71]. Experiments demonstrated that nanoparticles with glucan-shell encapsulating siRNA core structure are efficiently delivered to macrophages, both *in vitro* and *in vivo*. A systemic injection in mice bearing a 4T1 mammary tumor showed a dramatic reduction in macrophage infiltration after drug delivery [71]. Hypoxia in the tumor microenvironment is driving the invasiveness of tumor cells and macrophages located in the hypoxic cancer core, whilst also interacting with cancer cells to promote chemo resistance and cancer cell proliferation. With this in mind, Song *et al.* developed manganese dioxide nanoparticles (MnO₂ NPs) toward hydrogen peroxide (H₂O₂) loaded with hyaluronic acid (HA) that have the capability to repolarize the pro-tumoral M2 in order to pro-inflammatory M1 phenotypic state of TAMs. Using these NPs noticeably alleviated tumor hypoxia and enhanced chemotherapy responses in a murine 4T1 breast cancer model [72].

Table 1. Examples of nanotechnology-based systems for active macrophage targeting in disease models.

Disease Model	Ligand/Target	Carrier	Cargo	Strategy; Depletion, Imaging, Reprogramming	Reference
	Mannose/MR	BMA-PAA-DMAEMA Micelles	siRNA	Reprogramming	[67, 68]
	RR-11a/Legumain	Liposomes	Hydrazinocurcumin	Reprogramming	[69]
	β -(1-3)-(1-4)-glucan/CD11b	Glucan-based nanoparticle	MIF siRNA	Inhibiting recruitment and reprogramming	[70]
	Mannan	Manganese dioxide-MnO ₂	Hyaluronic acid	Reprogramming	[72]
	Folate receptor (FR)	USPIO	Ferumoxytol	Targeting	[74]
	Galactose/MGL	Alginate-based nanoparticles	CpG, anti-IL-10 and anti-IL-10R oligonucleotides	Pro-tumoral inhibition and reprogramming	[43]
	Folate receptor (FR)	Liposomes	Radio- and Fluorescent label	Targeting	[76]
		Folate receptor antibody	Pseudomonas endotoxin A	Depletion	[77]
	CD163 antibody	Glycol coated liposomes	Fluorescent label, doxorubicin	Depletion	[78, 79]
	NOTE: Phagocytic cells specific liposomes: MPS CELLS	Liposomes	Clodronate	Depletion	[83]
	PEGylation	Liposomes	Clodronate	Depletion	[85]
		Liposome- DOTAP	Clodronate	Depletion	[86]
	Folate receptor (FR)	Liposomes	Zoledronic acid	Depletion	[35]
	AAN/Legumain	Liposomes	Doxorubicin	Depletion	[24]
	Mannose surface-modification	PLGA	Doxorubicin	Depletion	[88]
	Polysaccharide from <i>Bletilla striata</i> /MR	Polysaccharide from <i>Bletilla striata</i> -drug conjugate	Alendronate	Depletion	[89]
	M2pep/M2 Macrophages	Peptide-based nanoparticle	Fluorescent label, pro- apoptotic peptide	Targeting	[38, 40]
	Mannose/MR	Liposomes	Radiolabel, fluorescent dye	Targeting	[39]

CANCER

Table 1. Examples of nanotechnology-based systems for active macrophage targeting in disease models. (continued)

Disease Model	Ligand/Target	Carrier	Cargo	Strategy; Depletion, Imaging, Reprogramming	Reference
CARDIOVASCULAR DISEASE (CVD)	Scavenger receptor (SRA)	M12PEG	Mucic acid (M12)	Reprogramming	[93]
	Receptors for Hyaluronic acid (e.g. stabilin-2 and CD44)	Hyaluronic acid	/	Targeting	[94]
	CD36 Receptor	Liposomes	Gadolinium	Targeting	[95]
	Lyp-1 peptide	Cage-like protein structure: Heat Shock Protein from <i>Methanococcus jannaschii</i> (MjHsp)	Fluorescent molecule : Cy5.5	Targeting	[96]
	Human Ferritin Protein	Human Ferritin Protein	Fluorescent Cy5.5 molecule or a magnetite nanoparticle	Targeting	[98]
METABOLIC DISEASE	siRNA particles (GeRPs)	Beta-1,3-D-glucan	/	Reprogramming	[103]
	1,3-β-glucan	Glucan shell	Rifabutin	Depletion	[46]

To regulate cell-specific functions a study was performed by Huang *et al.* in which they designed a nano-carrier system consisting of galactosylated cationic dextran so as to target the macrophage galactose-type lectin I receptor and encapsulate the anti-IL-10 and anti-IL-10R oligonucleotides. The aim was to alter the phenotype of TAMs and to potentially trigger their tumoricidal activity. The effectiveness and tumor suppression was noted when the galactosylated nano-carrier system was tested in mice bearing liver cancer [73].

In 2011 Daldrup-Link *et al.* showed that ultra-small superparamagnetic iron oxide (USPIO) nanoparticles could be used for the MRI imaging of macrophages in a tumor microenvironment. USPIO particles are phagocytosed by macrophages throughout the whole body, which enables enhanced molecular imaging. The basis of the imaging technique relied on the iron supplement ferumoxytol (Feraheme), which was FDA-approved for intravenous treatment of iron deficiency in patients.

As USPIO compound ferumoxytol provides a strong signal on an MRI showing excellent contrast agent properties [74]. The authors proved that when intravenously injected into the PyMT mouse mammary model, USPIO enhanced the MRI signaling in tumor tissues. Later on, the authors engrafted the nanoparticles targeting the folate receptor (FR) in order to increase even more particle uptake by macrophages. In a more recent study, ferumoxytol significantly inhibited the growth of subcutaneous adenocarcinomas in mice. In addition, intravenous ferumoxytol treatment given before an intravenous tumor cell challenge prevented the development of liver metastasis. The observed tumor growth inhibition was accompanied by an increased presence of pro-inflammatory M1 macrophages in tumor tissues [75].

2.4.2. Macrophage Depletion

Eradication of macrophages by directly killing them is called a macrophage depletion strategy. The basis of this strategy is either depletion via antibodies or via molecules with targeted toxicity against macrophages.

2.4.3. Depletion via Monoclonal Antibodies

Turk *et al.* found that the folate receptor (FR) is highly expressed on macrophages. The study investigated the folate-targeted liposome distribution in a mouse model of ovarian cancer. It was found that the uptake was tenfold greater in macrophages when compared to the ovarian cancer cells [76]. In a follow-up study, the presence of a folate- β -receptor (FR- β) subtype was discovered on the surface of macrophages within the tumor microenvironment. *Pseudomonas* exotoxin A was coupled to an antibody directed towards FR- β . Macrophage depletion was observed after the injection of the immunotoxin into C6 glioma xenografts in nude mice [77].

CD163, the hemoglobin scavenger receptor, is mainly expressed in tissue resident macrophages of the M2 phenotype as well in macrophages in inflammation and at the

tumor growth site. Etzerodt et al. developed liposomes specifically targeting the CD163 receptor through the binding of the CD163 monoclonal antibody to glycol-coated liposomes, or the so called 'stealth liposomes' [78, 79]. Cargo doxorubicin was used and when applied strong cytotoxic effects were seen in vitro studies using the CD163-expressing human monocytes.

The colony stimulating factor 1 receptor (CSF1R) recruits macrophages to the tumor microenvironment and drives the phenotypic switch towards a pro-tumorigenic phenotype. In a study by Strachan et al. BLZ945 is used as an inhibitor of CSF1R and showed that the BLZ945 decreases the growth of malignant cells in mouse mammary tumors. It also propagates the infiltration of CD8+ T cells showing that inhibiting CSF1R could be essential for macrophage depletion [80]. In another study, a monoclonal antibody was generated (RG7155) that inhibits the CSF-1R receptor activation. Studies in vitro resulted in cell death of CSF-1R expressing macrophages. In vivo trials of the RG7155 antibody showed to reduce the macrophage population in various cancer models [81]. A very recent study from Kyriakos et al. applied the AMG 820, a fully human CSF1R antibody that inhibits binding of the ligands CSF1R, and IL34. This first-in-human phase 1 study demonstrated the safety and tolerability of the CSF1R antibody AMG820 in patients ≥ 18 years old who had pathologically confirmed advanced solid tumors, most common tumor types were colorectal cancer (CRC:44%) and non-small cell lung cancer (NSCLC;12%). However, AMG820 showed limited anticancer activity [82].

2.4.4. Depletion via Molecules Exerting Specific Toxicity Against Macrophages

In the early 1990s, Van Rooijen et al. developed a 'suicide' technique where a dichloromethylene-bisphosphonate (Cl₂MBP or Clodronate) was encapsulated into a liposome structure for a transient depletion of macrophages. Clodronate is a bisphosphonate when encapsulated in liposomes. The particles are rapidly recognized and engulfed by macrophages, which is what causes apoptotic cell death. This technique is known as 'liposome-mediated macrophage suicide' [83]. A major inhibitory action of clodronate liposomes in murine tumors is based on the depletion of macrophages and is associated with the volume reduction of the total tumor mass [84]. Inhibition of tumor angiogenesis and growth was observed by depleting macrophages via clodronate liposomes in a teratocarcinoma model [86]. To avoid the massive uptake by monocytes and macrophages clodronate containing liposomal formulations have been coated with PEG, a synthetic hydrophilic polymer, which improves their stability and prolongs their half-lives in circulations [85]. A new version of clodronate liposomes has been established by Piaggio et al. named the Clo-Lipo-DOTA version, with physicochemical properties well suited for safe storage and injections. The new version of liposomes containing clodronate showed no general toxicity. Furthermore, they were cell specific since no immune cells other than macrophages were affected. In vitro studies of the novel clodronate liposomes showed

to induce apoptosis of macrophage-like cell lines in a dose and time manner. On the other hand, the *in vivo* assays showed a significant reduction of F4/80- positive cells and a reduction of general tumor mass compared to the controls [86]. The anti-tumor effect of zoledronic acid (ZA) was tested by Hattori et al., in which zoledronic acid was encapsulated in folate modified liposomes to selectively eradicate macrophages in the tumor microenvironment. However, results showed no anti-tumoral effect and injections of the folate-linked liposome containing zoledronic acid were lethal for tumor-bearing mice [35]. Recently an elegant multi-target peptide was developed by Song et al., the so called “tadpole”-like peptide or the cyclic nRGD peptide. A tumor homing peptide (iRGD) was combined with the substrate of the endoprotease legumain (AAN), which could bind specifically to macrophages. When nanoparticles were targeted by conjugating them with nRGD-AAN loaded with doxorubicin and applied to 4T1 tumor bearing mice, macrophage depletion was observed in the tumor microenvironment [87]. In another study, doxorubicin was delivered to macrophages in the tumor microenvironment using nanoparticles with a functionalized surface by PEGylation and mannose modification (i.e. DOX-AS-M-PLGA-NPs) [88]. Targeted nanoparticles were more efficient in tumor growth reduction than non-targeted ones, proving that there is a need to design a targeted-therapy for a more efficient control of tumor growth. Another example of macrophage depletion strategy is represented by alendronate-glucomannan, in which the polysaccharide from *Bletilla striata* was conjugated to the bisphosphonate alendronate. It was shown that alendronate-glucomannan accumulates within a certain preference in macrophages and does induce apoptosis *in vitro* [89].

2.5. Active Nano-targeting of Macrophages in Cardiovascular Diseases

Cardiovascular disease (CVD) is one of the leading causes of death across the world [90]. Atherosclerosis is the most common type of CVD caused by atherosclerotic plaques due to lipid retention in the arterial wall. Macrophages play a crucial role in the disease progression where they promote the formation of unstable plaques maintaining a pro-inflammatory microenvironment. On the contrary, the anti-inflammatory phenotype of macrophages stabilizes the plaque formation in the arterial wall [91].

A more adjuvant anti-atherosclerotic therapy is needed, such as the vascular-targeted nanocarrier strategy, to allow more specific drug delivery and reduce the macrophage accumulation to the lesion site. In order to specifically target macrophages within the atherosclerotic plaques the two most popular moieties are incorporated into the nanosystems targeting ligands like antibodies, peptides, aptamers, or small molecules that are specific for the components within the plaques and PEGylation of the nanocarriers that stabilize the particles *in vivo* [92].

Usually, the most common material used for nanoparticle-mediated investigations in atherosclerosis is polystyrene, which is a biomaterial that is widely used for *in vitro* studies

and *in vivo* biodistribution [93]. Metallic and inorganic materials are mainly used for the imaging of atherosclerotic plaques with MRI as the classical modality due to the ultra-small supermagnetic nanoparticles of iron oxide (USPIOs) or gadolinium (Gd)-based materials. Until now the nanoparticles-mediated specific targeting of atherosclerosis was done mainly for imaging purposes. Many possible targets have been identified that are either overexpressed at the cell of interest, or are disproportionately expressed at the plaque site.

The key point for atherosclerosis progression is the uptake of low density lipoprotein (LDL), a process mediated by macrophages, via the scavenger receptor-A (SR-A) and scavenger receptor B (CD36). Many strategies have been developed in order to interrupt this process. One study shows the development of nanoparticles that competitively bind to cells via scavenger receptors and inhibit the uptake of modified lipids by macrophages. Nanoparticles were designed with a basis on a hydrophobic mucic acid core and amphiphilic shells, and act in two ways to prevent the lipid uptake: the direct competition with the uptake of oxidized LDL via the scavenger receptors SR-A and CD36, plus the decrease of surface expression of the scavenger receptors after incubation with the nanoparticles *in vitro*. The most important finding of this study is the ability of the nanoparticles to switch the highly atherosclerotic macrophage phenotype towards an athero-resistant phenotype which forms the basis for future nanomedicine strategies battling with atherosclerotic plaques [94].

Lee et al. constructed hyaluronic nanoparticles (HA-NPs) to actively target macrophages in atherosclerotic plaques both *in vitro* and *in vivo* since the hallmark of atherosclerosis is the overexpression of receptors for hyaluronic acid (e.g. stabilin-2 and CD44). In conclusion, it was evident that the particles selectively did accumulate in the atherosclerotic regions by active targeting, thus demonstrating their potential as a nanocarrier for diagnosis and therapy [95].

Techniques for imaging such as cardiovascular magnetic resonance (CMR) provide possibilities to identify atherosclerotic plaques in several ways. Delliner et al. developed an atherosclerotic-targeting agent (ATCA) in which gadolinium was formulated into liposomes along with CD36 ligands in the lipid bilayer. This was to specifically target the macrophage population within the atherosclerotic plaques. The system when applied provided an enhanced and optimized visualization of plaques in the arterial walls [96].

The LyP-1 peptide was used to construct a protein caged nanoparticles system for enhanced imaging of macrophage-rich vascular lesions in a study by Uchida et al. The LyP-1 peptide has been shown to specifically target macrophages in the tumor microenvironment. Within this study, the LyP-1 was fused to a heat shock protein from *Methanococcus jannaschii* (MjHsp) with the near infrared fluorescent molecule (Cy5.5) placed onto the interior cavity. A design like this showed specificity for macrophages *in vitro*, and when being injected *in vivo* models it allowed visualization of macrophage-rich murine carotid

lesions by *in situ* and *ex vivo* fluorescence imaging. The authors showed the potential of LyP-1 conjugates as a possible nanoscale platform for delivering imaging agents to carotid lesion for diagnosis [97].

In a recent *in vivo* study of intravascular optical imaging, macrophages were targeted via nanocarriers by specifically targeting the mannose receptor (CD206). The authors developed an injectable near-infrared fluorescence probe (NIRF) via chemical conjugation of a thiolated glycol chitosan with cholesteryl chloroformate, a NIRF dye and maleimide-polyethylene glycol-mannose as mannose binding receptor ligands to target specifically macrophages within atherosclerotic plaques. The probe showed high specificity and low toxicity, and allowed the direct visualization of murine carotid atheroma. This novel imaging platform allows identification of high-risk plaques in *in vivo* models [98].

Ferritin protein has been shown to accumulate in macrophages in human atherosclerotic plaques and the hypothesis of the authors in one study was that ferritin could serve as an intrinsic nanoplatform to target vascular macrophages in order to detect atherosclerotic plaques. The authors have developed an engineered imaging platform consisting of a human ferritin protein either conjugated to the NIRF Cy5.5 molecule or encapsulating a magnetite nanoparticle. They showed that those nanoparticles are taken up *in vivo* by macrophages in murine atherosclerotic plaques and can be imaged via MRI and fluorescence imaging. Results show that human ferritin can serve as a nanoparticle platform to specifically visualize inflammation *in vivo* [99]. Researches are constantly looking for novel targets to image, diagnose and treat atherosclerosis utilizing nanosystems, and with the advances in recent studies it's becoming an achievable target.

2.6. Active Nano-targeting of Macrophages in Metabolic Disease

Metabolic syndrome is a cluster of several conditions including the occurrence of insulin resistance, formation of atherosclerotic arterial plaques and excess accumulation of adipose tissue around the waist. These symptoms tend to occur together and increase the risk of cardiovascular disease, stroke and diabetes. The cross talk between the immune and metabolic system is pivotal for the metabolic health since the immune system provides the anti-infectious anti-neoplastic protection. The omnipresence of macrophages in tissues and metabolic organs is greatly considered as having a crucial impact on metabolic disease progression.

A study relating to macrophages in obesity used polysaccharides based on biocompatible glucose polymers as delivery systems used to target adipose tissue macrophages [100]. The particles were designed with tunable sizes that carried contrast agents for positron emission tomography (PET), fluorophores for optical microscopy, and anti-inflammatory drugs for modulation of macrophage phenotype. Observations in obese mice 24h post administration showed that an uptake of 63% of the larger conjugates of the injected dose remained in visceral adipose tissue; 24 h post administration resulting in >2 fold

increased local concentration compared to liver. A single dose treatment resulted in inflammatory marker reduction. All the components are clinically approved and ready for future studies as promising nano-based drug delivery systems.

For the treatment of metabolic diseases, liposomes remain of interest because they are easily engineered to target macrophage subsets. Clodronate-loaded-liposomes have shown to induce apoptosis when internalized, and the strategy has been used to deplete visceral adipose tissue macrophages (ATMs). This resulted in improved insulin and glucose tolerance and reduced weight gain when fed with a high-fat diet compared to the control group [101].

Experimental evidence highlighted the possibility that gene silencing by double-stranded RNAs is an interesting approach to interfere with the inflammatory responses caused by macrophages in diseases such as rheumatoid arthritis, atherosclerosis, inflammatory bowel disease and diabetes [102]. For example, Aouadi et al. conducted a study where beta-1,3-D-glucan encapsulated siRNA particles (GeRPs) were engineered and orally delivered to silence TNF α in mouse macrophages [103]. In another study, an oligopeptide consisting of an adipocyte-targeting sequence and 9-arginine (ATS-9R) was shown to selectively transfects mature adipocytes by binding to prohibitin. The injection in mice of an oligopeptide complex consisting of ATS-9R and short hairpin shRNA for silencing fatty acid binding protein 4 proved to be a safe therapeutic approach to regress and treat obesity as well as obesity-induced metabolic syndromes [104]. Later, another group showed that ATS-9R can target also visceral adipose tissue macrophages (ATMs). In this study, ATS-9R was complexed with shRNA for silencing tumor necrosis factor- α converting enzyme (TACE) enzyme, which is a transmembrane enzyme that induces the enzymatic cleavage and release of inflammatory cytokines [105]. This therapeutic approach alleviated visceral fat inflammation and improved type 2 diabetes by reducing whole body inflammation [106].

CONCLUSION

The nanoparticle based drugs presented here that actively targets macrophages seems to demonstrate efficacy in preclinical models. However, one limitation of this approach is represented by the continuous changes in phenotype/activation of macrophages in response to environmental stimuli, which may lead to unspecific targeting of tissue-resident macrophages that play a pivotal role in tissue homeostasis and body defense. For example, the depletion of macrophages is frequently associated with an increased risk of infection. Moreover, a combination of strategies, for example, depletion and re-educating, using different nanocarriers to deliver different drugs may be a preferential way to achieve clinical significance. Ultimately, the increased understanding of macrophage diversity, tissue

distribution and plasticity is essential for refining targeting strategies and will lead to more effective therapies.

CONSENT FOR PUBLICATION

Not applicable.

FUNDING

We thank the European Commission (MSCA-ITN-2015-ETN, project acronym 'ISPIC'; and H2020-MSCA-RISE-2018, project acronym 'Cancer') for grant support of our work in this area and Mrs. Joanne Everett for English language editing.

CONFLICT OF INTEREST

The authors declare no conflict of interest, financial or other- wise.

ACKNOWLEDGEMENTS

Macrophage biology is an enormous field with thousands of references published each year. This means we are unable to cite every important paper published and for this, we apologize to the macrophage biology scientific community.

REFERENCES

- [1] Wynn TA, Chawla A, Pollard JW. Macrophage biology in development, homeostasis and disease. *Nature* 2013; 496(7446): 445-55. [<http://dx.doi.org/10.1038/nature12034>] [PMID: 23619691]
- [2] Hume DA, Irvine KM, Pridans C. The mononuclear phagocyte system: The relationship between monocytes and macrophages. *Trends Immunol* 2018; pii: S1471-4906(18): 30226-6.
- [3] Gordon S. The macrophage: Past, present and future. *Eur J Immunol* 2007; 37(Suppl. 1): S9-S17. [<http://dx.doi.org/10.1002/eji.200737638>] [PMID: 17972350]
- [4] Gentek R, Molawi K, Sieweke MH. Tissue macrophage identity and self-renewal. *Immunol Rev* 2014; 262(1): 56-73. [<http://dx.doi.org/10.1111/imr.12224>] [PMID: 25319327]
- [5] Epelman S, Lavine KJ, Randolph GJ. Origin and functions of tissue macrophages. *Immunity* 2014; 41(1): 21-35. [<http://dx.doi.org/10.1016/j.immuni.2014.06.013>] [PMID: 25035951]
- [6] Yang M, McKay D, Pollard JW, Lewis CE. Diverse functions of macrophages in different tumor micro-environments. *Cancer Res* 2018; 78(19): 5492-503. [<http://dx.doi.org/10.1158/0008-5472.CAN-18-1367>] [PMID: 30206177]
- [7] Cassetta L, Pollard JW. Targeting macrophages: Therapeutic approaches in cancer. *Nat Rev Drug Discov* 2018; 17: 887-904. [<http://dx.doi.org/10.1038/nrd.2018.169>]
- [8] Metschnikoff, Elias Ueber den Kampf der Zellen gegen Erysipelkokken. *Archiv fur pathologische anatomie und phycologie und fur klinische medicin.* 1887; 1432-2307. 107(2): 209-249
- [9] Gordon S, Martinez FO. Alternative activation of macrophages: Mechanism and functions. *Immunity* 2010; 32(5): 593-604. [<http://dx.doi.org/10.1016/j.immuni.2010.05.007>] [PMID: 20510870]
- [10] Martinez FO, Sica A, Mantovani A, Locati M. Macrophage activation and polarization. *Front Biosci* 2008; 13: 453-61. [<http://dx.doi.org/10.2741/2692>] [PMID: 17981560]
- [11] Bertrand N, Wu J, Xu X, Kamaly N, Farokhzad OC. Cancer nanotechnology: The impact of passive and active targeting in the era of modern cancer biology. *Adv Drug Deliv Rev* 2014; 66: 2-25. [<http://dx.doi.org/10.1016/j.addr.2013.11.009>] [PMID: 24270007]
- [12] Mostafavi SH, Jayachandra Babu. Nano-Sized Drug Delivery. *J Mol Pharm Org Process Res* 2013; 1(3): e108. [<http://dx.doi.org/10.4172/2329-9053.1000e108>]
- [13] Jaracz S, Chen J, Kuznetsova LV, Ojima I. Recent advances in tumor-targeting anticancer drug conjugates. *Bioorg Med Chem* 2005; 13(17): 5043-54. [<http://dx.doi.org/10.1016/j.bmc.2005.04.084>] [PMID: 15955702]
- [14] Danhier F, Feron O, Pr at V. To exploit the tumor microenvironment: Passive and active tumor targeting of nanocarriers for anti-cancer drug delivery. *J Control Release* 2010; 148(2): 135-46. [<http://dx.doi.org/10.1016/j.jconrel.2010.08.027>] [PMID: 20797419]
- [15] Shi J, Kantoff PW, Wooster R, Farokhzad OC. Cancer nanomedicine: Progress, challenges and opportunities. *Nat Rev Cancer* 2017; 17(1): 20-37. [<http://dx.doi.org/10.1038/nrc.2016.108>] [PMID: 27834398]
- [16] Miller MA, Gadde S, Pfirsche C, et al. Predicting therapeutic nanomedicine efficacy using a companion magnetic resonance imaging nanoparticle. *Sci Transl Med* 2015; 7(314): 314ra183. [<http://dx.doi.org/10.1126/scitranslmed.aac6522>]
- [17] Miller MA, Zheng YR, Gadde S, et al. Tumour-associated macrophages act as a slow-release reservoir of nano-therapeutic Pt(IV) pro-drug. *Nat Commun* 2015; 6: 8692. [<http://dx.doi.org/10.1038/ncomms9692>] [PMID: 26503691]
- [18] Wakaskar RR. Passive and Active Targeting in Tumor Microenvironment. *Int J Drug Dev Res* 2017; 9: 2.

- [19] Ponzoni M, Pastorino F, Di Paolo D, Perri P, Brignole C. Targeting Macrophages as a Potential Therapeutic Intervention: Impact on Inflammatory Diseases and Cancer. *Int J Mol Sci* 2018; 19(7): 1953. [http://dx.doi.org/10.3390/ijms19071953] [PMID: 29973487]
- [20] Toy R, Roy K. Engineering nanoparticles to overcome barriers to immunotherapy. *Bioeng Transl Med* 2016; 1(1): 47-62. [http://dx.doi.org/10.1002/btm2.10005] [PMID: 29313006]
- [21] Edgington-Mitchell LE, Wartmann T, Fleming AK, et al. Legumain is activated in macrophages during pancreatitis. *Am J Physiol Gastrointest Liver Physiol* 2016; 311(3): G548-60. [http://dx.doi.org/10.1152/ajpgi.00047.2016] [PMID: 27514475]
- [22] Liu C, Sun C, Huang H, Janda K, Edgington T. Overexpression of legumain in tumors is significant for invasion/metastasis and a candidate enzymatic target for prodrug therapy. *Cancer Res* 2003; 63(11): 2957-64. [PMID: 12782603]
- [23] Solberg R, Smith R, Almlöf M, et al. Legumain expression, activity and secretion are increased during monocyte-to-macrophage differentiation and inhibited by atorvastatin. *Biol Chem* 2015; 396(1): 71-80.
- [24] Binnemars-Postma K, Storm G, Prakash J. Nanomedicine strategies to target Tumor-associated macrophages. *Int J Mol Sci* 2017; 18(5): 979. [http://dx.doi.org/10.3390/ijms18050979]
- [25] Liu Z, Xiong M, Gong J, et al. Legumain protease-activated TAT-liposome cargo for targeting tumours and their microenvironment. *Nat Commun* 2014; 5: 4280. [http://dx.doi.org/10.1038/ncomms5280] [PMID: 24969588]
- [26] Zhang X, Tian W, Cai X, et al. Hydrazinocurcumin Encapsulated nanoparticles “re-educate” tumor-associated macrophages and exhibit anti-tumor effects on breast cancer following STAT3 suppression. *PLoS One* 2013; 8(6): e65896. [http://dx.doi.org/10.1371/journal.pone.0065896] [PMID: 23825527]
- [27] Casals C, Campanero-Rhodes MA, García-Fojeda B, et al. The Role of Collectins and Galectins in Lung Innate Immune Defense. *Front Immunol* 1998; 2018: 9. [PMID: 30233589]
- [28] Chavez-Santoscoy AV, Roychoudhury R, Pohl NL, Wannemuehler MJ, Narasimhan B, Ramer-Tait AE. Tailoring the immune response by targeting C-type lectin receptors on alveolar macrophages using “pathogen-like” amphiphilic polyanhydride nanoparticles. *Biomaterials* 2012; 33(18): 4762-72. [http://dx.doi.org/10.1016/j.biomaterials.2012.03.027] [PMID: 22465338]
- [29] Porcheray F, Viaud S, Rimaniol AC, et al. Macrophage activation switching: An asset for the resolution of inflammation. *Clin Exp Immunol* 2005; 142(3): 481-9. [http://dx.doi.org/10.1111/j.1365-2249.2005.02934.x] [PMID: 16297160]
- [30] Yu SS, Lau CM, Barham WJ, et al. Macrophage-specific RNA interference targeting via “click”, mannoseylated polymeric micelles. *Mol Pharm* 2013; 10(3): 975-87. [http://dx.doi.org/10.1021/mp300434e] [PMID: 23331322]
- [31] Düffels A, Green LG, Ley SV, Miller AD. Synthesis of high-mannose type neoglycolipids: Active targeting of liposomes to macrophages in gene therapy. *Chemistry* 2000; 6(8): 1416-30. [http://dx.doi.org/10.1002/(SICI)1521-3765(20000417)6:8<1416::AID-CHEM1416>3.0.CO;2-O] [PMID: 10840965]
- [32] Ortega RA, Barham W, Sharman K, Tikhomirov O, Giorgio TD, Yull FE. Manipulating the NF- κ B pathway in macrophages using mannoseylated, siRNA-delivering nanoparticles can induce immunostimulatory and tumor cytotoxic functions. *Int J Nanomedicine* 2016; 11: 2163-77. [http://dx.doi.org/10.2147/IJN.S93483] [PMID: 27274241]
- [33] Song Y, Tang C, Yin C. Combination antitumor immunotherapy with VEGF and PIGF siRNA via systemic delivery of multifunctionalized nanoparticles to tumor-associated macrophages and breast cancer cells. *Biomaterials* 2018; 185: 117-32. [http://dx.doi.org/10.1016/j.biomaterials.2018.09.017] [PMID: 30241030]

- [34] Nimje N, Agarwal A, Saraogi GK, et al. Mannosylated nanoparticulate carriers of rifabutin for alveolar targeting. *J Drug Target* 2009; 17(10): 777-87. [<http://dx.doi.org/10.3109/10611860903115308>] [PMID: 19938949]
- [35] Turk MJ, Breur GJ, Widmer WR, et al. Folate-targeted imaging of activated macrophages in rats with adjuvant-induced arthritis. *Arthritis Rheum* 2002; 46(7): 1947-55. [<http://dx.doi.org/10.1002/art.10405>] [PMID: 12124880]
- [36] Hattori Y, Yamashita J, Sakaida C, Kawano K, Yonemochi E. Evaluation of antitumor effect of zoledronic acid entrapped in folate-linked liposome for targeting to tumor-associated macrophages. *J Liposome Res* 2015; 25(2): 131-40. [<http://dx.doi.org/10.3109/08982104.2014.954128>] [PMID: 25203609]
- [37] Turk MJ, Waters DJ, Low PS. Folate-conjugated liposomes preferentially target macrophages associated with ovarian carcinoma. *Cancer Lett* 2004; 213(2): 165-72. [<http://dx.doi.org/10.1016/j.canlet.2003.12.028>] [PMID: 15327831]
- [38] Penn CA, Yang K, Zong H, et al. Therapeutic Impact of Nanoparticle Therapy Targeting Tumor-Associated Macrophages. *Mol Cancer Ther* 2018; 17(1): 96-106. [<http://dx.doi.org/10.1158/1535-7163.MCT-17-0688>] [PMID: 29133618]
- [39] Cieslewicz M, Tang J, Yu JL, et al. Targeted delivery of proapoptotic peptides to tumor-associated macrophages improves survival. *Proc Natl Acad Sci USA* 2013; 110(40): 15919-24. [<http://dx.doi.org/10.1073/pnas.1312197110>] [PMID: 24046373]
- [40] Kakoschky B, Pleli T, Schmithals C, et al. Selective targeting of tumor associated macrophages in different tumor models. *PLoS One* 2018; 13(2): e0193015. [<http://dx.doi.org/10.1371/journal.pone.0193015>] [PMID: 29447241]
- [41] Qian Y, Qiao S, Dai Y, et al. Molecular-Targeted Immunotherapeutic Strategy for Melanoma via Dual-Targeting Nanoparticles Delivering Small Interfering RNA to Tumor-Associated Macrophages. *ACS Nano* 2017; 11(9): 9536-49. [<http://dx.doi.org/10.1021/acsnano.7b05465>] [PMID: 28858473]
- [42] Scodeller P, Simón-Gracia L, Kopanchuk S, et al. Precision Targeting of Tumor Macrophages with a CD206 Binding Peptide. *Sci Rep* 2017; 7(1): 14655. [<http://dx.doi.org/10.1038/s41598-017-14709-x>] [PMID: 29116108]
- [43] Lee C, Jeong H, Bae H. Development of melittin-based anti-cancer drug for targeting tumor-associated macrophages. *The Journal of Immunology* 2018; 200(1 Supplement): 56.22.56.22;
- [44] Jain S, Amiji M. Tuftsin-modified alginate nanoparticles as a non-condensing macrophage-targeted DNA delivery system. *Biomacromolecules* 2012; 13(4): 1074-85. [<http://dx.doi.org/10.1021/bm2017993>] [PMID: 22385328]
- [45] Soto ER, Caras AC, Kut LC, Castle MK, Ostroff GR. Glucan particles for macrophage targeted delivery of nanoparticles. *J Drug Deliv* 2012; 2012: 143524-4. [<http://dx.doi.org/10.1155/2012/143524>] [PMID: 22013535]
- [46] Zhang M, Kim JA, Huang AY-C. Optimizing Tumor Microenvironment for Cancer Immunotherapy: B-Glucan-Based Nanoparticles. *Front Immunol* 2018; 9: 341-1. [<http://dx.doi.org/10.3389/fimmu.2018.00341>] [PMID: 29535722]
- [47] Upadhyay TK, Fatima N, Sharma D, Saravanakumar V, Sharma R. Preparation and characterization of beta-glucan particles containing a payload of nanoembedded rifabutin for enhanced targeted delivery to macrophages. *EXCLI J* 2017; 16: 210-28. [PMID: 28507467]
- [48] Hoffmann F, Ender F, Schmutte I, et al. Origin, Localization, and Immunoregulatory Properties of Pulmonary Phagocytes in Allergic Asthma. *Front Immunol* 2016; 7(107): 107. [<http://dx.doi.org/10.3389/fimmu.2016.00107>] [PMID: 27047494]

- [49] Tsapis N, Bennett D, Jackson B, Weitz DA, Edwards DA. Trojan particles: Large porous carriers of nanoparticles for drug delivery. *Proc Natl Acad Sci USA* 2002; 99(19): 12001-5. [<http://dx.doi.org/10.1073/pnas.182233999>] [PMID: 12200546]
- [50] Tsugita M, Morimoto N, Tashiro M, Kinoshita K, Nakayama M. SR-B1 Is a Silica Receptor that Mediates Canonical Inflammasome Activation. *Cell Rep* 2017; 18(5): 1298-311. [<http://dx.doi.org/10.1016/j.celrep.2017.01.004>] [PMID: 28147282]
- [51] Geiser M, Wigge C, Conrad ML, et al. Nanoparticle uptake by airway phagocytes after fungal spore challenge in murine allergic asthma and chronic bronchitis. *BMC Pulm Med* 2014; 14(1): 116. [<http://dx.doi.org/10.1186/1471-2466-14-116>] [PMID: 25027175]
- [52] Al Faraj A, Shaik AS, Afzal S, Al Sayed B, Halwani R. MR imaging and targeting of a specific alveolar macrophage subpopulation in LPS-induced COPD animal model using antibody-conjugated magnetic nanoparticles. *Int J Nanomedicine* 2014; 9: 1491-503. [<http://dx.doi.org/10.2147/IJN.S59394>] [PMID: 24711699]
- [53] Al Faraj A, Shaik AS, Afzal S, Al-Muhsen S, Halwani R. Specific targeting and noninvasive magnetic resonance imaging of an asthma biomarker in the lung using polyethylene glycol functionalized magnetic nanocarriers. *Contrast Media Mol Imaging* 2016; 11(3): 172-83. [<http://dx.doi.org/10.1002/cmml.1678>] [PMID: 26708935]
- [54] Halwani R, Sultana Shaik A, Ratemi E, et al. A novel anti-IL4R α nanoparticle efficiently controls lung inflammation during asthma. *Exp Mol Med* 2016; 48(10): e262. [<http://dx.doi.org/10.1038/emm.2016.89>] [PMID: 27713399]
- [55] Chung S, Lee TJ, Reader BF, et al. FoxO1 regulates allergic asthmatic inflammation through regulating polarization of the macrophage inflammatory phenotype. *Oncotarget* 2016; 7(14): 17532-46. [<http://dx.doi.org/10.18632/oncotarget.8162>] [PMID: 27007158]
- [56] Firestein GS. Evolving concepts of rheumatoid arthritis. *Nature* 2003; 423(6937): 356-61. [<http://dx.doi.org/10.1038/nature01661>] [PMID: 12748655]
- [57] Nogueira E, Gomes AC, Preto A, Cavaco-Paulo A. Folate-targeted nanoparticles for rheumatoid arthritis therapy. *Nanomedicine (Lond)* 2016; 12(4): 1113-26. [<http://dx.doi.org/10.1016/j.nano.2015.12.365>] [PMID: 26733257]
- [58] Paulos CM, Turk MJ, Breur GJ, et al. Folate receptor-mediated targeting of therapeutic and imaging agents to activated macrophages in rheumatoid arthritis. *Adv Drug Deliv Rev* 2004; 56(8): 1205-17. [<http://dx.doi.org/10.1016/j.addr.2004.01.012>]
- [59] Alekseeva AA, Moiseeva EV, Onishchenko NR, et al. Liposomal formulation of a methotrexate lipophilic prodrug: Assessment in tumor cells and mouse T-cell leukemic lymphoma. *Int J Nanomedicine* 2017; 12: 3735-49. [<http://dx.doi.org/10.2147/IJN.S133034>] [PMID: 28553111]
- [60] Zhou M, Hou J, Zhong Z, Hao N, Lin Y, Li C. Targeted delivery of hyaluronic acid-coated solid lipid nanoparticles for rheumatoid arthritis therapy. *Drug Deliv* 2018; 25(1): 716-22. [<http://dx.doi.org/10.1080/10717544.2018.1447050>] [PMID: 29516758]
- [61] Poupot R, Goursat C, Fruchon S. Multivalent nanosystems: Targeting monocytes/macrophages. *Int J Nanomedicine* 2018; 13: 5511-21. [<http://dx.doi.org/10.2147/IJN.S146192>] [PMID: 30271144]
- [62] Xiao B, Laroui H, Ayyadurai S, et al. Mannosylated bioreducible nanoparticle-mediated macrophage-specific TNF- α RNA interference for IBD therapy. *Biomaterials* 2013; 34(30): 7471-82. [<http://dx.doi.org/10.1016/j.biomaterials.2013.06.008>] [PMID: 23820013]
- [63] Harrison C. Inflammatory disorders: Monocytes derailed by microparticles. *Nat Rev Drug Discov* 2014; 13(3): 175. [<http://dx.doi.org/10.1038/nrd4263>] [PMID: 24525780]

- [64] Gan J, Dou Y, Li Y, et al. Producing anti-inflammatory macrophages by nanoparticle-triggered clustering of mannose receptors. *Biomaterials* 2018; 178: 95-108. [<http://dx.doi.org/10.1016/j.biomaterials.2018.06.015>] [PMID: 29920405]
- [65] Ahsan F, Rivas IP, Khan MA, Torres Suarez AI. Targeting to macrophages: Role of physicochemical properties of particulate carriers--liposomes and microspheres--on the phagocytosis by macrophages. *J Control Release* 2002; 79(1-3): 29-40. [[http://dx.doi.org/10.1016/S0168-3659\(01\)00549-1](http://dx.doi.org/10.1016/S0168-3659(01)00549-1)] [PMID: 11853916]
- [66] Lee WH, Loo CY, Traini D, Young PM. Nano- and micro-based inhaled drug delivery systems for targeting alveolar macrophages. *Expert Opin Drug Deliv* 2015; 12(6): 1009-26. [<http://dx.doi.org/10.1517/17425247.2015.1039509>] [PMID: 25912721]
- [67] Ortega RA, Barham WJ, Kumar B, et al. Biocompatible mannose-lated endosomal-escape nanoparticles enhance selective delivery of short nucleotide sequences to tumor associated macrophages. *Nanoscale* 2015; 7(2): 500-10. [<http://dx.doi.org/10.1039/C4NR03962A>] [PMID: 25408159]
- [68] Mantovani A, Marchesi F, Malesci A, Laghi L, Allavena P. Tumor-associated macrophages as treatment targets in oncology. *Nat Rev Clin Oncol* 2017; 14(7): 399-416. [<http://dx.doi.org/10.1038/nrclinonc.2016.217>] [PMID: 28117416]
- [69] Zhang M, Gao Y, Caja K, Zhao B, Kim JA. Non-viral nanoparticle delivers small interfering RNA to macrophages in vitro and in vivo. *PLoS One* 2015; 10(3): e0118472. [<http://dx.doi.org/10.1371/journal.pone.0118472>] [PMID: 25799489]
- [70] Nishihira J. Macrophage migration inhibitory factor (MIF): Its essential role in the immune system and cell growth. *J Interferon Cytokine Res* 2000; 20(9): 751-62. [<http://dx.doi.org/10.1089/10799900050151012>] [PMID: 11032394]
- [71] Bifulco C, McDaniel K, Leng L, Bucala R. Tumor growth-promoting properties of macrophage migration inhibitory factor. *Curr Pharm Des* 2008; 14(36): 3790-801. [<http://dx.doi.org/10.2174/138161208786898608>] [PMID: 19128232]
- [72] Song M, Liu T, Shi C, Zhang X, Chen X. Bioconjugated Manganese Dioxide Nanoparticles Enhance Chemotherapy Response by Priming Tumor-Associated Macrophages toward M1-like Phenotype and Attenuating Tumor Hypoxia. *ACS Nano* 2016; 10(1): 633-47. [<http://dx.doi.org/10.1021/acsnano.5b06779>] [PMID: 26650065]
- [73] Huang Z, Zhang J, Jiang Y, et al. Targeted delivery of oligonucleotides into tumor-associated macrophages for cancer immunotherapy. *J Control Release* 2012; 158(2): 286-92. [<http://dx.doi.org/10.1016/j.jconrel.2011.11.013>] [PMID: 22119956]
- [74] Daldrup-Link HE, Golovko D, Ruffell B, et al. MRI of tumor-associated macrophages with clinically applicable iron oxide nanoparticles. *Clin Cancer Res* 2011; 17(17): 5695-704. [<http://dx.doi.org/10.1158/1078-0432.CCR-10-3420>] [PMID: 21791632]
- [75] Zanganeh S, Hutter G, Spitler R, et al. Iron oxide nanoparticles inhibit tumour growth by inducing pro-inflammatory macrophage polarization in tumour tissues. *Nat Nanotechnol* 2016; 11(11): 986-94. [<http://dx.doi.org/10.1038/nnano.2016.168>] [PMID: 27668795]
- [76] Turk MJ, Waters DJ, Low PS. Folate-conjugated liposomes preferentially target macrophages associated with ovarian carcinoma. *Cancer Lett* 2004; 213(2): 165-72. [<http://dx.doi.org/10.1016/j.canlet.2003.12.028>] [PMID: 15327831]
- [77] Nagai T, Tanaka M, Tsuneyoshi Y, et al. Targeting tumor-associated macrophages in an experimental glioma model with a recombinant immunotoxin to folate receptor β . *Cancer Immunol Immunother* 2009; 58(10): 1577-86. [<http://dx.doi.org/10.1007/s00262-009-0667-x>] [PMID: 19238383]
- [78] Etzerodt A, Maniecki MB, Graversen JH, Møller HJ, Torchilin VP, Moestrup SK. Efficient intracellular drug-targeting of macrophages using stealth liposomes directed to the hemoglobin scavenger receptor

CD163. *J Control Release* 2012; 160(1): 72-80. [<http://dx.doi.org/10.1016/j.jconrel.2012.01.034>] [PMID: 22306335]

- [79] Gabizon AA. Stealth liposomes and tumor targeting: One step further in the quest for the magic bullet. *Clin Cancer Res* 2001; 7(2): 223-5. [PMID: 11234871]
- [80] Ries CH, Cannarile MA, Hoves S, et al. Targeting tumor-associated macrophages with anti-CSF-1R antibody reveals a strategy for cancer therapy. *Cancer Cell* 2014; 25(6): 846-59. [<http://dx.doi.org/10.1016/j.ccr.2014.05.016>] [PMID: 24898549]
- [81] Strachan DC, Ruffell B, Oei Y, et al. CSF1R inhibition delays cervical and mammary tumor growth in murine models by attenuating the turnover of tumor-associated macrophages and enhancing infiltration by CD8+ T cells. *Oncol Immunology* 2013; 2(12): E26968-8. [<http://dx.doi.org/10.4161/onci.26968>] [PMID: 24498562]
- [82] Papadopoulos KP, Gluck L, Martin LP, et al. First-in-Human Study of AMG 820, a Monoclonal Anti-Colony-Stimulating Factor 1 Receptor Antibody, in Patients with Advanced Solid Tumors. *Clin Cancer Res* 2017; 23(19): 5703-10. [<http://dx.doi.org/10.1158/1078-0432.CCR-16-3261>] [PMID: 28655795]
- [83] Van Rooijen N, Sanders A. Liposome mediated depletion of macrophages: Mechanism of action, preparation of liposomes and applications. *J Immunol Methods* 1994; 174(1-2): 83-93. [[http://dx.doi.org/10.1016/0022-1759\(94\)90012-4](http://dx.doi.org/10.1016/0022-1759(94)90012-4)] [PMID: 8083541]
- [84] Banciu M, Metselaar JM, Schiffelers RM, Storm G. Antitumor activity of liposomal prednisolone phosphate depends on the presence of functional tumor-associated macrophages in tumor tissue. *Neoplasia* 2008; 10(2): 108-17. [<http://dx.doi.org/10.1593/neo.07913>] [PMID: 18283332]
- [85] Zeisberger SM, Odermatt B, Marty C, Zehnder-Fjällman AH, Ballmer-Hofer K, Schwendener RA. Clodronate-liposome-mediated depletion of tumour-associated macrophages: A new and highly effective antiangiogenic therapy approach. *Br J Cancer* 2006; 95(3): 272-81. [<http://dx.doi.org/10.1038/sj.bjc.6603240>] [PMID: 16832418]
- [86] Piaggio F, Kondylis V, Pastorino F, et al. A novel liposomal Clodronate depletes tumor-associated macrophages in primary and metastatic melanoma: Anti-angiogenic and anti-tumor effects. *J Control Release* 2016; 223: 165-77. [<http://dx.doi.org/10.1016/j.jconrel.2015.12.037>] [PMID: 26742942]
- [87] Song X, Wan Z, Chen T, et al. Development of a multi-target peptide for potentiating chemotherapy by modulating tumor microenvironment. *Biomaterials* 2016; 108: 44-56. [<http://dx.doi.org/10.1016/j.biomaterials.2016.09.001>] [PMID: 27619239]
- [88] Niu M, Valdes S, Naguib YW, Hursing SD, Cui Z. Tumor-Associated Macrophage-Mediated Targeted Therapy of Triple-Negative Breast Cancer. *Mol Pharm* 2016; 13(6): 1833-42. [<http://dx.doi.org/10.1021/acs.molpharmaceut.5b00987>] [PMID: 27074028]
- [89] Zhan X, Jia L, Niu Y, et al. Targeted depletion of tumour-associated macrophages by an alendronate-glucomannan conjugate for cancer immunotherapy. *Biomaterials* 2014; 35(38): 10046-57. [<http://dx.doi.org/10.1016/j.biomaterials.2014.09.007>] [PMID: 25245263]
- [90] Ross R. Atherosclerosis--an inflammatory disease. *N Engl J Med* 1999; 340(2): 115-26. [<http://dx.doi.org/10.1056/NEJM199901143400207>] [PMID: 9887164]
- [91] Bobryshev YV, Ivanova EA, Chistiakov DA, Nikiforov NG, Orekhov AN. Macrophages and Their Role in Atherosclerosis: Pathophysiology and Transcriptome Analysis. *BioMed Res Int* 2016; 2016: 9582430. [<http://dx.doi.org/10.1155/2016/9582430>] [PMID: 27493969]
- [92] DiStasio N, Lehoux S, Khademhosseini A, Tabrizian M. The Multifaceted Uses and Therapeutic Advantages of Nanoparticles for Atherosclerosis Research. *Materials (Basel)* 2018; 11(5): 75493. [<http://dx.doi.org/10.3390/ma11050754>] [PMID: 29738480]

- [93] Petersen LK, York AW, Lewis DR, et al. Amphiphilic nanoparticles repress macrophage atherogenesis: Novel core/shell designs for scavenger receptor targeting and down-regulation. *Mol Pharm* 2014; 11(8): 2815-24. [<http://dx.doi.org/10.1021/mp500188g>] [PMID: 24972372]
- [94] Lee GY, Kim JH, Choi KY, et al. Hyaluronic acid nanoparticles for active targeting atherosclerosis. *Biomaterials* 2015; 53: 341-8. [<http://dx.doi.org/10.1016/j.biomaterials.2015.02.089>] [PMID: 25890732]
- [95] Dellinger A, Olson J, Link K, et al. Functionalization of gadolinium metallofullerenes for detecting atherosclerotic plaque lesions by cardiovascular magnetic resonance. *J Cardiovasc Magn Reson* 2013; 15(1): 7. [<http://dx.doi.org/10.1186/1532-429X-15-7>] [PMID: 23324435]
- [96] Uchida M, Kosuge H, Terashima M, et al. Protein cage nanoparticles bearing the LyP-1 peptide for enhanced imaging of macrophage-rich vascular lesions. *ACS Nano* 2011; 5(4): 2493-502. [<http://dx.doi.org/10.1021/nn102863y>] [PMID: 21391720]
- [97] Kim JB, Park K, Ryu J, et al. Intravascular optical imaging of high-risk plaques in vivo by targeting macrophage mannose receptors. *Sci Rep* 2016; 6: 22608. [<http://dx.doi.org/10.1038/srep22608>] [PMID: 26948523]
- [98] Terashima M, Uchida M, Kosuge H, et al. Human ferritin cages for imaging vascular macrophages. *Biomaterials* 2011; 32(5): 1430-7. [<http://dx.doi.org/10.1016/j.biomaterials.2010.09.029>] [PMID: 21074263]
- [99] Peterson KR, Cottam MA, Kennedy AJ, Hasty AH. Macrophage-Targeted Therapeutics for Metabolic Disease. *Trends Pharmacol Sci* 2018; 39(6): 536-46. [<http://dx.doi.org/10.1016/j.tips.2018.03.001>] [PMID: 29628274]
- [100] Ma L, Liu TW, Wallig MA, et al. Efficient Targeting of Adipose Tissue Macrophages in Obesity with Polysaccharide Nanocarriers. *ACS Nano* 2016; 10(7): 6952-62. [<http://dx.doi.org/10.1021/acsnano.6b02878>] [PMID: 27281538]
- [101] Bu L, Gao M, Qu S, Liu D. Intraperitoneal injection of clodronate liposomes eliminates visceral adipose macrophages and blocks high-fat diet-induced weight gain and development of insulin resistance. *AAPS J* 2013; 15(4): 1001-11. [<http://dx.doi.org/10.1208/s12248-013-9501-7>] [PMID: 23821353]
- [102] Duffield JS. The inflammatory macrophage: A story of Jekyll and Hyde. *Clin Sci (Lond)* 2003; 104(1): 27-38. [<http://dx.doi.org/10.1042/CS20020240>] [PMID: 12519085]
- [103] Aouadi M, Tesz GJ, Nicoloso SM, et al. Orally delivered siRNA targeting macrophage Map4k4 suppresses systemic inflammation. *Nature* 2009; 458(7242): 1180-4. [<http://dx.doi.org/10.1038/nature07774>] [PMID: 19407801]
- [104] Won Y-W, Adhikary PP, Lim KS, Kim HJ, Kim JK, Kim YH. Oligopeptide complex for targeted non-viral gene delivery to adipocytes. *Nat Mater* 2014; 13(12): 1157-64. [<http://dx.doi.org/10.1038/nmat4092>] [PMID: 25282508]
- [105] Black RA. Tumor necrosis factor- α converting enzyme. *Int J Biochem Cell Biol* 2002; 34(1): 1-5. [[http://dx.doi.org/10.1016/S1357-2725\(01\)00097-8](http://dx.doi.org/10.1016/S1357-2725(01)00097-8)] [PMID: 11733179]
- [106] Yong S-B, Song Y, Kim Y-H. Visceral adipose tissue macrophage-targeted TACE silencing to treat obesity-induced type 2 diabetes. *Biomaterials* 2017; 148: 81-9. [<http://dx.doi.org/10.1016/j.biomaterials.2017.09.023>] [PMID: 28985514]

Chapter 7

Summary & Concluding remarks

Summary & Concluding remarks

Molecular imaging became a part of standard care for cancer. By visualization what is happening in the body at a cellular level, molecular imaging provides unique information in detection, diagnosis and treatment of cancer. During the last century much research has been performed in order to enhance pre- and post- operative imaging for early detection and therapy efficacy. Despite efforts, targeting cancer remains challenging due to intra- and inter- tumor heterogeneity. In order to fully advance cancer diagnosis and management using molecular imaging, one would like to bridge together fundamental advances in imaging modalities that can provide different information enabling to cross-examine the disease from several angles.

Within this thesis we performed preclinical studies in different models with the ultimate aim of using molecular imaging for better cancer management. For this purpose, we developed new 'smart' tools for multi-modality imaging of cancer in which optical imaging modalities, like bioluminescence (BLI) and fluorescence (FLI) imaging and radionuclide methods, like (SPECT) were used. Although radionuclide-based modalities are the most advanced ones within the clinical setting, innovative optical molecular imaging modalities, such as those discussed in the chapters of this thesis, are beneficial for better understanding treatment mechanisms and response, and to test and optimize new therapies.

Visualizing Viral Infection by Optical Imaging

Cancer immunotherapy aims to enhance and facilitate an immune response against tumor by inducing patient's own immune response. Most forms of cancer immunotherapy are focused on T- cells, since they are able to kill tumor cells based on the ability to recognize specific tumor- and neo-epitopes. The growing understanding of cell compartment within tumor microenvironment (TME), and recent clinical success of cancer immunotherapy, led to the development of novel imaging tools, and better monitoring of the immune system. In recent decades, impressive responses were observed in the clinic using cancer immunotherapy. Nevertheless, many patients do not respond, or temporarily respond to therapy, which raises the need for improved immunotherapeutic drugs and 'smart' imaging tools to better understand treatment mechanism and patient's response (1). Oncolytic viruses are a newer class of immunotherapy (2, 3). These viruses are either genetically modified, or naturally occurring viruses that selectively disrupt and replicate in cancer cells (4-6). These viruses were shown to turn 'cold' (immune-suppressive) tumors into 'hot' (immune-active) tumors by induction of T- cell infiltration in tumors (7-9).

An important tool to monitor the process of viral infection are reporter viruses. Nevertheless, generating recombinant reporter viruses remains a challenge; the smaller the inserted reporter gene, the more stable the viral genome remains.

Since most viruses do not tolerate large genome alterations (10), we propose a solution to this problem in **Chapter 2**. We used the NanoLuc® Binary Technology (NanoBiT®)

which is a two-subunit system based on split NanoLuc® luciferase consisting of the small HiBiT (11 amino acids) that, when in close proximity, will reconstitute with its complementary large part (LgBiT). The very small HiBiT (33 base pairs/11 amino-acids) can be used as a tag which can be inserted anywhere within the viral genome, without substantially altering its properties (11). In our system, the HiBiT tag was inserted into the viral genome of a clinically used oncolytic virus, that upon infection of prostate cancer cells (PC-3), expressing the LgBiT, will reconstitute into the full NanoLuc enzyme that can generate strong bioluminescent light in the presence of its substrate. Having generated these tools, we demonstrate the power of our system, by monitoring infection dynamics of the HiBiT-reporter virus in living mice over the course of 6 weeks, using established PC-3-LgBiT tumors and hydrofurimazine as the novel water soluble NanoLuc substrate. We anticipate that pre-clinical research into (oncolytic) viral infections, and a wide range of other viruses, especially those ones not tolerating large genome alterations, will strongly benefit from our BL-based viral screening tool, enabling fast and simple readout protocols applicable for rapid drug screening both *in vitro* and *in vivo*.

Identification of Preferred Luciferase/Substrate Pairings for *in Vivo* BLI

Bioluminescence imaging (BLI) has become a vital tool in preclinical *in vitro* and *in vivo* studies for visualizing molecular events at cellular level (12). The superiority of BLI lies in the high signal/noise ratios and quantum efficiencies of luciferase/luciferin systems, leading to an extremely high detectability in cell based assays, and for *in vivo* molecular imaging (13, 14). Thousands of bioluminescent species are represented by ~700 genera among which 90% originate from marine organisms (15, 16) (e.g. NanoLuc or Renilla). These luciferases mainly utilize coelenterazine, varguline or analogues of these two luciferins as substrates. The other big subset of luciferase genes are terrestrial luciferases that require D-luciferin analogues, such as firefly or click beetle luciferases. Bioluminescence reactions are highly dependent on the interaction between the luciferase enzyme and its substrate, and any modification of the substrate can lead to a different emission spectrum and reaction sensitivity.

During recent years the BL toolbox was immensely expanded with newly engineered luciferase genes, with different emission characteristic, and luciferin analogues that enhance *in vivo* light emission and increase detection sensitivity in deeper tissues (17). These advances expanded the potential of BLI where numerous processes can be monitored in the same animal, lowering the amount of needed animal models, lowering costs and saving time.

Improving the performance of luciferase enzymes, substrates and their mutants for BLI is an important part in improving the tools available for life science research (18).

In **Chapter 3** and **Chapter 4** we investigated BLI properties of novel substrate analogues. We provide a detailed *in vitro* and *in vivo* analysis of brightness and emission spectra in or-

der to detect the best performing luciferase/luciferin pairings with a final aim of increased detection sensitivity. Inter alia, we anticipate that the luciferase/luciferin pairings, used and described within this thesis, will serve as a stepping stone for development of more sensitive imaging approaches. We expect that the obtained results of such analysis will be beneficial for researchers in order to choose the most optimal luciferase/luciferin pairing in different experimental setups.

NanoLuc (NLuc) is a marine derived luciferase and represents an important addition to the marine BLI-toolset. It gained popularity due to its small size (19 kDa) and superior bioluminescence performance offering increased sensitivity, fast response dynamics and low background auto-luminescence (19, 20). For *in vivo* imaging applications, NanoLuc has been limited by its substrate furimazine, which has low solubility and *in vivo* bio-availability. Within **Chapter 4** we compared performances of recently reported NanoLuc substrates for *in vivo* imaging in mice, since recently they have demonstrated to be better suited for *in cellulo* and *in vivo* NLuc based imaging (21-23). Two substrates with improved aqueous solubility, hydrofurimazine and fluorofurimazine, were evaluated along with three stabilized *O*-acetylated furimazine analogues, the hikarazines (21, 22). All 5 analogues, when tested *in vitro*, displayed greater signal intensity and reaction duration, in comparison to the standard NLuc substrate, furimazine. NanoLuc/fluorofurimazine pairing demonstrated the highest bioluminescence intensity. It was found to be around 9-fold brighter compared to the NanoLuc/furimazine combination. Excitingly, despite the fact that NanoLuc/fluorofurimazine emits mostly blue light, which gets easily absorbed by surrounding tissue in small animals, we proved that cells trapped in mice lung vasculature could be visualized *via* the NanoLuc/fluorofurimazine pairing. Among all tested analogues, fluorofurimazine enables higher substrate loading and improved *in vivo* optical imaging sensitivity, upgrading NanoLuc derived bioluminescent systems for deep tissue imaging.

Sensitivity of BL reactions in animals primarily depends on the amount of photons emitted by luciferases at wavelengths greater than 620 nm, where tissue penetration is high (24). Firefly (Luc2), click beetle (CBR and CBR2) systems with D-Luciferin and its analogues, dominate this field of BLI. In order to further improve light emission from deep tissues, several attempts have been made in order to shift the emission to the near infrared (NIR) (650-900 nm), resulting with improved luciferase/luciferin systems (24). In **Chapter 5**, for the first time, we directly compared *in vivo* spectral characteristics of firefly (Luc2), click beetle green (CBG99), click beetle red 2 (CBR2), and AkaLuc luciferases when paired with different D-luciferin (D-LH2) analogues (AkaLuc, CycLuc1 and amino-naphthyl (NH₂-NpLH2)). From our *in vivo* results we could clearly conclude: the best substrate, in terms of signal strength, for firefly luciferase (Luc2), click beetle green (CBG99) and click beetle red 2 (CBR2) was clearly D-Luciferin; the emission spectra of firefly (Luc2) and click beetle red 2 (CBR2) was shifted to a longer wavelength when we used AkaLumine as substrate; Click beetle red 2 (CBR2) produced the brightest signals

with the near-infrared substrate (NIR), amino-naphthyl (NH₂-NpLH₂); AkaLuc, paired either with CycLuc1 or AkaLumine, was brighter than when paired with D-Luciferin.

We expect that the obtain results will be of benefit for researches, enabling selection of best performing enzyme/substrate pairings for applications of interest.

Bioluminescence & Radionuclide Based Reporter Gene System

Reporter genes represent a straight forward means for monitoring emerging tumors and enables *in vivo* visualization and distribution of cells targeting the tumor, such as T- cells and their interaction with cancer cells. Generating specific multi-modality imaging probes will facilitate the translation of molecular-genetic imaging into clinical application for cancer diagnosis and therapy (25). An attractive approach, and a compensation on limitations of each individual imaging technique, is the coupling of nuclear (SPECT/PET) with optical (BLI/FLI) imaging modalities. SPECT/PET scans provide whole body 3D images and quantitative analyses of reporter expression, and on the other hand, optical imaging modalities (BLI/FLI) provide 2D images with high sensitivity but limited tissue penetration (1-2 cm) (25, 26).

In **Chapter 5** we dare to ask the question: ‘Can we shift a bioluminescence reporter system towards a nuclear imaging one?’ In this study we developed a reporter gene system that supports bioluminescence (BLI) imaging in addition to nuclear (SPECT/PET) imaging. We used the LgBiT subunit, and combined it with the radioactively labelled HiBiT peptide from the BL ‘NanoBiT[®]’ split-system. We first constructed a chimeric transmembrane reporter gene (TM-LgBiT) and expressed it on the membrane of HEK-293T and PC-3 cells. Secondly, a reliable procedure for labelling HiBiT with indium-111 was established where we generated the [111In]In-DOTA-6-Ahx-HiBiT probe. We were able to detected specific binding of DOTA-6-Ahx-HiBiT, using bioluminescence imaging *in vitro* from cells, and *in vivo* from tumors expressing the TM-LgBiT reporter. Preliminary SPECT/CT scans showed specific [111In]In-DOTA-6-Ahx-HiBiT tracer uptake in mice implanted with target positive cells, which was confirmed by *ex vivo* biodistribution studies. To answer the question: ‘Can we shift a bioluminescence reporter system towards a nuclear imaging one?’- yes, we can. Future optimization of our system, such as: injecting higher amounts of HiBiT tracer (e.g. 1 nmol) to animals, and evaluation of most suitable imaging time point, after probe administration, are essential.

We believe that our system will be of great benefit in future cell tracking studies and in diagnostic/prognostic settings, and when we can show that this approach does not induce an immune response, it can even be translated into clinical practice i.e. to monitor cell based therapies.

Targeting Macrophages

Molecular imaging revolutionized the way we perceive and approach the human body, plan and approach drug design and diagnose disease (27). Bioluminescence optical imaging is a well suited imaging technique for visualization of the immune system, allowing real time insight in immune cell dynamics, which often change location and expand in number. Different cell tracking methods emerged over past years, and in comparison to optical imaging, alternative imaging methods of injected molecules or cells offer advantages, such as excellent spatial resolution (MRI) and absolute resolution in case of nuclear imaging modalities (28-30). Macrophages play a role in almost every disease and became an attractive therapeutic target. Understanding macrophage diversity, tissue distribution and plasticity will help in defining precise targeting strategies and effective therapies. In **Chapter 6** we highlight recent progress on active nanotechnology-based systems, which are playing central roles, in targeting macrophage subsets for therapeutic purposes in diseased tissues.

Concluding remarks

Within this work, we discussed several applications, that contribute to our knowledge on the value of imaging and cell tracking, particularly in the field of oncology. In spite of the many efforts on designing and optimizing the ‘perfect’ imaging approach, the ‘perfect’ results have yet not been found. Designing novel imaging approaches, and improving the current, remains vital for how we diagnose, understand and treat patients. In other words, the search must continue.

No current available imaging modality provides all answers. Within this thesis, the focus was to generate new ‘smart’ imaging tools, and optimize the currently available ones, for more sensitive cellular imaging.

In order to image and monitor viral infection in real time, we developed a novel imaging platform based on the bioluminescent ‘NanoBiT[®]’ system where we show that light emitting luciferase enzymes, when incorporated into viral genome, enable bioluminescence detection from infected cells, using sensitive charge-coupled device (CCD) camera systems. Furthermore, with several advances within the BL toolkit, such as novel mutated luciferase enzymes and substrate analogues, within this thesis, we evaluated the best marine- and terrestrial- derived luciferase/substrate pairings that will be beneficial for researchers, in order to choose the most suitable enzyme/substrate pairing, depending on the experimental setup.

We took the next step in our quest and developed a reporter gene system that simultaneously supports bioluminescence imaging (BLI) in addition to nuclear (SPECT/PET) imaging. This combination of optical and nuclear imaging modalities may further facilitate research and potentially find application in personalized health care for cell tracking.

In summary, with continuous evolution of newer multi-modality imaging reporters/probes and equipment, it will be possible to better track cells, monitor biological processes, improve diagnosis and drug development and better determine therapy efficacy, finally resulting in better quality of life of cancer patients.

REFERENCES

1. Kurtz DM, Gambhir SS. Tracking cellular and immune therapies in cancer. *Adv Cancer Res.* 2014;124:257-96.
2. Jiang H, Shin DH, Nguyen TT, Fueyo J, Fan X, Henry V, et al. Localized Treatment with Oncolytic Adenovirus Delta-24-RGDOX Induces Systemic Immunity against Disseminated Subcutaneous and Intracranial Melanomas. *Clinical Cancer Research.* 2019;25(22):6801.
3. Kaufman HL, Kohlhapp FJ, Zloza A. Oncolytic viruses: a new class of immunotherapy drugs. *Nat Rev Drug Discov.* 2015;14(9):642-62.
4. Lichty BD, Breitbach CJ, Stojdl DF, Bell JC. Going viral with cancer immunotherapy. *Nature Reviews Cancer.* 2014;14(8):559-67.
5. Jiang H, Gomez-Manzano C, Rivera-Molina Y, Lang FF, Conrad CA, Fueyo J. Oncolytic adenovirus research evolution: from cell-cycle checkpoints to immune checkpoints. *Curr Opin Virol.* 2015;13:33-9.
6. Russell SJ, Peng KW, Bell JC. Oncolytic virotherapy. *Nat Biotechnol.* 2012;30(7):658-70.
7. Lang FF, Conrad C, Gomez-Manzano C, Yung WKA, Sawaya R, Weinberg JS, et al. Phase I Study of DNX-2401 (Delta-24-RGD) Oncolytic Adenovirus: Replication and Immunotherapeutic Effects in Recurrent Malignant Glioma. *J Clin Oncol.* 2018;36(14):1419-27.
8. Jiang H, Rivera-Molina Y, Gomez-Manzano C, Clise-Dwyer K, Bover L, Vence LM, et al. Oncolytic Adenovirus and Tumor-Targeting Immune Modulatory Therapy Improve Autologous Cancer Vaccination. *Cancer Res.* 2017;77(14):3894-907.
9. Jiang H, Clise-Dwyer K, Ruisaard KE, Fan X, Tian W, Gumin J, et al. Delta-24-RGD Oncolytic Adenovirus Elicits Anti-Glioma Immunity in an Immunocompetent Mouse Model. *PLOS ONE.* 2014;9(5):e97407.
10. Cai H, Liu M, Russell CJ. Directed Evolution of an Influenza Reporter Virus To Restore Replication and Virulence and Enhance Noninvasive Bioluminescence Imaging in Mice. *Journal of Virology.* 2018;92(16):e00593-18.
11. Gaspar N, Zambito G, Dautzenberg IJC, Cramer SJ, Hoeben RC, Lowik C, et al. NanoBiT System and Hydrofurimazine for Optimized Detection of Viral Infection in Mice—A Novel in Vivo Imaging Platform. *International Journal of Molecular Sciences.* 2020;21(16).
12. Kaijzel EL, van der Pluijm G, Löwik CWGM. Whole-Body Optical Imaging in Animal Models to Assess Cancer Development and Progression. *Clinical Cancer Research.* 2007;13(12):3490.
13. Roda A, Pasini P, Mirasoli M, Michelini E, Guardigli M. Biotechnological applications of bioluminescence and chemiluminescence. *Trends Biotechnol.* 2004;22(6):295-303.
14. Roda A, Guardigli M, Michelini E, Mirasoli M. Bioluminescence in analytical chemistry and in vivo imaging. *TrAC Trends in Analytical Chemistry.* 2009;28:307-22.
15. Shimomura O. *Bioluminescence: Chemical principles and methods*, revised edition 2012. 1-468 p.
16. Martini S, Haddock SHD. Quantification of bioluminescence from the surface to the deep sea demonstrates its predominance as an ecological trait. *Scientific Reports.* 2017;7(1):45750.
17. Adams ST, Jr., Miller SC. Beyond D-luciferin: expanding the scope of bioluminescence imaging in vivo. *Curr Opin Chem Biol.* 2014;21:112-20.
18. Markova SV, Vysotski ES. Coelenterazine-dependent luciferases. *Biochemistry (Moscow).* 2015;80(6):714-32.
19. Hall MP, Unch J, Binkowski BF, Valley MP, Butler BL, Wood MG, et al. Engineered Luciferase Reporter from a Deep Sea Shrimp Utilizing a Novel Imidazopyrazinone Substrate. *ACS Chemical Biology.* 2012;7(11):1848-57.

20. Dale NC, Johnstone EKM, White CW, Pflieger KDG. NanoBRET: The Bright Future of Proximity-Based Assays. *Frontiers in Bioengineering and Biotechnology*. 2019;7(56).
21. Morse D, Tannous BA. A water-soluble coelenterazine for sensitive in vivo imaging of coelenterate luciferases. *Molecular therapy : the journal of the American Society of Gene Therapy*. 2012;20(4):692-3.
22. Schwinn MK, Machleidt T, Zimmerman K, Eggers CT, Dixon AS, Hurst R, et al. CRISPR-Mediated Tagging of Endogenous Proteins with a Luminescent Peptide. *ACS Chemical Biology*. 2018;13(2):467-74.
23. Inouye S, Sato J, Sahara-Miura Y, Yoshida S, Kurakata H, Hosoya T. C6-Deoxy coelenterazine analogues as an efficient substrate for glow luminescence reaction of nanoKAZ: the mutated catalytic 19 kDa component of Oplophorus luciferase. *Biochem Biophys Res Commun*. 2013;437(1):23-8.
24. Hall MP, Woodrooffe CC, Wood MG, Que I, van't Root M, Ridwan Y, et al. Click beetle luciferase mutant and near infrared naphthyl-luciferins for improved bioluminescence imaging. *Nature Communications*. 2018;9(1):132.
25. Kang JH, Chung JK. Molecular-genetic imaging based on reporter gene expression. *J Nucl Med*. 2008;49 Suppl 2:164S-79S.
26. Akins EJ, Dubey P. Noninvasive Imaging of Cell-Mediated Therapy for Treatment of Cancer. *Journal of Nuclear Medicine*. 2008;49(Suppl 2):180S.
27. James ML, Gambhir SS. A molecular imaging primer: modalities, imaging agents, and applications. *Physiol Rev*. 2012;92(2):897-965.
28. Kherlopian AR, Song T, Duan Q, Neimark MA, Po MJ, Gohagan JK, et al. A review of imaging techniques for systems biology. *BMC Syst Biol*. 2008;2:74.
29. Penet M-F, Mikhaylova M, Li C, Krishnamachary B, Glunde K, Pathak AP, et al. Applications of molecular MRI and optical imaging in cancer. *Future Med Chem*. 2010;2(6):975-88.
30. Wu C, Have F, Vastenhouw B, Dierckx R, Paans A, Beekman F. Absolute quantitative total-body small-animal SPECT with focusing pinholes. *Eur J Nucl Med Mol Imaging*. 2010;37:2127-35.

Nederlandse Samenvatting

Samenvatting en conclusie

Tegenwoordig is moleculaire beeldvorming een onderdeel geworden van de standaardzorg voor kanker. Door te zien wat er op cellulair niveau in het lichaam gebeurt, levert moleculaire beeldvorming unieke informatie op bij het opsporen, diagnosticeren en behandelen van kanker. In de afgelopen eeuw is er veel onderzoek gedaan om pre- en postoperatieve beeldvorming voor vroege detectie te verbeteren. Ondanks inspanningen blijft het bestrijden van kanker een uitdaging vanwege intra- en inter tumor heterogeniteit. Om de behandeling en de diagnose van kanker volledig te verbeteren, door middel van moleculaire beeldvorming, is het nodig om fundamentele vorderingen in beeldvormingsmodaliteiten te gebruiken om zo de ziekte vanuit verschillende hoeken te onderzoeken.

Binnen dit proefschrift hebben we preklinische studies uitgevoerd in verschillende modellen met als uiteindelijk doel het gebruik van moleculaire beeldvorming bij de studering en behandeling van kanker. Een multi-modaliteits beeldperspectief, waarin optische beeldvormingsmodaliteiten, zoals bioluminescentie (BLI) en fluorescentie (FLI) beeldvorming en radionuclidemethoden zoals (SPECT) werden gebruikt om 'slimme' tools voor kankerdetectie te ontwikkelen. Hoewel op radionucliden gebaseerde modaliteiten de meest geavanceerde zijn binnen de klinische setting, zijn innovatieve optische moleculaire beeldvormingsmodaliteiten, zoals die besproken in de hoofdstukken van dit proefschrift, gunstig om diagnose en behandeling in de goede richting te leiden.

Virale infectie visualiseren door optische beeldvorming

Immunotherapie bij kanker heeft tot doel de immuunrespons te versterken en te vergemakkelijken door een eigen immuunrespons op te wekken. De meeste vormen van kankerimmunotherapie zijn gericht op T-cellen, omdat ze tumorcellen kunnen doden op basis van het vermogen om gemuteerde eiwitten te onderscheiden. Het groeiende begrip van de cel in de micro-omgeving van tumoren en het recente klinische succes van kankerimmunotherapie, hebben geleid tot de ontwikkeling van nieuwe beeldvormingsinstrumenten voor een betere monitoring van het immuunsysteem. In de kliniek werden de afgelopen decennia indrukwekkende reacties waargenomen na immunotherapie tegen kanker. Echter slechts een relatief klein percentage (<20%) patiënten reageert op de therapie waardoor er een grote behoefte is aan verbeterde immunotherapiemedicijnen en 'slimme' beeldvormingsinstrumenten om de behandeling en de respons van de patiënten beter te begrijpen (1). Oncolytische virussen zijn een nieuwere klasse van immunotherapie-medicijnen (2, 3). Deze virussen zijn ofwel genetisch gemodificeerd, ofwel natuurlijk voorkomende virussen die zich selectief in kankercellen kunnen vermenigvuldigen en de kankercellen kunnen doden (4-6). Deze virussen blijken 'koude' (immuun-onderdrukkende) tumoren om te kunnen zetten in 'hete' (immuun-actieve) tumoren door inductie van T-celinfiltratie in tumoren (7-9).

Een belangrijk hulpmiddel om de routes van virale infectie te bestuderen, zijn reportervirussen. Echter, het genereren van recombinante virussen blijft een uitdaging. Hoe kleiner het ingevoegde reporter gen, des te stabielier blijft het virale genoom. Aangezien de meeste virussen geen grote genoomveranderingen tolereren (10), dragen we in Hoofdstuk 2 een oplossing aan voor dit probleem. We gebruikten de HiBiT-tag, de kleinste bioluminescente reporter, die overal in het virale genoom kan worden ingevoegd, zonder de eigenschappen ervan wezenlijk te veranderen (11). In ons systeem werd de HiBiT-tag (33 basenparen / 11 aminozuren) ingebracht in het virale genoom van een klinisch gebruikt oncolytisch virus. Na infectie van kankercellen, die het complementaire grote deel (LgBiT) tot expressie brengen, met het HiBiT-gelabelde virus, zal HiBiT met LgBiT reconstitueren tot het volledige NanoLuc-luciferase. Als vervolgens het substraat wordt toegediend zal het gereconstitueerde NanoLuc enorm veel bioluminescentielicht genereren. Met deze tools demonstreren vervolgens we de kracht van ons systeem door de infectiedynamiek van het HiBiT-reportervirus in levende muizen in de loop van 6 weken te volgen. Dit wordt gedaan in muizen met PC-3-LgBiT prostaattumoren en hydrofurimazine als het nieuwe in wateroplosbare NanoLuc-substraat. We verwachten dat preklinisch onderzoek naar oncolytische virale infecties en een breed scala aan andere virussen, vooral virussen die geen grote genoomveranderingen verdragen, sterk zullen profiteren van onze op BL gebaseerde virale screeningstool, waardoor snelle en eenvoudige uitleesprotocollen mogelijk zijn voor snelle screening van geneesmiddelen.

Identificatie van luciferase / substraat-paren die de voorkeur hebben voor in vivo BLI

Bioluminescentiebeeldvorming (BLI) is een essentieel instrument geworden in preklinische in vitro en in vivo studies voor het visualiseren van moleculaire processen op cellulair niveau (12). De superioriteit van BLI ligt in de hoge signaal/ruisverhoudingen en lichtquantum-opbrengst van luciferase/ luciferinesystemen, wat leidt tot een extreem hoge detecteerbaarheid van cellen in celgebaseerde onderzoeken en voor in vivo moleculaire beeldvorming (13, 14). Duizenden lichtgevende soorten worden vertegenwoordigd door ~ 700 geslachten, waarvan 90% afkomstig is van mariene organismen (15, 16) (bijv. NanoLuc of Renilla). Deze luciferasen gebruiken hoofdzakelijk coelenterazine, varguline of analogen van deze twee luciferinen als substraten. De andere grote subset van luciferasegenen zijn terrestrische luciferasen die D-luciferine-analogen vereisen, zoals vuurvlieg- of klik-kever luciferasen. Bioluminescentiereacties zijn sterk afhankelijk van de interactie tussen het luciferase-enzym en zijn substraat, en elke wijziging van het substraat kan leiden tot een ander emissiespectrum en reactiegevoeligheid.

De afgelopen jaren is de BL-toolbox enorm uitgebreid met nieuw ontwikkelde luciferasegenen, met verschillende emissiekenmerken, en luciferine-analogen die de in vivo lichtemissie verbeteren en de detectiegevoeligheid in diepere weefsels verhogen (17). Deze

voortgang vergroot het potentieel van BLI, waar meerdere processen kunnen worden gevolgd in hetzelfde diermodel, waardoor kosten worden verlaagd en tijd wordt bespaard.

Het verbeteren van de prestaties van luciferase-enzymen, -substraten en hun mutanten voor BLI is een belangrijk onderdeel van het verbeteren van de tools die beschikbaar zijn voor biowetenschappelijk onderzoek (18).

In Hoofdstuk 3 en Hoofdstuk 4 hebben we de BLI-eigenschappen van nieuwe substraatanalogen onderzocht. We bieden een gedetailleerde *in vitro* en *in vivo* analyse van helderheid en emissiespectra om de best presterende luciferase / luciferine-paringen te vinden met als uiteindelijk doel een verhoogde detectiegevoeligheid. We verwachten onder meer dat de luciferase / luciferine-paren, gebruikt en beschreven in dit proefschrift, zullen dienen als een springplank voor de ontwikkeling van meer gevoelige beeldvormende benaderingen. We verwachten dat de verkregen resultaten van een dergelijke analyse gunstig zullen zijn voor onderzoekers om de meest optimale luciferase / luciferine paren in verschillende experimentele opstellingen te kiezen.

NanoLuc (NLuc) is een mariene luciferase en vormt een belangrijke aanvulling op de mariene BLI-toolset. Het won aan populariteit vanwege zijn relatief kleine formaat (19 kDa) en superieure bioluminescentieprestaties met verhoogde gevoeligheid, snelle reactiedynamiek en lage auto luminescentie op de achtergrond (19, 20). Voor *in vivo* beeldvormingstoepassingen werd NanoLuc beperkt door zijn substraat furimazine, dat een lage oplosbaarheid en *in vivo* biologische beschikbaarheid heeft. In Hoofdstuk 4 vergeleken we de prestaties van recent gerapporteerde NanoLuc-substraten voor *in vivo* beeldvorming bij muizen, aangezien recentelijk is aangetoond dat ze beter geschikt zijn voor *in cellulo* en *in vivo* NLuc gebaseerde beeldvorming (21-23). Twee substraten met verbeterde oplosbaarheid in water, hydrofurimazine en fluorofurimazine, werden geëvalueerd samen met drie gestabiliseerde O-geacetylerde furimazine-analogen, de hikarazines (21, 22). Alle vijf analogen vertoonden, wanneer ze *in vitro* werden getest, een grotere signaalintensiteit en reactieduur, in vergelijking met het standaard NLuc-substraat, furimazine. NanoLuc / fluorofurimazine-koppeling vertoonde de hoogste bioluminescentie-intensiteit. Het bleek ongeveer negen keer helderder te zijn in vergelijking met de NanoLuc / furimazine-combinatie. Interessant is dat ondanks het feit dat NanoLuc / fluorofurimazine voornamelijk blauw licht uitzendt, dat gemakkelijk wordt geabsorbeerd door het omringende weefsel bij kleine dieren, hebben we aangetoond dat cellen die na inspuiting zich bevinden in de vasculatuur van de longen van muizen gevisualiseerd konden worden via de NanoLuc / fluorofurimazine-koppeling. Van alle geteste analogen maakt fluorofurimazine een hogere substraatbelasting en verbeterde *in vivo* optische beeldvormingsgevoeligheid mogelijk, waardoor NanoLuc-afgeleide bioluminescente systemen ook gebruikt kunnen worden voor diepe weefselbeeldvorming.

De gevoeligheid van BLI in dieren hangt voornamelijk af van de hoeveelheid fotonen die wordt uitgezonden door luciferasen bij golflengten groter dan 620 nm, waar de weef-

selpenetratie van licht hoog is (24). Firefly (Luc2), klikkever (CBR en CBR2) systemen met D-Luciferine en zijn analogen domineren het veld van BLI. Om de lichtemissie uit diepe weefsels verder te verbeteren, zijn verschillende pogingen gedaan om de emissie te verschuiven naar het nabij-infrarood (NIR) (650-900 nm), resulterend in verbeterde luciferase / luciferinesystemen (24). In Hoofdstuk 5 hebben we voor de eerste keer in vivo spectrale kenmerken van vuurvlieg (Luc2), klikkever groen (CBG99), klikkever rood 2 (CBR2) en AkaLuc luciferases vergeleken met verschillende D-luciferine (D- LH2) analogen (AkaLuc, CycLuc1 en amino-naftyl (NH₂-NpLH2)). Uit onze in vivo resultaten konden we duidelijk concluderen: het beste substraat, in termen van signaalsterkte, voor vuurvlieg luciferase (Luc2), klikkever groen luciferase (CBG99) en klikkever rood 2 luciferase (CBR2) was duidelijk D-luciferine; de emissiespectra van vuurvlieg luciferase (Luc2) en klikkever rood 2 luciferase (CBR2) werden verschoven naar een langere golflengte toen we AkaLucine als substraat gebruikten; Klikkever rood 2 luciferase (CBR2) produceerde de helderste signalen met het nabij-infraroodsubstraat (NIR), amino-naftyl (NH₂-NpLH2); AkaLuc, gecombineerd met CycLuc1 of AkaLucine, was helderder dan in combinatie met D-Luciferin.

We verwachten dat de verkregen resultaten van nut zullen zijn voor veel onderzoekers, die het mogelijk maakt om de best presterende enzym / substraat-paren te selecteren voor hun onderzoekstoepassingen.

Bioluminescentie en op radionucliden gebaseerd reportergensysteem

Reporter (marker) genen vertegenwoordigen een eenvoudige manier voor het volgen van opkomende tumoren, en die het mogelijk maakt om bepaalde cel-interacties en biodistributie van bepaalde cellen te bestuderen zoals zoals b.v. de interactie tussen T-cellen en kankercellen. Het genereren van multi-modale beeldvormingsprobes waar een enkele probe gebruikt kan worden voor verschillende imagingmodaliteiten zal de vertaling van moleculair-genetische beeldvorming naar de kliniek voor kanker-diagnose en -therapie vergemakkelijken (25). Een aantrekkelijke benadering en een compensatie voor de beperkingen van elke individuele beeldvormingstechniek, is het gebruik van duale beeldvormingsreporters/probes voor zowel nucleaire (SPECT / PET) als optische (BLI / FLI) beeldvormingsmodaliteiten. SPECT / PET-scans bieden 3D-beelden en kwantitatieve analyses van reporterexpressie, en aan de andere kant bieden optische beeldvormingsmodaliteiten (BLI / FLI) 2D-beelden met een hoge gevoeligheid (25, 26).

In Hoofdstuk 5 durven we de vraag te stellen: ‘Kunnen we een bioluminescentiereportersysteem ook gebruiken voor een nucleair beeldvormingssysteem? In deze studie hebben we een reporter-gen-systeem ontwikkeld dat zowel voor bioluminescentie (BLI) beeldvorming gebruikt kan worden alsook voor nucleaire (SPECT / PET) beeldvorming. Voor dit gebruikten de LgBiT-subeenheid van het NanoLuc en combineerden deze met het radioactief gelabelde complementaire HiBiT-peptide van het ‘NanoBiT’ split-luciferase

systeem. Eerst hebben we een chimeer transmembraanreportergen (TM-LgBiT) geconstrueerd en het tot expressie gebracht op het membraan van HEK-293T- en PC-3-cellen. Vervolgens werd een betrouwbare procedure voor het labelen van HiBiT met indium-111 vastgesteld, waar we [¹¹¹In] In-DOTA-6-Ahx-HiBiT als tracer verkregen. We waren in staat om specifieke opname van niet-radioactief DOTA-6-Ahx-HiBiT te detecteren, met behulp van bioluminescentie-beeldvorming in vitro van cellen en in vivo van tumoren die TM-LgBiT-reporter tot expressie brengen. Voorlopige SPECT / CT-scans van radioactief [¹¹¹In] In-DOTA-6-Ahx-HiBiT liet specifiek traceropname zien in muizen die waren geïmplant met doelwit-positieve cellen, wat werd bevestigd door ex vivo bio distributie studies. Om de vraag te beantwoorden: ‘Kunnen we een bioluminescentie-reportersysteem ook gebruiken voor een nucleaire beeldvorming?’ - ja, dat kunnen we. Toekomstige optimalisatie van ons systeem zoals het injecteren van grotere hoeveelheden HiBiT-tracer (bijv. 1 nmol) bij dieren, en evaluatie van het meest geschikte tijdpunt voor beeldvorming, na toediening van de probe, zijn essentieel.

Wij zijn van mening dat ons systeem van groot nut zal zijn bij toekomstige cel-tracering studies en mogelijk ook in diagnostische / prognostische evaluaties.

Richten op macrofagen

Moleculaire beeldvorming heeft een revolutie teweeggebracht in de manier waarop we het menselijk lichaam waarnemen en benaderen, het ontwikkelen van geneesmiddelen plannen en benaderen en ziekten diagnosticeren (27). Bioluminescentie optische beeldvorming is een zeer geschikte beeldvormingstechniek voor visualisatie van het immuunsysteem, waardoor real-time inzicht mogelijk wordt gemaakt in de dynamiek van immuuncellen, die vaak van locatie veranderen en in aantal toenemen. Verschillende celtraceringstechnieken zijn de afgelopen jaren naar voren gekomen en in vergelijking met optische beeldvorming bieden alternatieve beeldvormingsmethoden van geïnjecteerde moleculen of cellen voordelen, zoals een uitstekende ruimtelijke resolutie bij MRI en absolute resolutie in het geval van nucleaire beeldvormingsmodaliteiten (28-30). Macrofagen spelen een rol bij bijna elke ziekte en werden een aantrekkelijk therapeutisch doelwit. Inzicht in de diversiteit van macrofagen, wefseldistributie en plasticiteit zal helpen bij het definiëren van precieze richtstrategieën en effectieve therapieën. In Hoofdstuk 6 belichten we de recente vooruitgang van actieve op nanotechnologie gebaseerde systemen die een centrale rol spelen bij het richten op macrofaag subsets voor therapeutische doeleinden in zieke weefsels.

Afsluitende opmerkingen

In het beschreven onderzoek hebben we verschillende toepassingen besproken die bijdragen aan onze kennis over de waarde van beeldvorming en celtracering, met name op het gebied van oncologie. Ondanks de vele inspanningen om de ‘perfecte’ beeldvormingsbenadering te ontwerpen en te optimaliseren, zijn de ‘perfecte’ resultaten nog niet gevonden. Het

ontwerpen van nieuwe beeldvormende benaderingen en het verbeteren van de huidige, blijft van vitaal belang voor de manier waarop we patiënten diagnosticeren, hun ziekte begrijpen en behandelen. Met andere woorden, de zoektocht moet worden voortgezet.

Geen enkele huidige beschikbare beeldvormingsmodaliteit biedt alle antwoorden. Binnen dit proefschrift lag de focus op het genereren van 'smart' tools en het optimaliseren van de momenteel beschikbare tools voor gevoeliger cellulaire beeldvorming.

Om virale infectie in realtime in beeld te brengen en te volgen, hebben we een nieuw beeldvormingsplatform ontwikkeld op basis van het bioluminescente 'NanoBiT'-systeem, waarin we aantonen dat lichtgevende luciferase-enzymen, wanneer ze worden opgenomen in het virale genoom, bioluminescentiedetectie van geïnfecteerde cellen mogelijk maken met CCD-camerasystemen (charge-coupled device). Bovendien hebben we met verschillende vorderingen binnen het bioluminescentieonderzoek, zoals nieuwe luciferase-enzymen en substraatanalogen, binnen dit proefschrift de beste mariene en terrestrische afgeleide luciferase / substraat-paren geëvalueerd. Een dergelijke analyse zal gunstig zijn voor onderzoekers om de meest geschikte enzym / substraatparing te kiezen, afhankelijk van de experimentele opstelling.

In onze zoektocht hebben we een volgende stap gezet en ontwikkelden een reporter (marker) gensysteem dat zowel voor bioluminescentie (BLI) alsook nucleaire (SPECT / PET) beeldvorming gebruikt kan worden. Deze combinatie van optische en nucleaire beeldvormingsmodaliteiten kan onderzoek verder vergemakkelijken en mogelijk toepassing vinden in gepersonaliseerde gezondheidszorg voor celtracering in diagnostische / prognostische omgevingen.

Samenvattend, met de voortdurende evolutie van nieuwere beeldvormingsmodaliteiten en -apparatuur, zal het mogelijk zijn om cel veranderingen van normale naar zieke toestand vooraf te kwantificeren en in beeld te brengen, en zullen patiënten van ongemak worden behoed (31).

Moleculaire beeldvorming werd een onderdeel van de standaardzorg voor kanker. Door te zien wat er op cellulair niveau in het lichaam gebeurt, levert moleculaire beeldvorming unieke informatie op bij het opsporen, diagnosticeren en behandelen van kanker. In de afgelopen eeuw is er veel onderzoek gedaan om pre- en postoperatieve beeldvorming voor vroege detectie te verbeteren. Ondanks inspanningen blijft het bestrijden van kanker een uitdaging vanwege intra- en inter tumor heterogeniteit. Om de behandeling en de diagnose van kanker volledig te bevorderen, door middel van moleculaire beeldvorming, is het de bedoeling om fundamentele vorderingen in beeldvormingsmodaliteiten te overbruggen en de ziekte vanuit verschillende hoeken te onderzoeken.

Binnen dit proefschrift hebben we preklinische studies uitgevoerd in verschillende modellen met als uiteindelijk doel het gebruik van moleculaire beeldvorming bij de behandeling van kanker. Een multimodaliteitsbeeldperspectief, waarin optische beeldvormingsmodaliteiten, zoals bioluminescentie (BLI) en fluorescentie (FLI) beeldvorming en

radionuclidemethoden zoals (SPECT) werden gebruikt om ‘slimme’ instrumenten voor kankerdetectie te ontwikkelen. Hoewel op radionucliden gebaseerde modaliteiten de meest geavanceerde zijn binnen de klinische setting, zijn innovatieve optische moleculaire beeldvormingsmodaliteiten, zoals die besproken in de hoofdstukken van dit proefschrift, gunstig om diagnose en behandeling in de goede richting te leiden.

Virale infectie visualiseren door optische beeldvorming

Immunotherapie bij kanker heeft tot doel de immuunrespons te versterken en te vergemakkelijken door een eigen immuunrespons op te wekken. De meeste vormen van kankerimmunotherapie zijn gericht op T-cellen, omdat ze tumorcellen kunnen doden op basis van het vermogen om zelf gemuteerde eiwitten te onderscheiden. Het groeiende begrip van de cel in de micro-omgeving van tumoren en het recente klinische succes van kankerimmunotherapie, hebben geleid tot de ontwikkeling van nieuwe beeldvormingsinstrumenten en een betere monitoring van het immuunsysteem. In de klinieken werden de afgelopen decennia indrukwekkende reacties waargenomen na immunotherapie tegen kanker. Echter sommige patiënten reageren niet op therapie wat de behoefte doet toenemen aan verbeterde immunotherapiemedicijnen en ‘slimme’ beeldvormingsinstrumenten om het behandelingsmechanisme en de respons van de patiënt beter te begrijpen (1). Oncolytische virussen zijn een nieuwere klasse van immunotherapie-medicijnen (2, 3). Deze virussen zijn ofwel genetisch gemodificeerd, ofwel natuurlijk voorkomende virussen die selectief kankercellen verstoren en vermenigvuldigen (4-6). Deze virussen bleken ‘koude’ (immuun onderdrukkende) tumoren om te zetten in ‘hete’ (immuun actieve) tumoren door inductie van T-celinfiltratie in tumoren (7-9).

Een belangrijk hulpmiddel om de routes van virale infectie te deconvuleren, zijn reportervirussen. Desalniettemin blijft het genereren van recombinante virussen een uitdaging; hoe kleiner het ingevoegde reporter gen, des te stabielier blijft het virale genoom. Aangezien de meeste virussen geen grote genoomveranderingen tolereren (10), stellen we in **Hoofdstuk 2** een oplossing voor dit probleem voor. We gebruikten de HiBiT-tag, de kleinste bioluminescente reporter, die overal in het virale genoom kan worden ingevoegd, zonder de eigenschappen ervan wezenlijk te veranderen (11). In ons systeem werd de HiBiT-tag (33 basenparen/11 aminozuren) ingebracht in het virale genoom van een klinisch gebruikt oncolytisch virus, en wanneer het reageert met zijn complementaire grote deel (LgBiT), dat tot expressie werd gebracht in kankercellen na infectie met het HiBiT-gelabelde virus, reconstitueert het de volledige NanoLuc-luciferase. Nadat we deze tools hebben gegenereerd, demonstreren we de kracht van ons systeem door de infectiedynamiek van het HiBiT-reportervirus in levende muizen in de loop van 6 weken te volgen, met behulp van gevestigde PC-3-LgBiT-tumoren en hydrofurimazine als het nieuwe in water oplosbare NanoLuc-substraat. We verwachten dat preklinisch onderzoek naar (oncolytische) virale infecties en een breed scala aan andere virussen, vooral virussen die geen

grote genomveranderingen verdragen, sterk zullen profiteren van onze op BL gebaseerde virale screeningstool, waardoor snelle en eenvoudige uitleesprotocollen mogelijk zijn voor een snelle screening van geneesmiddelen.

Identificatie van luciferase/substraat-paren die de voorkeur hebben voor *in vivo* BLI

Bioluminescentiebeeldvorming (BLI) is een essentieel instrument geworden in preklinische *in vivo* en *in vitro* studies voor het visualiseren van moleculaire gebeurtenissen op cellulair niveau (12). De superioriteit van BLI ligt in de hoge signaal/ ruisverhoudingen en quantumopbrengst van luciferas /luciferine systemen, wat leidt tot een extreem hoge detecteerbaarheid in op cellen gebaseerde onderzoeken en voor *in vivo* moleculaire beeldvorming (13, 14). Duizenden lichtgevende soorten worden vertegenwoordigd door ~ 700 geslachten, waarvan 90% afkomstig is van mariene organismen (15, 16) (bijv. NanoLuc of Renilla). Deze luciferasen gebruiken hoofdzakelijk coelenterazine, varguline of analogen van deze twee luciferinen als substraten. De andere grote subset van luciferasegenen zijn terrestrische luciferasen die D-luciferine-analogen vereisen, zoals vuurvlieg of klikkever luciferasen. Bioluminescentiereacties zijn sterk afhankelijk van de interactie tussen het luciferase-enzym en zijn substraat, en elke wijziging van het substraat kan leiden tot een ander emissiespectrum en reactiegevoeligheid.

De afgelopen jaren is de BL-toolbox enorm uitgebreid met nieuw ontwikkelde luciferasegenen, met verschillende emissiekenmerken, en luciferine-analogen die de verbetering en de detectiegevoeligheid in diepere weefsels verhogen (17). Deze vooruitgang vergroot het potentieel van BLI, waar meerdere processen kunnen worden gevolgd vanuit hetzelfde diermodel, waardoor kosten worden verlaagd en tijd wordt bespaard.

Het verbeteren van de prestaties van luciferase-enzymen, substraten en hun mutanten voor BLI is een belangrijk onderdeel van het verbeteren van de tools die beschikbaar zijn voor biowetenschappelijk onderzoek (18).

In **Hoofdstuk 3** en **Hoofdstuk 4** hebben we de BLI-eigenschappen van nieuwe substraatanalogen onderzocht. We bieden een gedetailleerde *in vitro* en *in vivo* analyse van helderheid en emissiespectra om de best presterende luciferase/luciferine-paringen te detecteren met als uiteindelijk doel een verhoogde detectiegevoeligheid. We verwachten onder meer dat de luciferase/luciferine-paren, gebruikt en beschreven in dit proefschrift, zullen dienen als een springplank voor de ontwikkeling van meer gevoelige beeldvormende benaderingen. We verwachten dat de verkregen resultaten van een dergelijke analyse gunstig zullen zijn voor onderzoekers om de meest optimale luciferase / luciferine paren in verschillende experimentele opstellingen te kiezen.

NanoLuc (NLuc) is een mariene luciferase en vormt een belangrijke aanvulling op de mariene BLI-toolset. Het won aan populariteit vanwege zijn kleine formaat (19 kDa) en superieure bioluminescentieprestaties met verhoogde gevoeligheid, snelle reactiedynamiek en lage auto luminescentie op de achtergrond (19, 20). Voor *in vivo* beeldvormingstoepas-

singen werd NanoLuc beperkt door zijn substraat furimazine, dat een lage oplosbaarheid en *in vivo* biologische beschikbaarheid heeft. In **Hoofdstuk 4** vergeleken we de prestaties van recent gerapporteerde NanoLuc-substraten voor *in vivo* beeldvorming bij muizen, aangezien recentelijk is aangetoond dat ze beter geschikt zijn voor in cellulo en *in vivo* NLuc gebaseerde beeldvorming (21-23). Twee substraten met verbeterde oplosbaarheid in water, hydrofurimazine en fluorofurimazine, werden geëvalueerd samen met drie gestabiliseerde O-geacetylerde furimazine-analogen, de hikarazines (21, 22). Alle vijf analogen vertoonden, wanneer ze *in vitro* werden getest, een grotere signaalintensiteit en reactieduur, in vergelijking met het standaard NLuc-substraat, furimazine. NanoLuc/fluorofurimazine-koppeling vertoonde de hoogste bioluminescentie-intensiteit. Het bleek ongeveer negen keer helderder te zijn in vergelijking met de NanoLuc/furimazine-combinatie. Opwindend, ondanks het feit dat NanoLuc/fluorofurimazine voornamelijk blauw licht uitzendt, dat gemakkelijk wordt geabsorbeerd door het omringende weefsel bij kleine dieren, hebben we bewezen dat cellen die vastzitten in de vasculatuur van de longen van muizen gevisualiseerd konden worden via de NanoLuc / fluorofurimazine-koppeling. Van alle geteste analogen maakt fluorofurimazine een hogere substraatbelasting en verbeterde *in vivo* optische beeldvormingsgevoeligheid mogelijk, waardoor NanoLuc-afgeleide bioluminescente systemen worden geüpgraded voor diepe weefselbeeldvorming.

De gevoeligheid van BL-reacties bij dieren hangt voornamelijk af van de hoeveelheid fotonen die wordt uitgezonden door luciferasen bij golflengten groter dan 620 nm, waar de weefselpenetratie hoog is (24). Firefly (Luc2), klikkever (CBR en CBR2) systemen met D-Luciferine en zijn analogen domineren dit veld van BLI. Om de lichtemissie uit diepe weefsels verder te verbeteren, zijn verschillende pogingen gedaan om de emissie te verschuiven naar het nabij-infrarood (NIR) (650-900 nm), resulterend in verbeterde luciferase/luciferinesystemen (24). In **Hoofdstuk 5** hebben we voor de eerste keer *in vivo* spectrale kenmerken van vuurvlieg (Luc2), klikkever groen (CBG99), klikkever rood 2 (CBR2) en AkaLuc luciferases vergeleken met verschillende D-luciferine (D- LH2) analogen (AkaLuc, CycLuc1 en amino-naftyl (NH₂-NpLH₂)). Uit onze *in vivo* resultaten konden we duidelijk concluderen: het beste substraat, in termen van signaalsterkte, voor vuurvlieg luciferase (Luc2), klikkever groen (CBG99) en klikkever rood 2 (CBR2) was duidelijk D-luciferine; de emissiespectra van vuurvlieg (Luc2) en klikkever rood 2 (CBR2) werden verschoven naar een langere golflengte toen we AkaLumine als substraat gebruikten; Klikkever rood 2 (CBR2) produceerde de helderste signalen met het nabij-infraroodsubstraat (NIR), amino-naftyl (NH₂-NpLH₂); AkaLuc, gecombineerd met CycLuc1 of AkaLumine, was helderder dan in combinatie met D-Luciferin.

We verwachten dat de verkregen resultaten van nut zullen zijn voor onderzoeken, waardoor de selectie van de best presterende enzym / substraat-paren voor toepassingen mogelijk zal zijn.

Bioluminescentie en op radionucliden gebaseerd reportergensysteem

Reporter genen vertegenwoordigen een ongecompliceerd middel voor het volgen van opkomende tumoren, waardoor *in vivo* visualisatie en distributie van doelcellen mogelijk is zoals de interactie tussen T-cellen en kankercellen. Het samenvoegen van verschillende beeldvormingsmodaliteiten in een specifieke beeldvormingsprobe zal de vertaling van moleculair-genetische beeldvorming naar klinische toepassing voor kankerdiagnose en -therapie vergemakkelijken (25). Een aantrekkelijke benadering en een compensatie voor de beperkingen van elke individuele beeldvormingstechniek, is de koppeling van nucleaire (SPECT/PET) met optische (BLI/FLI) beeldvormingsmodaliteiten. SPECT/PET-scans bieden 3D-beelden en kwantitatieve analyses van reporterexpressie, en aan de andere kant bieden optische beeldvormingsmodaliteiten (BLI / FLI) 2D-beelden met een hoge gevoeligheid (25, 26).

In **Hoofdstuk 5** durven we de vraag te stellen: ‘Kunnen we een bioluminescentiereportersysteem verschuiven naar een nucleair beeldvormingssysteem? In deze studie hebben we een reporter-gen-systeem ontwikkeld dat bioluminescentie (BLI) beeldvorming ondersteunt naast nucleaire (SPECT/PET) beeldvorming. We gebruikten de LgBiT-subeenheid en combineerden deze met het radioactief gelabelde HiBiT-peptide van het BL ‘NanoBiT’ split-systeem. Aanvankelijk hebben we een chimeer transmembraanreportergen (TM-LgBiT) geconstrueerd en het tot expressie gebracht op het membraan van HEK-293T en PC-3-cellen. Bovendien werd een betrouwbare procedure voor het labelen van HiBiT met indium-111 vastgesteld, waar we [¹¹¹In] In-DOTA-6-Ahx-HiBiT-probe verkregen. We waren in staat om specifieke opname van DOTA-6-Ahx-HiBiT te detecteren, met behulp van bioluminescentie-beeldvorming *in vitro* van cellen en *in vivo* van tumoren die TM-LgBiT-reporter tot expressie brengen. Voorlopige SPECT/CT-scans lieten specifieke [¹¹¹In] In-DOTA-6-Ahx-HiBiT-traceropname zien in muizen die waren geïmplant met doelwit-positieve cellen, wat werd bevestigd door *ex vivo* bio distributie studies. Om de vraag te beantwoorden: ‘Kunnen we een bioluminescentie-reportersysteem verschuiven naar een nucleaire beeldvorming?’ - ja, dat kunnen we. Toekomstige optimalisatie van ons systeem zoals het injecteren van grotere hoeveelheden HiBiT-tracer (bijv. 1 nmol) bij dieren, en evaluatie van het meest geschikte tijdpunt voor beeldvorming, na toediening van de sonde, zijn essentieel.

Wij zijn van mening dat ons systeem van groot nut zal zijn bij toekomstige cel tracers studies en in diagnostische / prognostische omgevingen.

Richten op macrofagen

Moleculaire beeldvorming heeft een revolutie teweeggebracht in de manier waarop we het menselijk lichaam waarnemen en benaderen, het ontwerp van geneesmiddelen plannen en benaderen en ziekten diagnosticeren (27). Bioluminescentie optische beeldvorming is een zeer geschikte beeldvormingstechniek voor visualisatie van het immuunsysteem, waardoor

real-time inzicht mogelijk wordt gemaakt in de dynamiek van immuuncellen, die vaak van locatie veranderen en in aantal toenemen. Verschillende celtraceringstechnieken zijn de afgelopen jaren naar voren gekomen en in vergelijking met optische beeldvorming bieden alternatieve beeldvormingsmethoden van geïnjecteerde moleculen of cellen voordelen, zoals een uitstekende ruimtelijke resolutie (MRI) en absolute resolutie in het geval van nucleaire beeldvormingsmodaliteiten (28-30). Macrofagen spelen een rol bij bijna elke ziekte en werden een aantrekkelijk therapeutisch doelwit. Inzicht in de diversiteit van macrofagen, weefseldistributie en plasticiteit zal helpen bij het definiëren van precieze richtstrategieën en effectieve therapieën. In **Hoofdstuk 6** belichten we de recente vooruitgang van actieve op nanotechnologie gebaseerde systemen die een centrale rol spelen bij het richten op macrofaag subsets voor therapeutische doeleinden in zieke weefsels.

Afsluitende opmerkingen

Binnen dit werk hebben we verschillende toepassingen besproken die bijdragen aan onze kennis over de waarde van beeldvorming en celtracering, met name op het gebied van oncologie. Ondanks de vele inspanningen om de 'perfecte' beeldvormingsbenadering te ontwerpen en te optimaliseren, zijn de 'perfecte' resultaten nog niet gevonden. Het ontwerpen van nieuwe beeldvormende benaderingen en het verbeteren van de huidige, blijft van vitaal belang voor de manier waarop we patiënten diagnosticeren, begrijpen en behandelen. Met andere woorden, de zoektocht moet worden voortgezet.

Geen enkele huidige beschikbare beeldvormingsmodaliteit biedt alle antwoorden. Binnen dit proefschrift lag de focus op het leveren van 'smart' en het optimaliseren van de momenteel beschikbare tools voor gevoeliger cellulaire beeldvorming.

Om virale infectie in realtime in beeld te brengen en te volgen, hebben we een nieuw beeldvormingsplatform ontwikkeld op basis van het bioluminescente 'NanoBiT'-systeem, waarin we aantonen dat lichtgevend luciferase-enzymen, wanneer ze worden opgenomen in het virale genoom, bioluminescentiedetectie van geïnfecteerde cellen mogelijk maken met CCD-camerasystemen (charge-coupled device). Bovendien hebben we met verschillende vorderingen binnen de BL toolkit, zoals nieuwe luciferase-enzymen en substraat-analogen, binnen dit proefschrift de beste mariene en terrestrische afgeleide luciferase/substraat-paren geëvalueerd. Een dergelijke analyse zal gunstig zijn voor onderzoekers om de meest geschikte enzym/substraatparing te kiezen, afhankelijk van de experimentele opstelling.

We zetten de volgende stap in onze zoektocht en ontwikkelden een reporter (marker) gensysteem dat tegelijkertijd bioluminescentie (BLI) ondersteunt naast nucleaire (SPECT/PET) beeldvorming. Deze combinatie van optische en nucleaire beeldvormingsmodaliteiten kan onderzoek verder vergemakkelijken en mogelijk toepassing vinden in gepersonaliseerde gezondheidszorg voor celtracering.

Samengevat, door de continue evolutie van nieuwe multi-modale beeldverwerkings reporters/probes en apparatuur, wordt het mogelijk om cellen beter te volgen en biologische processen te monitoren, diagnose en medicijn ontwikkeling te verbeteren alsmede beter de effectiviteit van behandeling te bepalen wat uiteindelijk leidt tot betere kwaliteit van leven van de kankerpatiënt.

REFERENTIES

1. Kurtz DM, Gambhir SS. Tracking cellular and immune therapies in cancer. *Adv Cancer Res.* 2014;124:257-96.
2. Jiang H, Shin DH, Nguyen TT, Fueyo J, Fan X, Henry V, et al. Localized Treatment with Oncolytic Adenovirus Delta-24-RGDOX Induces Systemic Immunity against Disseminated Subcutaneous and Intracranial Melanomas. *Clinical Cancer Research.* 2019;25(22):6801.
3. Kaufman HL, Kohlhapp FJ, Zloza A. Oncolytic viruses: a new class of immunotherapy drugs. *Nat Rev Drug Discov.* 2015;14(9):642-62.
4. Lichty BD, Breitbach CJ, Stojdl DF, Bell JC. Going viral with cancer immunotherapy. *Nature Reviews Cancer.* 2014;14(8):559-67.
5. Jiang H, Gomez-Manzano C, Rivera-Molina Y, Lang FF, Conrad CA, Fueyo J. Oncolytic adenovirus research evolution: from cell-cycle checkpoints to immune checkpoints. *Curr Opin Virol.* 2015;13:33-9.
6. Russell SJ, Peng KW, Bell JC. Oncolytic virotherapy. *Nat Biotechnol.* 2012;30(7):658-70.
7. Lang FF, Conrad C, Gomez-Manzano C, Yung WKA, Sawaya R, Weinberg JS, et al. Phase I Study of DNX-2401 (Delta-24-RGD) Oncolytic Adenovirus: Replication and Immunotherapeutic Effects in Recurrent Malignant Glioma. *J Clin Oncol.* 2018;36(14):1419-27.
8. Jiang H, Rivera-Molina Y, Gomez-Manzano C, Clise-Dwyer K, Bover L, Vence LM, et al. Oncolytic Adenovirus and Tumor-Targeting Immune Modulatory Therapy Improve Autologous Cancer Vaccination. *Cancer Res.* 2017;77(14):3894-907.
9. Jiang H, Clise-Dwyer K, Ruisaard KE, Fan X, Tian W, Gumin J, et al. Delta-24-RGD Oncolytic Adenovirus Elicits Anti-Glioma Immunity in an Immunocompetent Mouse Model. *PLOS ONE.* 2014;9(5):e97407.
10. Cai H, Liu M, Russell CJ. Directed Evolution of an Influenza Reporter Virus To Restore Replication and Virulence and Enhance Noninvasive Bioluminescence Imaging in Mice. *Journal of Virology.* 2018;92(16):e00593-18.
11. Gaspar N, Zambito G, Dautzenberg IJC, Cramer SJ, Hoeben RC, Lowik C, et al. NanoBiT System and Hydrofurimazine for Optimized Detection of Viral Infection in Mice—A Novel in Vivo Imaging Platform. *International Journal of Molecular Sciences.* 2020;21(16).
12. Kaijzel EL, van der Pluijm G, Löwik CWGM. Whole-Body Optical Imaging in Animal Models to Assess Cancer Development and Progression. *Clinical Cancer Research.* 2007;13(12):3490.
13. Roda A, Pasini P, Mirasoli M, Michelini E, Guardigli M. Biotechnological applications of bioluminescence and chemiluminescence. *Trends Biotechnol.* 2004;22(6):295-303.
14. Roda A, Guardigli M, Michelini E, Mirasoli M. Bioluminescence in analytical chemistry and in vivo imaging. *TrAC Trends in Analytical Chemistry.* 2009;28:307-22.
15. Shimomura O. *Bioluminescence: Chemical principles and methods*, revised edition 2012. 1-468 p.
16. Martini S, Haddock SHD. Quantification of bioluminescence from the surface to the deep sea demonstrates its predominance as an ecological trait. *Scientific Reports.* 2017;7(1):45750.
17. Adams ST, Jr., Miller SC. Beyond D-luciferin: expanding the scope of bioluminescence imaging in vivo. *Curr Opin Chem Biol.* 2014;21:112-20.
18. Markova SV, Vysotski ES. Coelenterazine-dependent luciferases. *Biochemistry (Moscow).* 2015;80(6):714-32.
19. Hall MP, Unch J, Binkowski BF, Valley MP, Butler BL, Wood MG, et al. Engineered Luciferase Reporter from a Deep Sea Shrimp Utilizing a Novel Imidazopyrazinone Substrate. *ACS Chemical Biology.* 2012;7(11):1848-57.

20. Dale NC, Johnstone EKM, White CW, Pflieger KDG. NanoBRET: The Bright Future of Proximity-Based Assays. *Frontiers in Bioengineering and Biotechnology*. 2019;7(56).
21. Morse D, Tannous BA. A water-soluble coelenterazine for sensitive in vivo imaging of coelenterate luciferases. *Molecular therapy : the journal of the American Society of Gene Therapy*. 2012;20(4):692-3.
22. Schwinn MK, Machleidt T, Zimmerman K, Eggers CT, Dixon AS, Hurst R, et al. CRISPR-Mediated Tagging of Endogenous Proteins with a Luminescent Peptide. *ACS Chemical Biology*. 2018;13(2):467-74.
23. Inouye S, Sato J, Sahara-Miura Y, Yoshida S, Kurakata H, Hosoya T. C6-Deoxy coelenterazine analogues as an efficient substrate for glow luminescence reaction of nanoKAZ: the mutated catalytic 19 kDa component of Oplophorus luciferase. *Biochem Biophys Res Commun*. 2013;437(1):23-8.
24. Hall MP, Woodrooffe CC, Wood MG, Que I, van't Root M, Ridwan Y, et al. Click beetle luciferase mutant and near infrared naphthyl-luciferins for improved bioluminescence imaging. *Nature Communications*. 2018;9(1):132.
25. Kang JH, Chung JK. Molecular-genetic imaging based on reporter gene expression. *J Nucl Med*. 2008;49 Suppl 2:164S-79S.
26. Akins EJ, Dubey P. Noninvasive Imaging of Cell-Mediated Therapy for Treatment of Cancer. *Journal of Nuclear Medicine*. 2008;49(Suppl 2):180S.
27. James ML, Gambhir SS. A molecular imaging primer: modalities, imaging agents, and applications. *Physiol Rev*. 2012;92(2):897-965.
28. Kherlopian AR, Song T, Duan Q, Neimark MA, Po MJ, Gohagan JK, et al. A review of imaging techniques for systems biology. *BMC Syst Biol*. 2008;2:74.
29. Penet M-F, Mikhaylova M, Li C, Krishnamachary B, Glunde K, Pathak AP, et al. Applications of molecular MRI and optical imaging in cancer. *Future Med Chem*. 2010;2(6):975-88.
30. Wu C, Have F, Vastenhouw B, Dierckx R, Paans A, Beekman F. Absolute quantitative total-body small-animal SPECT with focusing pinholes. *Eur J Nucl Med Mol Imaging*. 2010;37:2127-35.

Scientific Contributions & PhD Portfolio

SCIENTIFIC CONTRIBUTIONS

Orals & Posters

1. **ERASMUS MC 2017 Research on the Move:** ‘Preclinical Imaging of Viral Infection Using NanoLuc Binary Technology’ (*Poster Session*)
2. **European Society for Molecular Imaging Summer Workshop Dedicated to Optical Molecular Imaging (ESMI TOPIM TECH):** ‘Combining luciferases and novel D-luciferin analogues for accurate multicolor bioluminescence imaging’ (*Poster Session*)
3. **European Molecular Imaging Meeting Conference (EMIM 2018):** ‘Sensitive Bioluminescent Imaging of Viral Infection Using NanoLuc Binary Technology’ (*Poster Session*)
4. **The World Molecular Imaging Congress (WMIC 2019):** ‘Optical Molecular Imaging of Oncolytic Virus using NanoLuc Luciferase Complementation Assay’ (*Poster Session*)
5. **European Molecular Imaging Meeting Conference (EMIM 2020):** ‘Novel NanoBiT *in Vivo* Application- Visualizing Infection’ (*Oral Presentation-online*)

List of Publications

1. ‘Imaging Modalities for Biological and Preclinical Research, Volume 2: A compendium’
Book Chapter II. 4.b.: Optical imaging: Bioluminescence (**Published chapter**)
Authors: Laura Mezzanotte & **Natasa Gaspar**
2. ‘Active Nano-targeting of Macrophages’ (**Published Article**)
Authors: **Natasa Gaspar**, Giorgia Zambito, Clemens M.W.G. Löwik, and Laura Mezzanotte
3. ‘NanoBiT System and Hydrofurimazine for Optimized Detection of Viral Infection in Mice- A Novel *in Vivo* Imaging Platform’ (**Published Article**)
Authors: **Natasa Gaspar**, Giorgia Zambito, Iris J. C. Dautzenberg, Steve J. Cramer, Rob C. Hoeben, Clemens Lowik, Joel R. Walker, Thomas A. Kirkland, Thomas P. Smith, Wytse M. van Weerden, Jeroen de Vrij and Laura Mezzanotte
4. ‘Evaluation of NanoLuc Substrates for Bioluminescence Imaging of Transferred Cells in Mice’ (**Published Article**)
Authors: **Natasa Gaspar**, Joel R. Walker, Giorgia Zambito, Kranthi Marella-Panth, Clemens Lowik, Thomas A. Kirkland, Laura Mezzanotte (**Published Article**)
5. ‘Evaluating Brightness and Spectral Properties of Click Beetle and Firefly Luciferases Using Luciferin Analogues: Identification of Preferred Pairings of Luciferase and Substrate for *in Vivo* Bioluminescence Imaging’ (**Published Article**)

Authors: Giorgia Zambito, Natasa Gaspar, Yanto Ridwan, Mary P Hall, Ce Shi, Thomas A Kirkland, Lance P Encell, Clemens Löwik, Laura Mezzanotte

6. **'Red-shifted click beetle luciferase mutant expands the multicolor bioluminescent palette for deep tissue imaging' (Published Article)**

Authors: Giorgia Zambito, Mary P. Hall, Monika G Wood, Natasa Gaspar, Yanto Ridwan, Fabio F. Stellari, Ce Shi Thomas A. Kirkland, Lance P. Encell, Clemens Löwik, Laura Mezzanotte

7. **Can We Transform a Bioluminescent Reporter Gene Towards a Reporter for Radionuclide-based Imaging? (Manuscript in Preparation) Authors: Natasa Gaspar,**

Maryana Handula, Marcus C. M. Stroet, Kranthi Marella-Panth, Joost Haeck, Thomas Kirkland, Mary Hall, Lance Encell, Simone Dalm, Marion De Jong, Clemens Lowik, Yann Seimbille, Laura Mezzanotte

PHD PORTFOLIO

PhD portfolio

Name PhD Student: Natasa Gaspar

Erasmus MC Departments: Molecular Genetics, Radiology & Nuclear Medicine

Promotor: Prof. dr. Clemens Löwik

Supervisor: Dr. Laura Mezzanotte

<i>Courses</i>	<i>Year</i>	<i>ECTS</i>
Laboratory Animal Science (Article 9)	2017	3
Working with Radionuclides level 5B	2017	1
8 TH LUMC FCF User Course Flow Cytometry for Starters	2018	0.5
Basic Introduction Course on SPSS	2018	1
Course on Research Integrity	2018	0.5
GraphPad Prism Version 7 Course	2018	0.3
Biomedical English Writing Course	2019	2
Personal Leadership & Communication for PhD Students and Post Docs	2020	1
Photoshop and Illustrator CC 2019 Workshop for PhD-students and other Researchers	2020	0.3
Annual Course on Molecular Medicine	2020	0.7

<i>Conferences & Symposia</i>	<i>Year</i>	<i>ECTS</i>
European Molecular Imaging Meeting Conference-EMIM	2018	1
Annual Molecular Medicine Conference	2018	0.7
Stem Cells, Organoids And Regenerative Medicine Symposium	2018	1
European <i>in vivo</i> Optical Imaging User Group Meeting	2019	0.7
The World Molecular Imaging Congress (WMIC)	2019	1
15 th European Molecular Imaging Meeting (on line)	2020	1
Monocytes, Macrophages, Dendritic Cells and Metabolism Symposium	2019	0.15

<i>Seminars & Workshops</i>	<i>Year</i>	<i>ECTS</i>
Weekly Molecular Genetics Department Work Discussion Meeting	2016-2021	3
Weekly Meeting – Laboratory Journal	2016-2021	3
Translational Imaging Workshop in Molecular Imaging (AMIE)	2017	1.4
European Society for Molecular Imaging Summer Workshop Dedicated to Optical Molecular Imaging	2017	1
Optoacoustic imaging workshop -Visualsonics	2017	0.2
Seminar on 3D cell culture (Sigma-Aldrich)	2017	0.1
People in Science Workshop	2018	0.2
Monocyte Lunch	2019	0.1

Monthly Virology Department Laboratory Journal	2018-2020	1
Monthly Radiology & Nuclear Medicine Joint Meeting	2018-2021	2
Career Development for PhD Candidates	2019	0.15
Workshop on Presenting Skills	2019	1

<i>Teaching & other Activities</i>	<i>Year</i>	<i>ECTS</i>
Supervising Students	2017-2021	7
ML-II Laboratory, Rules and Regulations on Safety Procedures	2017	0.5
PhD Student Committee Member	-2019	0.5

<i>Presentations</i>	<i>Year</i>	<i>ECTS</i>
50+ Talks/Poster Sessions at different Groups, Workshops & Congresses	2016-2021	5

TOTAL		41.80
-------	--	-------

Acknowledgements

First of all,

I would like to express sincere gratitude and respect to my promotor and co-promotors; Prof. Dr. Clemens Löwik, Dr. Laura Mezzanotte and Dr. Alan Chan, for letting me be a part of this unique experience.

During the last couple of years, I have received a great deal of support and guidance from all of you. I will remember this throughout my future career.

I feel lucky that I could learn from you, thank you.

A very special *thanks* goes out to my 'main' supervisor, Dr. Laura Mezzanotte, whose constant presence, guidance and advice were the stepping-stones for this dissertation. Your feedback sharpened my thinking and brought my work and character to a higher level.

I would like to acknowledge my Colleagues, with a capital C. Colleagues from 'my' very special OMIR group, Molecular Genetics, Nuclear Medicine, Radiology, LUMC and all of you that I had the chance to meet during different courses, workshops, conferences, etc.

Writing these words here, brings back great memories.

I feel lucky to have met you all.

Thank You & I wish You well.

'Thank You'!

To Friends, that are still present, and to those that left to another place- *Your light is eternal!*

I highly cherish your support and loyalty.

Thank you for giving me many, many things to enjoy outside of the PhD.

To me, you are very special.

To my Parents.

If obtaining a doctorate can be called 'success', I completely dedicate it to You.

I owe You everything.

To experience, the good and the bad ones. All leads to wisdom, if we allow it.

To Self.

Curriculum Vitae

Natasa Gaspar was born on April 20th, 1990 in Benkovac, Croatia. She completed high school (Lyceum Jurja Barakovica, 2009) in Zadar, Croatia.

After high school, she studied Nutrition Science in Zagreb, University of Food Technology and Biotechnology, from 2009 to 2012. Her bachelor thesis research project was performed within the department of Biochemistry, under supervision of Prof. Dr. Slobodan Barbaric where she investigated the synthesis of β -glucanase by *Candida utilis*.



After her bachelor studies, Natasa performed her Master studies in Molecular Biotechnology at the same university from 2012 to 2014. During her masters, she participated in the LLP Erasmus exchange program for excellent students, at the Technical University of Kaiserslautern, Germany. Within this program she performed her master research project, under supervision of Prof. Dr. John Cullum and Prof. Dr. Daslav Hranueli, at the department of Molecular genetics. She investigated the effect of Photodynamic inactivation in the *Escherichia coli*.

In 2014, after graduating from university, Natasa started working for a pharmaceutical and cosmetic company (*Magdis d.o.o.*) in Zagreb, Croatia, as a Quality control assistant.

In 2016, she obtained the EU founded PhD scholarship, project: H2020- Marie Skłodowska-Curie Actions-ITN 2016, Acronym –ISPIC (Image Guided Surgery and Personalized Postoperative Immunotherapy). Natasa started her PhD research at the Erasmus MC in Rotterdam, within the Optical Molecular Imaging group (OMIR), at the departments of Molecular Genetics: Radiology and Nuclear Medicine. In collaboration with Prof. Dr. Clemens Lowik, Dr. Laura Mezzanotte and Dr. Alan Chan she performed the research documented within this thesis.